UNIVERSITY OF CALIFORNIA
RIVERSIDE

Synthesis and Properties of Helical Oligothiophenes and Molecular Gyroscopes

A Dissertation submitted in partial satisfaction
of the requirements for the degree of

Doctor of Philosophy

in

Chemistry

by

Shohreh Rahbarnia

June 2009

Dissertation Committee:

Dr. Michael J. Marsella, Chairperson
Dr. Christopher Switzer
Dr. Richard Hooley

The Dissertation of Shohreh Rahbarnia is approved:

_____

_____

_____

Committee Chairperson

University of California, Riverside

Acknowledgments

First and foremost, I would like to offer my deepest gratitude and admiration to my advisor Dr. Michael J. Marsella. He has been a an amazing mentor and a wonderful advisor, knowing instinctively when to allow me the freedom to explore my chemistry and when to offer advice and suggestions. I will forever be grateful for his encouragement, guidance, and support. A very special thanks goes to my committee members Dr. Christopher Switzer and Dr. Richard Hooley for their suggestions and assistance in editing and revising this dissertation.

I have had the great pleasure of working with many talented chemists in the Marsella lab. They have made the arduous journey through graduate school infinitely easier to bear. Special thanks to: Dr. Samia Estassi, and Dr. Paul Richardson for their support; Dr. Nathan Wilmot for conception of the gyroscope idea; Future Doctors Michael Guiterrez (synthesis of the gyroscopes) and Robert Carp (dynamics of the Kelly system) for collaborations on the gyroscope project. I specially want to acknowledge future Doctors Katie Hawkins and Angie Garcia who were “the best undergrads ever”, as well as wonderful friends.

Special thanks to: Dr. Dan Borchardt, and Mr. Mi Yang for NMR guidance, Dr. Richard Kondrat and Mr. Ron New for Mass Spectrometry, Dr. Fook Tham for X-

ray Crystallography, and all of the faculty and staff at UCR Chemistry Department.

I would have never made it through this process without the love and support of my family, and for that I am very grateful. Much love and appreciation goes to my mother, Tamineh Javadi for her never-ending support and love. She has been the best mother and grandmother anyone could ask for, and we are so very lucky to have you in our lives. A special thanks goes to my sisters, Tina and Ghazaleh Rahbarnia for their love and support and for reminding me that I have a life outside chemistry.

Finally and most important, I want to thank my husband Dr. Kourosh Tanara. He has been so understanding and patient throughout my studies, suffering through the frustrations and sharing the accomplishments. His faith, support and love have kept me going. Without his love and incredible friendship none of this would matter. I love you very much.

Dedicated to my husband Kourosh, my daughters Sahar
and her little sister to be, my mother Tamineh Javadi,
and in memory of my father Mohammad Javad Rahbarnia.

You all bring much joy to my life and I love you very much.

ABSTRACT OF THE DISSERTATION

Synthesis and Properties of Helical Oligothiophenes and Molecular Gyroscopes

by

Shohreh Rahbarnia

Doctor of Philosophy, Graduate Program in Chemistry
University of California, Riverside, June 2009
Dr. Michael J. Marsella, Chairperson

Molecular springs and molecular gyroscope, two diverse topics, are the subject of this dissertation. In Part I oligothiophenes are used as the bases of the molecular spring. The design is targeted in making non-ladder type helix with large extension range. Two non-transition metal cross-coupling strategies for assembling odd- and even-numbered helical oligoarenes are reported. Outer Valence Green Function predicts that the energies of the HOMO and LUMO vary non-linearly with extension from contracted form to extended form. Coupled with recent developments in STM, these molecules should be excellent candidates to demonstrate force-induced attenuation of conductivity. In part II, a non-gearing rotor composed of two nearly orthogonal rotational axes is analyzed by molecular dynamics and *ab initio* calculations. The isolated system is investigated for its ability to rotate and precess analogous to a conventional gyroscope. We find that correlated rotation and precession at equilibrium is possible, contingent on

symmetry, steric, and rotor mass prerequisites. *Ab initio* frequency calculations can be used to predict the likelihood of a molecular gyroscope to exhibit correlated rotation and precession at equilibrium.

Table of Contents

List of Figures

List of Schemes

Chapter 1

Conjugated Oligomers and Polymers

1.1 Introduction

The diversity in configuration and function of biological molecules is astonishing. Nature achieves this by only three major polymeric backbones: proteins, ribonucleic acids, and polysaccharides,[1] making copolymer sequence a dominant way to meet various chemical challenges. Studies on monomers similar to those found in nature have provided clues about these polymeric backbones. Looking beyond the biopolymers it is possible to imagine that other chain molecules are capable of similar functions. Testing of this concept has begun, raising questions of great fundamental interest.

Most of the functions carried out by biomacromolecules, such as molecular recognition, information storage, and catalysis, involve stable compact solution structures that approach conformational uniqueness. The spatial position of most of the backbone atoms is fixed, except for minor fluctuations about their equilibrium coordinates. Foldamers are unnatural oligomeric sequences that take on well-defined conformations in solution, and are defined as any oligomer that folds into a conformationally ordered state in solution, the structures of which are stabilized by a collection of noncovalent interactions between nonadjacent monomer units. There are two major classes of foldamers: single stranded foldamers that only fold and multiple-stranded foldamers that both associate and fold.[1] Different types of foldamer structures are shown in **Figure 1**.

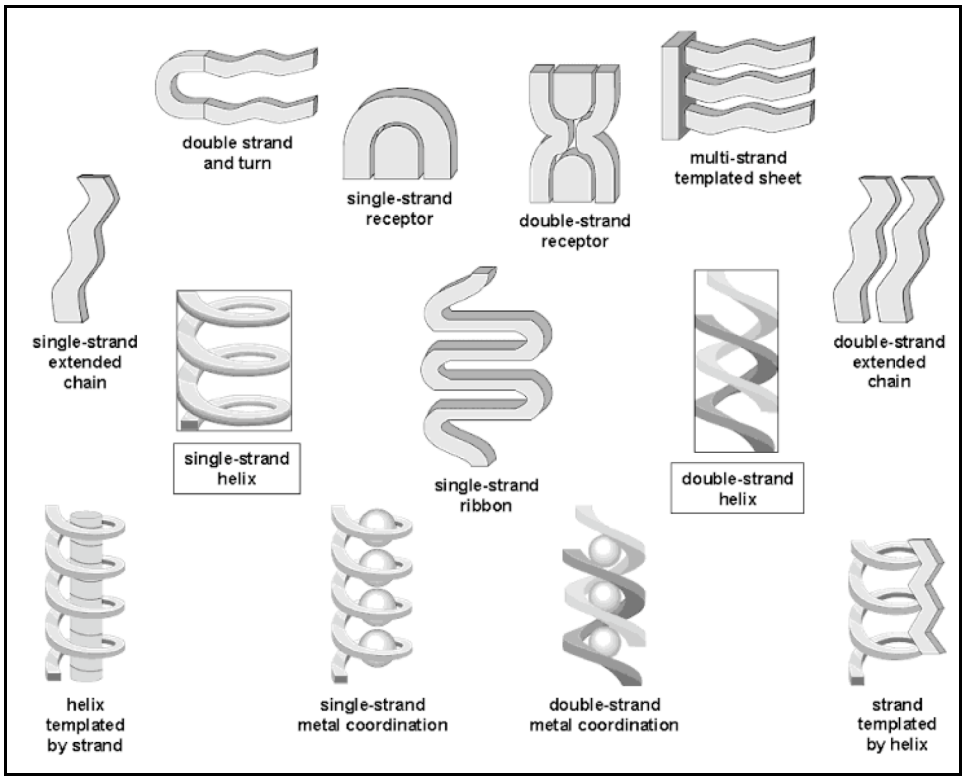

Figure 1: Illustrations depicting the different types of foldamer structures.

The foundation of foldamer research was laid in the early 20th century, after major breakthroughs in the field of structural biology. First was the discovery of the helical structure of α-amylose as proposed by Hanes in 1937,[2] which was further extended by Freudenberg.[3] And second, Pauling proposed the α-helical structure for natural polypeptides,[4] followed by Watson and Crick who determined the double helical structure of DNA[5] in the early 1950s.

These discoveries indicated that the helix was the most fundamental structure among naturally occurring macromolecules. It is of no surprise that synthetic

chemists find the helix attractive: its broad application and potential makes it a perfect tool for mimicking the high functionalities of biomacromolecules. As mentioned above, these include molecular recognition (separation, catalysis, sensory functions), a molecular scaffold for controlled spatial alignment of functional groups or chromophores, and ordered molecular alignment in the solid phase such as that in liquid crystalline materials.[6] Double-stranded helices enhance the properties derived from chirality, such as chiral currents and chiral optical properties. They also serve as a platform to orient pendant groups.[1]

The field of synthetic helical macromolecules dates back to 1955, when Natta found that stereoregular isotactic polypropylene has a helical structure in the solid state.[7] A helical structure for vinyl polymers in solution was realized for isotactic poly(3-methyl-1-pentene) by Pino in 1960.[8] Although the chiral side groups affect the helical conformation in the polyolefin, the single handed helix of poly(triphenylmethyl methacrylate) (**1**), shown in **Figure 2**, synthesized by Okamoto and Yuki in 1979 did not require chiral side chains. This was the first optically active vinyl polymer that was chiral due to its helicity.[9] The helicity of this vinyl polymer was dependent on the bulky side groups that caused isotactic polymerization, if the bulky groups were removed the vinyl polymer lost its helicity.

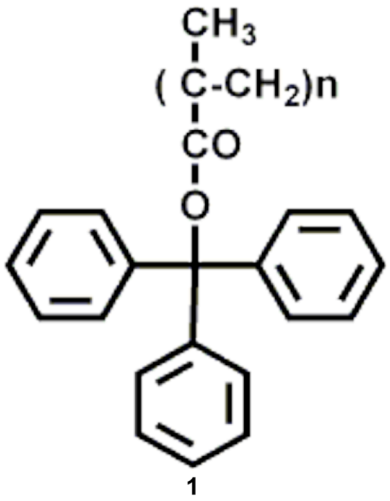

1

Figure 2: Structure of poly(triphenylmethylmethacrylate) (**1**).

The helical conformation of polyisocyanides with bulky side chains was first postulated by Millich[10] in 1969 and confirmed by Drenth and Nolte in 1974.[11] This aspect was later studied by Green,[12] Hoffman,[13] Salvadori,[14] and Goodman,[15] all of whom made significant contributions in understanding polyisocyanides.

In 1974 Ciardelli confirmed the helical conformation of polyacetylene derivatives with chiral side chains.[16] It was later extended and more clearly demonstrated via ring opening metathesis of the corresponding cyclooctatetraene derivative by Grubbs in 1991.[17]

The helical structure of polychloral was proposed by Vogl[18] in 1980 and was demonstrated by Ute, Hatada, and Vogl via a detailed conformational analysis of chloral oligomers.[19]

Polysilanes bearing a chiral side chain were synthesized and their conformations were studied. A helical conformation for this class of polymers in solution was found in 1994 independently by Fujiki[20] and Moller.[21] This was the first example of a helical polymer with an inorganic backbone. In 1992, however, Matyjaszewski[22] had pointed out such a conformation for chiral polysilanes in the solid state.

A related development in this is the discovery of helicates by Lehn in 1987[23], which are double and triple helical complexes of oligomeric ligands and metals. Later, they also discovered the helical conformations of oligoarylenes (**2**) (**Figure 3**) in 1995.[24] In this study they present three basic features for coiling a non-chiral linear molecule into a helical shape: (a) an alternating sequence of pyridine and pyrimidine units; (b) linkage of these units at appropriate positions; and (c) *transoid* conformations around the linkage bonds based on the preference for a *trans* orientation of nitrogen sites and concomitant *cisoid* orientation of CH and N sites as found in the 2,2'-bipyridine structure.

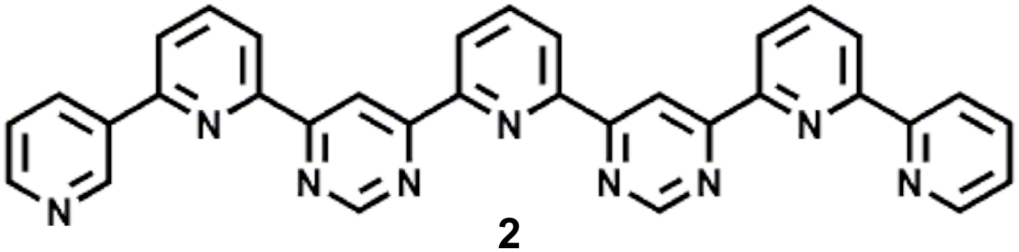

2

Figure 3: Oligoarylenes (**2**): a linear non-chiral molecule that curles up into a helix.

Also noteworthy are the discovery of helical oligo(aryleneethynylenes) by Moore and coworkers, as well as the double helical π-conjugated topology of octaphenylenes by Rajca and coworkers, both in 1997.[25,26]

An outline of the historical aspect of helical polymers has been discussed. The following sections will explore significant work done by Moore, Rajca, and Katz related to our work.

1.2 Solvophobically-Driven Folding of Nonbiological Oligomers

Proteins and polynucleotides exemplify intramolecular self-organization in solution, as seen by their spontaneous and reversible folding into well-defined conformations. Until 1997, no such system was reported for synthetic chain molecules. Moore et al. reported the folding of an aromatic hydrocarbon backbone using phenylacetylene oligomers whose cooperative transition can be

driven, just as for proteins, by both solvent and temperature changes. The oligomer is guided to a folded, helical conformation by non-directional interactions and local constraints caused by the covalent structure of the backbone. A significant number of open chain conformations are available to an all *meta*-phenylacetylene oligomer, whereas the compact helical conformation has a well defined tubular cavity that is potentially useful for binding (**Figure 4**).[27]

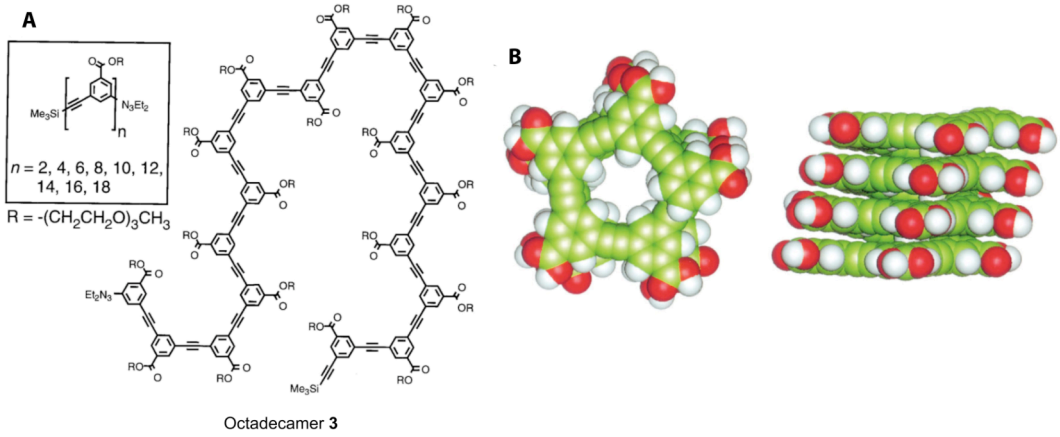

Figure 4: (A) Phenylacetylene oligomers with a range of n values (inset, upper left). Also shown is octadecamer (**3**) with n=18 in a representative random coil conformation. (B) Helical conformation of a meta-substituted phenylacetylene octadecamer (n=18), where R=H and the end groups have been removed for clarity.

Moore et al. were able to show that by changing the size of the helical cavity it can act as a host to rod like guest[28], as shown in **Figure 5**. The stability gained from folding can be used to control the synthesis of oligomers from short chain segments reversibly ligated through an imine metathesis reaction. In this case folding shifts the ligation equilibrium in favor of conformationally ordered sequences. This approach selectively prepares macromolecules with stable

conformations and directly connects folding and synthesis, emphasizing molecular function rather than structure in polymer synthesis.

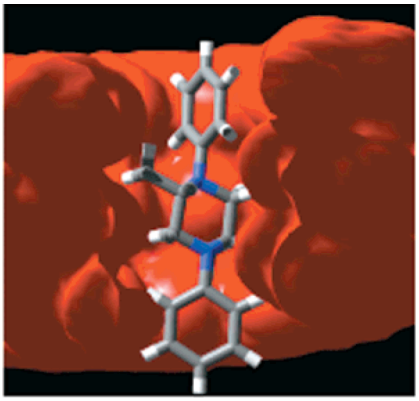

Figure 5: Minimized structure of *m*-phenylene ethynylene oligomer (n=18) with *cis*-(2S,5S)-2,5-dimethyl-N,N'-diphenylpiperazine (**4**) determined by Monte Carlo docking algorithm.

The helical conformation of oligo(*meta*-phenylene ethynylenes) was investigated by placing a pair of 2,2,6,6-tetramethylpiperidine-1-oxyl (TEMPO) spin labels on the backbone, as shown in **Figure 6**.[29] Four, five, and six repeating units separated the two radicals. After the measurement and analysis of the electron spin resonance (ESR) spectra in both chloroform and ethyl acetate, it was found that six repeating units make one helical turn. The oligomer was disordered in chloroform and folded in ethyl acetate.

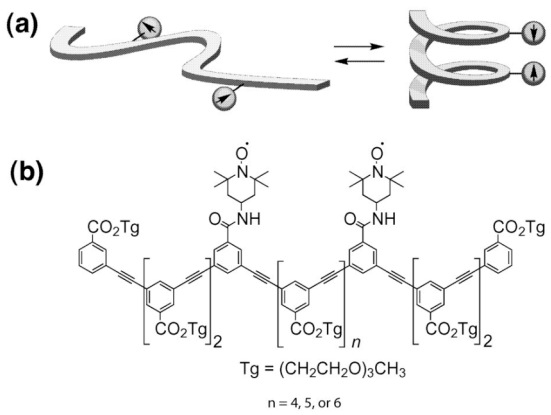

Figure 6: (a) Schematic diagram illustrating a doubly spin labeled phenylene ethynylene oligomer in the unfolded and helical conformation. (b) A representative Chemical structure of an oligomer.

1.3 Aggregation of Conjugated Helical Molecules

In 1903, Meisenheimer and Witte prepared the first synthetic helical molecule (termed a helicene) via *ortho* fusion of aromatic rings. The interest in these compounds did not garner widespread interest until almost a hundred years later, when Newman noted the chirality of helicenes and Lednicer synthesized the fist nonracemic variants.[30] Nevertheless, almost no applications were found for helicenes, even though their helical structures endow useful physical and chemical properties.

In the past Katz and coworkers have changed the outlook for helicenes. By combining bis enol ethers of aromatic species with *p*-benzoquinone, they have provided a large quantity of helicenes with five to eight fused carbocyclic and

heterocyclic rings. Like planar aromatic compounds surrounded by alkyl chains, helicenes also stack into long columns in both liquid, and solid phase. Unlike the columnar discotic liquid crystal phases formed by planar aromatic species, nonracemic helicene (when dissolved in saturated hydrocarbon solvents), assembles into helical columns within which the molecules appear to be stacked along their helical axis, as shown in **Figure 7**. In the pure material, the columnar assemblies are further ordered to long, micrometer-wide lamellar fibers. Analysis by electron and X-ray diffraction, electron and polarized light microscopy, as well as atomic force microscopy shows the fibers organized in parallel columns. In dodecane solutions of sufficient concentration, the molecules aggregate and the assembly into columns is apparent by circular dichroism (CD) and ultraviolet-visible (UV-vis) absorptions. Katz as well as other groups have since made significant contributions to furthering the understanding of helicene synthesis, functionalization of helicenes, and application.[31]

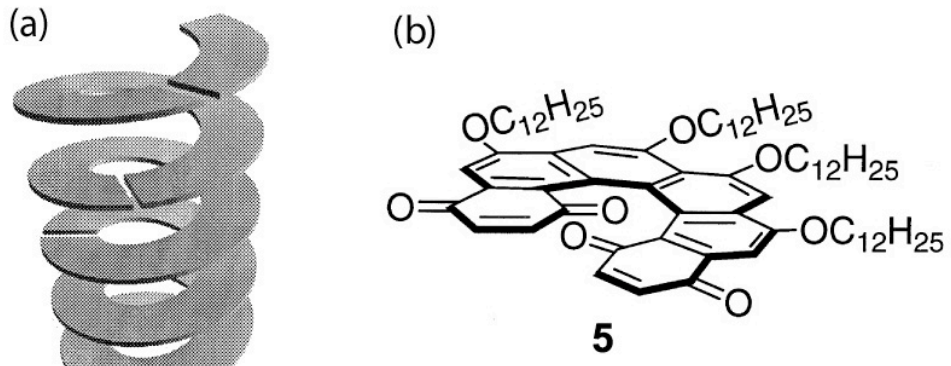

Figure 7: (a) Schematic representation of helicenes stacked into long columns. (b) Nonracemic helicene (**5**) synthesized by Katz el. al.

1.4 Helically Annelated and Cross-Conjugated β-Oligothiophenes

Oligothiophenes are among the most studied π-systems for organic materials, and show application as active components in electronic or optical devices.[32] The focus has primarily been on α-oligothiophenes, such as α-sexithiophene (**6**) (**Figure 8)**, that have thiophene rings connected with single carbon-carbon bonds at the α-position, forming a linearly extended conjugated π-system. Annelated α-oligothiophenes, such as pentathienoacene (**9**) (**Figure 8**), have also been reported. In 2000[33], Rajca and coworkers reported the synthesis and characterization of a novel oligothiophene, in which the thiophene rings are annelated into a [7]helicene (**10**) (**Figure 8**) with a cross-conjugated π-system.

[7]Helicene may be viewed as a fragment of the unprecedented carbon sulfur $(C_2S)_n$ helix, having a sulfur rich molecular periphery.

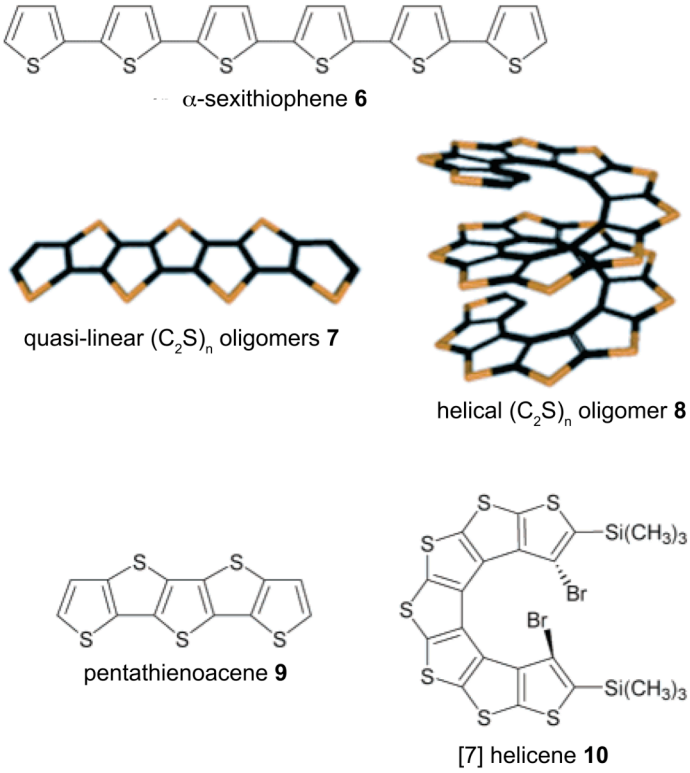

Figure 8: Oligothiophenes: α-sexithiophene (**6**), annelated carbon-sulfur $(C_2S)_n$ oligomers that are quasi-linear (**7**) and helical (**8**), pentathienoacene (**9**), and [7]helicene (**10**).

Racemic synthesis of [7]helicene is based upon iterative alternation of two steps: carbon-carbon homocoupling between the β-positions of thiophenes and annelation between the α-positions of thiophenes. Asymmetric synthesis is carried out using (-)sparteine-mediated annelation of the axially chiral bis(aryllithium) with an electrophilic sulfur equivalent. [7]helicene was characterized by X-ray crystallography as well as physicochemical studies.[34] In 2005,[35] Rajca and coworkers reported the asymmetric synthesis of [11]helicene

(**11**), **Figure 9**. The X-ray crystal structure of [11]helicene showed that the molecule is helical and posses an approximate two fold symmetry.

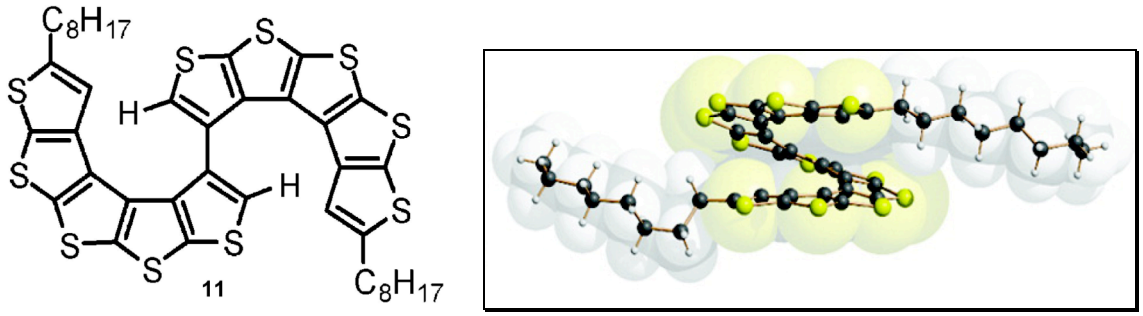

Figure 9: Chemical structure of [11]helicene (**11)** and its helical representation.

1.5 The Chemistry of Oligomers

A goal of synthetic polymer chemists is to generate high molecular weight tyligomers (a structure consisting of folding parts) with discrete chain lengths and primary sequences. Chemists are restricted in preparing high molecular weight substances in pure, monodisperse form, limiting the size of oligomers. Even with oligomers the synthetic challenges are significant. Three synthetic methods to heteromeric chain molecules have been developed; step-by-step, iterative, and polymeric growth.

Step-by-step growth is the lengthening of a chain by adding one monomer at a time. This allows for high sequence control, but the chain growth is slow.[36]

Iterative approach allows for a more rapid chain extension, specially through split pool divergent or convergent methods, while imposing some limits on sequence control. For example, dimer A-B can be coupled to a tetramer, A-B-A-B, which doubles the chain length but limits the variability.[37] The last approach, polymeric growth, offers rapid but statistical chain expansion to a heteropolymeric mixture with little control over length or sequence, which is why it has been avoided for the generation of foldamers. Adjustments have been made to narrow chain length distribution; but a consistent approach for heteromeric tyligomers has not been found. Use of this method has also been avoided due to difficulties with separation and purification of polymers.[36]

Chapter 2

α, β Oligothiophenes

2.1 Thiophene Chemistry

Thiophene, C_4H_4S, is a sulfur-containing heterocyclic [5]annulene (**Figure 10a**). Thiophene is aromatic, although theoretical calculations suggest that the degree of aromaticity is less than that of benzene. The electron pairs on sulfur are significantly delocalized within π-electron system (**Figure 10b**). As a consequence of its aromaticity, thiophene does not exhibit the properties seen for conventional thioethers. For example, the sulfur atom resists alkylation and oxidation.

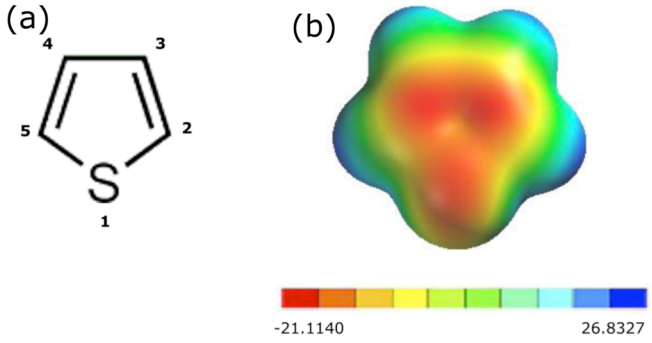

Figure 10: (a) Molecular structure of thiophene, (b) Molecular electrostatic potential map of thiophene.

The thiophene ring has two synthetic attributes that are highly desirable. First, the thiophene ring has two pairs of reactive sites for carbon-carbon bond formation, with each pair having unique chemical reactivity. In general, the 2- and 5-positions (α-positions) are more reactive than the 3- and 4-positions (β-positions) with respect to electrophilic aromatic substitution, Grignard formation

of the corresponding halothiophenes, thienyl lithium formation[38], and cross-coupling reactivity. Second, thiophyne is rarely observed under conditions that would otherwise convert *ortho*-substituted benzene to benzyne. The selective bromination at α-positions, and lithium-halogen exchange occurring exclusively at the 2-position of 2,3-dibromothiophene (without thiophyne formation[39]) are key transformations in many of our synthetic strategies (**Figure 11**) .[40-46]

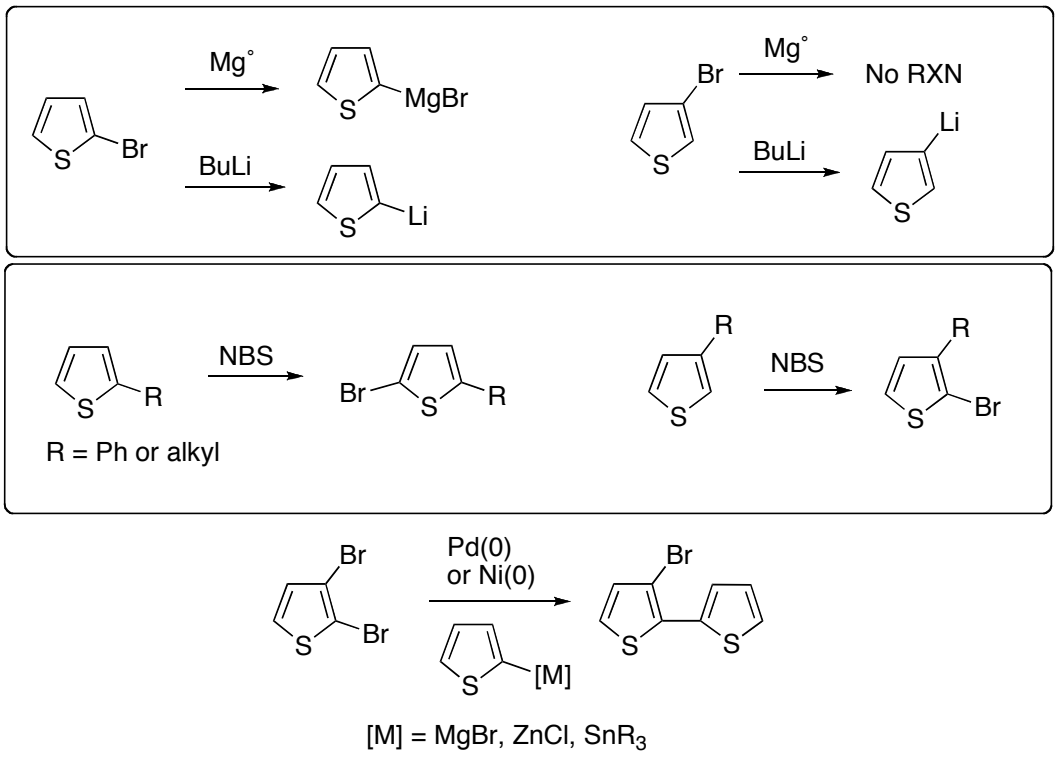

Figure 11: Reactivity of 2 vs 3 position of the thiophene ring. Thiophene is well-suited for iterative 2,3-coupling.

2.2 Previous Work

A prototypical example of conjugated helical oligomers, [1,1',2',1'',2'',1''']quaterphenyl (**12**), is shown in **Figure 12**, where single and double bonds are alternating and the molecule is helical. Helical oligomers and polymers are classified as either conformationally rigid, such as helicenes[47], or conformationally flexible, as polyisocyanates.[48] In the case of the conformationally flexible backbone, it is required that an external or internal force bias the conformational dynamics of the molecule to prefer a helical conformation over all other possibilities.[1]

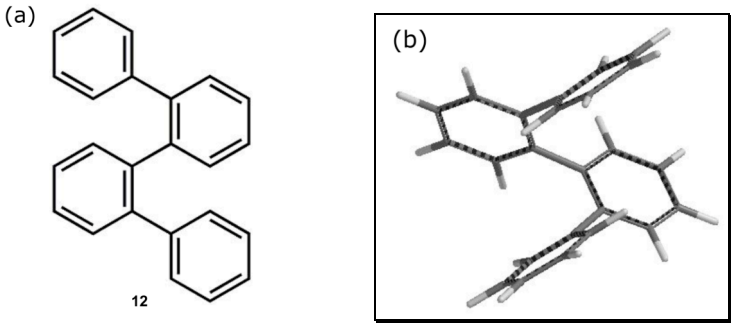

Figure 12: An example of conjugated helical oligomer (a) chemical structure of *ortho*-quaterphenyl (**12)**, (b) minimized representation.

Traditionally, oligothiophenes have a 2,5-connectivitiy at the thiophene rings. This type of connectivity creates a planar conducting polymer. There are two types of conformations for these polymers; the linear s-*trans* conformation, and the coiled s-*cis* conformation. The s-*cis* conformation is not a reliable helical

scaffold as there is no driving force for coiling. It takes thirteen thiophene rings to make one turn of the helix and the energy cost is approximately 13 kcal per mol higher than the all s-*trans* conformation (**Figure 13**).

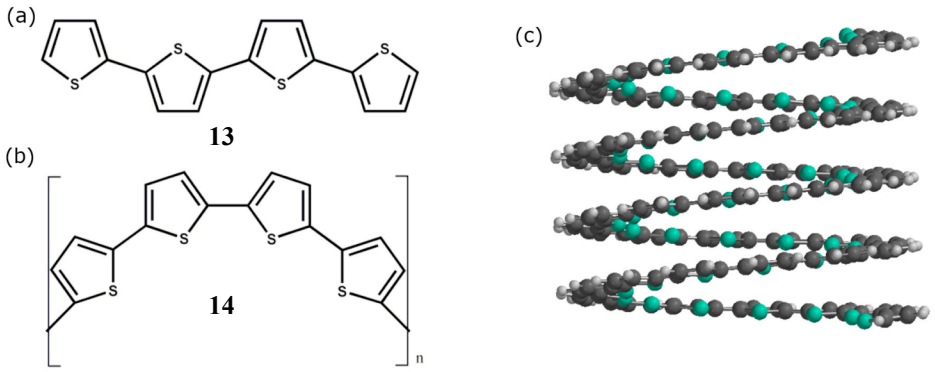

Figure 13: Oligothiophenes with 2,5-connectivity: (a)Linear (**13**) (b) Coil (**14**) (c) Helical representation.

In 1988, the X-ray crystal structure of [3, 3', 2', 2'', 3'', 3'''']-quaterthiophene (**15**) was reported.[49] The molecule, being the first to have this type of connectivity, had a partial helical structure composed of three isomorphic conformers due to sulfur-carbon (S-C) disorder in the two terminal thiophenes (**Figure 14**).

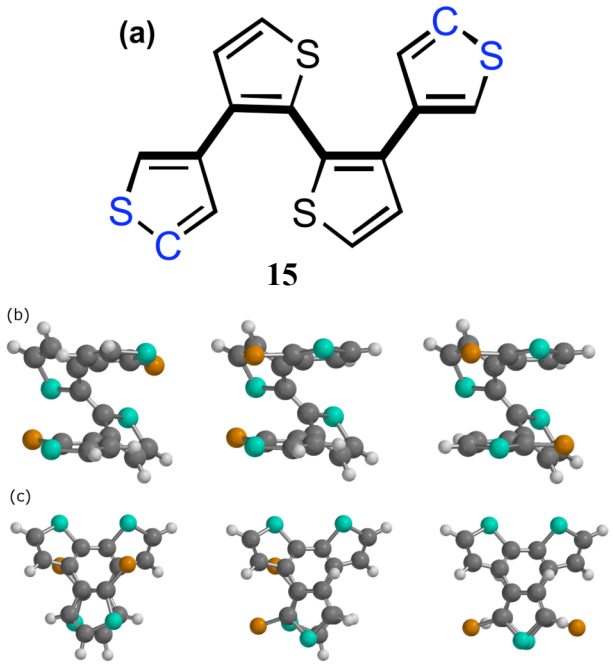

Figure 14: Structure of (a) quaterthiophene, (**15**) and its three isomorphic conformers outlined by the orange atom ((b) side view). Looking at (c), the view down the helix, the isomorphic behavior is seen by the position of the sulfur atoms: right and left, left and down, and both down.

Our group reported the synthesis of hexachlorohexa(2,3-thienylene) in 2001.[41] In this synthesis the cyclization step occurs via an intermediate hexamer similar to the tetramer mentioned above (**Figure 15**). Up to this point, there had been no reports of oligothiophenes with the [3, 3'; 2, 2'] connectivity.

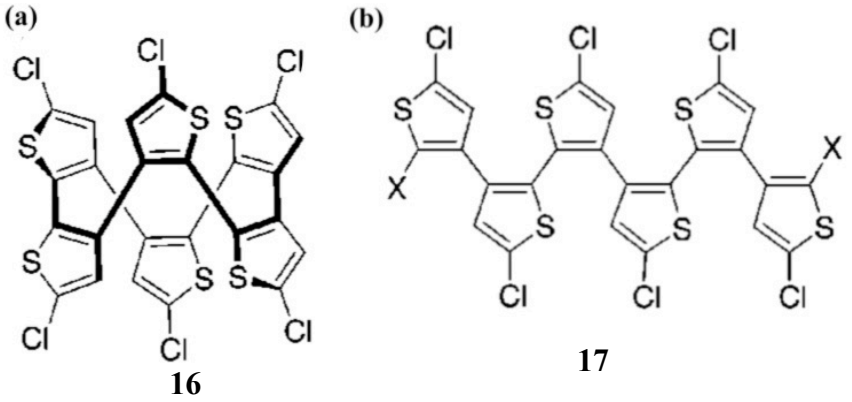

Figure 15: (a) Chemical structure of hexachlorohexa(2,3-thienylene) (**16**). (b) Intermediate hexamer (**17**).

In an effort to elucidate molecular structure as a function of variable substituents at the termini of the hexamer, our group reported the design, synthesis, crystal structure, and computational analysis of sexi(2,3-thienylene) (**17**).[44] Compounds **17a-c** were synthesized and compounds **17d-i** were analyzed by theoretical calculations (**Figure 16**).

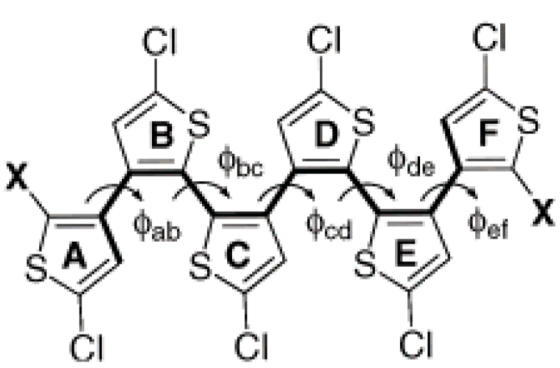

17a: X = H
17b: X = Cl
17c: X = Br
17d: X = I
17e: X = Me
17f: X = Et
17g: X = t-Bu
17h: X = Ph
17i: Cl = X = H

Figure 16: Chemical structure of sexi(2,3-thienylene) (**17**).

X-ray crystal structures of compounds **17a**, **17b**, and **17c** revealed that all three compounds have a nearly identical helical conformation, as illustrated by the superimposition of the three X-ray structures shown in **Figure 17a**. For each structure, no S-C disorder is observed in the terminal rings of the hexamer. Substituents (X) are oriented in the same relative direction. The X-ray crystal structure of compound **17a** was also compared to the computational analysis of the hexamer at both Merck molecular force field (MMFF)[50] level of theory and Becke's exchange functional and the gradient-corrected functional of Lee, Yang and Parr (BYLP) 6-31G(d)[50] level of theory. As illustrated by the overlay in **Figure 17b**, the helical orientation of the backbone is unaffected by either substituents' composition or orientation.

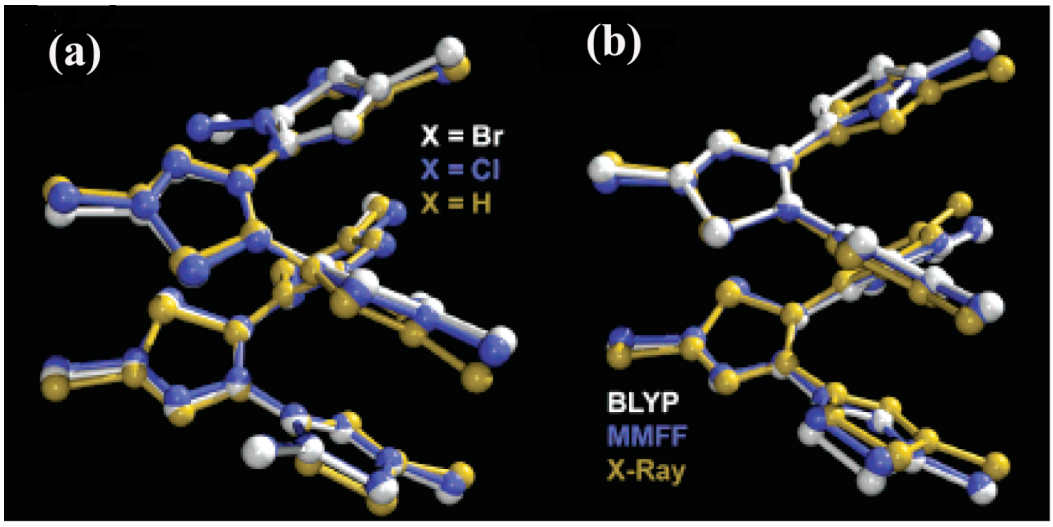

Figure 17: (a) Overlay of the three X-ray structure corresponding to **17a**, **17b**, and **17c**. (b) Overlay of **17a** as X-ray crystal structure and as MMFF and BLYP/6-31G(d) minimized structures.

To prove that the hexamers adopt a helical structure due to torsional strain, energy profiles corresponding to complete rotation about the three unique backbone dihedral angles of compound **17a** were calculated. The results were overlaid onto a single plot to yield a distinct energy well that coincides with the average of all experimentally determined dihedral angles (**Figure 18**), thus indicating that torsional strains cause the hexamer to form a helix.

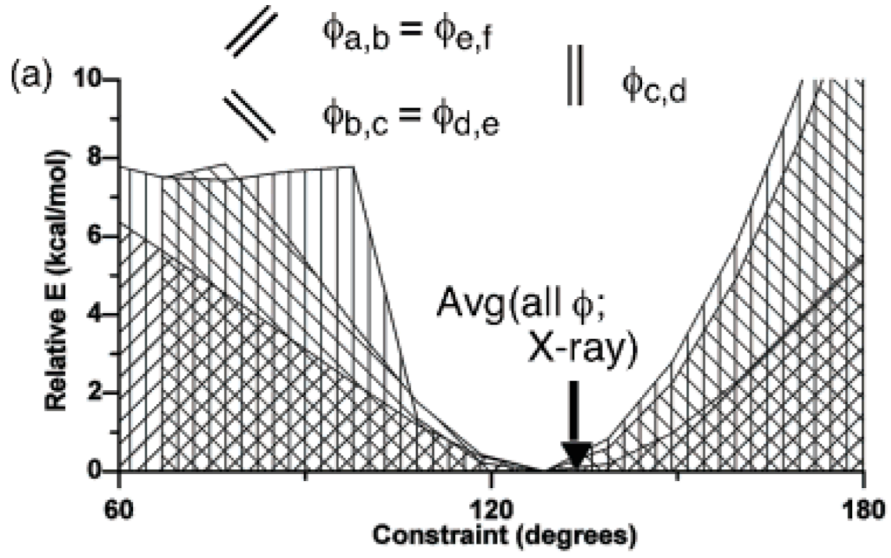

Figure 18: Graph of energy profile (MMFF) corresponding to constraints applied to the three symmetrically unique dihedral angles of compound **17a** (C_2 Symmetry). The arrow corresponds to the average of all five backbone dihedral angles ($\phi_{ab\text{-}ef}$) observed in the X-ray crystal structure of compound **17a** (C_1 symmetry).

Chapter 3

Molecular Springs

3.1 Introduction

A molecular spring is a device typically composed of coiled material, capable of being stretched (tension springs) and/or compressed (compression springs). For metal springs, a simple atomistic description states that atomic interactions are displaced from an equilibrium state when a force is applied, thus accessing a higher-energy state. A spring's restoring force is the return to the equilibrium. This is true of both coiled and non-coiled springs, such as leaf springs and spiral springs.

Given the above description, one could define almost any conformationally flexible molecule as a spring.[51] For example, consider a force applied to a molecule such that bond lengths, bond angles, and/or dihedral angles are perturbed from equilibrium, thus raising the energy of the molecule. Once the force is released, the molecule will return to its equilibrium conformation (that is, assuming a transition state between conformers is not reached in the process). Although most molecules can fit this definition to some extent, fewer satisfy the requirements of maximizing extension (or compression) within a deep-well global minimum. For example, conversion of a hydrocarbon from an all s-*trans* to all s-*cis* conformation would be analogous to compression. The energy barriers that lead to other conformers are easily overcome, thereby negating the concept of a restoring force. In other terms, the path between s-*trans* and s-*cis* does not exist

in a sufficiently deep energy well on the potential energy surface to avoid diversion to other conformations. **Figure 19** illustrates the analogy between spring function and bond rotation, using bithiophene as the example molecule. Oligothiophenes will serve as the basis of our molecular spring. Requirements for our molecular spring include both a helical and conjugated backbone.

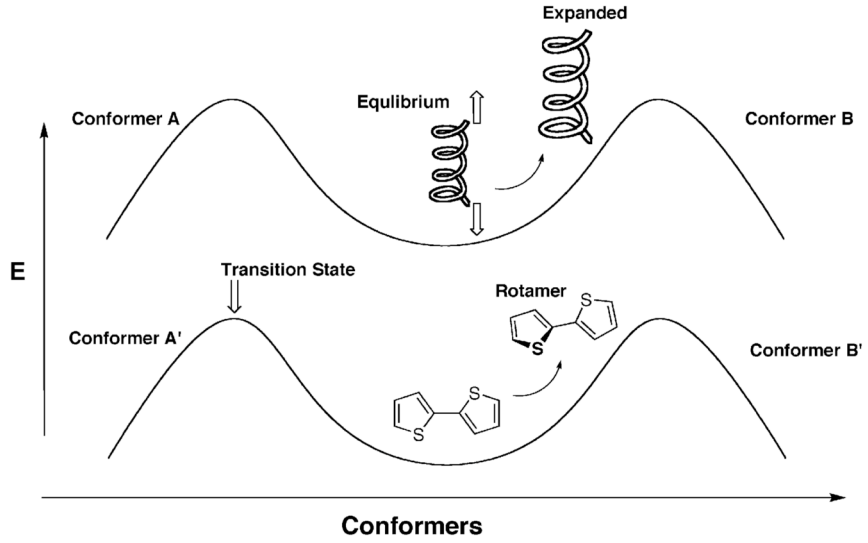

Figure 19: Showing the reversible behavior of macroscopic springs and molecules (bithiophene), as they are physically displaced from equilibrium geometry. As long as the displacement corresponds to energy less than the transition state boundaries, the perturbation will be reversible.

Polythiophenes that are entirely α-fused will not be the best candidates for helical polymers. *Ortho*-oligothiophenes (α,β-oligothiophenes), however, have proved otherwise.[52] The sterics associated with this regioisomer preclude the co-planarity of adjacent thiophene rings. Based on computational analysis (MMFF), the conformer search for these molecules demonstrate a compact helix at the

global minimum energy. The next highest energy conformer (ca. 0.8-2.2 kcal per mol) is and extended helix. (**Figure 20**).

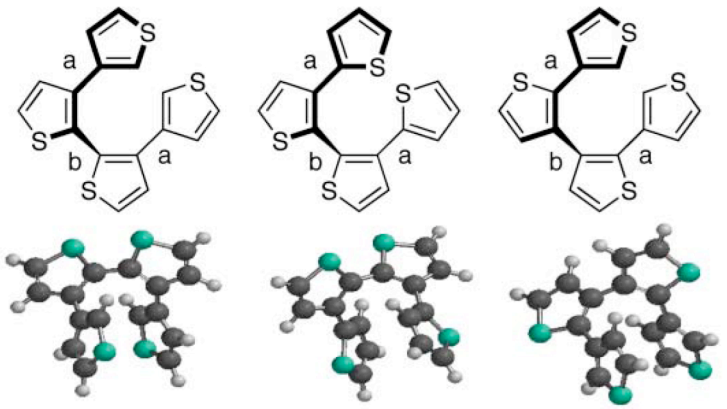

compact helix			
dihedral a:	46.6°	41.6°	41.2°
dihedral b:	58.6°	59.9°	58.1°
extended helix			
ΔE (kcal/mol):	1.9	2.2	0.8
dihedral a:	43.0°	41.2°	36.5°
dihedral b:	115.8°	110.6°	119.1°

Figure 20: Showing three α, β-tetrathiophene oligomers, and reporting dihedral angles for both the global minimum structure (compact helix; also shown as ball and stick structures), and higher energy extended helix conformer. The energy difference between compact and extended helix is also given. All values were determined from MMFF conformer searches.

3.2 Results and Discussion

We have synthesized conjugated helical oligomers with dipole moments, which will compress or elongate while placed in an external electrical field. Based on molecular modeling, the head-to-tail oligothiophene regioisomer (**18**) produces a larger dipole moment than the head-to-head regioisomers (**19**) (**Figure 21**). Computational studies have also shown that the alignment of the dipole along the

molecular axis depends on the number of thiophene rings in the helix. The shortest oligothiophene to produce a dipole that parallels the long molecular axis is a trimer. The trimer may then be end-capped with phenyl groups to create a helical pentamer; the phenyl groups extend the helix without affecting the dipole.

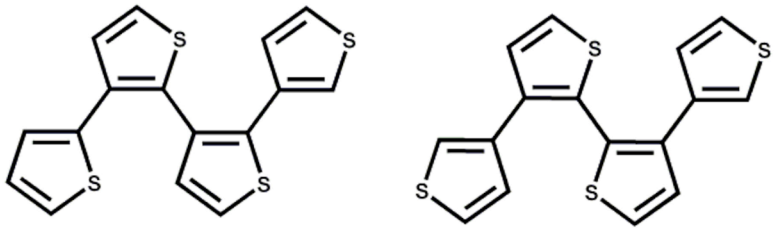

Head-to-Tail
18

Head-to-Head
19

Figure 21: Structures of Head-to-tail (**18**) and Head-to-head (**19**) oligothiophenes.

Calculations have shown that the dipole of the compressed helix (0.55 debye) is less than the dipole of the elongated helix (0.95 debye), as shown in **Figure 22**. It is predicted that applying a variable electric field to this system will then drive this compression-elongation actuation cycle.

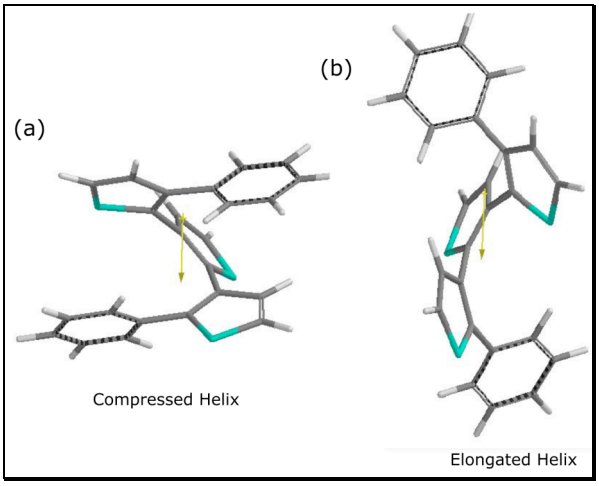

Figure 22: (a) Compressed helix with a dipole of 0.55 debye, (b) Elongated helix with a dipole of 0.95 debye. Dipole moments were obtained from Spartan 04[50], HF/3-21G(d).

The synthesis of α, β-oligothiophenes is facilitated by the reactivity of the α- and β-thienyl positions (as discussed in section 2.1). In general, biaryls and triaryls are prepared by nickel-catalyzed cross-coupling chemistry,[53] and halogenation is used to direct lithiation (via lithium–halogen exchange). The resultant organolithium species can be used as the nucleophile for a double addition–elimination with octafluorocyclopentene[54], or oxidatively coupled using Fe(III).

Scheme 1 provides the detailed synthesis of the one of the target molecules, helical pentamer **21**. As shown in the subsequent X-ray crystal structure (**Figure 23**), an unexpected rearrangement had taken place between the second and third thiophene rings. These two rings have rearranged from 2,3' to 2,2' linked thiophene bonds. The rearranged pentamer **21** gave a 41% yield.

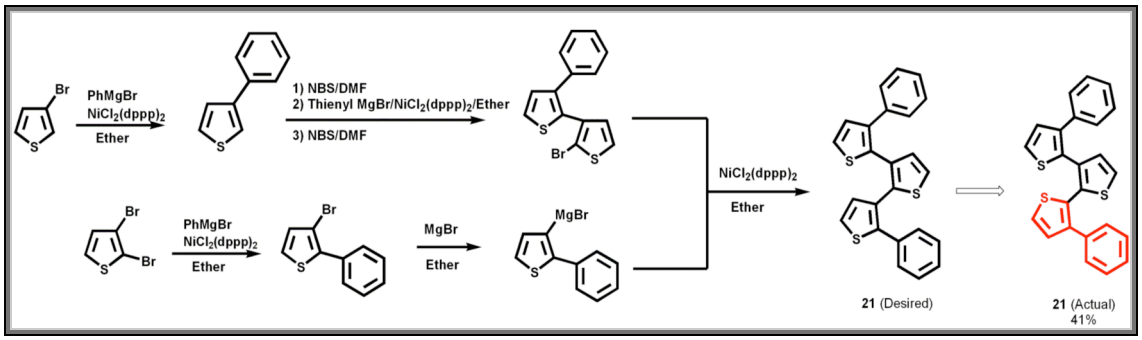

Scheme 1: Synthesis of helical pentamer **21**.

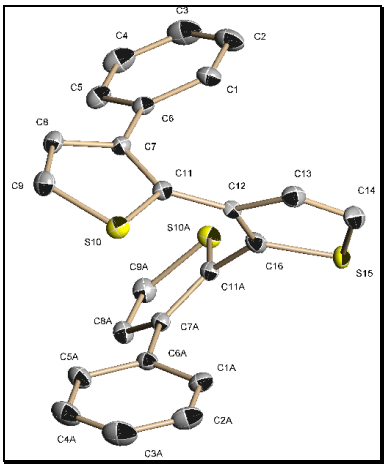

Figure 23: X-ray crystal structure of Pentamer **21**, revealing the rearrangement of the third thiophene ring from a 2,3' (α,β') to 2,2' (α,α') connectivity.

Based on previous studies done by Scott and coworkers[55-58], it was assumed that the rearrangement was the result of a spontaneous halide radical cleavage or a proton transfer. Therefore, a series of computational studies were performed on the trimer to explain the rearrangement observed in the X-ray crystal structure of pentamer **21**. Using Gaussian 03[59], density functional theory (DFT) at B3LYP 6-31G(d) level of theory, equilibrium geometry and transition states for the trimer were computed. Unfortunately, the movement of a radical

from optimized structures to the corresponding transition state does not account for the rearrangement observed in the X-ray structure of pentamer **21**. In fact, the computed energies for intermediate structures gave a high-energy pathway, which ruled out the possibility of radical mediated rearrangement.

Further investigation revealed that this rearrangement took place after the synthesis of 2-phenyl-3-bromothiophene (**20**), which when exposed to light converts to 2-bromo-3-phenylthiophen. It is interesting to note that, based on our calculations using Hartree-Fock (HF) 3-21G(d) level of theory, 2-phenyl-3-bromothiophene is lower in energy by 3.46 kcal per mol compared to 2-bromo-3-phenylthiophene. This type of rearrangement has been reported in literature by Wynberg[60-62] and coworkers. In their study valence bond isomerization reactions are proposed to account for the rearrangement results. **Figure 24** illustrates the details of their mechanism. Another study proposes that it undergoes a dewar thiophene, where the sulfur atom assists in a [1,3]shift to get the rearranged product (**Figure 25a**).[63] Yet another study proposes that the sulfur atom sits above the ring assisting in the rearrangement (**Figure 25b**). Although all of these mechanisms have been proposed, to date there has been no evidence to disprove their existence.[63]

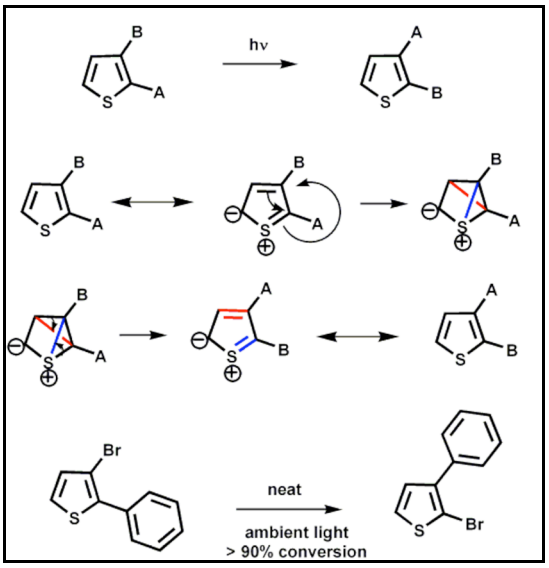

Figure 24: Proposed mechanism for rearrangement of 2-phenyl-3-bromothiophene to 2-bromo-3-phenylthiophene.

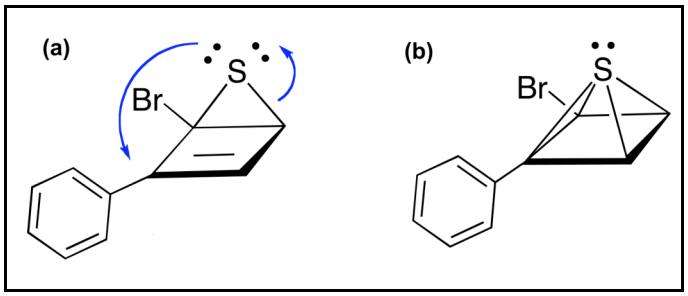

Figure 25: Proposed mechanism for thiophene rearrangement via **(a)** a dewar thiophene, and **(b)** sulfur atom above the ring methods.

The second strategy utilized iron (III) acetylacetone ($Fe(acac)_3$) as an oxidant to directly couple two equivalents of oligoaryl lithium, a homocoupling approach, as illustrated in **Scheme 2**. Consistent with previous observations, the lowest energy structure returned from MMFF conformer searches predicts the crystal structure of the molecular helix, hexamer **22**. Although the synthesis was successful, the yield was low at 44%.

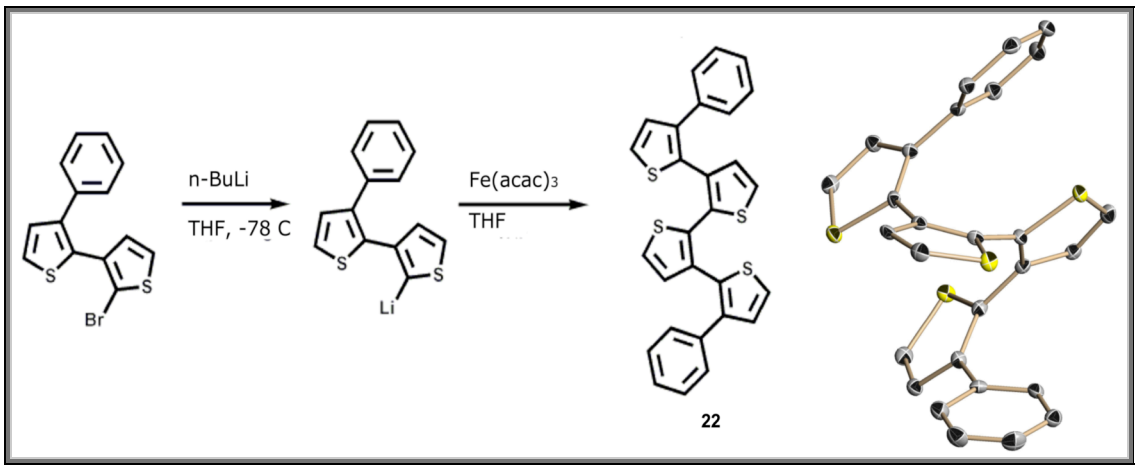

Scheme 2: Synthesis and X-ray crystal structure of helical hexamer **22**.

A new synthetic approach was necessary due to the poor yields and the unexpected rearrangements. To circumvent these problems, we aimed to limit "non-activated" cross-coupling chemistry to the synthesis of bi- and terthiophenes. Higher oligomers were achieved by coupling dimeric or trimeric systems with reactive, electron-deficient rings ("activated" coupling). Specifically, we utilized octafluorocyclopentene as the cornerstone that joins two partially helical oligoarene hemispheres. The concept of two hemispheres of short oligomers (n-mers) connecting at a single, activated "equator" ring system to yield a 2n+1-mer is illustrated in **Figure 26**. Unlike larger helical fragments, the synthesis of [n]ortho-arylenes (n=2 [biaryl], n=3 [teraryl]) remains within the limits of reliable cross-coupling methodology. Thus, the addition reaction between two

equivalents of [n]ortho-aryllithium and one equivalent of octafluorocyclopentene yields a helix with 2n+1 –HC=CH- backbone moieties.

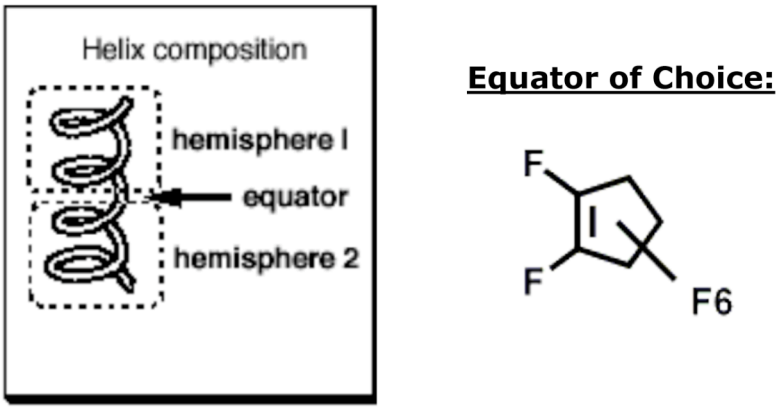

Figure 26: Illustrates “hemispheres” and active “equator” approach to helical oligothiophenes.

Three helical molecules were synthesized via this approach, as outlined in **Scheme 3**. For compounds **23** and **24** the compact helical conformation observed in the single crystal X-ray structural analysis was predicted by MMFF calculations of the equilibrium conformer. Compounds **23** and **24** were obtained in 60 and 62% yield, respectively. Compound **25**, regrettably, displayed another unexpected rearrangement. Its X-ray crystal structure showed that the trimer hemispheres had rearranged to give the non-helical structure. It is believed that this rearrangement was due to an exchanged between the kinetic and thermodynamic intermediate shown in **Figure 27**.

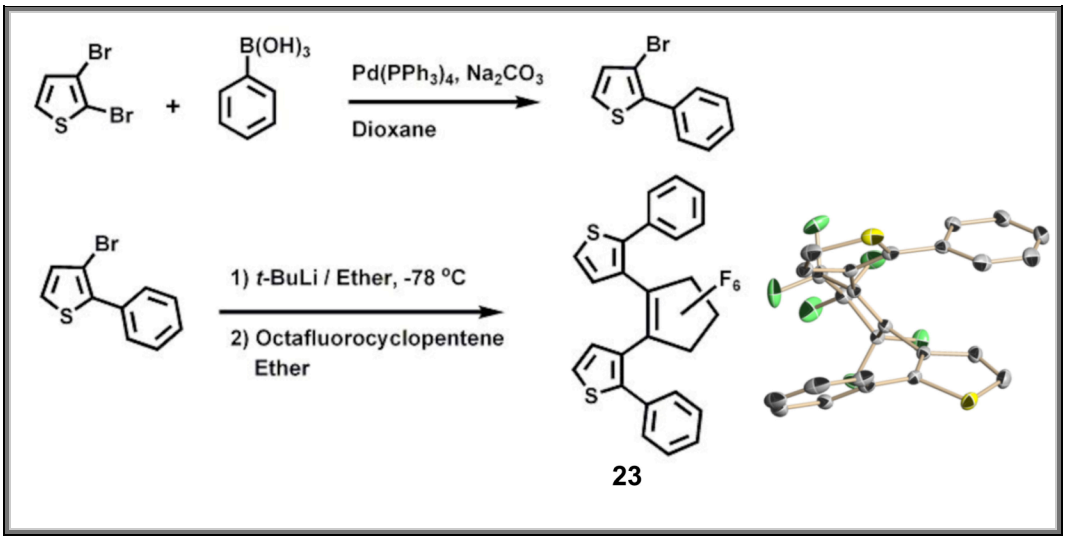

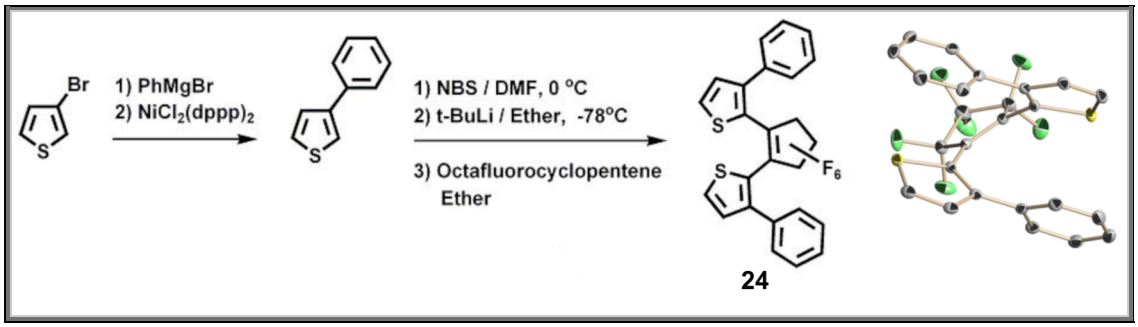

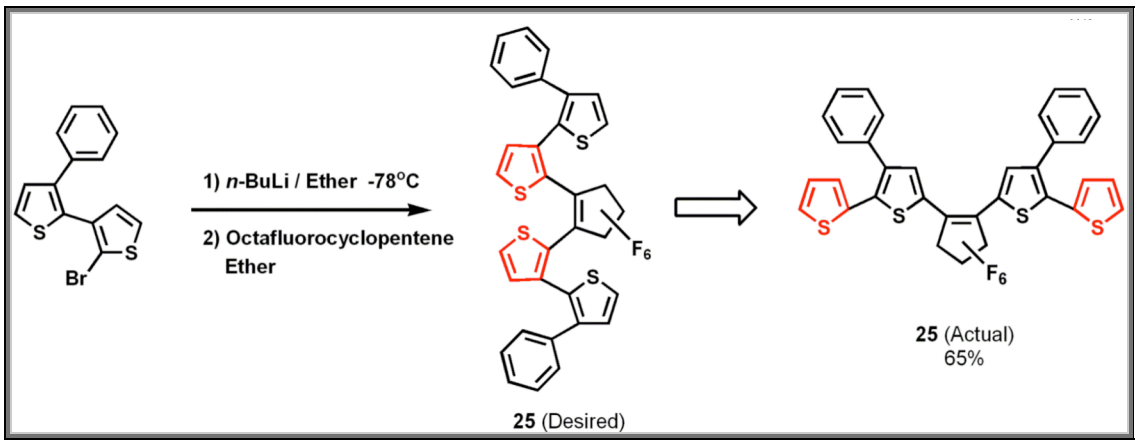

Scheme 3: Synthesis of helical pentamers **23**, **24**, and heptamer **25**, respectively. X-ray crystal structures for pentamers **23** and **24** are shown.

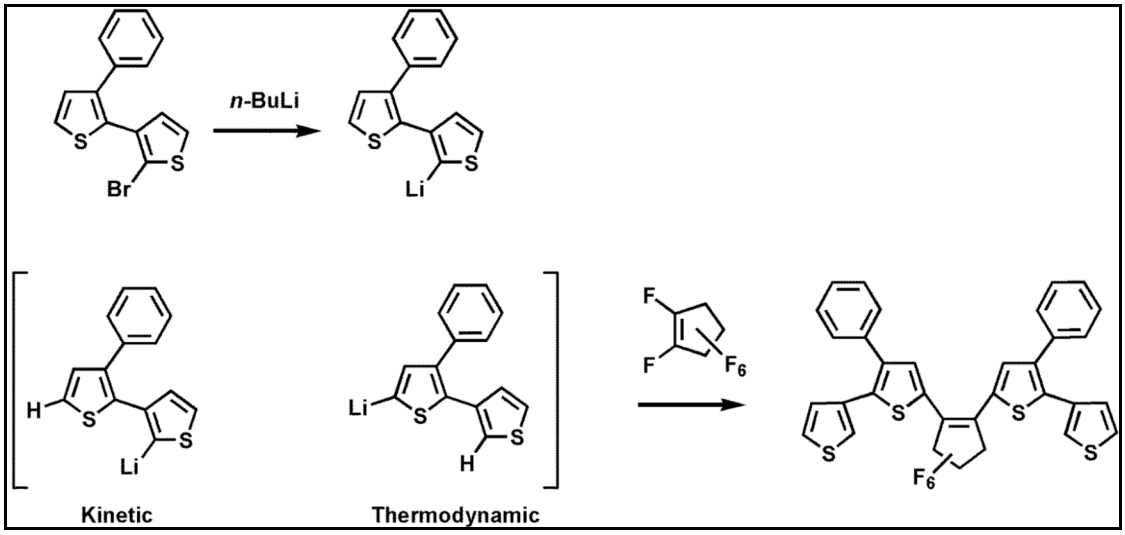

Figure 27: Rearrangement of the heptamer via an exchange between the kinetic and thermodynamic intermediate.

In order to have our helical compounds tested by scanning tunneling microscopy (STM), one or both ends of the helix needed to be functionalized. Attempts were made to incorporate amines onto the ends of these helical compounds, one example is shown in **Scheme 4**. Unfortunately the intended product was never isolated.

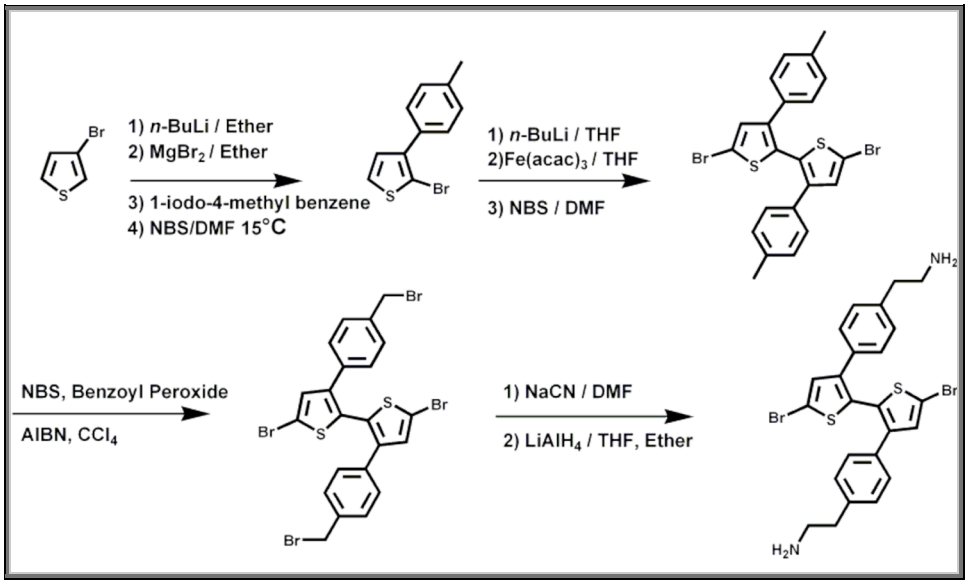

Scheme 4: Attempted synthesis for placing amines at the termini of a helical tetramer.

3.3 Helical Spring as a Molecular Muscles

We have previously published work on thiophene-fused [8]annulenes[43] which can act as "molecular muscles" capable of expansion and contraction under an electrical bias. Each unit of the polymer is defined as an "actuator synthon", capable of lengthening and contraction as a function of redox state. The polymer mimics a bellows, whereby each [8]annulene monomer is one convolution of the bellows and the pitch of each convolution changes as a function of oxidation state.

We propose our molecular spring as an actuator. Our molecular spring is a conjugated helix, with the possibility of p-orbital interactions not only in a side-on sense between adjacent rings, but also in a head-on sense between adjacent turns of the helix. Calculation predicted that upon oxidation or reduction, such a helix would contract from its equilibrium neutral conformer length. We predict that the contraction process is driven by increased orbital interaction, thus best delocalizing the charge. **Figure 28** illustrates this concept, showing (a) neutral redox state (non-ideal overlap of adjacent orbitals), and (b) charged redox state (improved side-on and head-to-head orbital interactions).

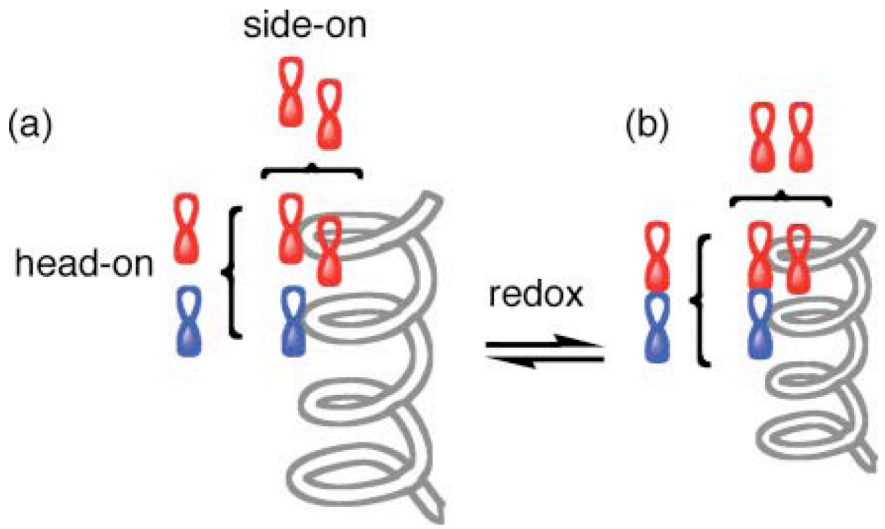

Figure 28: Showing (a) equilibrium conformer of a conjugated helix, and (b) contracted form of the same helix, as a result of oxidation or reduction. The red–red orbital interaction represents side-on overlap, and the red–blue orbital interaction represents head-to-head overlap. Contraction (form b) is believed to increase both types of overlap.

One example of head-on orbital interactions was shown by Stahl and coworkers in 2002[64]. In this report, neutral in-plane tris-homoaromaticity is evaluated in tris(bismethano)benzene in which the p-orbitals interact in the plane established

by the unsaturated carbon atoms. The six overlapping p-orbitals lie in-plane (head-on) as opposed to the orthogonally layout seen in benzene molecules, as shown in **Figure 29**. It was determined that such in-plane conjugation possesses more than one third the aromatic stabilization energy of benzene, thus constituting the best candidate yet proposed for neutral tri-homoaromatic compounds.

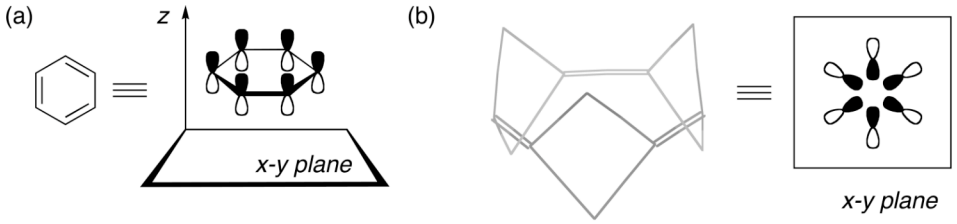

Figure 29: (a) Benzene p-orbitals are orthogonal to x-y plane (b) tris(bismethano)benzene, six p-orbitals lie in-plane (head-on).

To test this theory, we geometry optimized both compounds **Hex-26** and **Hex-26^{2+}** (HF 6–31G(d)). **Figure 30a** shows the three unique bonds (labeled **a**, **b**, and **c**) associated with the three unique dihedral angles for the given helical hexamer. In the neutral form, the calculated bond lengths range from (a) 1.475 Å, (b) 1.48 Å, and (c) 1.476 Å. The corresponding dihedral angles are (a) 63.6° and (b = c) *ca.* 46°.

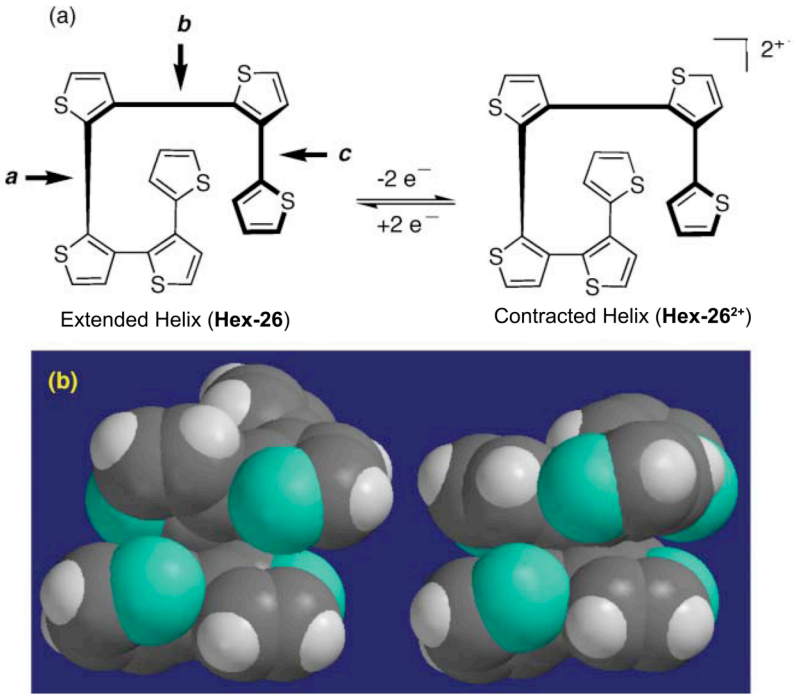

Figure 30: (a) Defining the bonds in **Hex-26** (b) Space filling models of **Hex-26** (left, extended form) and **Hex-26^{2+}** (right, contracted form).

The equilibrium geometry of **Hex-26^{2+}** reports the desired contraction. Bond ***a*** develops considerable double bond character, with its length decreasing from 1.775 Å to 1.339 Å. The corresponding dihedral angle is reduced from 63.6° to 5.3°. The dihedral angles associated with bonds ***b*** and ***c*** also decrease in value from 46° to 37.5°. Summing the NBO[65-70] atomic charges for each ring reveals that *ca.* 50% of the 2^+ charge is localized onto the central bithiophene unit. The closest carbon–carbon atomic contact in **Hex-26^{2+}**, reflecting the head-to-head orbital interaction discussed above, is 3.42 Å. In the neutral form, this same distance is 3.64 Å. In accord with prediction, contraction and oxidation are commensurate, and reinforce the ability of helical oligoarenes to function as

molecular muscles. This contraction can be viewed in **Figure 30b**, which shows space-filling models of **Hex-26** and **Hex-26**$^{2+}$.

3.4 Helical Springs as Molecular Rheostats

A rheostat can be defined as a variable resistor that is attenuated by a mechanical process. In our design, the macroscopic process of "turning a knob" to attenuate resistance (and hence current), is mimicked at the molecular level by stretching a conjugated helix. Specifically, we investigated the possibility of integrating STM experiments with helical oligomers, as a route into force-attenuated conductivity (i.e., a molecular rheostat).

STM experiments have been reported to yield reproducible measurements of single-molecule conductivity.[71] Nuckolls et al. showed that single molecule conductivity of terminal aliphatic and aromatic diamines could be reproducibly measured by STM.

By adsorbing one amine terminus onto a gold surface and the other onto the STM tip, conductance was measured as a function of tip–surface distance until either end was desorbed. The choice of amino functionality in the experiments was vital due to the single coordination geometry that exists between amine nitrogens and a gold surface. Amines only add to unsaturated gold sites, the so-

called “ad-atoms,” via donation of the nitrogen lone- pair to a vacant gold orbital in a well-defined geometry. More commonly employed functional groups, such as thiols, add in multiple geometries. This, combined with the consideration that amines are not subject to oxidative oligomerizations, leads to consistent conductivity curves for a given substrate over many cycles. It was found that clear conductance data could be obtained for aliphatic substrates as large as 1,8-octanediamine, and that minimal steric bulk about the nitrogen led to the most well defined conductance.

It is important to highlight that accurate measurements of single-molecule conductivity may be obtained via STM, with simultaneous physical “pulling” on the molecule. The assumption is that the STM tip may serve both as the mechanical element of the rheostat, as well as the probe to accurately measure changes in conductance through the extending helix.

In order for our molecular springs to behave like molecular rheostats four characteristics must be met. First, helical oligomers must demonstrate an effective conjugation length that varies as a function of molecular conformation. Second, any changes in conjugation must translate to changes in molecular conductance. Third, the termini of the helix must be functionalized to allow adsorption between metal surface and STM tip ad-atoms. And fourth, using the STM tip to generate mechanical force, the helix must stretch from a compact

helical conformation (dihedral angles less than 90°), to an extended helical conformation (dihedral angles greater than 90°).

Theoretical calculations were done to test our theory. In order to save computational time, we reduced the composition of the helical oligomer to a helical s-*cis*-z-polyene (1,3,5,7,9-decapentene). The length of this helix is a direct function of the dihedral angles between adjacent -HC=CH– moieties of the backbone. In an ideal case, the fully extended system, registering 180º dihedral angles throughout, would experience complete overlap of the π-system, establishing a conjugation maximum.

With one end of the helix fixed in space, a unidirectional external force could be applied such that the helix is pulled from its compact coil conformation to its fully extended state. Appropriately, conjugation would decrease to a minimum as the dihedral angles approach 90°. Further extension would again increase conjugation, as the dihedral angles are stretched beyond 90°. Overall, orbital overlap (effective conjugation length) should respond non-linearly as a function of lengthening from a compact coil to a fully extended state.

We employed outer valence green function (OVGF)[72] calculations to gain ionization potentials (I_p) and electron affinities (E_a), and used these differences in energy as a qualitative predictor of single molecule conductivity. We calculate

the energies of I_p (representing the highest occupied molecular orbital, or HOMO) and E_a (representing the lowest unoccupied molecular orbital, or LUMO), and use this difference as a probe of effective conjugation; the smaller the difference, the greater the effective conjugation, the greater the potential for increased carrier mobility, and the higher the molecular conductivity.

A HF/6–31G(d) OVGF analysis of the C_2-symmetric helical decapentene was performed, whereby C=C–C=C dihedral angles were constrained to values of 30°, 60°, 90°, 120°, 150°, and 180° (corresponding to an extension from compact coil to linear conformer), as shown in **Figure 31**. By definition, these values also report the angle between atomic *p*-orbitals on adjacent ethylene moieties of the polyene. A first-approximation mandates that there are no long-range orbital interactions at the 90° conformer, as all ethylene moieties are oriented such that adjacent *p*-orbitals are orthogonal and non-interacting.

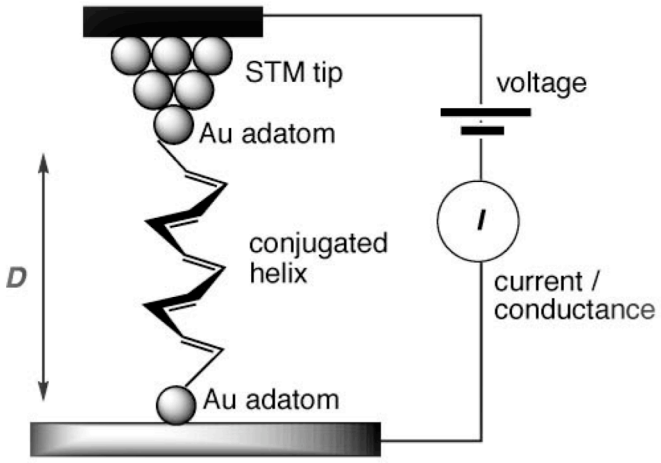

Figure 31: Conceptual illustration of a conjugated helix, in this case the 1,3,5,7,9-decapentene model, adsorbed onto metal surface (gold) and STM tip.

The I_p and E_a determined from OVGF calculations are plotted in **Figure 32**, as change in I_p and E_a relative to the 30° starting point. Note the plot is relative to the 30° dihedral angle conformer versus dihedral angle, and should not be misinterpreted as a crossing of I_p and E_a at *ca.* 150º. The values posted adjacent to data points report the pole strength, which is a measure of probability of each corresponding excitation (maximum value of pole strength is 1.0).

Thus, there are four parameters for each dihedral: ionization potential, electron affinity and the two corresponding values of pole strength. The most striking trend in the OVGF data is the non-linear change of both I_p and E_a, with inflection points occurring at the 90° dihedral conformation. This trend matches our

predictions. Given that π-orbital overlap, I_p, and E_a should qualitatively reflect conductance, it follows that a uniaxial force that extends the molecular helix should be capable of attenuating single-molecule conductance, thus establishing a molecular rheostat.

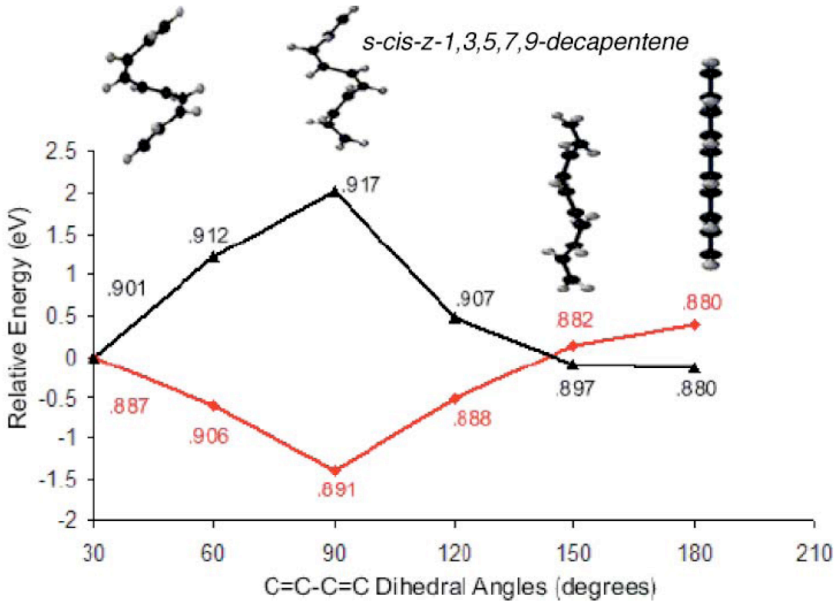

Figure 32: Plot of ionization potential (Ip; red) and electron affinity (Ea; black) as a function of conformation.

3.5 Conclusion

We have established two more synthetic pathways into helical oligoaryls that are predicted (by OVGF calculations) to illustrate a non-linear change in conductance as a function of an external, uniaxial compression and/or elongation force. Building on our previous observations, oligoaryls containing 4, 5, or 6 rings predictably yield helical conformations both theoretically (MMFF) and experimentally (crystallography). It is hoped that future studies will focus on synthetic inclusion of appropriate functional groups for reproducible surface adsorption (amines on gold ad-atoms), and subsequently, STM measurements of force-conductance profiles.

Chapter 4

Molecular Motors

4.1 Introduction

A molecular machine can be defined as an assembly of a discrete number of molecular components (that is, a supramolecular structure) designed to perform a function through the mechanical movements of its components, which occur under appropriate external stimulation.[73] Hence, molecular machines contain a motor part, capable of converting energy into mechanical work. Molecular motors and machines operate via nuclear rearrangements. Like their macroscopic counterparts, molecular motors are characterized by: the kind of energy input supplied to make them work; the manner in which their operation can be monitored; the possibility to repeat the operation at will (i.e., establishing a cyclic process); the time scale needed to complete a cycle of operation; and the performed function. Recently, prototypes of molecular motors and machines have been designed. The extension of the concept of machine to the molecular level is of great interest not only for basic research, but also for the growth of nano-science and the development of nanotechnology. The following sections will discuss remarkable progress made in molecular devices.

4.2 Molecular Gears

Macroscopic scale mechanical gears are used to produce and control rotational movement and create work in numerous mechanical devices, such as transmissions, drive trains, and clocks.[74] Examples of macroscopic mechanical gears are shown in **Figure 33**. There are four major classes of gears: spur gears, bevel gears, worm gears, and spiral (or helical) gears. Spur gears are the simplest and most commonly used in macroscopic machines; they are also the most efficient type of gears, with up to 99% efficiency. They contain two cylindrically-symmetric cogged wheels, with teeth cut parallel to the axis of rotation, and they transmit rotary power between parallel shafts. Bevel gears transmit rotary power to shafts at a 90° angle to one another. Worm gears transmit rotary power between two shafts that lie in different planes. A worm is a screw cut to mesh with the teeth of a worm wheel, which is essentially a spiral spur gear. These gears are known to be least efficient and produce more heat because of friction between the shafts. They are typically used when one shaft needs to turn at a much slower rate than the other. Helical or spiral gears offer a refinement over spur gears. Since the gear is curved, this angling causes the tooth shape to be a segment of a helix. They are used to transmit rotary power between shafts that are in different planes.

Figure 33: The four major classes of macroscopic gearing systems.

At the molecular level rotation around single bonds can serve as the molecular equivalent of axles. The major efforts aimed at synthesizing molecular gears have been focused on triptycene derivatives. Triptycene (Tp) is a rigid molecular unit with three blades each composed of a benzene ring. It represents a molecular mimic of a gearing element, **Figure 34**.

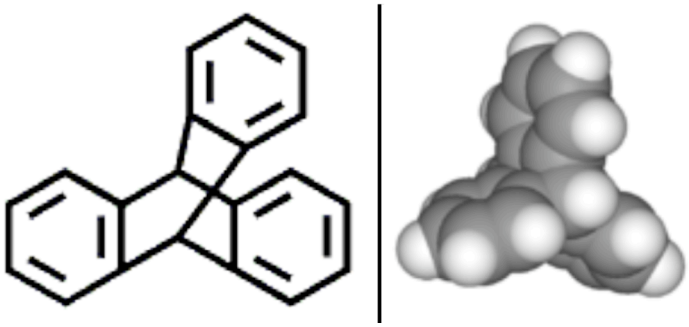

Figure 34: Chemical structure and space filling model of Triptycene.

Work by Oki and coworkers[75,76] presented the simplest triptycene molecular gears, using two triptycene derivatives connected by a bridge, such as CH_2, NH, O, SiH_2, or C=C. The laboratories of Iwamura and Mislow[77] reported the first

examples of truly geared rotation by using ditriptycyl ethers (Tp_2O) and ditriptycyl methanes (Tp_2CH_2).

The triptycene-based gears consist of two three-toothed gears; as illustrated in **Figure 35**. The intermeshing between the phenyl groups on the two triptycenes leads to little or no slippage, even at high temperature. Rotation on one triptycene unit causes the disrotation of the other in a frame of reference that keeps the central linker atom static.

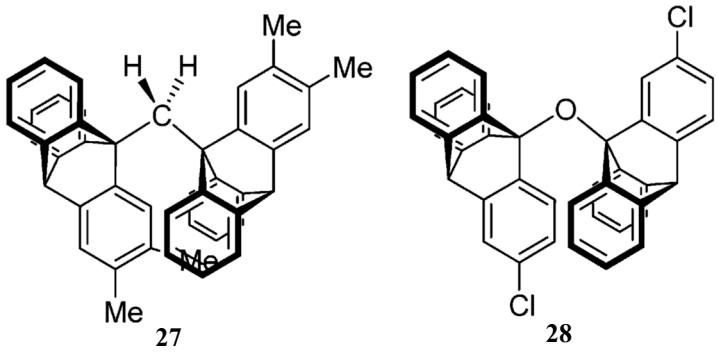

Figure 35: Triptycene based molecular gears.

According to empirical force field calculations the gearing barrier in Tp_2CH_2 from the C_s ground state through the C_2 transition state is only 1 kcal mol^{-1}.[78] The low energy barrier implies that correlated rotation is nearly barrier-less. Thus the triptycene gears are highly mobile, almost frictionless, and tightly meshed as well as securely interlocked bevel gears. NMR studies of these compounds show a very rapid correlated disrotation. The ^1H NMR spectra of Tp_2CH_2 and Tp_2O show no splitting of the benzene ring signals, even at low temperatures

(approximately -90°C). These results are in agreement with an upper limit of 7-8 kcal per mol for the gearing barrier.[79] The energy barrier for gear slippage is much higher and very dependent on the joint group. In a variable temperature ^{1}H NMR study, by both Iwamura[80] and Mislow[81], a barrier of *ca.* 20.4 kcal mol^{-1} for Tp_2SiH_2 and a barrier as high as 41.0 kcal per mol for Tp_2O was found. In these systems rotation happens in the absence of slippage giving rise to a particular case of stereoisomerism, called "phase isomerism" by Iwamura.[82] If two blades on each wheel are labeled, three stereisomers are produced, a racemic pair and a *meso* form.

In 1986, Iwamura and coworkers succeeded in synthesizing a more complex triptycene gear, a chemical gear train. This system consists of two labeled triptycenes connected by ether type bonds shown in **Figure 36**. The movements are more complex in these systems. The rotation rule is that the motion of the two terminal gears in a train is disrotatory if the number of gears is even and conrotatory if the number of gears is odd. This allows insight into the construction of macromolecular chains that can transfer information from one end of the molecule to the other by means of torsional motions along the chain.

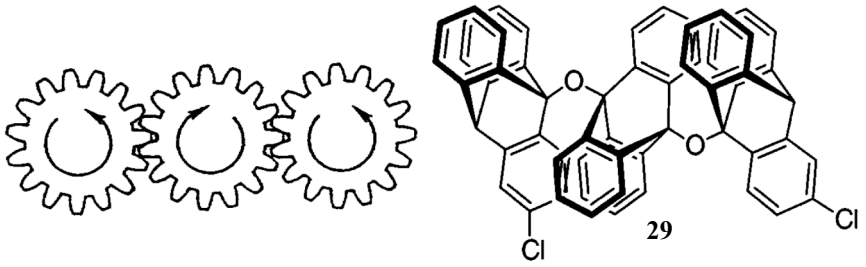

Figure 36: Depiction of a macroscopic drive train and its molecular analog.

4.3 Light-Driven Unidirectional Molecular Rotors

The transformation of chemical energy to mechanical energy is the key to controlled motion in living organisms. The efficiency and the rate at which nature's motors can engage in repetitive unidirectional rotations providing a challenge on synthetic systems. Three basic requirements need to be satisfied in order to be able to create a molecular motor: repetitive rotary motion, consumption of energy, and unidirectional rotation.

Feringa and coworkers have pioneered the field of chirooptic molecular switches.[83] In 1999, expanding on their findings with switches, they reported the first light driven mono-directional molecular rotor.[84] Feringa's system is based on a chiral helical alkene, which displays unidirectional rotation around the central carbon-carbon double bond in which each 360° rotation involves four discrete isomerization steps activated by ultraviolet light or a change in

temperature. Their first generation light-driven motors were the compounds shown in **Figure 37**.

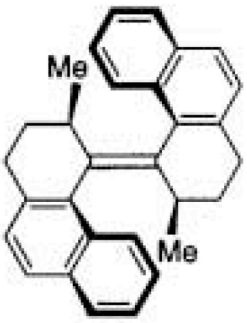

(3R, 3′R)-(P,P)-trans-**30a**
stable form
(two axial methyl groups)
ΔE = 0.0 kJ mol^{-1}

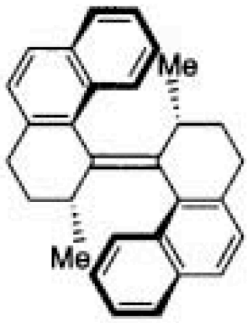

(3R, 3′R)-(M,M)-trans-**30a**
less-stable form
(two equatorial methyl groups)
ΔE = +35.9 kJ mol^{-1}

Figure 37: First generation light-driven molecular motors.

Upon examining the structure of the stable light-driven motor it was recognized that both a stereogenic center, with fixed stereochemistry, and a helical structure, the helicity of which can be changed by photoisomerization, are present in the same molecule. Another important feature of this system is that the methyl substituents can adopt two distinct orientations. The photochemical and thermal isomerization process is summarized in **Figure 38**. Even though light energy is essential to power this motor, the unidirectional rotation is directed by the methyl substituents. In the first step, photochemical *trans-cis* isomerization of stable **30a** to unstable **30b** results in helix inversion. It also forces the methyl substituents to adopt an unfavorable equatorial orientation. In the second step,

thermal interconverstion continues the rotary motion of the molecule from **30b** to the stable conformation **30c**. In this step strain is released and the methyl groups are back to the more favorable axial orientation. Once again the methyl groups are forced into the unstable equatorial orientation in the third step, with the photochemical isomerization of **30c** to **30d**. In the final thermal step, the original stable isomer **30a** (with the methyl groups at the axial position), is restored from **30d.**[85]

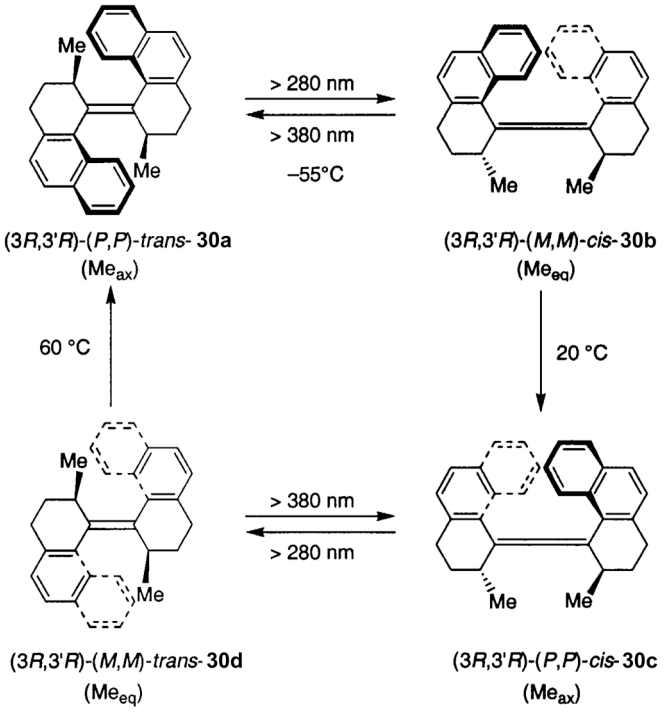

Figure 38: Photochemical and thermal isomerization of Feringa's first generation molecular rotor.

Feringa and coworkers redesigned their molecular rotor to have distinct upper and lower halves, so that the lower part could be used for connection to other molecules or surfaces while the upper part still behaved as a rotor, as illustrated in **Figure 39**.

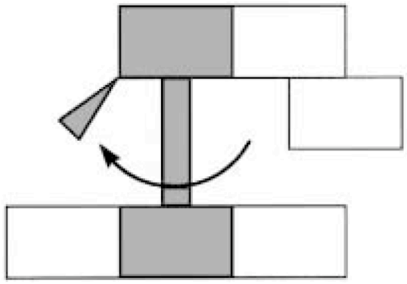

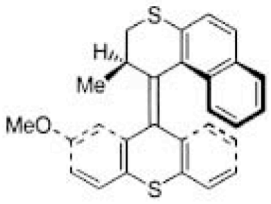

31

Figure 39: Second generation light-driven molecular motor.

This motor, which consisted of a (2R)-methyl-2,3-dihydronaphthothiopyran upper half and a thioxanthene lower half, undergoes two thermal and two photochemical isomerization steps as before, shown in **Figure 40**. The experimental results, observed by circular dichroism spectra, show that the upper naphthothiopyran moiety undergoes a full 360° rotation in a counterclockwise direction relative to the lower thioxanthene unit. In the second-generation molecular motors the presence of a single stereogenic center, the methyl group on the top fragment, dictates the unidirectional rotation.[86]

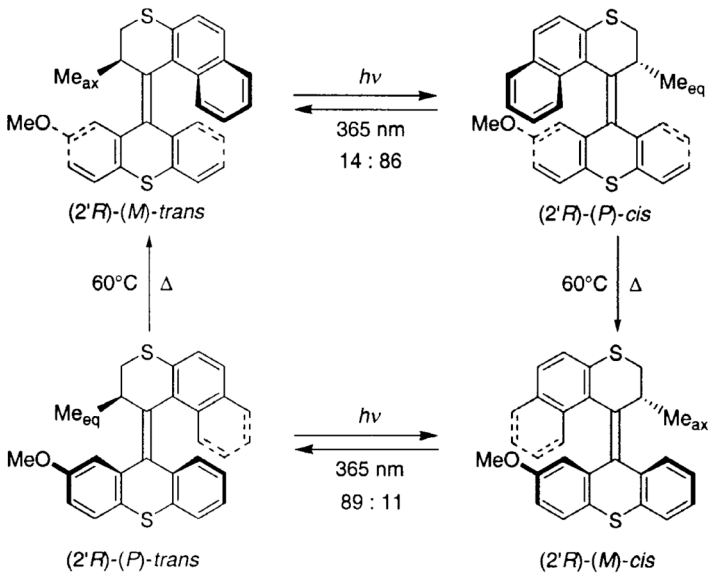

Figure 40: Photochemical and thermal isomerization of Feringa's second generation molecular rotor.

In 2002, in an attempt to vary the speed of rotary motion, Feringa and coworkers investigated the effects of changing the heteroatoms in the framework. It was found that by replacing a sulfur atom with oxygen on the lower half the barrier to rotation decreased by 1.2 kcal mol^{-1}. Changing the sulfur atom on the upper half of the molecule with a CH_2 group the rotation barrier decreased further (by 3.4 kcal per mol), lowering the half-life from 215 hours to 40 min. The results of this study are summarized in **Figure 41**.

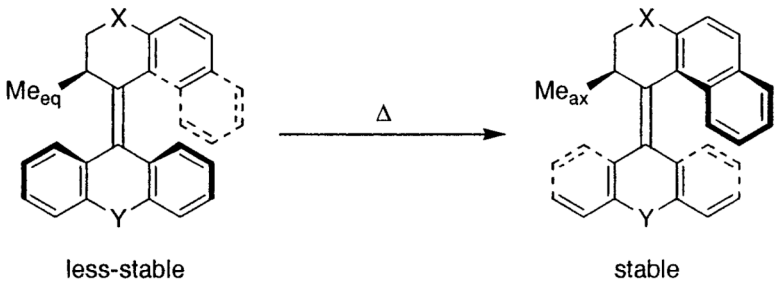

	$\Delta^{\ddagger}G^{\theta}$ (kJ·mol^{-1})	$t_{1/2}^{a}$ (h)
X = S, Y = S	105.7	215
X = S, Y = O	100.6	26.3
X = CH_2, Y = S	91.6	0.67 (40 min)

a: at room temperature (25 °C)

Figure 41: Summary of energies and half-lives for the thermally activated helix inversion.

4.4 Molecular Turnstiles

Molecular turnstiles demonstrate another example of rotary motion in a molecular system. The first molecular turnstile was designed and synthesized by Moore and Bedard.[87] The turnstile was composed of a hexa(phenylacetylene) macrocyclic frame with a diethynylarene bridge, as shown in **Figure 42**. The group observed the rotation of the internal phenylene group as a function of its substituents (R=H, CH_2OCH_3, CH_2O-3,5-di-*tert*-butylphenyl). The dynamic behavior of the system was studied using variable temperature ^{1}H NMR. Turnstile **32a** rotates too quickly to be studied by NMR methods, due to low rotational barrier in triple bonds. For the substituents CH_2OCH_3 and CH_2O-3,5-

di-*tert*-butylphenyl, the benzylic hydrogens are diastereotopic in the absence of rotation (doublet peaks) and enantiotopic under free rotation (singlet peak). For turnstile **32b**, the benzylic hydrogens appear as a doublet at a low temperature of -54°C; however, at 0°C it coalesces to a singlet, thus exhibiting spindle rotation. Upon further examination of turnstile **32b**, via molecular models, it was found that rotation requires distortion of the macrocyclic framework from a planar conformation. To date the mechanism of rotation has not been reported. In the case of turnstile **32c**, the benzylic hydrogens did not change at any temperature (up to 150°C), indicating that the spindle does not rotate on the NMR time scale. This is consistent with the idea that this turnstile is conformationally locked and cannot undergo spindle rotation. The group will investigate placing a dipole on the spindle. It is believed that this might allow rotation to be controlled rapidly and reversibly by an external field.

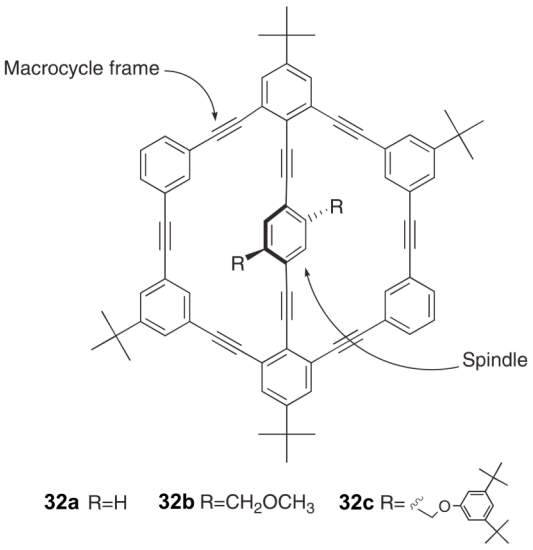

Figure 42: Chemical structure of molecular turnstile.

4.5 Molecular Ratchets

A macroscopic ratchet is a device that allows linear or rotary motion in only one direction, while preventing motion in the opposite direction. Ratchets are used in many mechanisms, including clocks, winders, jacks, etc. Ratchets contain three components: a) a toothed ratchet wheel, b) a pawl that prevents unintended rotation of the ratchet wheel, and c) a spring that holds the pawl in place (**Figure 43**). The ease and the direction of rotation are determined by both the tension of the spring and the contours of the ratchet wheel and pawl.

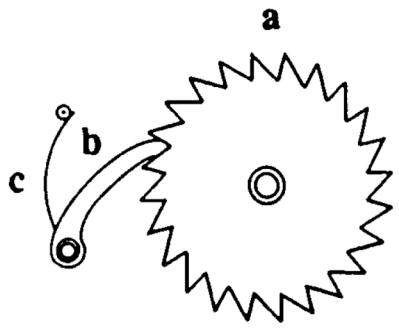

Figure 43: A mechanical ratchet's components: (a) ratchet wheel; (b) pawl; and (c) spring.

The first example of molecular ratchets was designed and synthesized by Kelly and coworkers.[88] They designed a molecule composed of triptycene, which would act as the ratchet wheel, connected to helicenes, acting simultaneously as the pawls and springs. Helicenes are helical polycyclic aromatic compounds. The helical structure is a result of steric repulsion of the terminal aromatic nuclei.[89] Kelly and coworkers choose helicenes for two reasons: First, the

inherent helicity promotes the unidirectional rotation needed to create a ratchet; and the rigid structure of helicenes resists deformation, which is a characteristic of springs. The two molecular ratchets they proposed are shown in **Figure 44**. Both systems have the same basic components, and vary only in the length of the helicene.

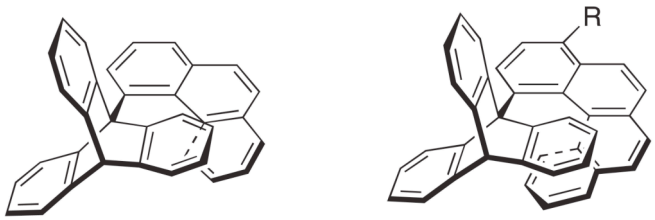

33 **34** **a**, R= H
b, R= Me

Figure 44: Molecular structure of Kelly's ratchet.

Molecular modeling calculations revealed that ratchet **33** presents a greater barrier to rotation than ratchet **34**. A distinct helical conformation is seen with the [4]helicene unit in **34**, and it is believed that the lower barrier to rotation is due to the longer helicene in ratchet **34**, which prevents it from relaxing to a stable ground state conformation in comparison to **33**. Manual rotation of the triptycene in computational models of **34** forces the helicene further and further out of planarity until the energy maximum is reached. The rotation is achieved more easily with a clockwise, instead of counterclockwise, turning of the triptycene unit, as expected of a ratchet. In order to establish the direction of rotation of the triptycene unit, spin polarization transfer NMR was used. The findings were unexpected, in that the triptycene unit demonstrated equal rotation in both

directions, which is in agreement with the second law of thermodynamics.[89,90] The comparison of theory and experimental findings in Kelly's work exemplifies the disconnection that may occur during the molecularization of a macroscopic device.

4.6 Molecular Gyroscopes

The creation of the macroscopic gyroscope is credited to the French scientist, Jean Foucault, in 1852.[91] His goal was to develop an instrument that would help visualize the rotation and precession of the Earth about its axis, **Figure 45**. Since then gyroscopes have played a significant role in our society and technology. Some practical applications of gyroscopes include the anti-roll stabilizers in ships and high-speed trains, gyrocompasses and airplane autopilots, and space station orientation and navigational systems.[92]

Figure 45: A replica of Foucault's gyroscope.

A simple gyroscope is a device with one degree of freedom, consisting of a spinning mass, called a rotator[90], with its spinning axis positioned through the center of the mass and mounted within a rigid frame, or stator. When the gyroscope is mounted on supports, or gimbals, it has three degrees of freedom.

The design of molecular analogs of macroscopic gyroscopes faces challenges and limitations, such as construction of a frictionless rotator, the need for flat or barrier-less potential energy surfaces, mechanisms to introduce a controlled impulse or a constant force to power the rotator, and perhaps the most significant challenge, the fact that momentum and energy are internally redistributed within a few picoseconds in dissipative molecular systems, making it difficult to induce unidirectional rotation.[93]

The first example of molecules resembling gyroscopes were introduced by Rose and coworkers in 1985.[94] In this system, a “double picket fence” porphyrin was first synthesized, and then bridges were introduced below and above the plane of the porphyrin ring system. Three of Rose’s “gyroscope-like” compounds are shown in **Figure 46**, with connectivity similar to two-spoke toy gyroscopes.

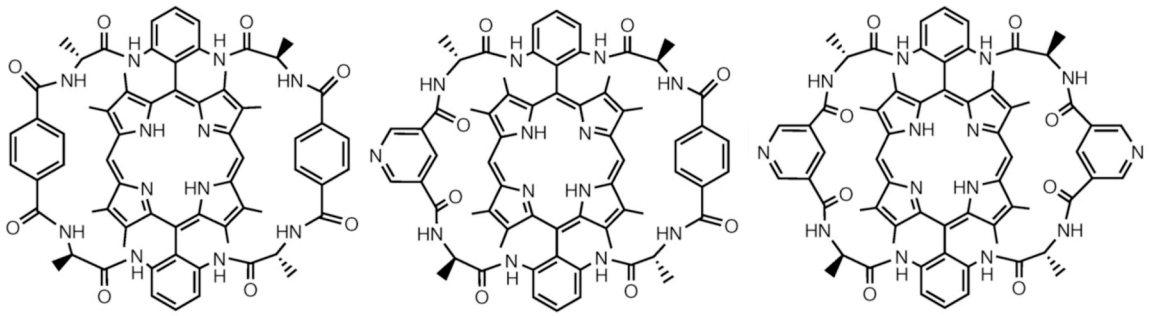

35 36 37

Figure 46: Rose’s “gyroscope-like” molecules.

The porphyrin cores are viewed as potential rotators, with phenyl groups capping the axes. The problem found with this system was that the outer periphery of the porphyrin hemisphere is made up of eleven atoms, while the spokes consist of only fifteen atoms. Considering the steric effects on the methyl groups of the porphyrin ring, it is clear that rotation is not possible.

In 1994 Gray and coworkers presented another molecule resembling a molecular gyroscope. In their system a molybdenum tetracarbonyl complex is surrounded with crown ethers, as seen in **Figure 47**. The macrocycle of this system is

symmetric about the $Mo(CO)_4$ plane and bisects one OC-Mo-CO angle. If rotation of the $Mo(CO)_4$ group on the NMR time scale is slow, two peaks would be observed on the ^{13}C NMR for the CO groups. NMR studies show one broadened signal at high temperatures, indicating a low barrier for the rotation of carbonyl ligand through the macrocycle. Upon further investigation, it was found that based on metrical parameters, rotation of the $Mo(CO)_4$ group is also favored. This system qualifies as a molecular rotor, perhaps even a gyroscope, however the group did not continue the research further.[95]

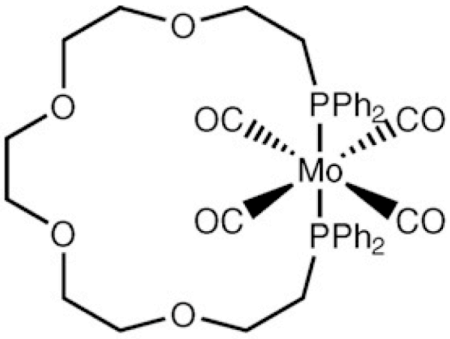

38

Figure 47: Chemical structure of a molybdenum complex representing a potential molecular gyroscope.

A major contribution to the field of molecular gyroscopes has been made by Gladysz and coworkers. By utilizing ring closing alkene metathesis, followed by hydrogenation reactions of complexes with *trans*-phosphine ligands, they have been able to synthesize a series of gyroscope-like molecules. **Figure 48** illustrates examples of such compounds, categorized as trigonal bipyramidal substrates, square planar substrates, and octahedral substrates, respectively.[96-98]

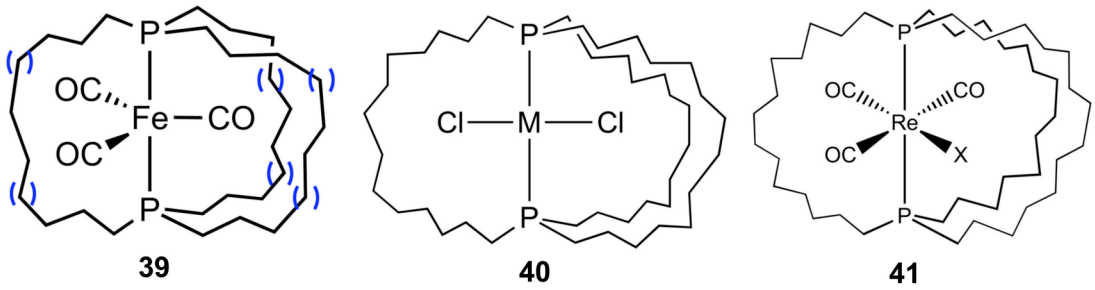

Figure 48: Gladysz's Organometallic molecular gyroscopes.

In compound **39**, a bipyramidal structure, the ligands on the pentacoordinated iron rotate within the cage formed by the methylene linkers. The group then replaced one CO ligand with NO and investigated the dynamics of the system using ^{13}C dynamic NMR (DNMR). Replacing the ligand with a NO group was found to introduce a dipole moment in the molecule, which opens possibilities for driven motion in a rotating electric field. The rotator is protected by the cage, which might allow for regular arrays of dipolar rotors capable of communicating through electrostatic interactions.[96]

For the square planar structure, compound **40,** the two chloride ligands can easily be substituted by bromide, iodide, and cyanide ligands. Analysis via low temperature ^{13}C NMR shows that in all cases the rotation is rapid on the NMR time scale. Introduction of longer ligands, such as thiocyanide, isothiocyanide and phenyl groups "brake" the rotation. Computational analyses were done to clarify the barrier to rotation, and it was found that platinum (Pt) and palladium

(Pd) complexes both have a considerably lower rotational barrier than the iron (Fe) analogs.[97]

In the case of compound **41**, the octahedral structure, rapid rotation was again observed via ^{13}C NMR. The complex can easily undergo substitution reactions to replace ligands in high yield. Further studies are currently underway to test other metals, different types of stators, and incorporation of a dipole moment in the rotators to favor unidirectional rotation.[98]

The Garcia-Garibay group have designed and investigated crystals in which phenylene groups rotate in a cavity created by the substituents on the phenylene rotator. The goal is to design a molecule that encompasses a fully enclosed cavity containing a chemically bonded rotator.[90]

The molecular gyroscope previously designed by the Garcia-Garibay group entails the use of a *para*-phenylene connected by alkynes at the 1,4 positions to triptycyl (**42**) or triarymethyl (**43**) (trityl) groups, as shown in **Figure 49**.[99-101] The choice of phenylene groups as rotators was due to ease in synthesis, as well as the correct symmetry for attachment of molecular axles along the center of mass. Alkynes are ideal as axles in that the intrinsic barriers for rotation of groups immediately linked to them are very low. The final piece of the Garcia-Garibay gyroscope is an encapsulating stator, either a triphenylmethyl (trityl) or triptycyl

group, which must provide the free volume needed to allow the phenylene group to rotate in a sterically unhindered manner. Its important to note that both trityl and triptycyl groups are relatively large, thus forming a cavity to shield the rotator, and can be modified to adjust crystal packing.

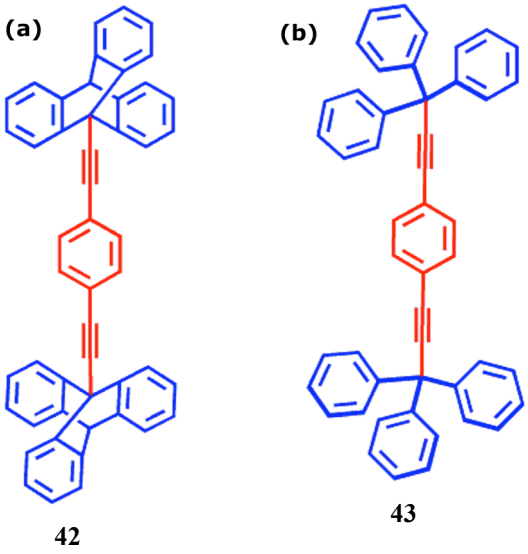

42 43

Figure 49: Structures of Molecular gyroscopes with (a) triptycle (**42**), and (b) trityl (**43**) stators.

To identify structural characterizations the authors used single crystal X-ray diffraction measurements, as well as ^{1}H and ^{13}C NMR. For dynamic properties a wide range of time scale measurements were taken by techniques that include variable-temperature solid-state NMR, cross-polarization and magic-angle spinning (CPMAS) NMR, broadband ^{2}H NMR, dielectric spectroscopy, and inelastic neutron scattering. These methods have complementary dynamic ranges and are relatively simple. Variable temperature CPMAS relies on

sufficient chemical shift differences between carbon atoms at exchanging positions[102], and ^{2}H NMR relies on spectral changes caused by dynamic averaging of the orientation dependent interactions between ^{2}H nuclear quadrupole moment and the electric field gradient at the nuclear position.[103] It should be noted that although site exchange rates determined by NMR methods provide information on the dynamic motion of the gyroscope, no information can be obtained on the directions of movement; it is believed that under thermal conditions and at equilibrium, either direction of rotation is equally possible. It is also important to note that NMR experiments cannot distinguish between continuous rotation in a single direction and random displacement in either direction.

Crystals molecular gyroscope with trityl end-groups from benzene formed a clathrate, and crystals from dichloromethane formed a solvent free structure.[100] Analysis of the packing structures confirmed that the molecules align parallel to each other due to aromatic edge-face interactions (**Figure 50**). In the benzene clathrate, this packing takes the form of a 6-fold trityl embrace. Thermal and spectroscopic analysis show that the benzene clathrate becomes solvent free between the temperatures of 80-100° C; the solvent free crystals were thermally stable with a melting point of 316° C. The rotary dynamics of the phenylene group turned out to be very efficient in both the benzene clathrate and the solvent free form, as determined by variable temperature ^{13}C CPMAS NMR and

quadrupolar echo ^{2}H NMR line-shape analysis. A splitting of 60 Hz at 255K was found from ^{13}C CPMAS NMR, giving a time constant of rotation of 7.7 milliseconds and a barrier of 12.8 kcal per mol. From ^{2}H NMR line-shape analysis, the upper limit of rotation was 10^{4} s^{-1}, giving an activation barrier of 14.6 kcal per mol for the desolvated structure, which is only 2 kcal per mol higher than the clathrate structure.[90,100]

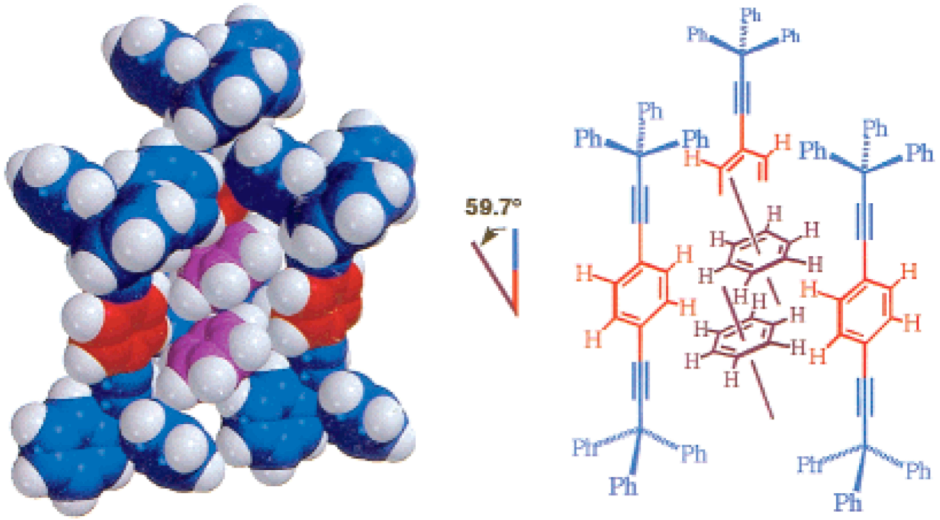

Figure 50: Space filling models and line formulas illustrating the packing arrangement of the trityl molecular gyroscope and the benzene solvent molecules.

The Garcia-Garibay group continued their effort on barrier-less rotation by placing substituents at the *meta* positions of each phenyl group on the trityl framework. Based on molecular mechanics calculations, it was believed that the substituents would diminish interdigitation of adjacent molecules and reduce the

hindrance for rotation of the central phenylene. The hexamethoxy derivatives[104] (**44**) and dodeca-*tert*-butyl derivatives[105] (**45**), as shown in **Figure 51**, were synthesized to analyze the effects on the central phenylene.

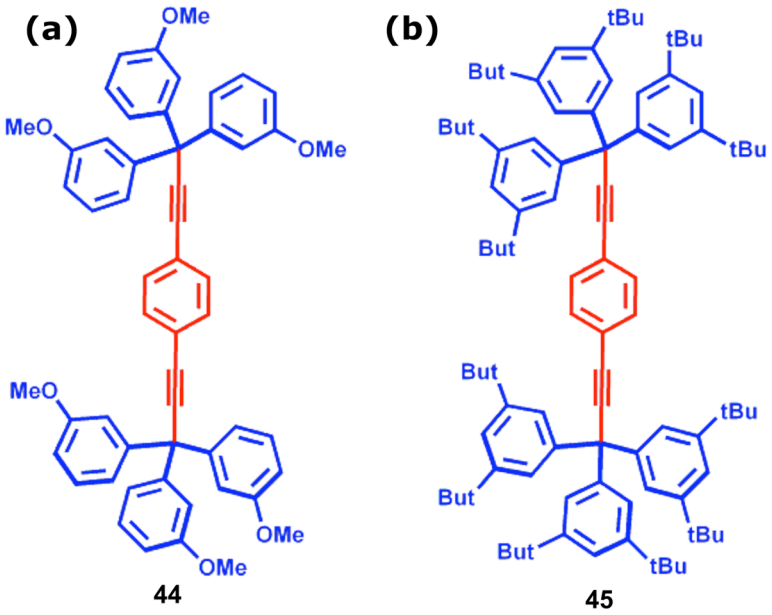

Figure 51: Structures of (a) hexamethoxy **44**, and (b) dodeca-tert-butyl **45** derivatives of the trityl molecular gyroscope.

The hexamethoxy derivative **44** was highly polymorphic. A well-characterized benzene clathrate of this molecule was used to investigate its rotational dynamics by CPMAS ^{13}C NMR and ^{2}H NMR line shape. A lower energy barrier, 11.7 kcal per mol, and faster rotation rates was observed for the methoxy substituents of **44** compared to the non-substituted trityl, due to better shielding and increased degrees of freedom resulting from the methoxy substituents.

The dynamic studies of dodeca-*tert*-butyl derivative **45** resulted in ambient temperature exchange rates that were greater than the upper limit of the ^{2}H NMR line shape analysis. X-ray diffraction-quality crystals of **45** obtained from CH_2Cl_2 were very fragile and lost their integrity upon cooling, and it was not possible to obtain an activation energy. The packing coefficients for both **44** (methoxy) and **45** (t-butyl) suggested that bulkier substituents helped the formation of more open structures in their solid state.

The Garcia-Garibay group also used triptycene units as stators[101], as seen in **Figure 48a**, in order to increase the shielding of the rotator. They also illustrated that various groups could be used as the rotator, such as anthracene, pyrene, and biphenyl, and analyzed the gas-phase rotational potentials, crystallization behavior, and thermal properties (**Figure 52**).

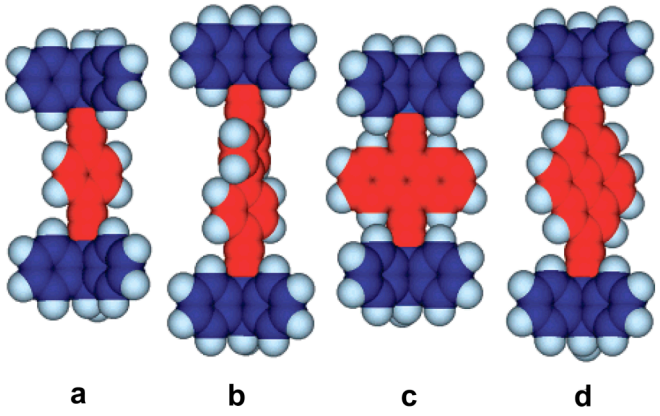

Figure 52: Space filling models of the triptycyl-based molecular gyroscope with rotators (a) phenylene, (b) biphenylene, (c) anthraceneylene, and (d) pyrenylene.

Even though these molecules did not have a dipole moment, they all rotated quickly on the NMR time scale, which was supported by semi-empirical AM1 calculations. The calculations also predicted a frictionless rotation. From X-ray crystallography, it was found that the close packing interactions that hinder the rotator's rotation come from interdigitation. It was seen that triptycenes fill the void space between two triptycenes on an adjacent molecule in the crystal. In an attempt to increase the free space around the phenylene rotator for ease of rotation, bulky substituents, in the form of *tert*-butyl groups were placed on the triptycene units, as shown in **Figure 53**. Analysis of the X-ray crystal structure showed there was more free space around the phenylene rotator, allowing it to turn. An estimated rotational barrier of 3.3 kcal per mol was found from the atomic displacement parameters in the crystal data.

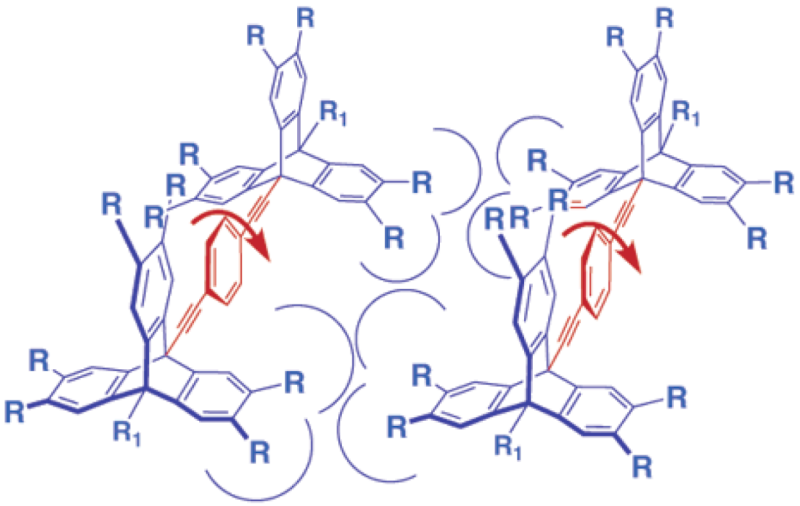

Figure 53: Illustration of the phenylene rotator with substituted triptycyl units. This design allows free space around the rotator, permitting it to rotate.

Garcia-Garibay and coworkers next introduced a dipole moment in their design, referring to it as a molecular compass. They synthesized the trityl molecular gyroscope with fluoro-, amino-, *ortho*-diamino-, *para*-aminonitro-, nitro-, and cyano- groups attached to the phenylene rotator[106], as illustrated in **Figure 54**. Based on semi-empirical AM1 calculations, the dipoles ranged from 0.74 to 7.30. Their calculated molecular volumes differ by only 5% from the parent molecule (**Figure 46b**)**.** Obtaining X-ray quality crystals for compounds with two polar substituents, **50** and **51** proved to be difficult. Samples of the mono-substituted compounds, **46-49**, crystallized from benzene gave triclinic clathrate structures, with two solvent molecules per unit cell. These crystals were desolvated by first-order phase transition between 60 and 130°C, which yielded crystals identical to crystals obtained from mixtures of CH_2Cl_2 and hexanes. The molecules were studied using ^{13}C CPMAS NMR, and due to overlapping signals from the trityl and phenylene groups, quantitative data was not obtained.

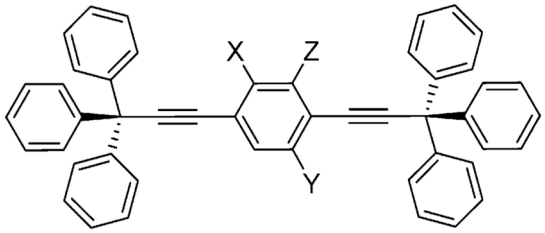

46 X = H; Y = F; Z = H
47 X = H; Y = CN; Z = H
48 X = H; Y = NO_2; Z = H
49 X = H; Y = NH_2; Z = H
50 X = NH_2; Y = H; Z = NH_2
51 X = H; Y = NH_2; Z = NO_2

Figure 54: Molecular compasses with dipole moment in the rotator.

Utilizing dielectric spectroscopy, ^{2}H NMR, and variable temperature X-ray crystallography, they were able to demonstrate a rapid thermal response of the molecular rotor to the applied electric field in the case of compound **46**. The barrier to rotation was found to be about 14 kcal per mol and twofold rotational potential was observed with well asymmetry of about 1.5 kcal per mol. The asymmetry was the result of steric interactions between the dipolar rotators and the non-rotating portions of neighboring molecules.[107,108]

They continued their work in the field of molecular machines via the synthesis of a triply-bridged molecular gyroscope,[109] shown in **Figure 55**. X-ray crystal structure revealed that the alkyl chain bridges do not provide sufficient steric shielding. While the bridges curve away from the center rotator to maximize the space around the phenylene group, bridges from neighboring molecules, as well as solvent molecules occupy that.[110-112]

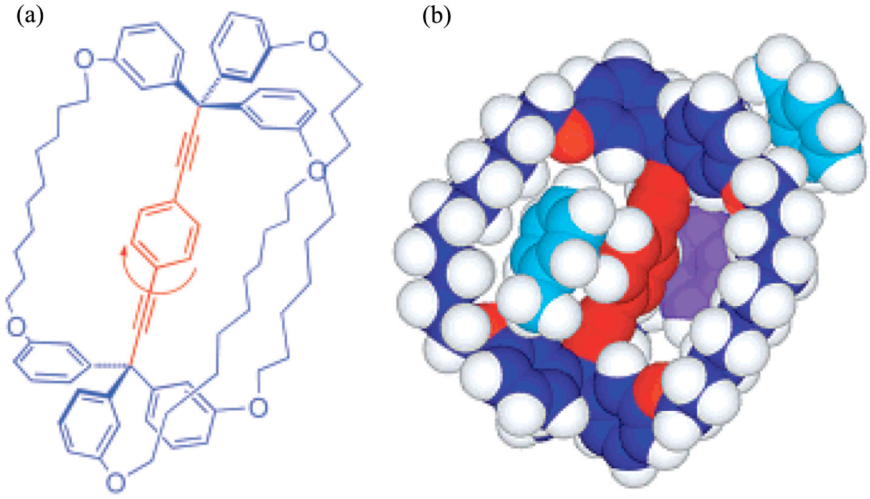

52

Figure 55: (a) Structure of a triply-bridged molecular gyroscope, (b) Space-filling model from the X-ray crystal structure showing the bridges (dark blue), the phenylene rotator (red) solvent molecules toluene (light blue) and benzene (purple).

Chapter 5

Molecular Gyroscopes: Does Precession Occur in the Absence of Gravity?

5.1 Introduction

A prior demonstration of the second law of thermodynamics in the context of the single molecule demonstrated the failure of a macroscopic machine (a ratchet) to be reproduced at the molecular level. The biased unidirectional rotation of a macroscopic ratchet does not translate to unidirectional rotation about a bond.[77,84,92,113-118] Specifically, Kelly and co-workers investigated compound **52a** (**Figure 56**), a molecule designed to emulate a true ratchet, having features characteristic of a toothed wheel (ipticene) and pawl (helicene) (Chapter 4, Section 4.5).[119] Evidence for the second law of thermodynamics was seen through the NMR analysis of the molecular ratchet, which demonstrated equal propensity for clockwise and counterclockwise rotation. The lesson is of significance in molecule-based nanotechnology, emphasizing that structural mimicry of macroscopic machines at the molecular level does not ensure analogous function.

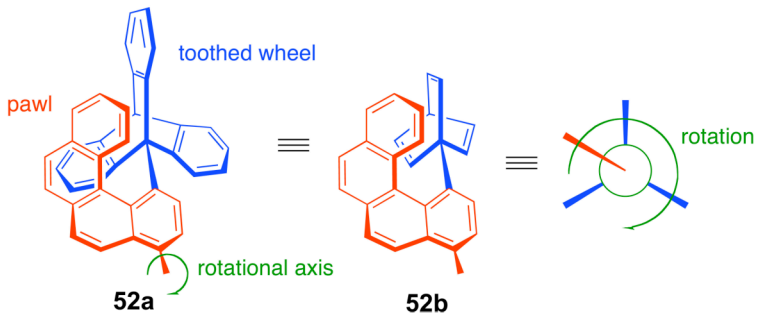

Figure 56: Kelly's molecular ratchet with ipticene as the toothed wheel, and helicene as the pawl.

Herein the consequence of mounting a molecular rotor on two orthogonal axes, as shown in **Figure 57,** (compound **53**) is explored. The macroscopic analog to this molecular system is a precessing gyroscope, and the "law" in question is conservation of angular momentum. Based on our computations (*ab initio* and molecular dynamics), functional equivalence of both molecular and macroscopic gyroscopes is predicted, with both systems demonstrating correlated rotation and precession. Our prediction supports a previous study implicating the methyl group of toluene to undergo both rotation *and* precession.[120]

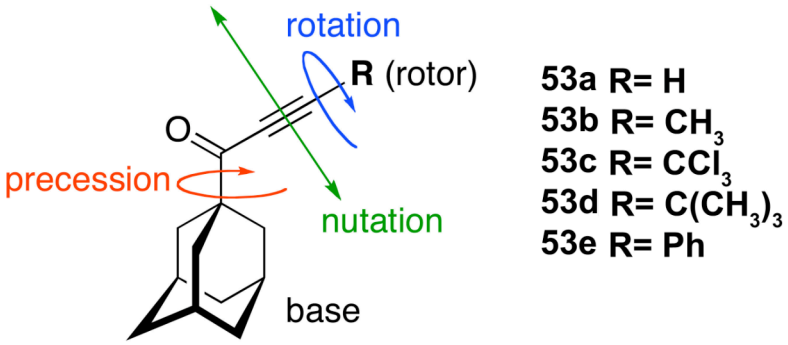

Figure 57: Precessing molecular gyroscope.

5.2 Results and Discussion

A macroscopic gyroscope is subject to three major torques: (i) the rotor generates a torque along the rotational axis, (ii) precession generates a torque along the precessional axis, and (iii) the force of gravity acting upon the rotor

generates the torque necessary to drive precession. In the third case, torque (τ) can be estimated by Equation 1:

$$\tau = m \times l \times g$$

(Eq. 1)

Where: **m** = rotor mass (kg), **l** = length of rotor axis (m), **g** = gravity (m/s^2)

The key observation is that a classical gyroscope functioning in the absence of gravity would generate no torque to drive precession, and thus correlated rotation and precession should not be observed. At the molecular level, the scenario of "zero gravity" applies, given that the Earth's gravitational field acting upon an object is dependant upon the object's mass. As an illustrative example, inserting into equation 1 a rotor with mass equivalent to one carbon atom and a rotational axis 10Å in length generates a torque of:

$$\tau = 1.66E^{-27}\ kg \times 1x10^{-10}\ m \times 9.81\ m/s^2 = 1.63 \times 10^{-36}\ Joules$$

Converting this quantity to kcal/mol, we obtain a value of $2.34x10^{-16}$ kcal/mol. In comparison, the energy required to rotate between two gauche conformers of ethane is 2.9 kcal per mol. With a difference of 16 orders of magnitude, it can safely be assumed that any forces due to gravity have insignificant impact on the

dynamic properties of small molecules. Indeed, the smallest mass that could be attached to a 100Å long rotational axis and generate 1 kcal of torque due to gravity is (by rearranging Eq. 1) the improbable value of $4.3x10^{+3}$ amu, or the mass equivalent of 355 carbon atoms (i.e., a 100 Å rotational axis terminated with six conjoined molecules of C_{60}). Of course, these calculations are gross approximations, useful only for emphatic purpose.

Compound **53** is designed to contain all elements necessary for rotation and precession in a classical gyroscope. The design includes an adamantane "base," a rotor (R), an axis of rotation, an axis of precession, and three-fold symmetry of both rotor and base (with the exception of R = H and Phenyl). In order for compound **53** to function in a manner analogous to a macroscopic precessing gyroscope, correlated rotation and precession must be manifested in the rotational states of the molecule. It follows that these states must absorb in the far-IR and/or microwave region of the electromagnetic spectrum.

As is known from experimental microwave spectroscopy,[121,122] extended lifetimes of rotational states require that molecules be isolated from any possibility of collision. This condition is also true of classical rotors, since an object striking a precessing gyroscope, of any size, would affect rotation and precession. As such, our theoretical analysis of an isolated gas phase molecule is appropriate, and used throughout our investigation.

One distinction in the design between compounds **52** and **53** is establishing a free versus hindered internal rotor. In the latter case, two interdigitated rotors are synonymous with a gearing process, and steric arguments logically explain correlated rotation. The base and rotor of gyroscope **52** are not interdigitated and therefore cannot be subject to traditional gearing mechanisms.

Using an analogy to classical physics, a free internal rotor implies that the torque driving precession exceeds the barrier to precession (compound **53**), otherwise, hindered rotation is observed (ratchet **52**). In the case of hindered rotation, rotational states are equated to a vibrational process centered at an energy minimum. At irregular time intervals, the vibrations have sufficient amplitude to jump the barrier to precession and into either of two adjacent symmetry sites (**Figure 58**). Subsequent to the next jump, vibrational processes resume, effectively destroying the momentum ("memory") of unidirectional motion. Due to the nature of this process, clockwise and counterclockwise movement has equal probability, and the events are non-periodic.

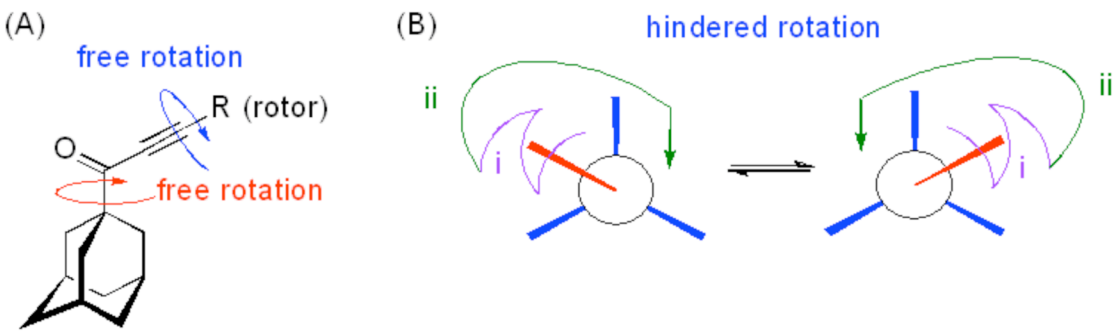

Figure 58: (A) Low barrier to rotation yields free rotation about both axes, facilitating periodic and correlated rotation and precession. (B) (i) pawl vibrates within the energy barrier until (ii) sufficient energy allows restricted rotation (ca. 120°) to the adjacent symmetry site. The barrier to 120° rotation is equal for clockwise and counterclockwise rotation, and the events are non-periodic.

Molecular dynamics[123] was employed to investigate compound **53**. The calculation isolated the molecule from any other molecule(s) (such as solvent), thus avoiding external forces that may result from collision. As a control experiment, compound **52b**, a molecular ratchet, was also investigated. Compounds **52a** and **52b** differ only by the magnitude of the barrier to rotation; with the [2.2.2] octatriene wheel of **52b** yielding a lower barrier than the iptycene wheel of **52a**. This simplification was employed to increase the frequency of rotations observed during molecular dynamics experiments.

In agreement with Kelly's findings, molecular dynamics predict that compound **52b** undergoes random rotation (both clockwise and counterclockwise) at irregular time intervals. This scenario is one of a hindered internal rotor. A graph

of the rotational data is shown in **Figure 59**. The data illustrates neither a unidirectional rotational bias nor a periodic process.

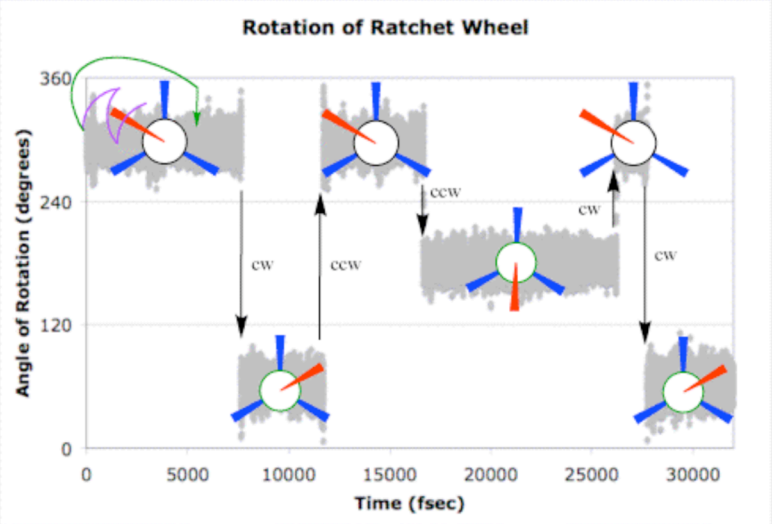

Figure 59: Molecular dynamics of compound **52b**. The frame of reference is such that the ratchet's "wheel" (blue) is fixed, and the "pawl" (red) rotates either clockwise (cw) or counterclockwise (ccw). Dihedral angles of 60, 180, and 320 degrees are arbitrarily chosen to correspond with the three symmetric minima of rotation.

Molecular dynamics[123] of compound **53** were investigated using two techniques. In the first case, all non-bonding intramolecular interactions were set to zero. This mimics infinitesimal activation barriers to rotation and precession, and it also omits all non-bonded interactions that may generate a torque between rotor axis and base. For all cases except **53a** (a rotor-less system), rates of rotation and precession are found to be constant at equilibrium. This is evident by examining the Fourier Transform, shown in **Figure 60**, of distance *d* over time: distance *d* reports both rotation and precession in a single measurement.

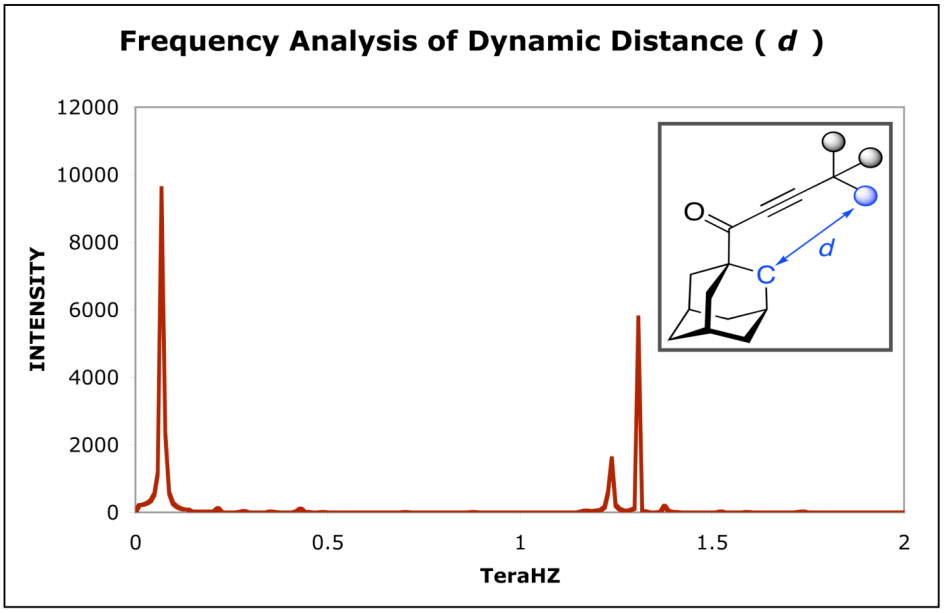

Figure 60: Fourier transform of distance d, plotted as frequency versus intensity. The three major peaks correspond to precession, nutation, and rotation (from left to right, respectively).

The second molecular dynamics study allowed normal non-bonding intramolecular interactions to be present. Barriers to rotation and precession (calculated at the MMFF level of theory) were predicted to be small. First, the linear alkyne axis presents minimal interaction with the adamantine base. Second, each axis in compounds **53b-d**, is a 3 x 2 = 6 fold barrier, mandating a small change in energy as a function of rotational conformer.[124] In the case of the phenyl rotor, the rotational axis is 2 x 2 = 4 fold, allowing a slightly higher rotational barrier. **Table 1** summarizes the results. Although the barrier to rotation varies, the barrier to precession is nearly equal in all cases.

Rotor	Precession Change in E (Kcal/mol)	Rotation Change in E (Kcal/mol)	Rotation Change in E (Kcal/mol)
		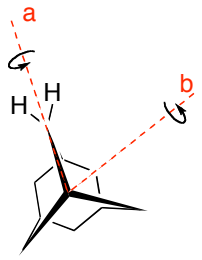	
		Symmetry A	**Symmetry B**
53b (CH_3)	7.79×10^{-2}	1.41×10^{-3}	2.83×10^{-4}
53c (CCl_3)	7.77×10^{-2}	3.13×10^{-2}	1.75×10^{-2}
53d ($C(CH_3)_3$)	7.84×10^{-2}	1.80×10^{-2}	5.90×10^{-2}
53e (Ph)	7.78×10^{-2}	1.40×10^{-2}	1.18×10^{-2}

Table 1: Energy Barriers of rotation and precession.

At equilibrium, rotor **53e** (phenyl rotor) regularly precesses, but only infrequently rotates. This likely reflects the lower symmetry and higher rotational activation barrier relative to compounds **53b-d**. Compound **53a** has a terminal alkyne as its rotational axis; the hydrogen is considered part of the axis, and therefore **53a** has no rotor. It is important to note that we define a rotor as having a diameter much larger than the diameter of the rotational axis. Here, precession is random both in rate and sense of direction. Compound **53b** (methyl rotor) rotates, but the precessional motion is limited to a back-and-forth vibration within one of the three low energy minima (i.e., 120° vibration versus 360° precession).

In contrast, compounds **53c** and **53d** show correlated rotation and precession. This is apparent by viewing either the frequency- (**Figure 60**) or the time-domain (**Figure 61**) plots.

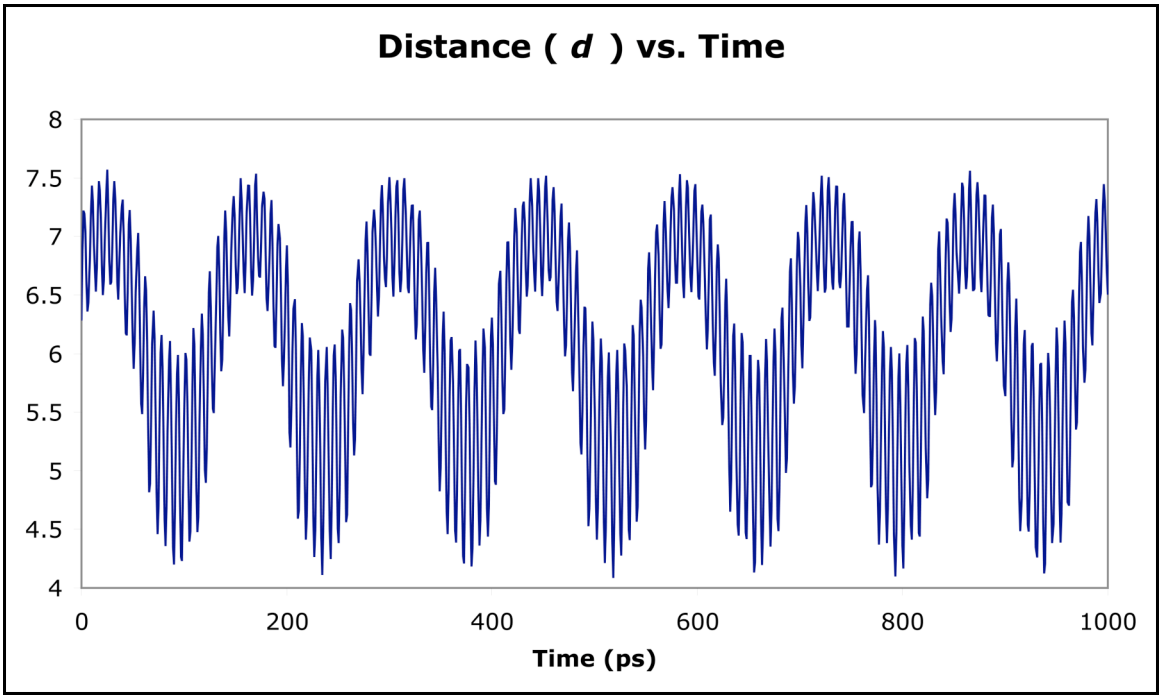

Figure 61: Plot of distance *d*, versus time (compound **53c**).

Figure 62 shows a multiple-exposure graphic from the molecular dynamics study of compound **53c**, illustrating more clearly both correlated and unidirectional rotation and precession (accompanied by nutation). Results indicate two correlated free internal rotors, an observation consistent with a classical gyroscope.

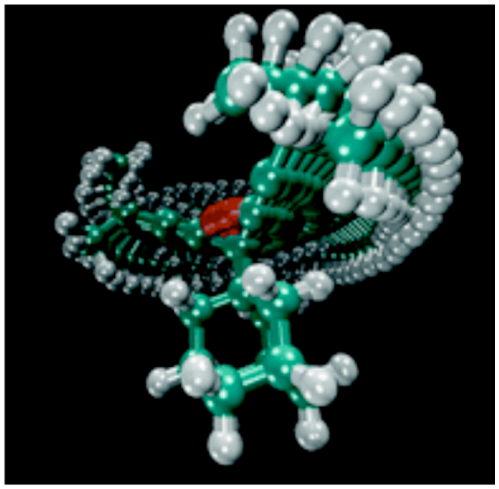

Figure 62: Multiple exposure graphic reflecting the rotational and precessional dynamics of compound **53c**.

From the perspective of Newtonian physics, correlated precession must arise from a force other than gravity. Given the differences observed in rotation and precession as a function of non-bonding interactions, we propose that precessional torque arises from non-bonding interactions between rotor and base. Because this torque is a function of the length of the precessional axis (a constant) and rotor mass (a variable), each system **53b-d** will generate a torque that scales with rotor mass. Precession does not occur with the methyl rotor **53b** because the torque associated with precession is not sufficient to surmount the barrier to precession. As rotor mass increases, as in **53c** and **53d**, so does the torque of precession, establishing unidirectionality.

Results from dynamics calculations were further supported by *ab initio* analysis of vibrational frequencies (HF-6/31G*).[50] For compounds **53c** and **53d** the

three lowest energy frequencies calculated correspond to: rotation (2.79, 13.15; for **53c** and **53d** respectively), precession (25.54, 27.17), and nutation (35.56, 44.47), from lowest to third lowest frequency. For those systems not demonstrating correlated rotation and precession in molecular dynamic studies (compounds **53a**, **53b**, and **53e**), it followed that vibrations corresponding to internal rotations were either absent, coupled, or at energies higher than other vibrational modes. Thus, there is empirical evidence suggesting that the exact ordering of frequencies corresponding to rotation, precession, and nutation may be used as a tool to predict correlated rotation and precession.

The possibility of designing, synthesizing, and isolating compound **53** on a surface, and then driving correlated rotation-precession with an external microwave source, appears to be feasible endeavor. With promising theoretical results in hand, the synthesis of compound **53d** was initiated.

As would be expected for nucleophilic addition of a carbanion to an acid chloride, treatment of acid chloride **54** (**Scheme 5**) with lithium phenyl acetylide gave predominantly the bis-adduct, alcohol **55**. Monoaddition of phenylacetylide to yield compound **53e** thus required conversion of the commercially available acid chloride **54** to the corresponding Weinreb amide **56**, prior to reaction with lithium phenylacetylide. In contrast, the *t*-butyl rotor, compound **53d**, could be prepared from the acid chloride without prior modification. These conflicting results likely

stem from the steric demands of the tetrahedral intermediate(s) formed during nucleophilic addition to the carbonyl carbon. This theory is further supported by the isodesmic reactions, shown in **Scheme 5**, that report a 2.74 kcal/mol difference for the corresponding bis-addition product alcohols, compounds **55** and **57**.

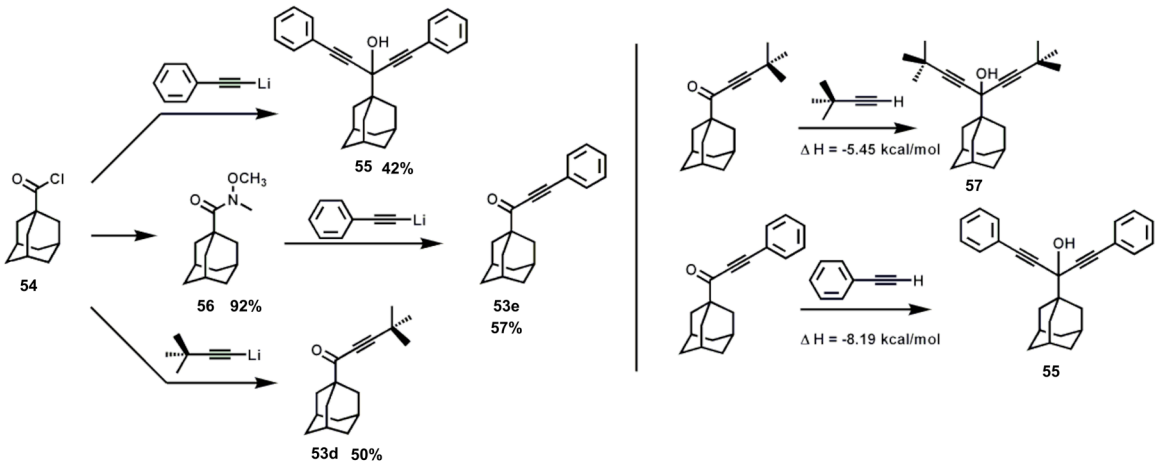

Scheme 5: Synthesis of molecular gyroscopes.

5.3 Conclusion

Correlated processes of rotation and precession, from the perspective of Newtonian physics, may be conserved from the macroscopic gyroscope down to the single molecule level, assuming certain requirements are met. For isolated molecular gyroscopes containing an axis of precession, an axis of rotation, and a rotor with mass greater than a methyl group, correlated rotation and precession is expected when the following criteria are met: (1) free internal rotation about each axis (low barriers to rotation), and (2) rotor and base of sufficient mass and symmetry. Support for designing a properly functioning system can be gained from molecular dynamics and frequency analysis. In the latter case, the two lowest-energy frequencies must correspond to rotation and precession, and may be of either conrotatory or disrotatory bias.[125]

References:

(1) Moore, J. S.; Hill, D. J.; Mio, M. J.; Prince, R. B.; Hughes, T. S. *Chemical Reviews* **2001**, *101*, 3893-4011.

(2) Hanes, C. S. *New Phytol* **1937**, *36*, 189.

(3) Fredenberg, K.; Schaaf, E.; Dumpert, G.; Ploetz, T. *Naturewissenschaften* **1939**, *27*, 850.

(4) Pauling, L.; Corey, R. B.; Branson, h. R. *Proceedings of the National Acadamy of Sciences U.S.A.* **1951**, *378*, 205.

(5) Watson, F. D.; Crick, F. H. C. *Nature* **1953**, *171*, 737.

(6) Okamoto, Y.; Nakano, T. *Chemical Review* **2001**, *101*, 4013-4038.

(7) Natta, G.; Pino, P.; Corradini, P.; Danusso, F.; Mantica, E.; Nazzanti, G.; Moraglio, G. *Journal of the American Chemical Society* **1955**, *77*, 1708.

(8) Pino, P.; Lorenzi, G. P. *Journal of the American Chemical Society* **1960**, *82*, 4745.

(9) Okamoto, Y.; Suzuki, K.; Ohta, K.; Hatada, K.; Yuki, H. *Journal of the American Chemical Society* **1979**, *101*, 4763.

(10) Millich, F.; Baker, G. K. *Macromolecules* **1969**, *2*, 122.

(11) Nolte, R. J. M.; Van Beijnen, A. J. M.; Drenth, W. *Journal of the American Chemical Society* **1974**, *96*, 5932.

(12) Green, M. M.; A., G. R.; Schilling, F. C.; Zero, K.; Crosby, C. *Macromolecules* **1987**, *20*, 992.

(13) Kollmar, C.; Hoffmann, R. *Journal of the American Chemical Society* **1990**, 8230.

(14) Pini, D.; Inuliano, A.; Salvadori, P. *Macromolecules* **1992**, *25*, 6054.

(15) Goodman, M.; Chen, S. C. *Macromolecules* **1970**, *3*, 398.

(16) Ciardelli, F.; Lanzillo, S.; Pieroni, O. *Macromolecules* **1974**, *7*.

(17) Moore, J. S.; Gorman, C. B.; Grubbs, R. H. *Journal of the American Chemical Society* **1991**, *113*, 1704.

(18) Corley, L. S.; Vogl, O. *Polymer Bulletin* **1980**, *2*, 211.

(19) Ute, K.; Hirose, K.; Kashimoto, H.; Hatada, K.; Vogl, O. *Journal of the American Chemical Society* **1991**, *113*, 6305.

(20) Fujiki, M. *Journal of the American Chemical Society* **1994**, *116*, 6017.

(21) Frey, H.; Moller, M.; Matyjaszewski, K. *Macromolecules* **1994**, *27*, 1814.

(22) Matyjaszewski, K. *Journal of Oranometalic Polymers* **1992**, *2*, 5.

(23) Lehn, J. M.; Rigault, A.; Siegel, J.; Harrowfield, J.; Chevrier, B.; Moras, D. *Proceedings of the National Acadamy of Sciences U.S.A.* **1987**, *84*, 2565.

(24) Hanan, G. S.; Lehn, J. M.; Kyritsakas, N.; Fischre, J. *Chemical Communications* **1995**, 765.

(25) Moore, J. S.; Nelson, J. C.; Saven, J. G.; Wolynes, P. G. *Science* **1997**, *277*.

(26) Rajca, A.; Safronov, A.; S., R.; Shoemaker, R. *Angewandte Chemie. International Edition in English* **1997**, *26*, 488.

(27) Moore, J. S.; Nelson, J. C.; Saven, J. G.; Wolynes, P. G. *Science* **1997**, *277*, 1793.

(28) Moore, J. S.; Tanatani, A.; Mio, M. J. *Journal of the American Chemical Society* **2001**, *123*, 1792.

(29) Moore, J. S.; Matsuda, K.; Stone, M. *Journal of the American Chemical Society* **2002**, *124*, 11836.

(30) Laarhoven, W. H.; Prinsen, W. J. C. *Topics in Current Chemistry* **1984**, *125*, 63.

(31) Katz, T. J. *Angewandte Chemie International Edition* **2000**, *39*, 1921.

(32) Barbarella, G.; Melucci, M.; Sotgiu, G. *Advanced Materials* **2005**, *17*, 1581.

(33) Rajca, A.; Wang, H.; Pink, M.; Rajca, S. *Angewandte Chemie. International Edition in English* **2000**, *39*, 4481.

(34) Rajca, A.; Miyasaka, M.; Pink, M.; Wang, H.; Rajca, S. *Journal of the American Chemical Society* **2004**, *126*, 15211.

(35) Rajca, A.; Miyasaka, M.; Pink, M.; Rajca, S. *Journal of the American Chemical Society* **2005**, *127*, 13806.

(36) Cowie, J. M. G. *Polymers: Chemistry and Physics of Modern Materals.*; 3rd ed. ed.; Boca Raton: CRC Press, 2008.

(37) Tour, J. M. *Chemical Review* **1996**, *96*, 537.

(38) Jones, E.; Moodie, M. *Organic Syntheses* **1988**, *6*, 979.

(39) Reinecke, M. G.; Newsom, J. G. *Journal of the American Chemical Society* **1976**, *98*, 3021.

(40) Marsella, M. J.; Reid, R. J. *Macromolecules* **1999**, *32*, 5982.

(41) Marsella, M. J.; Yoon, K.; Tham, F. S. *Organic Letters* **2001**, *3*, 2129.

(42) Marsella, M. J. *Accounts of Chemical Research***2002**, *35*, 944.

(43) Marsella, M. J.; Reid, R. J.; Estassi, S.; Wang, L. S. *Journal of the American Chemical Society* **2002**, *124*, 12507.

(44) Marsella, M. J.; Yoon, K.; Almutairi, A.; Butt, S. K.; Tham, F. S. *Journal of the American Chemical Society* **2003**, *125*, 13928.

(45) Almutairi, A.; Tham, F. S.; Marsella, M. J. *Tetrahedron* **2004**, *60*, 7187.

(46) Almutairi, A.; Yoon, K.; Tham, F. S.; Marsella, M. J. *Pure and Applied Chemistry* **2006**, *78*, 777.

(47) Paruch, K.; Katz, T. J.; Incarvito, C.; Lam, K. C.; Rhatigan, B.; Rheingold, A. L. *Journal of Organic Chemistry* **2000**, *65*, 7602.

(48) Green, M. M.; Park, J. W.; Sato, T.; Teramoton, A.; Lifson, S.; Selinger, R. L. B.; Selinger, J. V. *Angewandte Chemie International Edition* **1999**, *38*, 3138.

(49) Jayasuriya, N.; Kagan, J.; Huang, D. B.; Teo, B. *Heterocycles* **1988**, *27*, 1391.

(50) Spartan06, Wavefunction Inc., Irvine, CA.

(51) Ajami, D.; Rebek, J. J. *Journal of the American Chemical Society* **2006**, *128*, 15308.

(52) Marsella, M. J.; Rahbarnia, S.; Wilmot, N. *Organic and Biomolecular Chemistry* **2007**, *5*, 391.

(53) Tamao, K.; Kodama, S.; Nakajima, I.; Kumada, M. *Tetrahedron* **1982**, *38*, 3347.

(54) Irie, M. *Chemical Reviews* **2000**, *100*, 1683.

(55) Gerson, F.; Knobel, J.; Metzger, A.; Scott, L. T. *Journal of the American Chemical Society* **1986**, *108*, 7920.

(56) Brooks, M. A.; Scott, L. T. *Journal of the American Chemical Society* **1999**, *121*, 5444.

(57) Peng, L.; Scott, L. T. *Journal of the American Chemical Society* **2005**, *127*, 16518.

(58) Necula, A.; Scott, L. T. *Journal of the American Chemical Society* **2000**, *122*, 1548.

(59) (a) Gaussian 03, Revision, Frisch, M. J.; Trucks, G. W.; Schlegel, H. B.; Scuseria, G. E.; Robb, M. A.; Cheeseman, J. R.; Montgomery, Jr., J. A.; Vreven, T.; Kudin, K. N.; Burant, J. C.; Millam, J. M.; Iyengar, S. S.; Tomasi, J.; Barone, V.; Mennucci, B.; Cossi, M.; Scalmani, G.; Rega, N.; Petersson, G. A.; Nakatsuji, H.; Hada, M.; Ehara, M.; Toyota, K.; Fukuda, R.; Hasegawa, J.; Ishida, M.; Nakajima, T.; Honda, Y.; Kitao, O.; Nakai, H.; Klene, M.; Li, X.; Knox, J. E.; Hratchian, H. P.; Cross, J. B.; Bakken, V.; Adamo, C.; Jaramillo, J.; Gomperts, R.; Stratmann, R. E.; Yazyev, O.; Austin, A. J.; Cammi, R.; Pomelli, C.; Ochterski, J. W.; Ayala, P. Y.; Morokuma, K.; Voth, G. A.; Salvador, P.; Dannenberg, J. J.; Zakrzewski, V. G.; Dapprich, S.; Daniels, A. D.; Strain, M. C.; Farkas, O.; Malick, D. K.; Rabuck, A. D.; Raghavachari, K.; Foresman, J. B.; Ortiz, J. V.; Cui, Q.; Baboul, A. G.; Clifford, S.; Cioslowski, J.; Stefanov, B. B.; Liu, G.; Liashenko, A.; Piskorz, P.; Komaromi, I.; Martin, R. L.; Fox, D. J.; Keith, T.; Al-Laham, M. A.; Peng, C. Y.; Nanayakkara, A.; Challacombe, M.; Gill, P. M. W.; Johnson, B.; Chen, W.; Wong, M. W.; Gonzalez, C.; and

Pople, J. A.; Gaussian, Inc., Wallingford CT, 2004. (b) GaussView, Version 4.1, Dennington II, Roy; Keith, Todd; and Millam, John; Semichem, Inc., Shawnee Mission, KS, 2007.

(60) Wynberg, H. *Chemical Reviews* **1971**, *4*, 65.

(61) Perrine, D. M.; Owens, J. E.; Eugene, P. K. *Journal of Organic Chemistry* **1989**, *54*, 4203.

(62) Kellogg, R. M.; Dik, J. K.; Van Driel, H.; Wynberg, H. *Journal of Organic Chemistry* **1970**, *35*, 2737.

(63) Hlubucek, J. R.; Lowe, G. *Chemical Communications* **1974**, 419.

(64) Stahl, F.; Schleyer, P. V. R.; Jiao, H.; Schaefer, H. F.; Chen, K. H.; Allinger, N. L. *Journal of Organic Chemistry* **2002**, *67*, 6599.

(65) Reed, A. E.; Weinhold, F. *Journal of Chemical Physics* **1985**, *83*, 1736.
(66) Reed, A. E.; Weinstock, R. B.; Weinhold, F. *Journal of Chemical Physics* **1985**, *83*, 735.

(67) Reed, A. E.; Weinhold, F.; Curtiss, L. A.; Pochatki, D. J. *Journal of Chemical Physics* **1986**, *84*.

(68) Glendening, E. D.; Badenhoop, K.; Weinhold, F. *Journal of Computational Chemistry* **1998**, *19*, 628.

(69) Glendening, E. D.; Weinhold, F. *Journal of Computational Chemistry* **1998**, *19*, 593.

(70) Glendening, E. D.; Weinhold, F. *Journal of Computational Chemistry* **1998**, *19*, 610.

(71) Venkataraman, K.; Klare, J. E.; Tam, I. W.; Nuckolls, C.; Hybersten, M. S.; Steigerwald, M. L. *Nano Letters* **2006**, *6*, 458.

(72) (a) Gaussian 03, Revision, Frisch, M. J.; Trucks, G. W.; Schlegel, H. B.; Scuseria, G. E.; Robb, M. A.; Cheeseman, J. R.; Montgomery, Jr., J. A.; Vreven, T.; Kudin, K. N.; Burant, J. C.; Millam, J. M.; Iyengar, S. S.; Tomasi, J.; Barone, V.; Mennucci, B.; Cossi, M.; Scalmani, G.; Rega, N.; Petersson, G. A.; Nakatsuji, H.; Hada, M.; Ehara, M.; Toyota, K.; Fukuda, R.; Hasegawa, J.; Ishida, M.; Nakajima, T.; Honda, Y.; Kitao, O.; Nakai, H.; Klene, M.; Li, X.; Knox, J. E.; Hratchian, H. P.; Cross, J. B.; Bakken, V.; Adamo, C.; Jaramillo, J.; Gomperts, R.; Stratmann, R. E.; Yazyev, O.;

Austin, A. J.; Cammi, R.; Pomelli, C.; Ochterski, J. W.; Ayala, P. Y.; Morokuma, K.; Voth, G. A.; Salvador, P.; Dannenberg, J. J.; Zakrzewski, V. G.; Dapprich, S.; Daniels, A. D.; Strain, M. C.; Farkas, O.; Malick, D. K.; Rabuck, A. D.; Raghavachari, K.; Foresman, J. B.; Ortiz, J. V.; Cui, Q.; Baboul, A. G.; Clifford, S.; Cioslowski, J.; Stefanov, B. B.; Liu, G.; Liashenko, A.; Piskorz, P.; Komaromi, I.; Martin, R. L.; Fox, D. J.; Keith, T.; Al-Laham, M. A.; Peng, C. Y.; Nanayakkara, A.; Challacombe, M.; Gill, P. M. W.; Johnson, B.; Chen, W.; Wong, M. W.; Gonzalez, C.; and Pople, J. A.; Gaussian, Inc., Wallingford CT, 2004. (b) GaussView, Version 4.1, Dennington II, Roy; Keith, Todd; and Millam, John; Semichem, Inc., Shawnee Mission, KS, 2007.

(73) Ballardini, R.; Balzani, V.; Credi, A.; Gandolfi, M. T.; Venturi, M. *Accounts of Chemical Research* **2001**, *34*, 445.

(74) Brown, H. T. *507 Mechanical Movements*; Lindsay Publications: Bradley, Il, 1984; Vol. 17th Edition.

(75) Oki, M. *Angewandte Chemie International Edition* **1976**, *15*, 87.

(76) Oki, M. *Stereochemistry* **1983**, *14*, 1.

(77) Iwamura, H.; Mislow, K. *Accounts of Chemical Research***1988**, *21*, 175.

(78) Mislow, K.; Houndshell, W. D.; Johnson, C. A.; Guenzi, A.; Cozzi, F. *Proceedings of the National Acadamy of Sciences USA* **1980**, *77*, 6961.

(79) Iwamura, H.; Koga, N. *Chemistry Letters* **1986**, *16*, 247.

(80) Iwamura, H.; Kawada, Y. *Journal of the American Chemical Society* **1983**, *105*, 1449.

(81) Mislow, K.; Guenzi, A.; Johnson, C. A.; Cozzi, F. *Journal of the American Chemical Society* **1983**, *105*, 1438.

(82) Iwamura, H.; Kawada, Y. *Tetrahedron Lett.* **1981**, *22*, 1533.

(83) Feringa, B. L.; van Delden, R. A.; Koumura, N.; Geertsema, E. M. *Chemical Reviews* **2000**, *100*, 1789.

(84) Feringa, B. L.; Koumura, N.; Zijlstra, R. W.; van Delden, R. A.; Harada, N. *Nature* **1999**, *401*, 152.

(85) Feringa, B. L. *Accounts of Chemical Research* **2001**, *34*, 504.

(86) Feringa, B. L.; Koumura, N.; van Delden, R. A.; Ter Wiel, M. K. J. *Applied Physics A* **2002**, *75*, 301.

(87) Moore, J. S.; Bedard, T. C. *Journal of the American Chemical Society* **1995**, *117*, 10662.

(88) Kelly, T. R.; Sestelo, J. P.; Tellim, I. *Journal of Organic Chemistry* **1998**, *63*, 3655.

(89) Janke, R. H.; Haufe, G.; Wurthwein, E.; Borkent, J. H. *Journal of the American Chemical Society* **1996**, *118*, 6031.

(90) Michl, J.; Kottas, G. S.; Clarke, L. I.; Horinek, D. *Chemical Reviews* **2005**, *105*, 1281.

(91) Wagner, J. F.; The Institute of Navigation.

(92) Gladysz, J. A.; Skopek, K.; Hershberger, M. C. *Coordination Chemistry Reviews* **2007**, *251*, 1723.

(93) Astumian, R. D. *Science* **1997**, *276*, 917.

(94) Boitrel, B.; Lecas, A.; Renko, Z.; Rose, R. *Chemical Communications* **1985**, 1820.

(95) Gray, G. M.; Duffey, C. H. *Organomettalics* **1994**, *13*, 1542.

(96) Gladysz, J. A.; Shima, T.; Hampel, F. *Angewandte Chemie International Edition* **2004**, *43*, 5537.

(97) Gladysz, J. A.; Nawara, A. J.; Shima, T.; Hampel, F. *Journal of the American Chemical Society* **2006**, *128*, 4962.

(98) Gladysz, J. A.; Hess, G. D.; Hampel, F. *Organomettalics* **2007**, *26*, 5129.

(99) Garcia-Garibay, M. A.; Dominguez, Z.; Dang, H.; Strouse, M. J. *Journal of the American Chemical Society* **2002**, *124*, 2398.

(100) Garcia-Garibay, M. A.; Dominguez, Z.; Dang, H.; Strouse, M. J. *Journal of the American Chemical Society* **2002**, *124*, 7719.

(101) Garcia-Garibay, M. A.; Godinez, C. E.; Zepeda, G. *Journal of the American Chemical Society* **2002**, *124*, 4701.

(102) Lyerla, J. R.; Yannoni, C. S.; Fyfe, C. A. *Accounts of Chemical Research***1982**, *15*, 208.

(103) Hoatson, G. L.; Vold, R. L. *NMR, Basic Principles And Progress* **1994**, *32*, 1-67.

(104) Garcia-Garibay, M. A.; Nunez, J. E.; Khuong, T. A. V.; Campos, L. M.; Farfan, N.; Dang, H.; Karlen, S. D. *Crystal Growth and Design* **2006**, *6*, 866.

(105) Garcia-Garibay, M. A.; Khuong, T. A. V.; Zepeda, G.; Ruiz, R.; Khan, S. I. *Crystal. Growth and Dessign* **2004**, *4*, 15.

(106) Garcia-Garibay, M. A.; Dominguez, Z.; Khuong, T. A. V.; Dang, H.; Sanrame, C. N.; Nunez, J. E. *Journal of the American Chemical Society* **2003**, *125*, 8827.

(107) Horansky, R. D.; Clarke, L. I.; Price, J. C.; Khuong, T. A. V.; Jarowski, P. D.; Garcia-Garibay, M. A. *Physical Review B.* **2005**, *72*, 014302.

(108) Horansky, R. D.; Clarke, L. I.; Winston, E. B.; Price, J. C.; Karlen, S. D.; Jarowski, P. D.; Santillan, R.; Garcia-Garibay, M. A. *Physical Review B.* **2006**, *74*, 054306.

(109) Garcia-Garibay, M. A.; Nunez, J. E.; Natarajan, A.; Khan, S. I. *Organic Letters* **2007**, *9*, 3559.

(110) Garcia-Garibay, M. A.; Gould, S. L.; Tranchemontagne, D.; Yaghi, O. M. *Journal of the American Chemical Society* **2008**, *130*, 3246.

(111) Garcia-Garibay, M. A.; Jarowski, P. D.; Houk, K. N. *Journal of the American Chemical Society* **2007**, *129*, 3110.

(112) Garcia-Garibay, M. A.; Khuong, T. A. V.; Dang, H.; Jarowski, P. D.; Maverick, E. F. *Journal of the American Chemical Society* **2007**, *129*, 839.

(113) Feringa, B. L.; Koumura, N.; Geertsema, E. M.; Meetsma, A. *Journal of the American Chemical Society* **2000**, *122*, 12005.

(114) Garcia-Garibay, M. A. *Proceedings of the National Academy of Sciences* **2005**, *102*, 10771.

(115) Garcia-Garibay, M. A.; Khuong, T. A. V.; Nunez, J. E.; Godinez, C. E. *Accounts of Chemical Research***2006**, *39*, 413.

(116) Gladysz, J. A.; Skopek, K. *Journal of Organometalic Chemistry* **2008**, *693*, 857.

(117) Kelly, T. R.; Sestelo, J. P. *Structure and Bonding* **2001**, *99*, 19.

(118) Mislow, K. *Chemtracts: Organic Chemistry* **1988**, *2*, 151.

(119) Kelly, T. R.; Tellitu, I.; Sestelo, J. P. *Angewandte Chemie International Edition* **1997**, *36*, 1866.

(120) Pratt, D. W.; Tan, X. Q. *Journal of Chemical Physics* **1994**, *100*, 7061.

(121) Pratt, D. W. *Annual Review of Physical Chemistry* **1998**, *49*, 481.

(122) Hirota, E.; Endo, Y. *Advaced Series in Physical Chemistry* **1997**, *9*, 1.

(123) Tinker Version 4.2 June 2004, J. W. Ponder, http://dasher.wustl.edu/tinker/.

(124) Dougherty, D. A.; Anslyn, E. V. *Modern Physical Organic Chemistry.*; Universtiy Science: Sausalito, California, 2006.

(125) Goodman, L.; Pophristic, V. *Journal of Physical Chemistry* **2003**, *107*, 3538.

Appendix A

Experimental Procedure for Synthesis in Chapter 3

General Procedure:

All air and moisture-sensitive reactions were carried out in flame dried glassware using standard Schlenk techniques under an inert atmosphere of dry nitrogen unless otherwise noted. Anhydrous solvents were used by drying over alumina. Reagents were used as received from Acros, Aldrich, Lancaster, and Strem unless otherwise noted. ^{1}H, ^{13}C, and ^{19}F NMR spectra were recorded with Varian Inova 300 (300MHz) spectrometer. High-Resolution mass spectra were performed at the Southern California Regional Mass Spectrometry Facility (University of California at Riverside).

3-Phenylthiophene: A flame dried 300-mL round-bottomed three-neck flask equipped with a magnetic stir bar, reflux condenser, and N_2 inlet was charged with Magnesium turnings (3.46 g, 0.142 mol) in anhydrous ether (150 mL). Bromobenzene (22.4 g, 0.142 mol) was added dropwise and the reaction was set to reflux until all magnesium was consumed, then cooled to room temperature. In a separate 500 round-bottomed three-neck flask equipped with a magnetic stir bar, reflux condenser, and N_2 inlet, 3-Bromothiophene (23.2 g, 0.142 mol) and $NiCl_2$(dppp) (0.77 g, 1.42×10^{-3} mol) in anhydrous ether (200 mL) was set to reflux. Phenymagnesium bromide was then cannulated to the refluxing 3-bromothiophene. After refluxing overnight, the mixture was allowed to cool to room temperature and then quenched with ice-water. The layers were separated, and the aqueous layer was extracted with diethyl ether. The

combined organic layers were washed with 5% HCl, water, and brine then dried over $MgSO_4$. The solvent was removed under reduced pressure leaving a yellow oil as crude. The crude extract was purified by silica gel column chromatography using hexane, to give a pale yellow oil in 92% yield. Spectral data matched previously reported synthesis. [1]

2-Bromo-3-Phenylthiophene: A solution of 3-phenyl thiophene (2.26 g, 14.1 mmol) in DMF (30 mL) was cooled in an ice bath and a solution of NBS (2.51g, 14.1 mmol) in DMF (20 mL) was added dropwise. The resulting mixture was stirred overnight. The mixture was poured into water and extracted with diethyl ether. The combined organic layer was washed with 5% HCl, water, brine and dried over $MgSO_4$. The solvent was removed under reduced pressure and the crude extract was purified by silica gel column chromatography using hexane, to give a pale yellow oil in 95% yield. Spectral data matched previously reported synthesis.[2]

2'-Bromo-3-phenyl-[2,3'] bithiophenyl: A flame dried 100-mL round-bottomed three-neck flask equipped with a magnetic stir bar, reflux condenser, and N_2 inlet was charged with Magnesium turnings (0.49 g, 20.2 mmol) in anhydrous ether (150 mL). 1,2-Dibromoethane (3.97 g, 21.2 mmol) was added dropwise and the reaction was set to reflux until all magnesium was consumed, it was then cooled to room temperature. In a separate 100 mL round-bottomed three-neck flask

equipped with a magnetic stir bar, reflux condenser, and N_2 inlet, a solution of 3-Bromothiophene (23.2 g, 0.142 mol) in anhydrous ether (60 mL), n-butyllithium (12.1 mL, 19.3mmol) was added slowly at -78 ºC. The mixture stirred for an additional 50 min, and then the $MgBr_2$ mixture was cannulated to it, and allowed to reach room temperature. In another 500 mL round bottomed three neck flask, 2-Bromo-3-phenylthiophene (4.0g, 16.7 mmol) in anhydrous ether (120 mL) and $NiCl_2$(dppp) was set to reflux while 3-thienylmagnesium bromide was cannulated. After refluxing overnight, the mixture was allowed to cool to room temperature and then quenched with ice-water. The layers were separated, and the aqueous layer was extracted with diethyl ether. The combined organic layers were washed with 5% HCl, water, and brine then dried over $MgSO_4$. The solvent was removed under reduced pressure leaving a yellow oil as crude. The crude extract was purified by silica gel column chromatography using hexane, to give a pale yellow oil in 66 % yield. ^{1}H NMR (300 MHz, CDCl3): δ 6.89-6.91 (dd, 1H), 7.09-7.10 (d, 1H), 7.13-7.15 (dd, 1H), 7.18-7.20 (dd, 1H), 7.24-7.25 (d, 1H), 7.33-7.37 (m, 5H). ^{13}C NMR (300 MHz, CDCl3): δ 119.76, 122.60, 123.39, 125.45, 126.06, 126.34, 127.08, 128.09, 128.39, 129.05, 130.4, 134.61, 138.2; MS: 242.36 ($C_{14}H_{10}S_2^+$, calc. 242.36).

2'-Bromo-3-phenyl-[2,3']bithiophenyl: A solution of 2'-Bromo-3-phenyl-[2,3'] bithiophenyl (2.67 g, 0.011 mmol) in DMF (20 mL) was cooled in an ice bath and a solution of NBS (1.96g, 0.011 mmol) in DMF (17 mL) was added dropwise.

The resulting mixture was stirred overnight. The mixture was poured into water and extracted with diethyl ether. The combined organic layer was washed with 5% HCl, water, brine and dried over $MgSO_4$. The solvent was removed under reduced pressure and the crude extract was purified by silica gel column chromatography using hexane, to give a pale yellow solid in 91% yield. ^1H NMR (300 MHz, $CDCl_3$): d 6.73-6.74 (d, 1H), 7.18-7.19 (d, 1H), 7.25-7.31 (m, 5H), 7.34-7.35 (d, 1H), 7.42-7.43 (d, 1H); MS: 321.24 ($C_{14}H_9BrS_2^+$, calc. 321.26).

3-Bromo-2-phenyl-thiophene: To a stirring solution of 2,3-dibromothiophene (1mL, 8.83 mmol) and $Pd(PPh_3)_4$ (0.82g, 0.71 mmol) in dioxane (100 mL), a solution of phenyl boronic acid (1.19g, 9.72 mmol) in 2 M Na_2CO_3 (17.7 mL) was added. The mixture was heated to 100 ºC and stirred for four hours. The mixture was cooled to room temperature, diluted with t-butyl methylether, poured into water, and extracted with TBME. The combined organic layer was washed with brine, and dried over $MgSO_4$. The solvent was removed under reduced pressure and the crude was purifed by silica gel column chromatography using hexane, to give a pale yellow oil in 61% yield. Spectral data matched previously reported synthesis. [3]

Compound 21: A flame dried 25-mL round-bottomed three-neck flask equipped with a magnetic stir bar, reflux condenser, and N_2 inlet was charged with Magnesium turnings (0.042 g, 1.71 mmol) in anhydrous ether (5 mL). 1,2-

Dibromoethane (0.154 mL, 1.80 mmol) was added dropwise and the reaction was set to reflux until all magnesium was consumed, it was then cooled to room temperature. In a separate round-bottomed three-neck flask equipped with a magnetic stir bar and N_2 inlet, a solution of 3-Bromo-2-phenyl-thiophene (0.37 g, 1.56 mmol) in anhydrous ether (5 mL) was placed in a dry ice/acetone (-78 ºC). n-Butyllithium (1.02 mL, 1.63 mmol) was added slowly and the mixture stirred for an additional 50 min, and then the $MgBr_2$ mixture was cannulated to the lithiated species and allowed to reach room temperature. In another round bottomed three neck flask equipped with a magnetic stir bar, reflux condenser, and N_2 inlet 2'-Bromo-3-phenyl-[2,3']bithiophenyl (0.50g, 1.56 mmol) in anhydrous ether (10 mL) and $NiCl_2$(dppp) was set to reflux while previously made grignard compound was cannulated. After refluxing overnight, the mixture was allowed to cool to room temperature and then quenched with ice-water. The layers were separated, and the aqueous layer was extracted with diethyl ether. The combined organic layers were washed with 5% HCl, water, and brine then dried over $MgSO_4$. The solvent was removed under reduced pressure leaving a yellow oil as crude. The crude extract was purified by silica gel column chromatography using hexane, to give a white solid in 43 % yield. ^{1}H NMR (300 MHz, CDCl3): δ 6.75-6.76 (d, 1H), 6.96-7.00 (dd, 4H), 7.03-7.06 (dd, 2H), 7.17-7.30 (m, 10H); ^{13}C NMR (300 MHz, CDCl3): δ 125.26, 125.42, 126.44, 126.66, 126.88, 128.06, 128.63, 128.73, 128.82, 129.17, 130.19, 139.92; HR-MS: 400.041 ($C_{24}H_{16}S_3^+$, calc. 400.58).

Compound 22: To a flame dried 25mL three-neck flask equipped with a magnetic stir bar, reflux condenser, and N_2 inlet, 2'-bromo-3-phenyl-[2,3']bithiophenyl (0.18g, 0.56 mmol) in dry THF (6 mL) was added. The flask was placed in a dry ice /acetone bath (-78 ºC) n-Buthyl Lithium (0.37mL, 0.59 mmol) was added dropwise allowed to stir for 50 minutes at -78 °C. In a separate flame dried flask, equipped with a magnetic stir bar, reflux condenser, and N_2 inlet $Fe(acac)_3$ (0.20 g, 0.56mmol) was dissolved in dry THF (1ml) and refluxed. The lithiated compound was then slowly added to this mixture via a cannula and refluxed overnight. The mixture was cooled to room temperature, diluted with ether and extracted with NH_4Cl, water, and brine and dried over $MgSO_4$. The solvent was removed using reduced pressure and the crude was re-crystallized from hexane to give pure compound 22 in 41% yield. ^{1}H NMR (300 MHz, CDCl3): δ 6.66−6.68 (d, 2H), 6.93-6.96 (q, 4H), 7.02-7.04 (d, 2H), 7.14-7.16 (d, 2H), 7.17-7.19 (t, 6H), 7.24-7.25 (d, 2H); ^{13}C NMR (300 MHz, CDCl3): δ 125.28, 126.04, 126.61, 128.07, 128.55, 128.96, 129.95, 132.04 HR-MS: 482.029 ($C_{28}H_{18}S_4^+$, calc. 482.70).

Compound 23: To a flame dried 25mL three-neck flask equipped with a magnetic stir bar, reflux condensor, and N_2 inlet 2-phenyl-3-bromo thiophene (200 mg, 0.84 mmol) in anhydrous diethyl ether (3 mL) was added. t-Buthyl Lithium (1.12 mL, 1.68 mmol) was added dropwise over the course of about 5 minutes and allowed to stir for 30 minutes at -78 °C. In a separate flame dried

flask, under N_2 at -78 °C, octafluorocyclopentene (0.056mL, 0.42 mmol) in anhydrous diethyl ether (4 mL) is added. The lithiothiophene species is added via cannula to the octafluorocyclopentene flask slowly. The reaction is allowed to slowly warm to room temperature and stir for an additional three hours at room temperature. The reaction is quenched with ice chips and saturated aqueous NH_4Cl. The product is extracted three times with ether, washed with brine, dried ($MgSO_4$) and the solvent removed under reduced pressure to yield the crude solid. Purification is done on silica using hexane as eluant, followed be recrystallization from hexane to yield pure compound 23 in 60% yield. ^{1}H NMR (300 MHz, CDCl3): δ 6.66-6.68 (d, 2H), 7.02-7.04 (d, 2H), 7.14-7.26 (m, 10H); ^{13}C NMR (300 MHz, CDCl3): δ 124.84, 127.34, 127.82, 127.98, 128.55, 221.72; ^{19}F NMR (300 MHz, CDCl3, C6F6): δ -132.39, -112.44; HR-MS: 492.044 ($C_{25}H_{14}F_6S_2^+$, calc. 492.50).

Compound 24: To a flame dried 25 mL 3-neck flask at -78 ^{o}C under a nitrogen atmosphere, 2-bromo-3-phenyl thiophene **(**200 mg, 0.84 mmol) in anhydrous diethyl ether (2.8 mL) was added. t-Buthyl Lithium (1.1 mL, 0.0017 mmol) was added dropwise over the course of about 5 minutes and allowed to stir for 30 minutes at -78 ^{o}C. In a separate flame dried flask, under N_2 at -78 ^{o}C, octafluorocyclopentene (89 mg, 0.42 mmol) in anhydrous diethyl ether (1 mL) is added. The lithiothiophene species is added via cannula to the octafluorocyclopentene flask slowly. The reaction is allowed to slowly warm to

room temperature and stir for an additional three hours at room temperature. The reaction is quenched with ice chips and saturated aqueous NH_4Cl. The product is extracted three times with ether, washed with brine, dried ($MgSO_4$) and the solvent removed under reduced pressure to yield the crude solid. Purification is done on silica using hexane as eluant, followed be recrystallization from hexane to yield pure compound 3 in 68% yield. ^1H NMR (300 MHz, $CDCl_3$): d= 6.79-6.85 (m, 4H), 7.19 – 7.26 (m, 5H); ^{19}F NMR (300 MHz, $CDCl_3$, C_6F_6): d-114.82 (t, *J* = 20 Hz), -134.44 (p, *J* = 20 Hz); HR-MS: 492.0441 ($C_{25}H_{14}F_6S_2^+$, calc. 492.0441).

Compound 25: To a flame dried 25 mL 3-neck flask at -78 ^oC under a nitrogen atmosphere, 2'-Bromo-3-phenyl-[2,3'] bithiophenyl **(**.510 g, 1.587 mmol) in anhydrous diethyl ether (2 mL) was added. t-Buthyl Lithium (0.99 mL, 1.587 mmol) was added dropwise over the course of about 5 minutes and allowed to stir for 30 minutes at -78 ^oC. In a separate flame dried flask, under N_2 at -78 ^oC, octafluorocyclopentene (0.11 mL, 0.7935 mmol) in anhydrous diethyl ether (1 mL) is added. The lithiothiophene species is added via cannula to the octafluorocyclopentene flask slowly. The reaction is allowed to slowly warm to room temperature and stir for an additional three hours at room temperature. The reaction is quenched with ice chips and saturated aqueous NH_4Cl. The product is extracted three times with ether, washed with brine, dried ($MgSO_4$) and the solvent removed under reduced pressure to yield the crude solid. Purification is

done on silica using hexane as eluant, followed be recrystallization from hexane to yield pure compound 25 in 50% yield. X-ray crystal structure showed a rearranged product.

Reference:

1. Robitaille, L.; Leclerc, M.; Callender C. L.; *Chem. Mater.* **1993**, *5*, 1755.
2. Kellogg, R. M.; Schaap, A. P.; Harper, E. T.; Wynberg, H.; *J. Org. Chem.* **1968**, *33*, 2902.
3. Pereira, R.; Iglesias, B.; De Lera, A. R.; *Tetrahedron*, **2001**, *57*, 7871.

Appendix B

Calculations for Compounds in Chapter 3

Computational Details: All calculations were performed using the Gaussian 031 molecular modeling package. Dihedral angles were fixed at defined values, and geometry optimized under those constraints, first at HF/3-21G* and then at HF/6-31G*. Single point OVGF (Outer Valence Green's Theorem) calculations were performed at HF/6-31G* level of theory. Gaussian log files follow for each single point calculation are included below.

60 Degree Dihedral Angles:

```
Entering Link 1 = C:\G03W\l1.exe PID=      3248.

 Copyright (c) 1988,1990,1992,1993,1995,1998,2003,
Gaussian, Inc.
                  All Rights Reserved.

 This is the Gaussian(R) 03 program.  It is based on the
 the Gaussian(R) 98 system (copyright 1998, Gaussian,
Inc.),
 the Gaussian(R) 94 system (copyright 1995, Gaussian,
Inc.),
 the Gaussian 92(TM) system (copyright 1992, Gaussian,
Inc.),
 the Gaussian 90(TM) system (copyright 1990, Gaussian,
Inc.),
 the Gaussian 88(TM) system (copyright 1988, Gaussian,
Inc.),
 the Gaussian 86(TM) system (copyright 1986, Carnegie
Mellon
 University), and the Gaussian 82(TM) system (copyright
1983,
 Carnegie Mellon University). Gaussian is a federally
registered
 trademark of Gaussian, Inc.

 This software contains proprietary and confidential
information,
 including trade secrets, belonging to Gaussian, Inc.
```

Cite this work as:
Gaussian 03, Revision B.05,
M. J. Frisch, G. W. Trucks, H. B. Schlegel, G. E.
Scuseria,
M. A. Robb, J. R. Cheeseman, J. A. Montgomery, Jr., T.
Vreven,
K. N. Kudin, J. C. Burant, J. M. Millam, S. S. Iyengar, J.
Tomasi,
V. Barone, B. Mennucci, M. Cossi, G. Scalmani, N. Rega,
G. A. Petersson, H. Nakatsuji, M. Hada, M. Ehara, K.
Toyota,
R. Fukuda, J. Hasegawa, M. Ishida, T. Nakajima, Y. Honda,
O. Kitao,
H. Nakai, M. Klene, X. Li, J. E. Knox, H. P. Hratchian, J.
B. Cross,
C. Adamo, J. Jaramillo, R. Gomperts, R. E. Stratmann, O.
Yazyev,
A. J. Austin, R. Cammi, C. Pomelli, J. W. Ochterski, P. Y.
Ayala,
K. Morokuma, G. A. Voth, P. Salvador, J. J. Dannenberg,
V. G. Zakrzewski, S. Dapprich, A. D. Daniels, M. C.
Strain,
O. Farkas, D. K. Malick, A. D. Rabuck, K. Raghavachari,
J. B. Foresman, J. V. Ortiz, Q. Cui, A. G. Baboul, S.
Clifford,
J. Cioslowski, B. B. Stefanov, G. Liu, A. Liashenko, P.
Piskorz,

```
 I. Komaromi, R. L. Martin, D. J. Fox, T. Keith, M. A. Al-
Laham,
 C. Y. Peng, A. Nanayakkara, M. Challacombe, P. M. W. Gill,
 B. Johnson, W. Chen, M. W. Wong, C. Gonzalez, and J. A.
Pople,
 Gaussian, Inc., Pittsburgh PA, 2003.

 ******************************************
 Gaussian 03:  x86-Win32-G03RevB.05  8-Nov-2003
                  28-Feb-2006
 ******************************************
 %chk=60.chk
 %mem=64MB
 %nproc=1
 Will use up to    1 processors via shared memory.
 Default route:  MaxDisk=2000MB
 ----------------------------------------------------------
----
 # hf/6-31g(d) geom=(modredundant,connectivity) symm=loose
ovgf
 ----------------------------------------------------------
----
 1/18=120,38=1,57=2/1;
 2/17=4,18=3,40=1/2;
 3/5=1,6=6,7=1,11=9,16=1,25=1,30=1/1,2,3;
 4//1;
 5/5=2,38=5/2;
 8/6=4,9=120000,10=2,27=262144000/1,4;
 9/11=20000,27=262144000/8;
 6/7=2,8=2,9=2,10=2/1;
 99/5=1,9=1/99;
 --
 60
 --
 Symbolic Z-matrix:
 Charge =  0 Multiplicity = 1
 C                     1.34204   0.83075   0.27319
 C                     0.9563    1.62883  -0.71125
 C                     0.55818   0.35562   1.43633
 C                    -0.55818  -0.35562   1.43633
 C                    -1.34204  -0.83075   0.27319
 C                    -0.9563   -1.62883  -0.71125
 H                     0.99089   0.59456   2.39597
 H                    -0.99089  -0.59456   2.39597
 H                     1.676     1.83911  -1.48774
```

```
 H                     2.36707   0.49297   0.26147
 H                    -1.676    -1.83911  -1.48774
 H                    -2.36707  -0.49297   0.26147
 C                    -0.36987   2.25649  -0.90994
 H                    -0.8464    2.04278  -1.85458
 C                    -0.9563    3.08844  -0.07016
 H                    -0.50779   3.35422   0.87046
 H                    -1.91104   3.53023  -0.2946
 C                     0.36987  -2.25649  -0.90994
 H                     0.8464   -2.04278  -1.85458
 C                     0.9563   -3.08844  -0.07016
 H                     1.91104  -3.53023  -0.2946
 H                     0.50779  -3.35422   0.87046

 The following ModRedundant input section has been read:
 D    5    6   18   20 60.000 F
 D    3    4    5    6 60.000 F
 D    2    1    3    4 60.000 F
 D    1    2   13   15 60.000 F
 Iteration  1 RMS(Cart)=  0.00000044 RMS(Int)=  0.00000012
 Iteration  1 RMS(Cart)=  0.00000022 RMS(Int)=  0.00000006
                         Input orientation:
 ---------------------------------------------------------------
-----------
 Center     Atomic     Atomic              Coordinates
(Angstroms)
 Number     Number      Type              X           Y
Z
 ---------------------------------------------------------------
-----------
    1          6             0        1.342038    0.830750
0.273189
    2          6             0        0.956300    1.628828
-0.711247
    3          6             0        0.558176    0.355616
1.436331
    4          6             0       -0.558176   -0.355616
1.436331
    5          6             0       -1.342038   -0.830750
0.273189
    6          6             0       -0.956300   -1.628828
-0.711247
    7          1             0        0.990889    0.594562
2.395972
```

```
    8          1             0       -0.990889   -0.594562
2.395972
    9          1             0        1.676003    1.839114
-1.487740
   10          1             0        2.367070    0.492970
0.261466
   11          1             0       -1.676003   -1.839114
-1.487740
   12          1             0       -2.367070   -0.492970
0.261466
   13          6             0       -0.369874    2.256490
-0.909940
   14          1             0       -0.846398    2.042781
-1.854578
   15          6             0       -0.956300    3.088438
-0.070162
   16          1             0       -0.507792    3.354219
0.870460
   17          1             0       -1.911039    3.530232
-0.294594
   18          6             0        0.369874   -2.256490
-0.909940
   19          1             0        0.846398   -2.042781
-1.854578
   20          6             0        0.956300   -3.088438
-0.070162
   21          1             0        1.911039   -3.530232
-0.294594
   22          1             0        0.507792   -3.354219
0.870460
 -------------------------------------------------------------
-----------
                    Distance matrix (angstroms):
                    1          2          3          4
5
     1  C    0.000000
     2  C    1.324702   0.000000
     3  C    1.480909   2.528174   0.000000
     4  C    2.524119   3.292985   1.323666   0.000000
     5  C    3.156714   3.507278   2.524119   1.480909
0.000000
     6  C    3.507278   3.777614   3.292985   2.528174
1.324702
     7  H    2.164555   3.275013   1.079466   2.055079
3.461253
```

```
     8  H    3.461253   4.288335   2.055079   1.079466
2.164555
     9  H    2.056502   1.079414   3.464173   4.284692
4.397455
    10  H    1.079316   2.055874   2.161312   3.264578
3.938255
    11  H    4.397455   4.422509   4.284692   3.464173
2.056502
    12  H    3.938255   4.061156   3.264578   2.161312
1.079316
    13  C    2.522532   1.480599   3.159048   3.516183
3.446149
    14  H    3.284153   2.174461   3.955937   4.082335
3.609741
    15  C    3.239969   2.489877   3.468642   3.780150
3.953065
    16  H    3.185357   2.760857   3.232354   3.753082
4.308905
    17  H    4.265219   3.465627   4.378506   4.463873
4.434446
    18  C    3.446149   3.934345   3.516183   3.159048
2.522532
    19  H    3.609741   3.847077   4.082335   3.955937
3.284153
    20  C    3.953065   4.760630   3.780150   3.468642
3.239969
    21  H    4.434446   5.263177   4.463873   4.378506
4.265219
    22  H    4.308905   5.247258   3.753082   3.232354
3.185357
                   6          7          8          9
10
     6  C    0.000000
     7  H    4.288335   0.000000
     8  H    3.275013   2.311160   0.000000
     9  H    4.422509   4.135397   5.302670   0.000000
    10  H    4.061156   2.541714   4.124892   2.312876
0.000000
    11  H    1.079414   5.302670   4.135397   4.976475
4.984453
    12  H    2.055874   4.124892   2.541714   4.984453
4.835717
    13  C    3.934345   3.942427   4.409445   2.166488
3.460210
```

```
    14  H    3.847077   4.851818   5.004361   2.557060
4.148003
    15  C    4.760630   4.011581   4.432551   3.240271
4.229801
    16  H    5.247258   3.491266   4.260685   3.553253
4.101518
    17  H    5.263177   4.927321   5.009965   4.141298
5.276019
    18  C    1.480599   4.409445   3.942427   4.337487
3.594511
    19  H    2.174461   5.004361   4.851818   3.986467
3.635948
    20  C    2.489877   4.432551   4.011581   5.177670
3.863513
    21  H    3.465627   5.009965   4.927321   5.505335
4.086970
    22  H    2.760857   4.260685   3.491266   5.822072
4.316092
                   11         12         13         14
15
    11  H    0.000000
    12  H    2.312876   0.000000
    13  C    4.337487   3.594511   0.000000
    14  H    3.986467   3.635948   1.079392   0.000000
    15  C    5.177670   3.863513   1.319568   2.071139
0.000000
    16  H    5.822072   4.316092   2.096152   3.043083
1.075439
    17  H    5.505335   4.086970   2.091951   2.404063
1.075676
    18  C    2.166488   3.460210   4.573206   4.566770
5.570657
    19  H    2.557060   4.148003   4.566770   4.422373
5.723921
    20  C    3.240271   4.229801   5.570657   5.723921
6.466208
    21  H    4.141298   5.276019   6.250389   6.410576
7.216565
    22  H    3.553253   4.101518   5.951485   6.195746
6.673542
                   16         17         18         19
20
    16  H    0.000000
    17  H    1.832330   0.000000
    18  C    5.951485   6.250389   0.000000
```

```
    19  H    6.195746   6.410576   1.079392   0.000000
    20  C    6.673542   7.216565   1.319568   2.071139
0.000000
    21  H    7.389436   8.028602   2.091951   2.404063
1.075676
    22  H    6.784876   7.389436   2.096152   3.043083
1.075439
                  21         22
    21  H    0.000000
    22  H    1.832330   0.000000
 Stoichiometry    C10H12
 Framework group  C2[X(C10H12)]
 Deg. of freedom    31
 Full point group                 C2      NOp   2
 Largest Abelian subgroup         C2      NOp   2
 Largest concise Abelian subgroup C2      NOp   2
                         Standard orientation:
 ---------------------------------------------------------
-----------
 Center     Atomic     Atomic              Coordinates
(Angstroms)
 Number     Number      Type              X           Y
Z
 ---------------------------------------------------------
-----------
    1          6             0        1.342038    0.830750
0.273189
    2          6             0        0.956300    1.628828
-0.711247
    3          6             0        0.558176    0.355616
1.436331
    4          6             0       -0.558176   -0.355616
1.436331
    5          6             0       -1.342038   -0.830750
0.273189
    6          6             0       -0.956300   -1.628828
-0.711247
    7          1             0        0.990889    0.594562
2.395972
    8          1             0       -0.990889   -0.594562
2.395972
    9          1             0        1.676003    1.839114
-1.487740
   10          1             0        2.367070    0.492970
0.261466
```

```
   11          1             0       -1.676003   -1.839114
-1.487740
   12          1             0       -2.367070   -0.492970
0.261466
   13          6             0       -0.369874    2.256490
-0.909940
   14          1             0       -0.846398    2.042781
-1.854578
   15          6             0       -0.956300    3.088438
-0.070163
   16          1             0       -0.507792    3.354219
0.870460
   17          1             0       -1.911039    3.530232
-0.294594
   18          6             0        0.369874   -2.256490
-0.909940
   19          1             0        0.846398   -2.042781
-1.854578
   20          6             0        0.956300   -3.088438
-0.070163
   21          1             0        1.911039   -3.530232
-0.294594
   22          1             0        0.507792   -3.354219
0.870460
 ---------------------------------------------------------
-----------
 Rotational constants (GHZ):      2.1828635      0.8288598
0.8089055
 Standard basis: 6-31G(d) (6D, 7F)
 There are    87 symmetry adapted basis functions of A
symmetry.
 There are    87 symmetry adapted basis functions of B
symmetry.
 Integral buffers will be    262144 words long.
 Raffenetti 1 integral format.
 Two-electron integral symmetry is turned on.
   174 basis functions,   328 primitive gaussians,   174
cartesian basis functions
    36 alpha electrons       36 beta electrons
       nuclear repulsion energy       468.3790477886
Hartrees.
 NAtoms=   22 NActive=   22 NUniq=   11 SFac= 5.66D+00
NAtFMM=   60 Big=F
 One-electron integrals computed using PRISM.
 NBasis=   174 RedAO= T  NBF=    87    87
```

```
 NBsUse=   174 1.00D-06 NBFU=    87    87
 Harris functional with IExCor=  205 diagonalized for
initial guess.
 ExpMin= 1.61D-01 ExpMax= 3.05D+03 ExpMxC= 4.57D+02 IAcc=1
IRadAn=         1 AccDes= 1.00D-06
 HarFok:  IExCor= 205 AccDes= 1.00D-06 IRadAn=         1
IDoV=1
 ScaDFX=  1.000000  1.000000  1.000000  1.000000
 Initial guess orbital symmetries:
       Occupied  (A) (B) (B) (A) (A) (B) (A) (B) (A) (B)
(A) (B)
                 (A) (B) (A) (B) (A) (B) (A) (B) (A) (A)
(B) (A)
                 (B) (A) (B) (A) (B) (A) (B) (B) (A) (B)
(A) (B)
       Virtual   (A) (B) (A) (B) (A) (A) (A) (B) (A) (B)
(B) (A)
                 (A) (B) (A) (B) (B) (A) (B) (B) (A) (A)
(B) (B)
                 (A) (A) (B) (B) (A) (A) (B) (A) (B) (A)
(B) (A)
                 (B) (B) (A) (A) (B) (B) (A) (A) (B) (A)
(B) (A)
                 (A) (B) (B) (A) (B) (B) (A) (B) (A) (B)
(A) (B)
                 (A) (B) (A) (A) (B) (A) (A) (B) (B) (A)
(B) (B)
                 (A) (A) (B) (B) (B) (A) (A) (B) (A) (B)
(B) (A)
                 (B) (B) (A) (A) (B) (A) (B) (A) (B) (A)
(A) (B)
                 (A) (A) (B) (B) (A) (B) (A) (B) (A) (A)
(B) (A)
                 (B) (A) (B) (B) (A) (A) (B) (A) (A) (B)
(B) (B)
                 (A) (A) (B) (A) (B) (B) (A) (B) (A) (B)
(A) (B)
                 (A) (B) (A) (B) (A) (B)
 The electronic state of the initial guess is 1-A.
 Requested convergence on RMS density matrix=1.00D-08
within 128 cycles.
 Requested convergence on MAX density matrix=1.00D-06.
 Requested convergence on             energy=1.00D-06.
 No special actions if energy rises.
```

```
 Integral accuracy reduced to 1.0D-05 until final
iterations.
 Initial convergence to 1.0D-05 achieved.  Increase
integral accuracy.
 SCF Done:  E(RHF) =  -385.549638782     A.U. after   13
cycles
             Convg  =    0.9801D-08             -V/T =
2.0008
             S**2   =   0.0000
 ExpMin= 1.61D-01 ExpMax= 3.05D+03 ExpMxC= 4.57D+02 IAcc=1
IRadAn=         1 AccDes= 1.00D-06
 HarFok:  IExCor= 205 AccDes= 1.00D-06 IRadAn=         1
IDoV=1
 ScaDFX=  1.000000  1.000000  1.000000  1.000000
 Range of M.O.s used for correlation:    11   174
 NBasis=   174 NAE=    36 NBE=    36 NFC=    10 NFV=     0
 NROrb=    164 NOA=    26 NOB=    26 NVA=   138 NVB=   138
 Semi-Direct transformation.
 ModeAB=           4 MOrb=            25 LenV=
7786580
 LASXX=     25541776 LTotXX=    25541776 LenRXX=
51559950
 LTotAB=    26018174 MaxLAS=    31365984 LenRXY=
0
 NonZer=    77101726 LenScr=   123368960 LnRSAI=
30159600
 LnScr1=    51404800 LExtra=     2955347 Total=
259448657
 MaxDsk=   262144000 SrtSym=           T ITran=
4
 JobTyp=0 Pass  1:  I=   1 to  13.
 JobTyp=0 Pass  2:  I=  14 to  26.
 Spin components of T(2) and E(2):
     alpha-alpha T2 =       0.5634358735D-01 E2=     -
0.1567331676D+00
     alpha-beta  T2 =       0.3424046216D+00 E2=     -
0.9427908386D+00
     beta-beta   T2 =       0.5634358735D-01 E2=     -
0.1567331676D+00
 ANorm=    0.1206271858D+01
 E2=       -0.1256257174D+01 EUMP2=       -
0.38680589595605D+03
 GREENY: Electron Propagator Program
 Petite list used in FoFDir.
 MinBra= 0 MaxBra= 2 Meth= 1.
```

```
 IRaf=       0 NMat=   1 IRICut=       1 DoRegI=T DoRafI=F
ISym2E=-1 JSym2E=1.

 Orbital window will be selected automatically

    Alpha HOMO is orbital  26

 GREENY has selected a window containing alpha orbitals

             8 through  27

 from symmetry group number 1 of the 2 total symmetry
operations

 Summary of results for alpha spin-orbital   8  OVGF:
 Koopmans theorem:            -0.77167D+00 au  -20.998 eV
 Converged second order pole: -0.66158D+00 au  -18.002 eV
0.843 (PS)
 Converged third  order pole: -0.68946D+00 au  -18.761 eV
0.853 (PS)
 Outer Valence Approximation: -0.67892D+00 au  -18.474 eV
0.842 (PS)

 Summary of results for alpha spin-orbital   9  OVGF:
 Koopmans theorem:            -0.72271D+00 au  -19.666 eV
 Converged second order pole: -0.62266D+00 au  -16.944 eV
0.853 (PS)
 Converged third  order pole: -0.64891D+00 au  -17.658 eV
0.869 (PS)
 Outer Valence Approximation: -0.63905D+00 au  -17.389 eV
0.858 (PS)

 Summary of results for alpha spin-orbital  10  OVGF:
 Koopmans theorem:            -0.67629D+00 au  -18.403 eV
 Converged second order pole: -0.58460D+00 au  -15.908 eV
0.858 (PS)
 Converged third  order pole: -0.61003D+00 au  -16.600 eV
0.875 (PS)
 Outer Valence Approximation: -0.60063D+00 au  -16.344 eV
0.864 (PS)

 Summary of results for alpha spin-orbital  11  OVGF:
 Koopmans theorem:            -0.66439D+00 au  -18.079 eV
 Converged second order pole: -0.57168D+00 au  -15.556 eV
0.851 (PS)
```

```
 Converged third  order pole: -0.60059D+00 au  -16.343 eV
0.875 (PS)
 Outer Valence Approximation: -0.58935D+00 au  -16.037 eV
0.862 (PS)

 Summary of results for alpha spin-orbital  12  OVGF:
 Koopmans theorem:            -0.64441D+00 au  -17.535 eV
 Converged second order pole: -0.55980D+00 au  -15.233 eV
0.868 (PS)
 Converged third  order pole: -0.58214D+00 au  -15.841 eV
0.886 (PS)
 Outer Valence Approximation: -0.57315D+00 au  -15.596 eV
0.876 (PS)

 Summary of results for alpha spin-orbital  13  OVGF:
 Koopmans theorem:            -0.63098D+00 au  -17.170 eV
 Converged second order pole: -0.54641D+00 au  -14.869 eV
0.865 (PS)
 Converged third  order pole: -0.56961D+00 au  -15.500 eV
0.884 (PS)
 Outer Valence Approximation: -0.56002D+00 au  -15.239 eV
0.874 (PS)

 Summary of results for alpha spin-orbital  14  OVGF:
 Koopmans theorem:            -0.60195D+00 au  -16.380 eV
 Converged second order pole: -0.52345D+00 au  -14.244 eV
0.874 (PS)
 Converged third  order pole: -0.54370D+00 au  -14.795 eV
0.891 (PS)
 Outer Valence Approximation: -0.53536D+00 au  -14.568 eV
0.883 (PS)

 Summary of results for alpha spin-orbital  15  OVGF:
 Koopmans theorem:            -0.60130D+00 au  -16.362 eV
 Converged second order pole: -0.51053D+00 au  -13.892 eV
0.864 (PS)
 Converged third  order pole: -0.53810D+00 au  -14.642 eV
0.896 (PS)
 Outer Valence Approximation: -0.52472D+00 au  -14.278 eV
0.884 (PS)

 Summary of results for alpha spin-orbital  16  OVGF:
 Koopmans theorem:            -0.57874D+00 au  -15.748 eV
 Converged second order pole: -0.49902D+00 au  -13.579 eV
0.875 (PS)
```

```
 Converged third  order pole: -0.52029D+00 au  -14.158 eV
0.896 (PS)
 Outer Valence Approximation: -0.51096D+00 au  -13.904 eV
0.888 (PS)

 Summary of results for alpha spin-orbital  17  OVGF:
 Koopmans theorem:            -0.56771D+00 au  -15.448 eV
 Converged second order pole: -0.48992D+00 au  -13.331 eV
0.878 (PS)
 Converged third  order pole: -0.51154D+00 au  -13.920 eV
0.900 (PS)
 Outer Valence Approximation: -0.50197D+00 au  -13.659 eV
0.892 (PS)

 Summary of results for alpha spin-orbital  18  OVGF:
 Koopmans theorem:            -0.53470D+00 au  -14.550 eV
 Converged second order pole: -0.46248D+00 au  -12.585 eV
0.883 (PS)
 Converged third  order pole: -0.48340D+00 au  -13.154 eV
0.903 (PS)
 Outer Valence Approximation: -0.47458D+00 au  -12.914 eV
0.895 (PS)

 Summary of results for alpha spin-orbital  19  OVGF:
 Koopmans theorem:            -0.50377D+00 au  -13.708 eV
 Converged second order pole: -0.43422D+00 au  -11.816 eV
0.886 (PS)
 Converged third  order pole: -0.45519D+00 au  -12.386 eV
0.907 (PS)
 Outer Valence Approximation: -0.44628D+00 au  -12.144 eV
0.899 (PS)

 Summary of results for alpha spin-orbital  20  OVGF:
 Koopmans theorem:            -0.47996D+00 au  -13.060 eV
 Converged second order pole: -0.40981D+00 au  -11.152 eV
0.886 (PS)
 Converged third  order pole: -0.43192D+00 au  -11.753 eV
0.910 (PS)
 Outer Valence Approximation: -0.42215D+00 au  -11.487 eV
0.901 (PS)

 Summary of results for alpha spin-orbital  21  OVGF:
 Koopmans theorem:            -0.46887D+00 au  -12.759 eV
 Converged second order pole: -0.39557D+00 au  -10.764 eV
0.882 (PS)
```

```
 Converged third  order pole: -0.41993D+00 au  -11.427 eV
0.908 (PS)
 Outer Valence Approximation: -0.40884D+00 au  -11.125 eV
0.899 (PS)

 Summary of results for alpha spin-orbital  22  OVGF:
 Koopmans theorem:            -0.40334D+00 au  -10.975 eV
 Converged second order pole: -0.36870D+00 au  -10.033 eV
0.889 (PS)
 Converged third  order pole: -0.38015D+00 au  -10.345 eV
0.904 (PS)
 Outer Valence Approximation: -0.37355D+00 au  -10.165 eV
0.898 (PS)

 Summary of results for alpha spin-orbital  23  OVGF:
 Koopmans theorem:            -0.39947D+00 au  -10.870 eV
 Converged second order pole: -0.36189D+00 au   -9.847 eV
0.881 (PS)
 Converged third  order pole: -0.37563D+00 au  -10.221 eV
0.899 (PS)
 Outer Valence Approximation: -0.36796D+00 au  -10.013 eV
0.892 (PS)

 Summary of results for alpha spin-orbital  24  OVGF:
 Koopmans theorem:            -0.37628D+00 au  -10.239 eV
 Converged second order pole: -0.34911D+00 au   -9.500 eV
0.895 (PS)
 Converged third  order pole: -0.35815D+00 au   -9.746 eV
0.907 (PS)
 Outer Valence Approximation: -0.35260D+00 au   -9.595 eV
0.903 (PS)

 Summary of results for alpha spin-orbital  25  OVGF:
 Koopmans theorem:            -0.33196D+00 au   -9.033 eV
 Converged second order pole: -0.31098D+00 au   -8.462 eV
0.895 (PS)
 Converged third  order pole: -0.31909D+00 au   -8.683 eV
0.907 (PS)
 Outer Valence Approximation: -0.31740D+00 au   -8.637 eV
0.904 (PS)

 Summary of results for alpha spin-orbital  26  OVGF:
 Koopmans theorem:            -0.30532D+00 au   -8.308 eV
 Converged second order pole: -0.28616D+00 au   -7.787 eV
0.891 (PS)
```

```
 Converged third  order pole: -0.29486D+00 au   -8.023 eV
0.906 (PS)
 Outer Valence Approximation: -0.29295D+00 au   -7.971 eV
0.902 (PS)
 DD1Dir will call FoFDir   4 times, MxPair=       176
 NAB=   351 NAA=     0 NBB=     0 NumPrc=  1.

 Summary of results for alpha spin-orbital  27  OVGF:
 Koopmans theorem:             0.13752D+00 au    3.742 eV
 Converged second order pole:  0.70769D-01 au    1.926 eV
0.904 (PS)
 Converged third  order pole:  0.10397D+00 au    2.829 eV
0.912 (PS)
 Outer Valence Approximation:  0.97670D-01 au    2.658 eV
0.910 (PS)


**********************************************************
**********

            Population analysis using the SCF density.


**********************************************************
**********

 Orbital symmetries:
       Occupied  (A) (B) (A) (B) (A) (B) (A) (B) (A) (B)
(A) (B)
                 (A) (B) (A) (B) (A) (B) (A) (B) (A) (B)
(A) (B)
                 (A) (A) (B) (A) (B) (A) (B) (A) (B) (B)
(A) (B)
       Virtual   (A) (B) (A) (A) (B) (A) (B) (A) (B) (A)
(B) (A)
                 (B) (A) (B) (A) (B) (A) (B) (A) (B) (A)
(B) (A)
                 (B) (A) (B) (B) (A) (A) (B) (A) (A) (B)
(B) (A)
                 (B) (A) (B) (B) (A) (A) (A) (B) (B) (A)
(B) (A)
                 (B) (A) (B) (B) (A) (A) (B) (A) (B) (B)
(A) (A)
                 (B) (A) (B) (A) (B) (A) (B) (A) (B) (A)
(B) (B)
```

```
                 (A) (A) (B) (B) (B) (A) (A) (B) (A) (B)
(B) (A)
                 (B) (B) (A) (A) (B) (A) (B) (A) (B) (A)
(A) (B)
                 (A) (B) (A) (B) (A) (B) (A) (B) (A) (A)
(B) (A)
                 (B) (A) (B) (B) (A) (A) (B) (A) (B) (A)
(B) (A)
                 (B) (A) (B) (A) (B) (B) (A) (B) (A) (B)
(A) (B)
                 (A) (B) (A) (B) (A) (B)
 The electronic state is 1-A.
 Alpha  occ. eigenvalues --  -11.22876 -11.22870 -11.22807
-11.22786 -11.22779
 Alpha  occ. eigenvalues --  -11.22677 -11.22666 -11.22621
-11.21565 -11.21565
 Alpha  occ. eigenvalues --   -1.11022  -1.08242  -1.04459
-1.00367  -0.96674
 Alpha  occ. eigenvalues --   -0.86373  -0.81985  -0.77167
-0.72271  -0.67629
 Alpha  occ. eigenvalues --   -0.66439  -0.64441  -0.63098
-0.60195  -0.60130
 Alpha  occ. eigenvalues --   -0.57874  -0.56771  -0.53470
-0.50377  -0.47996
 Alpha  occ. eigenvalues --   -0.46887  -0.40334  -0.39947
-0.37628  -0.33196
 Alpha  occ. eigenvalues --   -0.30532
 Alpha virt. eigenvalues --    0.13752   0.15296   0.19780
0.21790   0.23023
 Alpha virt. eigenvalues --    0.27405   0.28028   0.28909
0.29187   0.30244
 Alpha virt. eigenvalues --    0.30512   0.31667   0.34050
0.34206   0.34572
 Alpha virt. eigenvalues --    0.35383   0.36708   0.43174
0.48826   0.50639
 Alpha virt. eigenvalues --    0.51259   0.55771   0.56773
0.61741   0.62527
 Alpha virt. eigenvalues --    0.65366   0.66488   0.69020
0.72206   0.75121
 Alpha virt. eigenvalues --    0.76678   0.76937   0.78012
0.78940   0.79267
 Alpha virt. eigenvalues --    0.82085   0.83607   0.85609
0.87256   0.90326
 Alpha virt. eigenvalues --    0.92390   0.93136   0.93797
0.93818   0.95113
```

```
 Alpha virt. eigenvalues --    0.95424   0.98254   1.01903
1.04557   1.04607
 Alpha virt. eigenvalues --    1.09979   1.12583   1.12664
1.13859   1.14084
 Alpha virt. eigenvalues --    1.14358   1.14501   1.17187
1.17324   1.17470
 Alpha virt. eigenvalues --    1.18627   1.18760   1.22661
1.23635   1.25278
 Alpha virt. eigenvalues --    1.25309   1.28283   1.28391
1.34384   1.35119
 Alpha virt. eigenvalues --    1.39100   1.42391   1.43788
1.44628   1.49981
 Alpha virt. eigenvalues --    1.55686   1.61676   1.64044
1.74639   1.76735
 Alpha virt. eigenvalues --    1.80407   1.80989   1.83674
1.90023   1.90117
 Alpha virt. eigenvalues --    1.93802   1.97563   2.00551
2.04964   2.08660
 Alpha virt. eigenvalues --    2.10570   2.20207   2.20230
2.24639   2.26986
 Alpha virt. eigenvalues --    2.28388   2.28662   2.32371
2.32738   2.35588
 Alpha virt. eigenvalues --    2.36063   2.40615   2.44152
2.46105   2.52383
 Alpha virt. eigenvalues --    2.54631   2.56641   2.62134
2.62750   2.71135
 Alpha virt. eigenvalues --    2.73702   2.79539   2.79860
2.83020   2.84746
 Alpha virt. eigenvalues --    2.85581   2.89902   2.90447
2.99138   3.09372
 Alpha virt. eigenvalues --    3.10041   3.17662   3.18051
3.24729   3.27075
 Alpha virt. eigenvalues --    3.32768   3.48135   3.62694
4.48925   4.56086
 Alpha virt. eigenvalues --    4.59396   4.63166   4.64228
4.68751   4.79868
 Alpha virt. eigenvalues --    4.82100   4.90607   5.04910
          Condensed to atoms (all electrons):
               1          2          3          4          5
6
     1  C    4.921917   0.676225   0.379414  -0.050810  -
0.005463   0.000033
     2  C    0.676225   4.928649  -0.050407  -0.001868
0.000033  -0.001400
```

```
     3  C    0.379414  -0.050407   4.918074   0.679731  -
0.050810  -0.001868
     4  C   -0.050810  -0.001868   0.679731   4.918074
0.379414  -0.050407
     5  C   -0.005463   0.000033  -0.050810   0.379414
4.921917   0.676225
     6  C    0.000033  -0.001400  -0.001868  -0.050407
0.676225   4.928649
     7  H   -0.040400   0.001360   0.388568  -0.038973
0.003506  -0.000063
     8  H    0.003506  -0.000063  -0.038973   0.388568  -
0.040400   0.001360
     9  H   -0.039165   0.389855   0.003551  -0.000063  -
0.000027  -0.000034
    10  H    0.388211  -0.038748  -0.039835   0.001310
0.000180  -0.000212
    11  H   -0.000027  -0.000034  -0.000063   0.003551  -
0.039165   0.389855
    12  H    0.000180  -0.000212   0.001310  -0.039835
0.388211  -0.038748
    13  C   -0.052886   0.377118  -0.005803  -0.000776
0.000113   0.000190
    14  H    0.001596  -0.039189   0.000117  -0.000188
0.000306   0.000352
    15  C   -0.002973  -0.049371   0.001533  -0.000942  -
0.000121  -0.000005
    16  H    0.001674  -0.002595   0.000713   0.000083  -
0.000022   0.000000
    17  H    0.000004   0.003309  -0.000011  -0.000007
0.000001  -0.000001
    18  C    0.000113   0.000190  -0.000776  -0.005803  -
0.052886   0.377118
    19  H    0.000306   0.000352  -0.000188   0.000117
0.001596  -0.039189
    20  C   -0.000121  -0.000005  -0.000942   0.001533  -
0.002973  -0.049371
    21  H    0.000001  -0.000001  -0.000007  -0.000011
0.000004   0.003309
    22  H   -0.000022   0.000000   0.000083   0.000713
0.001674  -0.002595
              7          8          9         10         11
12
     1  C   -0.040400   0.003506  -0.039165   0.388211  -
0.000027   0.000180
```

```
     2  C    0.001360  -0.000063   0.389855  -0.038748  -
0.000034  -0.000212
     3  C    0.388568  -0.038973   0.003551  -0.039835  -
0.000063   0.001310
     4  C   -0.038973   0.388568  -0.000063   0.001310
0.003551  -0.039835
     5  C    0.003506  -0.040400  -0.000027   0.000180  -
0.039165   0.388211
     6  C   -0.000063   0.001360  -0.000034  -0.000212
0.389855  -0.038748
     7  H    0.507011  -0.004179  -0.000127   0.000396
0.000002  -0.000133
     8  H   -0.004179   0.507011   0.000002  -0.000133  -
0.000127   0.000396
     9  H   -0.000127   0.000002   0.507479  -0.004154  -
0.000002  -0.000001
    10  H    0.000396  -0.000133  -0.004154   0.503007  -
0.000001  -0.000006
    11  H    0.000002  -0.000127  -0.000002  -0.000001
0.507479  -0.004154
    12  H   -0.000133   0.000396  -0.000001  -0.000006  -
0.004154   0.503007
    13  C    0.000278  -0.000020  -0.041932   0.003467
0.000017   0.000469
    14  H   -0.000005  -0.000001   0.000343  -0.000125
0.000023   0.000086
    15  C   -0.000220  -0.000035   0.001487  -0.000073
0.000000   0.000314
    16  H   -0.000032  -0.000004   0.000160  -0.000040
0.000000  -0.000003
    17  H   -0.000004  -0.000002  -0.000112   0.000003
0.000000   0.000013
    18  C   -0.000020   0.000278   0.000017   0.000469  -
0.041932   0.003467
    19  H   -0.000001  -0.000005   0.000023   0.000086
0.000343  -0.000125
    20  C   -0.000035  -0.000220   0.000000   0.000314
0.001487  -0.000073
    21  H   -0.000002  -0.000004   0.000000   0.000013  -
0.000112   0.000003
    22  H   -0.000004  -0.000032   0.000000  -0.000003
0.000160  -0.000040
             13         14         15         16         17
18
```

```
     1  C   -0.052886   0.001596  -0.002973   0.001674
0.000004   0.000113
     2  C    0.377118  -0.039189  -0.049371  -0.002595
0.003309   0.000190
     3  C   -0.005803   0.000117   0.001533   0.000713  -
0.000011  -0.000776
     4  C   -0.000776  -0.000188  -0.000942   0.000083  -
0.000007  -0.005803
     5  C    0.000113   0.000306  -0.000121  -0.000022
0.000001  -0.052886
     6  C    0.000190   0.000352  -0.000005   0.000000  -
0.000001   0.377118
     7  H    0.000278  -0.000005  -0.000220  -0.000032  -
0.000004  -0.000020
     8  H   -0.000020  -0.000001  -0.000035  -0.000004  -
0.000002   0.000278
     9  H   -0.041932   0.000343   0.001487   0.000160  -
0.000112   0.000017
    10  H    0.003467  -0.000125  -0.000073  -0.000040
0.000003   0.000469
    11  H    0.000017   0.000023   0.000000   0.000000
0.000000  -0.041932
    12  H    0.000469   0.000086   0.000314  -0.000003
0.000013   0.003467
    13  C    4.905466   0.390537   0.658481  -0.042714  -
0.039806  -0.000073
    14  H    0.390537   0.501416  -0.038926   0.003423  -
0.003367  -0.000005
    15  C    0.658481  -0.038926   5.018622   0.397056
0.393218   0.000002
    16  H   -0.042714   0.003423   0.397056   0.489505  -
0.027534   0.000000
    17  H   -0.039806  -0.003367   0.393218  -0.027534
0.501792   0.000000
    18  C   -0.000073  -0.000005   0.000002   0.000000
0.000000   4.905466
    19  H   -0.000005  -0.000005   0.000000   0.000000
0.000000   0.390537
    20  C    0.000002   0.000000   0.000000   0.000000
0.000000   0.658481
    21  H    0.000000   0.000000   0.000000   0.000000
0.000000  -0.039806
    22  H    0.000000   0.000000   0.000000   0.000000
0.000000  -0.042714
             19         20         21         22
```

1	C	0.000306	-0.000121	0.000001	-0.000022
2	C	0.000352	-0.000005	-0.000001	0.000000
3	C	-0.000188	-0.000942	-0.000007	0.000083
4	C	0.000117	0.001533	-0.000011	0.000713
5	C	0.001596	-0.002973	0.000004	0.001674
6	C	-0.039189	-0.049371	0.003309	-0.002595
7	H	-0.000001	-0.000035	-0.000002	-0.000004
8	H	-0.000005	-0.000220	-0.000004	-0.000032
9	H	0.000023	0.000000	0.000000	0.000000
10	H	0.000086	0.000314	0.000013	-0.000003
11	H	0.000343	0.001487	-0.000112	0.000160
12	H	-0.000125	-0.000073	0.000003	-0.000040
13	C	-0.000005	0.000002	0.000000	0.000000
14	H	-0.000005	0.000000	0.000000	0.000000
15	C	0.000000	0.000000	0.000000	0.000000
16	H	0.000000	0.000000	0.000000	0.000000
17	H	0.000000	0.000000	0.000000	0.000000
18	C	0.390537	0.658481	-0.039806	-0.042714
19	H	0.501416	-0.038926	-0.003367	0.003423
20	C	-0.038926	5.018622	0.393218	0.397056
21	H	-0.003367	0.393218	0.501792	-0.027534
22	H	0.003423	0.397056	-0.027534	0.489505

Mulliken atomic charges:

		1
1	C	-0.181313
2	C	-0.193200
3	C	-0.183413
4	C	-0.183413
5	C	-0.181313
6	C	-0.193200
7	H	0.183077
8	H	0.183077
9	H	0.182697
10	H	0.185875
11	H	0.182697
12	H	0.185875
13	C	-0.152123
14	H	0.183613
15	C	-0.378049
16	H	0.180331
17	H	0.172506
18	C	-0.152123
19	H	0.183613
20	C	-0.378049
21	H	0.172506

```
    22  H    0.180331
 Sum of Mulliken charges=   0.00000
 Atomic charges with hydrogens summed into heavy atoms:
              1
     1  C    0.004562
     2  C   -0.010503
     3  C   -0.000336
     4  C   -0.000336
     5  C    0.004562
     6  C   -0.010503
     7  H    0.000000
     8  H    0.000000
     9  H    0.000000
    10  H    0.000000
    11  H    0.000000
    12  H    0.000000
    13  C    0.031490
    14  H    0.000000
    15  C   -0.025213
    16  H    0.000000
    17  H    0.000000
    18  C    0.031490
    19  H    0.000000
    20  C   -0.025213
    21  H    0.000000
    22  H    0.000000
 Sum of Mulliken charges=   0.00000
 Electronic spatial extent (au):  <R**2>=  1647.2795
 Charge=     0.0000 electrons
 Dipole moment (field-independent basis, Debye):
    X=     0.0000    Y=     0.0000    Z=    -0.0906  Tot=
0.0906
 Quadrupole moment (field-independent basis, Debye-Ang):
   XX=   -57.3734   YY=   -63.8789   ZZ=   -56.6788
   XY=    -1.8519   XZ=     0.0000   YZ=     0.0000
 Traceless Quadrupole moment (field-independent basis,
Debye-Ang):
   XX=     1.9370   YY=    -4.5686   ZZ=     2.6316
   XY=    -1.8519   XZ=     0.0000   YZ=     0.0000
 Octapole moment (field-independent basis, Debye-Ang**2):
  XXX=     0.0000  YYY=     0.0000  ZZZ=     0.7101  XYY=
0.0000
  XXY=     0.0000  XXZ=    -2.6634  XZZ=     0.0000  YZZ=
0.0000
  YYZ=     5.3301  XYZ=     0.6778
```

```
 Hexadecapole moment (field-independent basis, Debye-
Ang**3):
 XXXX=  -413.0386 YYYY= -1548.6674 ZZZZ=  -358.0820 XXXY=
39.9444
 XXXZ=     0.0000 YYYX=     5.6750 YYYZ=     0.0000 ZZZX=
0.0000
 ZZZY=     0.0000 XXYY=  -302.2516 XXZZ=  -129.0599 YYZZ=
-305.5614
 XXYZ=     0.0000 YYXZ=     0.0000 ZZXY=    23.7119
 N-N= 4.683790477886D+02 E-N=-1.834285768678D+03  KE=
3.852427277881D+02
 Symmetry A    KE= 1.928317612380D+02
 Symmetry B    KE= 1.924109665502D+02
 1|1|UNPC-UNK|SP|ROVGF-FC|6-31G(d)|C10H12|PCUSER|28-Feb-
2006|0||# HF/6-
 31G(D) GEOM=(MODREDUNDANT,CONNECTIVITY) SYMM=LOOSE
OVGF||60||0,1|C,0,1

.3420378805,0.8307501895,0.2731885939|C,0,0.9562999368,1.62
88284545,-0

.7112472133|C,0,0.5581759103,0.3556161409,1.4363305941|C,0,
-0.55817591
 03,-0.3556161409,1.4363305941|C,0,-1.3420378805,-
0.8307501895,0.273188
 5939|C,0,-0.9562999368,-1.6288284545,-
0.7112472133|H,0,0.9908889182,0.
 5945621229,2.395971595|H,0,-0.9908889182,-
0.5945621229,2.395971595|H,0
 ,1.6760029771,1.8391136684,-
1.487740118|H,0,2.3670698862,0.4929702081,
 0.2614655622|H,0,-1.6760029771,-1.8391136684,-
1.487740118|H,0,-2.36706
 98862,-0.4929702081,0.2614655622|C,0,-
0.3698739567,2.2564897614,-0.909
 9399552|H,0,-0.8463979776,2.0427812495,-1.854578055|C,0,-
0.9562999564,
 3.0884382735,-0.0701624716|H,0,-
0.5077919839,3.3542186807,0.870459709|
 H,0,-1.9110389287,3.5302324504,-
0.2945942412|C,0,0.3698739567,-2.25648
 97614,-0.9099399552|H,0,0.8463979776,-2.0427812495,-
1.854578055|C,0,0.
 9562999564,-3.0884382735,-0.0701624716|H,0,1.9110389287,-
3.5302324504,
```

```
 -0.2945942412|H,0,0.5077919839,-
3.3542186807,0.870459709||Version=x86-
 Win32-G03RevB.05|State=1-A|HF=-385.5496388|MP2=-
386.805896|RMSD=9.801e
 -009|PG=C02 [X(C10H12)]||@


 When I told the people of Northern Ireland that I was
 an atheist, a woman in the audience stood up and said,
 "Yes, but is it the God of the Catholics or the God
 of the Protestants in whom you don't believe?"
                                -- Quentin Crisp
 Job cpu time:  0 days  2 hours 29 minutes 58.0 seconds.
 File lengths (MBytes):  RWF=   1984 Int=      0 D2E=
0 Chk=     11 Scr=      1
 Normal termination of Gaussian 03 at Tue Feb 28 17:00:47
2006.
```

120 Degree Dihedral Angles:

```
Entering Link 1 = C:\G03W\l1.exe PID=      3996.

 Copyright (c) 1988,1990,1992,1993,1995,1998,2003,
Gaussian, Inc.
                  All Rights Reserved.

 This is the Gaussian(R) 03 program.  It is based on the
 the Gaussian(R) 98 system (copyright 1998, Gaussian,
Inc.),
 the Gaussian(R) 94 system (copyright 1995, Gaussian,
Inc.),
 the Gaussian 92(TM) system (copyright 1992, Gaussian,
Inc.),
 the Gaussian 90(TM) system (copyright 1990, Gaussian,
Inc.),
 the Gaussian 88(TM) system (copyright 1988, Gaussian,
Inc.),
 the Gaussian 86(TM) system (copyright 1986, Carnegie
Mellon
 University), and the Gaussian 82(TM) system (copyright
1983,
```

```
 ---------------------------------------------------------------
-----
 Warning -- This program may not be used in any manner that
 competes with the business of Gaussian, Inc. or will
provide
 assistance to any competitor of Gaussian, Inc.  The
licensee
 of this program is prohibited from giving any competitor
of
 Gaussian, Inc. access to this program.  By using this
program,
 the user acknowledges that Gaussian, Inc. is engaged in
the
 business of creating and licensing software in the field
of
 computational chemistry and represents and warrants to the
 licensee that it is not a competitor of Gaussian, Inc. and
that
 it will not use this program in any manner prohibited
above.
 ---------------------------------------------------------------
-----


 Cite this work as:
 Gaussian 03, Revision B.05,
 M. J. Frisch, G. W. Trucks, H. B. Schlegel, G. E.
Scuseria,
 M. A. Robb, J. R. Cheeseman, J. A. Montgomery, Jr., T.
Vreven,
 K. N. Kudin, J. C. Burant, J. M. Millam, S. S. Iyengar, J.
Tomasi,
 V. Barone, B. Mennucci, M. Cossi, G. Scalmani, N. Rega,
 G. A. Petersson, H. Nakatsuji, M. Hada, M. Ehara, K.
Toyota,
 R. Fukuda, J. Hasegawa, M. Ishida, T. Nakajima, Y. Honda,
O. Kitao,
 H. Nakai, M. Klene, X. Li, J. E. Knox, H. P. Hratchian, J.
B. Cross,
 C. Adamo, J. Jaramillo, R. Gomperts, R. E. Stratmann, O.
Yazyev,
 A. J. Austin, R. Cammi, C. Pomelli, J. W. Ochterski, P. Y.
Ayala,
 K. Morokuma, G. A. Voth, P. Salvador, J. J. Dannenberg,
```

```
 V. G. Zakrzewski, S. Dapprich, A. D. Daniels, M. C.
Strain,
 O. Farkas, D. K. Malick, A. D. Rabuck, K. Raghavachari,
 J. B. Foresman, J. V. Ortiz, Q. Cui, A. G. Baboul, S.
Clifford,
 J. Cioslowski, B. B. Stefanov, G. Liu, A. Liashenko, P.
Piskorz,
 I. Komaromi, R. L. Martin, D. J. Fox, T. Keith, M. A. Al-
Laham,
 C. Y. Peng, A. Nanayakkara, M. Challacombe, P. M. W. Gill,
 B. Johnson, W. Chen, M. W. Wong, C. Gonzalez, and J. A.
Pople,
 Gaussian, Inc., Pittsburgh PA, 2003.

 ******************************************
 Gaussian 03:  x86-Win32-G03RevB.05  8-Nov-2003
                  28-Feb-2006
 ******************************************
 %chk=120.chk
 %mem=64MB
 %nproc=1
 Will use up to    1 processors via shared memory.
 Default route:  MaxDisk=2000MB
 ----------------------------------------------------------
----
 # hf/6-31g(d) geom=(modredundant,connectivity) symm=loose
ovgf
 ----------------------------------------------------------
----
 1/18=120,38=1,57=2/1;
 2/17=4,18=3,40=1/2;
 3/5=1,6=6,7=1,11=9,16=1,25=1,30=1/1,2,3;
 4//1;
 5/5=2,38=5/2;
 8/6=4,9=120000,10=2,27=262144000/1,4;
 9/11=20000,27=262144000/8;
 6/7=2,8=2,9=2,10=2/1;
 99/5=1,9=1/99;
 ---
 120
 ---
 Symbolic Z-matrix:
 Charge =  0 Multiplicity = 1
 C                    -0.71958   1.32317   0.54956
 C                    -0.33104   2.55816   0.82871
```

```
 C                    -0.33104   0.57388  -0.67139
 C                     0.33104  -0.57388  -0.67139
 C                     0.71958  -1.32317   0.54956
 C                     0.33104  -2.55816   0.82871
 H                    -0.56074   1.0372   -1.61693
 H                     0.56074  -1.0372   -1.61693
 H                    -0.67325   3.01219   1.74442
 H                    -1.31367   0.793     1.2757
 H                     0.67325  -3.01219   1.74442
 H                     1.31367  -0.793     1.2757
 C                     0.48421   3.4103   -0.07442
 H                     1.43308   3.00914  -0.39254
 C                     0.08696   4.57611  -0.55026
 H                    -0.8613    5.00839  -0.27957
 H                     0.70124   5.14614  -1.22423
 C                    -0.48421  -3.4103   -0.07442
 H                    -1.43308  -3.00914  -0.39254
 C                    -0.08696  -4.57611  -0.55026
 H                    -0.70124  -5.14614  -1.22423
 H                     0.8613   -5.00839  -0.27957

 The following ModRedundant input section has been read:
 D    1    2   13   15 120.00 F
 D    2    1    3    4 120.00 F
 D    3    4    5    6 120.00 F
 D    5    6   18   20 120.00 F
 Iteration  1 RMS(Cart)=  0.00000040 RMS(Int)=  0.00000025
 Iteration  1 RMS(Cart)=  0.00000020 RMS(Int)=  0.00000013
                         Input orientation:
 ---------------------------------------------------------------
-----------
 Center     Atomic     Atomic              Coordinates
(Angstroms)
 Number     Number      Type              X           Y
Z
 ---------------------------------------------------------------
-----------
    1          6             0       -0.719575    1.323165
0.549558
    2          6             0       -0.331044    2.558156
0.828706
    3          6             0       -0.331044    0.573875
-0.671394
    4          6             0        0.331044   -0.573875
-0.671394
```

```
    5          6             0        0.719575   -1.323165
0.549558
    6          6             0        0.331044   -2.558156
0.828706
    7          1             0       -0.560741    1.037196
-1.616930
    8          1             0        0.560741   -1.037196
-1.616930
    9          1             0       -0.673251    3.012194
1.744420
   10          1             0       -1.313670    0.793002
1.275699
   11          1             0        0.673251   -3.012194
1.744420
   12          1             0        1.313670   -0.793002
1.275699
   13          6             0        0.484211    3.410296
-0.074419
   14          1             0        1.433078    3.009142
-0.392535
   15          6             0        0.086960    4.576111
-0.550263
   16          1             0       -0.861298    5.008391
-0.279566
   17          1             0        0.701237    5.146140
-1.224225
   18          6             0       -0.484211   -3.410296
-0.074419
   19          1             0       -1.433078   -3.009142
-0.392535
   20          6             0       -0.086960   -4.576111
-0.550263
   21          1             0       -0.701237   -5.146140
-1.224225
   22          1             0        0.861298   -5.008391
-0.279566
 -------------------------------------------------------------
-----------
                    Distance matrix (angstroms):
                    1          2          3          4
5
     1  C    0.000000
     2  C    1.324418   0.000000
     3  C    1.484290   2.487503   0.000000
     4  C    2.488631   3.535291   1.325025   0.000000
```

```
     5  C    3.012344   4.030680   2.488631   1.484290
0.000000
     6  C    4.030680   5.158975   3.535291   2.487503
1.324418
     7  H    2.191045   2.889155   1.077713   2.069992
3.450244
     8  H    3.450244   4.438803   2.069992   1.077713
2.191045
     9  H    2.069458   1.077862   3.449443   4.438992
4.707759
    10  H    1.077637   2.069088   2.191972   2.892163
3.023165
    11  H    4.707759   5.733754   4.438992   3.449443
2.069458
    12  H    3.023165   3.759674   2.892163   2.191972
1.077637
    13  C    2.488888   1.485402   3.011030   4.031558
4.780210
    14  H    2.892053   2.192474   3.020002   3.759023
4.490603
    15  C    3.527288   2.479601   4.025828   5.157190
6.034175
    16  H    3.780003   2.741000   4.483261   5.721617
6.578389
    17  H    4.447488   3.460894   4.719834   5.758579
6.708096
    18  C    4.780210   6.038338   4.031558   3.011030
2.488888
    19  H    4.490603   5.805233   3.759023   3.020002
2.892053
    20  C    6.034175   7.270413   5.157190   4.025828
3.527288
    21  H    6.708096   7.981713   5.758579   4.719834
4.447488
    22  H    6.578389   7.739676   5.721617   4.483261
3.780003
                   6          7          8          9
10
     6  C    0.000000
     7  H    4.438803   0.000000
     8  H    2.889155   2.358140   0.000000
     9  H    5.733754   3.900249   5.405457   0.000000
    10  H    3.759674   2.998972   3.902607   2.356829
0.000000
```

```
    11  H    1.077862   5.405457   3.900249   6.173031
4.318225
    12  H    2.069088   3.902607   2.998972   4.318225
3.068928
    13  C    6.038338   3.017096   4.708013   2.192346
3.450424
    14  H    5.805233   3.059906   4.316592   3.000535
3.903704
    15  C    7.270413   3.752494   5.733364   2.879119
4.428071
    16  H    7.739676   4.201103   6.352941   2.848979
4.515860
    17  H    7.981713   4.316274   6.197387   3.905867
5.409184
    18  C    1.485402   4.708013   3.017096   6.677746
4.492053
    19  H    2.192474   4.316592   3.059906   6.434314
4.153742
    20  C    2.479601   5.733364   3.752494   7.949319
5.802269
    21  H    3.460894   6.197387   4.316274   8.681707
6.472874
    22  H    2.741000   6.352941   4.201103   8.413152
6.387918
                  11         12         13         14
15
    11  H    0.000000
    12  H    2.356829   0.000000
    13  C    6.677746   4.492053   0.000000
    14  H    6.434314   4.153742   1.078179   0.000000
    15  C    7.949319   5.802269   1.320363   2.071787
0.000000
    16  H    8.413152   6.387918   2.099139   3.045310
1.076725
    17  H    8.681707   6.472874   2.093396   2.407085
1.075404
    18  C    2.192346   3.450424   6.889001   6.707189
8.020933
    19  H    3.000535   3.903704   6.707189   6.665928
7.737665
    20  C    2.879119   4.428071   8.020933   7.737665
9.153874
    21  H    3.905867   5.409184   8.714353   8.470870
9.777404
```

```
    22  H    2.848979   4.515860   8.429625   8.038690
9.619540
                   16         17         18         19
20
    16  H    0.000000
    17  H    1.831085   0.000000
    18  C    8.429625   8.714353   0.000000
    19  H    8.038690   8.470870   1.078179   0.000000
    20  C    9.619540   9.777404   1.320363   2.071787
0.000000
    21  H   10.199632  10.387394   2.093396   2.407085
1.075404
    22  H   10.163821  10.199632   2.099139   3.045310
1.076725
                   21         22
    21  H    0.000000
    22  H    1.831085   0.000000
 Stoichiometry    C10H12
 Framework group  C2[X(C10H12)]
 Deg. of freedom    31
 Full point group                 C2      NOp   2
 Largest Abelian subgroup         C2      NOp   2
 Largest concise Abelian subgroup C2      NOp   2
                         Standard orientation:
 ---------------------------------------------------------
-----------
 Center     Atomic     Atomic              Coordinates
(Angstroms)
 Number     Number      Type              X           Y
Z
 ---------------------------------------------------------
-----------
    1          6             0       -0.719574    1.323165
0.549558
    2          6             0       -0.331044    2.558157
0.828706
    3          6             0       -0.331044    0.573875
-0.671394
    4          6             0        0.331044   -0.573875
-0.671394
    5          6             0        0.719574   -1.323165
0.549558
    6          6             0        0.331044   -2.558157
0.828706
```

```
    7          1             0       -0.560740    1.037196
-1.616930
    8          1             0        0.560740   -1.037196
-1.616930
    9          1             0       -0.673250    3.012194
1.744420
   10          1             0       -1.313669    0.793003
1.275699
   11          1             0        0.673250   -3.012194
1.744420
   12          1             0        1.313669   -0.793003
1.275699
   13          6             0        0.484212    3.410296
-0.074419
   14          1             0        1.433078    3.009142
-0.392535
   15          6             0        0.086961    4.576111
-0.550263
   16          1             0       -0.861297    5.008391
-0.279565
   17          1             0        0.701238    5.146140
-1.224225
   18          6             0       -0.484212   -3.410296
-0.074419
   19          1             0       -1.433078   -3.009142
-0.392535
   20          6             0       -0.086961   -4.576111
-0.550263
   21          1             0       -0.701238   -5.146140
-1.224225
   22          1             0        0.861297   -5.008391
-0.279565
 -------------------------------------------------------------
-----------
 Rotational constants (GHZ):      5.3052467      0.4327807
0.4237209
 Standard basis: 6-31G(d) (6D, 7F)
 There are    87 symmetry adapted basis functions of A
symmetry.
 There are    87 symmetry adapted basis functions of B
symmetry.
 Integral buffers will be    262144 words long.
 Raffenetti 1 integral format.
 Two-electron integral symmetry is turned on.
```

```
   174 basis functions,   328 primitive gaussians,   174
cartesian basis functions
    36 alpha electrons       36 beta electrons
       nuclear repulsion energy       435.6270472138
Hartrees.
 NAtoms=   22 NActive=   22 NUniq=   11 SFac= 5.66D+00
NAtFMM=   60 Big=F
 One-electron integrals computed using PRISM.
 NBasis=   174 RedAO= T  NBF=    87    87
 NBsUse=   174 1.00D-06 NBFU=    87    87
 Harris functional with IExCor=  205 diagonalized for
initial guess.
 ExpMin= 1.61D-01 ExpMax= 3.05D+03 ExpMxC= 4.57D+02 IAcc=1
IRadAn=         1 AccDes= 1.00D-06
 HarFok:  IExCor= 205 AccDes= 1.00D-06 IRadAn=         1
IDoV=1
 ScaDFX=  1.000000  1.000000  1.000000  1.000000
 Initial guess orbital symmetries:
       Occupied  (B) (A) (A) (B) (A) (B) (A) (B) (A) (B)
(A) (B)
                 (A) (B) (A) (B) (A) (B) (A) (B) (A) (A)
(B) (A)
                 (B) (B) (A) (A) (B) (B) (A) (A) (B) (B)
(A) (B)
       Virtual   (A) (B) (A) (B) (A) (A) (B) (A) (B) (A)
(A) (B)
                 (A) (B) (A) (B) (B) (A) (B) (B) (A) (A)
(B) (A)
                 (B) (B) (B) (A) (A) (A) (B) (B) (A) (B)
(A) (A)
                 (B) (A) (B) (A) (B) (A) (B) (A) (B) (A)
(B) (A)
                 (B) (B) (A) (A) (B) (B) (A) (B) (A) (B)
(A) (B)
                 (A) (A) (B) (A) (A) (B) (B) (A) (B) (B)
(A) (A)
                 (B) (A) (B) (B) (B) (A) (B) (A) (B) (A)
(B) (B)
                 (A) (A) (A) (B) (B) (A) (B) (A) (B) (A)
(A) (B)
                 (A) (A) (B) (B) (A) (B) (A) (B) (A) (B)
(A) (A)
                 (B) (A) (B) (A) (B) (A) (B) (A) (A) (B)
(B) (B)
```

```
                 (A) (A) (B) (B) (A) (B) (A) (B) (A) (B)
(A) (B)
                 (A) (A) (B) (B) (A) (B)
 The electronic state of the initial guess is 1-A.
 Requested convergence on RMS density matrix=1.00D-08
within 128 cycles.
 Requested convergence on MAX density matrix=1.00D-06.
 Requested convergence on             energy=1.00D-06.
 No special actions if energy rises.
 Integral accuracy reduced to 1.0D-05 until final
iterations.
 Initial convergence to 1.0D-05 achieved.  Increase
integral accuracy.
 SCF Done:  E(RHF) =  -385.551577749     A.U. after   13
cycles
             Convg  =    0.4159D-08             -V/T =
2.0007
             S**2   =   0.0000
 ExpMin= 1.61D-01 ExpMax= 3.05D+03 ExpMxC= 4.57D+02 IAcc=1
IRadAn=         1 AccDes= 1.00D-06
 HarFok:  IExCor= 205 AccDes= 1.00D-06 IRadAn=         1
IDoV=1
 ScaDFX=  1.000000  1.000000  1.000000  1.000000
 Range of M.O.s used for correlation:    11   174
 NBasis=   174 NAE=    36 NBE=    36 NFC=    10 NFV=     0
 NROrb=    164 NOA=    26 NOB=    26 NVA=   138 NVB=   138
 Semi-Direct transformation.
 ModeAB=           4 MOrb=            26 LenV=
7798105
 LASXX=     25541776 LTotXX=    25541776 LenRXX=
51559950
 LTotAB=    26018174 MaxLAS=    27101984 LenRXY=
0
 NonZer=    77101726 LenScr=   123368960 LnRSAI=
27101984
 LnScr1=    45844480 LExtra=     2955347 Total=
250830721
 MaxDsk=   262144000 SrtSym=           T ITran=
4
 JobTyp=0 Pass  1:  I=   1 to  26.
 Spin components of T(2) and E(2):
     alpha-alpha T2 =       0.5602002508D-01 E2=     -
0.1561642180D+00
     alpha-beta  T2 =       0.3419856691D+00 E2=     -
0.9415797981D+00
```

```
     beta-beta   T2 =       0.5602002508D-01 E2=     -
0.1561642180D+00
 ANorm=    0.1205829888D+01
 E2=       -0.1253908234D+01 EUMP2=       -
0.38680548598306D+03
 GREENY: Electron Propagator Program
 Petite list used in FoFDir.
 MinBra= 0 MaxBra= 2 Meth= 1.
 IRaf=       0 NMat=   1 IRICut=       1 DoRegI=T DoRafI=F
ISym2E=-1 JSym2E=1.

 Orbital window will be selected automatically

    Alpha HOMO is orbital  26

 GREENY has selected a window containing alpha orbitals

            9 through  27

 from symmetry group number 1 of the 2 total symmetry
operations

 Summary of results for alpha spin-orbital   9  OVGF:
 Koopmans theorem:            -0.73823D+00 au  -20.088 eV
 Converged second order pole: -0.63855D+00 au  -17.376 eV
0.850 (PS)
 Converged third  order pole: -0.66273D+00 au  -18.034 eV
0.860 (PS)
 Outer Valence Approximation: -0.65397D+00 au  -17.795 eV
0.849 (PS)

 Summary of results for alpha spin-orbital  10  OVGF:
 Koopmans theorem:            -0.69417D+00 au  -18.889 eV
 Converged second order pole: -0.60207D+00 au  -16.383 eV
0.859 (PS)
 Converged third  order pole: -0.62482D+00 au  -17.002 eV
0.870 (PS)
 Outer Valence Approximation: -0.61662D+00 au  -16.779 eV
0.861 (PS)

 Summary of results for alpha spin-orbital  11  OVGF:
 Koopmans theorem:            -0.65531D+00 au  -17.832 eV
 Converged second order pole: -0.56505D+00 au  -15.376 eV
0.861 (PS)
```

```
 Converged third  order pole: -0.58916D+00 au  -16.032 eV
0.881 (PS)
 Outer Valence Approximation: -0.57881D+00 au  -15.750 eV
0.871 (PS)

 Summary of results for alpha spin-orbital  12  OVGF:
 Koopmans theorem:            -0.63902D+00 au  -17.389 eV
 Converged second order pole: -0.54577D+00 au  -14.851 eV
0.848 (PS)
 Converged third  order pole: -0.57567D+00 au  -15.665 eV
0.872 (PS)
 Outer Valence Approximation: -0.56356D+00 au  -15.335 eV
0.859 (PS)

 Summary of results for alpha spin-orbital  13  OVGF:
 Koopmans theorem:            -0.63863D+00 au  -17.378 eV
 Converged second order pole: -0.55425D+00 au  -15.082 eV
0.867 (PS)
 Converged third  order pole: -0.57522D+00 au  -15.653 eV
0.884 (PS)
 Outer Valence Approximation: -0.56612D+00 au  -15.405 eV
0.876 (PS)

 Summary of results for alpha spin-orbital  14  OVGF:
 Koopmans theorem:            -0.61355D+00 au  -16.695 eV
 Converged second order pole: -0.53237D+00 au  -14.486 eV
0.871 (PS)
 Converged third  order pole: -0.55247D+00 au  -15.033 eV
0.888 (PS)
 Outer Valence Approximation: -0.54374D+00 au  -14.796 eV
0.880 (PS)

 Summary of results for alpha spin-orbital  15  OVGF:
 Koopmans theorem:            -0.60755D+00 au  -16.532 eV
 Converged second order pole: -0.52952D+00 au  -14.409 eV
0.871 (PS)
 Converged third  order pole: -0.54920D+00 au  -14.945 eV
0.883 (PS)
 Outer Valence Approximation: -0.54192D+00 au  -14.747 eV
0.875 (PS)

 Summary of results for alpha spin-orbital  16  OVGF:
 Koopmans theorem:            -0.57410D+00 au  -15.622 eV
 Converged second order pole: -0.49409D+00 au  -13.445 eV
0.876 (PS)
```

```
 Converged third  order pole: -0.51471D+00 au  -14.006 eV
0.899 (PS)
 Outer Valence Approximation: -0.50454D+00 au  -13.729 eV
0.891 (PS)

 Summary of results for alpha spin-orbital  17  OVGF:
 Koopmans theorem:            -0.56384D+00 au  -15.343 eV
 Converged second order pole: -0.48266D+00 au  -13.134 eV
0.875 (PS)
 Converged third  order pole: -0.50369D+00 au  -13.706 eV
0.900 (PS)
 Outer Valence Approximation: -0.49327D+00 au  -13.423 eV
0.892 (PS)

 Summary of results for alpha spin-orbital  18  OVGF:
 Koopmans theorem:            -0.54933D+00 au  -14.948 eV
 Converged second order pole: -0.47228D+00 au  -12.851 eV
0.876 (PS)
 Converged third  order pole: -0.49466D+00 au  -13.460 eV
0.896 (PS)
 Outer Valence Approximation: -0.48512D+00 au  -13.201 eV
0.888 (PS)

 Summary of results for alpha spin-orbital  19  OVGF:
 Koopmans theorem:            -0.51383D+00 au  -13.982 eV
 Converged second order pole: -0.44291D+00 au  -12.052 eV
0.883 (PS)
 Converged third  order pole: -0.46368D+00 au  -12.617 eV
0.902 (PS)
 Outer Valence Approximation: -0.45512D+00 au  -12.384 eV
0.894 (PS)

 Summary of results for alpha spin-orbital  20  OVGF:
 Koopmans theorem:            -0.48446D+00 au  -13.183 eV
 Converged second order pole: -0.41489D+00 au  -11.290 eV
0.885 (PS)
 Converged third  order pole: -0.43588D+00 au  -11.861 eV
0.906 (PS)
 Outer Valence Approximation: -0.42673D+00 au  -11.612 eV
0.898 (PS)

 Summary of results for alpha spin-orbital  21  OVGF:
 Koopmans theorem:            -0.47343D+00 au  -12.883 eV
 Converged second order pole: -0.40364D+00 au  -10.984 eV
0.879 (PS)
```

```
 Converged third  order pole: -0.42619D+00 au  -11.597 eV
0.903 (PS)
 Outer Valence Approximation: -0.41573D+00 au  -11.313 eV
0.894 (PS)

 Summary of results for alpha spin-orbital  22  OVGF:
 Koopmans theorem:            -0.40895D+00 au  -11.128 eV
 Converged second order pole: -0.36670D+00 au   -9.978 eV
0.881 (PS)
 Converged third  order pole: -0.38089D+00 au  -10.365 eV
0.897 (PS)
 Outer Valence Approximation: -0.37365D+00 au  -10.168 eV
0.891 (PS)

 Summary of results for alpha spin-orbital  23  OVGF:
 Koopmans theorem:            -0.39855D+00 au  -10.845 eV
 Converged second order pole: -0.36618D+00 au   -9.964 eV
0.887 (PS)
 Converged third  order pole: -0.37651D+00 au  -10.245 eV
0.899 (PS)
 Outer Valence Approximation: -0.37051D+00 au  -10.082 eV
0.895 (PS)

 Summary of results for alpha spin-orbital  24  OVGF:
 Koopmans theorem:            -0.37294D+00 au  -10.148 eV
 Converged second order pole: -0.34548D+00 au   -9.401 eV
0.890 (PS)
 Converged third  order pole: -0.35457D+00 au   -9.648 eV
0.902 (PS)
 Outer Valence Approximation: -0.34891D+00 au   -9.494 eV
0.898 (PS)

 Summary of results for alpha spin-orbital  25  OVGF:
 Koopmans theorem:            -0.34224D+00 au   -9.313 eV
 Converged second order pole: -0.32064D+00 au   -8.725 eV
0.892 (PS)
 Converged third  order pole: -0.32843D+00 au   -8.937 eV
0.903 (PS)
 Outer Valence Approximation: -0.32311D+00 au   -8.792 eV
0.900 (PS)

 Summary of results for alpha spin-orbital  26  OVGF:
 Koopmans theorem:            -0.31041D+00 au   -8.447 eV
 Converged second order pole: -0.29130D+00 au   -7.927 eV
0.888 (PS)
```

```
 Converged third  order pole: -0.29920D+00 au   -8.142 eV
0.901 (PS)
 Outer Valence Approximation: -0.29750D+00 au   -8.095 eV
0.897 (PS)
 DD1Dir will call FoFDir   4 times, MxPair=       176
 NAB=   351 NAA=     0 NBB=     0 NumPrc=  1.

 Summary of results for alpha spin-orbital  27  OVGF:
 Koopmans theorem:             0.10453D+00 au    2.844 eV
 Converged second order pole:  0.43903D-01 au    1.195 eV
0.907 (PS)
 Converged third  order pole:  0.73675D-01 au    2.005 eV
0.913 (PS)
 Outer Valence Approximation:  0.68366D-01 au    1.860 eV
0.911 (PS)


**********************************************************
**********

            Population analysis using the SCF density.


**********************************************************
**********

 Orbital symmetries:
       Occupied  (A) (B) (A) (B) (A) (B) (A) (B) (B) (A)
(A) (B)
                 (A) (B) (A) (B) (A) (B) (A) (B) (A) (A)
(B) (A)
                 (B) (B) (A) (A) (B) (A) (B) (B) (A) (B)
(A) (B)
       Virtual   (A) (B) (A) (A) (B) (A) (B) (A) (B) (A)
(A) (B)
                 (B) (A) (B) (A) (B) (A) (B) (A) (B) (B)
(A) (A)
                 (B) (B) (B) (A) (A) (A) (B) (A) (B) (B)
(A) (A)
                 (B) (A) (B) (A) (B) (A) (B) (A) (B) (A)
(A) (B)
                 (B) (A) (B) (A) (B) (A) (B) (A) (B) (A)
(B) (A)
                 (B) (A) (A) (B) (A) (B) (B) (A) (B) (B)
(A) (A)
```

```
                 (B) (A) (B) (B) (B) (A) (B) (A) (B) (A)
(B) (B)
                 (A) (A) (B) (A) (B) (A) (B) (A) (B) (A)
(A) (B)
                 (A) (A) (B) (B) (A) (B) (A) (B) (A) (B)
(A) (A)
                 (B) (A) (B) (A) (B) (A) (B) (A) (B) (A)
(B) (B)
                 (A) (A) (B) (B) (A) (B) (A) (B) (A) (B)
(A) (B)
                 (A) (A) (B) (B) (A) (B)
 The electronic state is 1-A.
 Alpha  occ. eigenvalues --  -11.23215 -11.23215 -11.23079
-11.23075 -11.23029
 Alpha  occ. eigenvalues --  -11.22895 -11.22863 -11.22829
-11.22164 -11.22164
 Alpha  occ. eigenvalues --   -1.11423  -1.08963  -1.05198
-1.00850  -0.97043
 Alpha  occ. eigenvalues --   -0.84778  -0.81592  -0.77891
-0.73823  -0.69417
 Alpha  occ. eigenvalues --   -0.65531  -0.63902  -0.63863
-0.61355  -0.60755
 Alpha  occ. eigenvalues --   -0.57410  -0.56384  -0.54933
-0.51383  -0.48446
 Alpha  occ. eigenvalues --   -0.47343  -0.40895  -0.39855
-0.37294  -0.34224
 Alpha  occ. eigenvalues --   -0.31041
 Alpha virt. eigenvalues --    0.10453   0.16123   0.20742
0.21629   0.21901
 Alpha virt. eigenvalues --    0.28177   0.28475   0.29351
0.29391   0.30146
 Alpha virt. eigenvalues --    0.30979   0.31048   0.33179
0.33436   0.34612
 Alpha virt. eigenvalues --    0.35607   0.36406   0.42213
0.47370   0.49814
 Alpha virt. eigenvalues --    0.50462   0.53390   0.54464
0.59188   0.61464
 Alpha virt. eigenvalues --    0.64422   0.70419   0.70911
0.72274   0.76684
 Alpha virt. eigenvalues --    0.77048   0.79052   0.79687
0.79765   0.79970
 Alpha virt. eigenvalues --    0.81023   0.82247   0.83141
0.85243   0.85278
 Alpha virt. eigenvalues --    0.87153   0.88461   0.89615
0.92055   0.93405
```

```
 Alpha virt. eigenvalues --    0.94071   0.96648   0.97196
1.08746   1.10950
 Alpha virt. eigenvalues --    1.12331   1.12672   1.13272
1.13325   1.13984
 Alpha virt. eigenvalues --    1.14666   1.15821   1.16724
1.16969   1.18394
 Alpha virt. eigenvalues --    1.18898   1.19395   1.20392
1.20865   1.22184
 Alpha virt. eigenvalues --    1.22394   1.25221   1.27321
1.36011   1.38149
 Alpha virt. eigenvalues --    1.38212   1.40938   1.40976
1.45154   1.50293
 Alpha virt. eigenvalues --    1.55673   1.59441   1.59990
1.75333   1.75527
 Alpha virt. eigenvalues --    1.75811   1.79151   1.82072
1.91260   1.92625
 Alpha virt. eigenvalues --    1.96658   2.01367   2.01387
2.03565   2.08702
 Alpha virt. eigenvalues --    2.11970   2.22644   2.23665
2.24027   2.26243
 Alpha virt. eigenvalues --    2.26688   2.27927   2.28823
2.30950   2.35675
 Alpha virt. eigenvalues --    2.37978   2.40515   2.49063
2.50493   2.55446
 Alpha virt. eigenvalues --    2.56492   2.58511   2.60184
2.60301   2.65045
 Alpha virt. eigenvalues --    2.66073   2.71487   2.73592
2.79305   2.88951
 Alpha virt. eigenvalues --    2.91632   2.92550   2.92961
3.02912   3.06579
 Alpha virt. eigenvalues --    3.07952   3.13361   3.15385
3.29186   3.30655
 Alpha virt. eigenvalues --    3.40187   3.42043   3.49963
4.53290   4.54645
 Alpha virt. eigenvalues --    4.56422   4.59253   4.63222
4.73086   4.73124
 Alpha virt. eigenvalues --    4.78726   4.88776   5.00428
          Condensed to atoms (all electrons):
               1          2          3          4          5
6
     1  C    4.952228   0.653843   0.401685  -0.060340  -
0.006246   0.000160
     2  C    0.653843   4.944335  -0.060350  -0.001930
0.000160  -0.000048
```

```
     3  C    0.401685  -0.060350   4.954490   0.651690  -
0.060340  -0.001930
     4  C   -0.060340  -0.001930   0.651690   4.954490
0.401685  -0.060350
     5  C   -0.006246   0.000160  -0.060340   0.401685
4.952228   0.653843
     6  C    0.000160  -0.000048  -0.001930  -0.060350
0.653843   4.944335
     7  H   -0.037041  -0.002429   0.391336  -0.039157
0.003214  -0.000083
     8  H    0.003214  -0.000083  -0.039157   0.391336  -
0.037041  -0.002429
     9  H   -0.038747   0.393091   0.003273  -0.000080  -
0.000008   0.000001
    10  H    0.390859  -0.038538  -0.037007  -0.002488
0.003259   0.000937
    11  H   -0.000008   0.000001  -0.000080   0.003273  -
0.038747   0.393091
    12  H    0.003259   0.000937  -0.002488  -0.037007
0.390859  -0.038538
    13  C   -0.061599   0.397135  -0.006470   0.000215  -
0.000015   0.000000
    14  H   -0.002373  -0.036930   0.003186   0.000880  -
0.000007   0.000001
    15  C   -0.001874  -0.055589   0.000219  -0.000031
0.000000   0.000000
    16  H    0.000369  -0.001523   0.000020   0.000001
0.000000   0.000000
    17  H   -0.000071   0.002909  -0.000006   0.000001
0.000000   0.000000
    18  C   -0.000015   0.000000   0.000215  -0.006470  -
0.061599   0.397135
    19  H   -0.000007   0.000001   0.000880   0.003186  -
0.002373  -0.036930
    20  C    0.000000   0.000000  -0.000031   0.000219  -
0.001874  -0.055589
    21  H    0.000000   0.000000   0.000001  -0.000006  -
0.000071   0.002909
    22  H    0.000000   0.000000   0.000001   0.000020
0.000369  -0.001523
              7          8          9         10         11
12
     1  C   -0.037041   0.003214  -0.038747   0.390859  -
0.000008   0.003259
```

```
     2  C   -0.002429  -0.000083   0.393091  -0.038538
0.000001   0.000937
     3  C    0.391336  -0.039157   0.003273  -0.037007  -
0.000080  -0.002488
     4  C   -0.039157   0.391336  -0.000080  -0.002488
0.003273  -0.037007
     5  C    0.003214  -0.037041  -0.000008   0.003259  -
0.038747   0.390859
     6  C   -0.000083  -0.002429   0.000001   0.000937
0.393091  -0.038538
     7  H    0.482121  -0.003324  -0.000069   0.002721
0.000002  -0.000057
     8  H   -0.003324   0.482121   0.000002  -0.000057  -
0.000069   0.002721
     9  H   -0.000069   0.000002   0.486955  -0.003633
0.000000  -0.000002
    10  H    0.002721  -0.000057  -0.003633   0.483805  -
0.000002  -0.000538
    11  H    0.000002  -0.000069   0.000000  -0.000002
0.486955  -0.003633
    12  H   -0.000057   0.002721  -0.000002  -0.000538  -
0.003633   0.483805
    13  C    0.003374  -0.000009  -0.037553   0.003279
0.000000  -0.000011
    14  H   -0.000520   0.000000   0.002694  -0.000062
0.000000  -0.000019
    15  C    0.000868   0.000001  -0.001026  -0.000092
0.000000   0.000000
    16  H   -0.000014   0.000000   0.001377  -0.000015
0.000000   0.000000
    17  H   -0.000010   0.000000  -0.000090   0.000002
0.000000   0.000000
    18  C   -0.000009   0.003374   0.000000  -0.000011  -
0.037553   0.003279
    19  H    0.000000  -0.000520   0.000000  -0.000019
0.002694  -0.000062
    20  C    0.000001   0.000868   0.000000   0.000000  -
0.001026  -0.000092
    21  H    0.000000  -0.000010   0.000000   0.000000  -
0.000090   0.000002
    22  H    0.000000  -0.000014   0.000000   0.000000
0.001377  -0.000015
             13         14         15         16         17
18
```

```
     1  C   -0.061599  -0.002373  -0.001874   0.000369  -
0.000071  -0.000015
     2  C    0.397135  -0.036930  -0.055589  -0.001523
0.002909   0.000000
     3  C   -0.006470   0.003186   0.000219   0.000020  -
0.000006   0.000215
     4  C    0.000215   0.000880  -0.000031   0.000001
0.000001  -0.006470
     5  C   -0.000015  -0.000007   0.000000   0.000000
0.000000  -0.061599
     6  C    0.000000   0.000001   0.000000   0.000000
0.000000   0.397135
     7  H    0.003374  -0.000520   0.000868  -0.000014  -
0.000010  -0.000009
     8  H   -0.000009   0.000000   0.000001   0.000000
0.000000   0.003374
     9  H   -0.037553   0.002694  -0.001026   0.001377  -
0.000090   0.000000
    10  H    0.003279  -0.000062  -0.000092  -0.000015
0.000002  -0.000011
    11  H    0.000000   0.000000   0.000000   0.000000
0.000000  -0.037553
    12  H   -0.000011  -0.000019   0.000000   0.000000
0.000000   0.003279
    13  C    4.916313   0.392901   0.645082  -0.045135  -
0.036844   0.000000
    14  H    0.392901   0.484666  -0.040298   0.003278  -
0.003224   0.000000
    15  C    0.645082  -0.040298   5.042642   0.397269
0.394203   0.000000
    16  H   -0.045135   0.003278   0.397269   0.493431  -
0.027197   0.000000
    17  H   -0.036844  -0.003224   0.394203  -0.027197
0.491309   0.000000
    18  C    0.000000   0.000000   0.000000   0.000000
0.000000   4.916313
    19  H    0.000000   0.000000   0.000000   0.000000
0.000000   0.392901
    20  C    0.000000   0.000000   0.000000   0.000000
0.000000   0.645082
    21  H    0.000000   0.000000   0.000000   0.000000
0.000000  -0.036844
    22  H    0.000000   0.000000   0.000000   0.000000
0.000000  -0.045135
             19         20         21         22
```

1	C	-0.000007	0.000000	0.000000	0.000000
2	C	0.000001	0.000000	0.000000	0.000000
3	C	0.000880	-0.000031	0.000001	0.000001
4	C	0.003186	0.000219	-0.000006	0.000020
5	C	-0.002373	-0.001874	-0.000071	0.000369
6	C	-0.036930	-0.055589	0.002909	-0.001523
7	H	0.000000	0.000001	0.000000	0.000000
8	H	-0.000520	0.000868	-0.000010	-0.000014
9	H	0.000000	0.000000	0.000000	0.000000
10	H	-0.000019	0.000000	0.000000	0.000000
11	H	0.002694	-0.001026	-0.000090	0.001377
12	H	-0.000062	-0.000092	0.000002	-0.000015
13	C	0.000000	0.000000	0.000000	0.000000
14	H	0.000000	0.000000	0.000000	0.000000
15	C	0.000000	0.000000	0.000000	0.000000
16	H	0.000000	0.000000	0.000000	0.000000
17	H	0.000000	0.000000	0.000000	0.000000
18	C	0.392901	0.645082	-0.036844	-0.045135
19	H	0.484666	-0.040298	-0.003224	0.003278
20	C	-0.040298	5.042642	0.394203	0.397269
21	H	-0.003224	0.394203	0.491309	-0.027197
22	H	0.003278	0.397269	-0.027197	0.493431

Mulliken atomic charges:

		1
1	C	-0.197298
2	C	-0.194993
3	C	-0.199139
4	C	-0.199139
5	C	-0.197298
6	C	-0.194993
7	H	0.199076
8	H	0.199076
9	H	0.193814
10	H	0.197598
11	H	0.193814
12	H	0.197598
13	C	-0.170664
14	H	0.195826
15	C	-0.381376
16	H	0.178139
17	H	0.179018
18	C	-0.170664
19	H	0.195826
20	C	-0.381376
21	H	0.179018

```
   22  H    0.178139
 Sum of Mulliken charges=   0.00000
 Atomic charges with hydrogens summed into heavy atoms:
              1
    1  C    0.000300
    2  C   -0.001179
    3  C   -0.000063
    4  C   -0.000063
    5  C    0.000300
    6  C   -0.001179
    7  H    0.000000
    8  H    0.000000
    9  H    0.000000
   10  H    0.000000
   11  H    0.000000
   12  H    0.000000
   13  C    0.025162
   14  H    0.000000
   15  C   -0.024219
   16  H    0.000000
   17  H    0.000000
   18  C    0.025162
   19  H    0.000000
   20  C   -0.024219
   21  H    0.000000
   22  H    0.000000
 Sum of Mulliken charges=   0.00000
 Electronic spatial extent (au):  <R**2>=  2629.8984
 Charge=     0.0000 electrons
 Dipole moment (field-independent basis, Debye):
    X=     0.0000    Y=     0.0000    Z=    -0.0326  Tot=
0.0326
 Quadrupole moment (field-independent basis, Debye-Ang):
   XX=   -61.0698   YY=   -57.1997   ZZ=   -59.4005
   XY=    -0.8950   XZ=     0.0000   YZ=     0.0000
 Traceless Quadrupole moment (field-independent basis,
Debye-Ang):
   XX=    -1.8465   YY=     2.0237   ZZ=    -0.1772
   XY=    -0.8950   XZ=     0.0000   YZ=     0.0000
 Octapole moment (field-independent basis, Debye-Ang**2):
  XXX=     0.0000  YYY=     0.0000  ZZZ=     1.4058  XYY=
0.0000
  XXY=     0.0000  XXZ=     0.2417  XZZ=     0.0000  YZZ=
0.0000
  YYZ=   -12.4544  XYZ=    -9.5548
```

```
 Hexadecapole moment (field-independent basis, Debye-
Ang**3):
 XXXX=  -176.0159 YYYY= -3108.7707 ZZZZ=  -241.1586 XXXY=
6.3552
 XXXZ=     0.0000 YYYX=   -53.9401 YYYZ=     0.0000 ZZZX=
0.0000
 ZZZY=     0.0000 XXYY=  -564.6728 XXZZ=   -67.1959 YYZZ=
-573.8862
 XXYZ=     0.0000 YYXZ=     0.0000 ZZXY=    -3.1737
 N-N= 4.356270472138D+02 E-N=-1.768538596746D+03  KE=
3.852637415038D+02
 Symmetry A    KE= 1.928699879399D+02
 Symmetry B    KE= 1.923937535639D+02
 1|1|UNPC-UNK|SP|ROVGF-FC|6-31G(d)|C10H12|PCUSER|28-Feb-
2006|0||# HF/6-
 31G(D) GEOM=(MODREDUNDANT,CONNECTIVITY) SYMM=LOOSE
OVGF||120||0,1|C,0,
 -0.7195745848,1.3231652296,0.5495581212|C,0,-
0.3310440968,2.5581564725
 ,0.8287057592|C,0,-0.3310436664,0.5738751925,-
0.671393882|C,0,0.331043
 6664,-0.5738751925,-0.671393882|C,0,0.7195745848,-
1.3231652296,0.54955
 81212|C,0,0.3310440968,-2.5581564725,0.8287057592|H,0,-
0.5607406826,1.
 0371961988,-1.6169298749|H,0,0.5607406826,-1.0371961988,-
1.6169298749|
 H,0,-0.673251003,3.0121935089,1.7444197762|H,0,-
1.3136695755,0.7930022
 572,1.2756991489|H,0,0.673251003,-
3.0121935089,1.7444197762|H,0,1.3136
 695755,-
0.7930022572,1.2756991489|C,0,0.4842107773,3.4102964596,-
0.074
 4193666|H,0,1.4330777471,3.0091424619,-
0.3925354596|C,0,0.0869599493,4
 .5761107169,-0.5502628798|H,0,-0.8612979052,5.0083908313,-
0.2795655528
 |H,0,0.7012369527,5.1461398199,-1.2242247896|C,0,-
0.4842107773,-3.4102
 964596,-0.0744193666|H,0,-1.4330777471,-3.0091424619,-
0.3925354596|C,0
 ,-0.0869599493,-4.5761107169,-0.5502628798|H,0,-
0.7012369527,-5.146139
```

```
 8199,-1.2242247896|H,0,0.8612979052,-5.0083908313,-
0.2795655528||Versi
 on=x86-Win32-G03RevB.05|State=1-A|HF=-385.5515777|MP2=-
386.805486|RMSD
 =4.159e-009|PG=C02 [X(C10H12)]||@


 EDUCATION IS NOT TRAINING BUT RATHER THE PROCESS THAT
EQUIPS YOU TO
 ENTERTAIN YOURSELF, A FRIEND, OR AN IDEA.  -- WALLACE
STERLING
 Job cpu time:  0 days  2 hours 13 minutes 18.0 seconds.
 File lengths (MBytes):  RWF=   1933 Int=      0 D2E=
0 Chk=     18 Scr=      1
 Normal termination of Gaussian 03 at Tue Feb 28 13:17:08
2006.
```

150 Degree Dihedral Angles:

```
Entering Link 1 = C:\G03W\l1.exe PID=      1676.

 Copyright (c) 1988,1990,1992,1993,1995,1998,2003,
Gaussian, Inc.
                  All Rights Reserved.

 This is the Gaussian(R) 03 program.  It is based on the
 the Gaussian(R) 98 system (copyright 1998, Gaussian,
Inc.),
 the Gaussian(R) 94 system (copyright 1995, Gaussian,
Inc.),
 the Gaussian 92(TM) system (copyright 1992, Gaussian,
Inc.),
 the Gaussian 90(TM) system (copyright 1990, Gaussian,
Inc.),
 the Gaussian 88(TM) system (copyright 1988, Gaussian,
Inc.),
 the Gaussian 86(TM) system (copyright 1986, Carnegie
Mellon
 University), and the Gaussian 82(TM) system (copyright
1983,
 Carnegie Mellon University). Gaussian is a federally
registered
 trademark of Gaussian, Inc.
```

Cite this work as:
Gaussian 03, Revision B.05,
M. J. Frisch, G. W. Trucks, H. B. Schlegel, G. E. Scuseria,
M. A. Robb, J. R. Cheeseman, J. A. Montgomery, Jr., T. Vreven,
K. N. Kudin, J. C. Burant, J. M. Millam, S. S. Iyengar, J. Tomasi,
V. Barone, B. Mennucci, M. Cossi, G. Scalmani, N. Rega,
G. A. Petersson, H. Nakatsuji, M. Hada, M. Ehara, K. Toyota,
R. Fukuda, J. Hasegawa, M. Ishida, T. Nakajima, Y. Honda, O. Kitao,
H. Nakai, M. Klene, X. Li, J. E. Knox, H. P. Hratchian, J. B. Cross,
C. Adamo, J. Jaramillo, R. Gomperts, R. E. Stratmann, O. Yazyev,
A. J. Austin, R. Cammi, C. Pomelli, J. W. Ochterski, P. Y. Ayala,
K. Morokuma, G. A. Voth, P. Salvador, J. J. Dannenberg,
V. G. Zakrzewski, S. Dapprich, A. D. Daniels, M. C. Strain,
O. Farkas, D. K. Malick, A. D. Rabuck, K. Raghavachari,

```
 J. B. Foresman, J. V. Ortiz, Q. Cui, A. G. Baboul, S.
Clifford,
 J. Cioslowski, B. B. Stefanov, G. Liu, A. Liashenko, P.
Piskorz,
 I. Komaromi, R. L. Martin, D. J. Fox, T. Keith, M. A. Al-
Laham,
 C. Y. Peng, A. Nanayakkara, M. Challacombe, P. M. W. Gill,
 B. Johnson, W. Chen, M. W. Wong, C. Gonzalez, and J. A.
Pople,
 Gaussian, Inc., Pittsburgh PA, 2003.

 ******************************************
 Gaussian 03:  x86-Win32-G03RevB.05  8-Nov-2003
                  28-Feb-2006
 ******************************************
 %chk=150.chk
 %mem=64MB
 %nproc=1
 Will use up to    1 processors via shared memory.
 Default route:  MaxDisk=2000MB
 ----------------------------------------------------------
----
 # hf/6-31g(d) geom=(modredundant,connectivity) symm=loose
ovgf
 ----------------------------------------------------------
----
 1/18=120,38=1,57=2/1;
 2/17=4,18=3,40=1/2;
 3/5=1,6=6,7=1,11=9,16=1,25=1,30=1/1,2,3;
 4//1;
 5/5=2,38=5/2;
 8/6=4,9=120000,10=2,27=262144000/1,4;
 9/11=20000,27=262144000/8;
 6/7=2,8=2,9=2,10=2/1;
 99/5=1,9=1/99;
 ---
 150
 ---
 Symbolic Z-matrix:
 Charge =  0 Multiplicity = 1
 C                    -0.1897    1.51211   0.65756
 C                     0.1897    2.78481   0.73912
 C                    -0.08601   0.66015  -0.53681
 C                     0.08601  -0.66015  -0.53681
 C                     0.1897   -1.51211   0.65756
```

```
 C                    -0.1897   -2.78481   0.73912
 H                    -0.13033   1.15785  -1.48993
 H                     0.13033  -1.15785  -1.48993
 H                     0.03414   3.29991   1.67272
 H                    -0.58281   1.04992   1.54619
 H                    -0.03414  -3.29991   1.67272
 H                     0.58281  -1.04992   1.54619
 C                     0.72747   3.60393  -0.35877
 H                     1.23992   3.09078  -1.15443
 C                     0.56502   4.91436  -0.43935
 H                     0.05241   5.47129   0.32636
 H                     0.9453    5.47875  -1.27141
 C                    -0.72747  -3.60393  -0.35877
 H                    -1.23992  -3.09078  -1.15443
 C                    -0.56502  -4.91436  -0.43935
 H                    -0.9453   -5.47875  -1.27141
 H                    -0.05241  -5.47129   0.32636

 The following ModRedundant input section has been read:
 D    1    2   13   15 150.00 F
 D    2    1    3    4 150.00 F
 D    3    4    5    6 150.00 F
 D    5    6   18   20 150.00 F
 Iteration  1 RMS(Cart)=  0.00000028 RMS(Int)=  0.00000024
 Iteration  1 RMS(Cart)=  0.00000014 RMS(Int)=  0.00000012
                         Input orientation:
 ---------------------------------------------------------
-----------
 Center     Atomic     Atomic              Coordinates
(Angstroms)
 Number     Number      Type              X           Y
Z
 ---------------------------------------------------------
-----------
    1          6             0       -0.189704    1.512107
0.657558
    2          6             0        0.189704    2.784807
0.739118
    3          6             0       -0.086013    0.660147
-0.536812
    4          6             0        0.086013   -0.660147
-0.536812
    5          6             0        0.189704   -1.512107
0.657558
```

```
    6          6             0       -0.189704   -2.784807
0.739118
    7          1             0       -0.130326    1.157845
-1.489929
    8          1             0        0.130326   -1.157845
-1.489929
    9          1             0        0.034138    3.299909
1.672723
   10          1             0       -0.582810    1.049919
1.546192
   11          1             0       -0.034138   -3.299909
1.672723
   12          1             0        0.582810   -1.049919
1.546192
   13          6             0        0.727465    3.603925
-0.358768
   14          1             0        1.239918    3.090782
-1.154426
   15          6             0        0.565021    4.914358
-0.439347
   16          1             0        0.052409    5.471285
0.326355
   17          1             0        0.945302    5.478746
-1.271410
   18          6             0       -0.727465   -3.603925
-0.358768
   19          1             0       -1.239918   -3.090782
-1.154426
   20          6             0       -0.565021   -4.914358
-0.439347
   21          1             0       -0.945302   -5.478746
-1.271410
   22          1             0       -0.052409   -5.471285
0.326355
 ---------------------------------------------------------
-----------
                    Distance matrix (angstroms):
                    1          2          3          4
5
     1  C    0.000000
     2  C    1.330552   0.000000
     3  C    1.470751   2.493631   0.000000
     4  C    2.494239   3.675113   1.331454   0.000000
     5  C    3.047921   4.297688   2.494239   1.470751
0.000000
```

```
     6  C    4.297688   5.582522   3.675113   2.493631
1.330552
     7  H    2.177321   2.778142   1.076150   2.064057
3.441332
     8  H    3.441332   4.529534   2.064057   1.076150
2.177321
     9  H    2.068067   1.077566   3.444535   4.535061
4.920392
    10  H    1.076021   2.063488   2.176611   2.776789
2.819650
    11  H    4.920392   6.159992   4.535061   3.444535
2.068067
    12  H    2.819650   3.938404   2.776789   2.176611
1.076021
    13  C    2.499964   1.471562   3.059293   4.315724
5.243653
    14  H    2.796305   2.186797   2.836816   3.972709
5.056958
    15  C    3.653508   2.462647   4.304841   5.595897
6.530201
    16  H    3.980378   2.721468   4.889915   6.191983
6.992590
    17  H    4.554490   3.445353   4.982183   6.242117
7.291356
    18  C    5.243653   6.546942   4.315724   3.059293
2.499964
    19  H    5.056958   6.336551   3.972709   2.836816
2.796305
    20  C    6.530201   7.825314   5.595897   4.304841
3.653508
    21  H    7.291356   8.580022   6.242117   4.982183
4.554490
    22  H    6.992590   8.269949   6.191983   4.889915
3.980378
                   6          7          8          9
10
     6  C    0.000000
     7  H    4.529534   0.000000
     8  H    2.778142   2.330313   0.000000
     9  H    6.159992   3.823330   5.466552   0.000000
    10  H    3.938404   3.071550   3.821101   2.336470
0.000000
    11  H    1.077566   5.466552   3.823330   6.600172
4.386121
```

```
    12  H    2.063488   3.821101   3.071550   4.386121
2.401664
    13  C    6.546942   2.828186   4.930574   2.167968
3.445089
    14  H    6.336551   2.392985   4.403929   3.080651
3.844580
    15  C    7.825314   3.962149   6.177729   2.710926
4.493748
    16  H    8.269949   4.683807   6.873887   2.554978
4.630333
    17  H    8.580022   4.458129   6.690014   3.774317
5.467039
    18  C    1.471562   4.930574   2.828186   7.236707
5.030712
    19  H    2.186797   4.403929   2.392985   7.103304
4.987037
    20  C    2.462647   6.177729   3.962149   8.502589
6.286119
    21  H    3.445353   6.690014   4.458129   9.310855
7.119955
    22  H    2.721468   6.873887   4.683807   8.874348
6.655481
                   11         12         13         14
15
    11  H    0.000000
    12  H    2.336470   0.000000
    13  C    7.236707   5.030712   0.000000
    14  H    7.103304   4.987037   1.076567   0.000000
    15  C    8.502589   6.286119   1.322919   2.071775
0.000000
    16  H    8.874348   6.655481   2.100506   3.044616
1.076679
    17  H    9.310855   7.119955   2.096502   2.408912
1.074931
    18  C    2.167968   3.445089   7.353226   7.023017
8.616157
    19  H    3.080651   3.844580   7.023017   6.660430
8.237197
    20  C    2.710926   4.493748   8.616157   8.237197
9.893466
    21  H    3.774317   5.467039   9.280409   8.844529
10.535181
    22  H    2.554978   4.630333   9.134388   8.784750
10.432119
```

```
                    16         17         18         19
20
    16  H    0.000000
    17  H    1.830346   0.000000
    18  C    9.134388   9.280409   0.000000
    19  H    8.784750   8.844529   1.076567   0.000000
    20  C   10.432119  10.535181   1.322919   2.071775
0.000000
    21  H   11.110872  11.119399   2.096502   2.408912
1.074931
    22  H   10.943073  11.110872   2.100506   3.044616
1.076679
                    21         22
    21  H    0.000000
    22  H    1.830346   0.000000
 Stoichiometry    C10H12
 Framework group  C2[X(C10H12)]
 Deg. of freedom    31
 Full point group                 C2      NOp   2
 Largest Abelian subgroup         C2      NOp   2
 Largest concise Abelian subgroup C2      NOp   2
                         Standard orientation:
 ---------------------------------------------------------
-----------
 Center     Atomic     Atomic              Coordinates
(Angstroms)
 Number     Number      Type              X           Y
Z
 ---------------------------------------------------------
-----------
    1          6             0       -0.189704    1.512107
0.657558
    2          6             0        0.189704    2.784807
0.739118
    3          6             0       -0.086013    0.660147
-0.536812
    4          6             0        0.086013   -0.660147
-0.536812
    5          6             0        0.189704   -1.512107
0.657558
    6          6             0       -0.189704   -2.784807
0.739118
    7          1             0       -0.130326    1.157845
-1.489929
```

```
     8          1             0        0.130326   -1.157845
-1.489929
     9          1             0        0.034138    3.299909
1.672723
    10          1             0       -0.582810    1.049919
1.546192
    11          1             0       -0.034138   -3.299909
1.672723
    12          1             0        0.582810   -1.049919
1.546192
    13          6             0        0.727464    3.603925
-0.358768
    14          1             0        1.239917    3.090782
-1.154426
    15          6             0        0.565021    4.914358
-0.439347
    16          1             0        0.052409    5.471285
0.326355
    17          1             0        0.945302    5.478746
-1.271410
    18          6             0       -0.727464   -3.603925
-0.358768
    19          1             0       -1.239917   -3.090782
-1.154426
    20          6             0       -0.565021   -4.914358
-0.439347
    21          1             0       -0.945302   -5.478746
-1.271410
    22          1             0       -0.052409   -5.471285
0.326355
 ---------------------------------------------------------
-----------
 Rotational constants (GHZ):      7.2753932      0.3778073
0.3644662
 Standard basis: 6-31G(d) (6D, 7F)
 There are    87 symmetry adapted basis functions of A
symmetry.
 There are    87 symmetry adapted basis functions of B
symmetry.
 Integral buffers will be    262144 words long.
 Raffenetti 1 integral format.
 Two-electron integral symmetry is turned on.
   174 basis functions,   328 primitive gaussians,   174
cartesian basis functions
    36 alpha electrons       36 beta electrons
```

```
      nuclear repulsion energy       428.1033358716
Hartrees.
 NAtoms=   22 NActive=   22 NUniq=   11 SFac= 5.66D+00
NAtFMM=   60 Big=F
 One-electron integrals computed using PRISM.
 NBasis=   174 RedAO= T  NBF=    87    87
 NBsUse=   174 1.00D-06 NBFU=    87    87
 Harris functional with IExCor=  205 diagonalized for
initial guess.
 ExpMin= 1.61D-01 ExpMax= 3.05D+03 ExpMxC= 4.57D+02 IAcc=1
IRadAn=         1 AccDes= 1.00D-06
 HarFok:  IExCor= 205 AccDes= 1.00D-06 IRadAn=         1
IDoV=1
 ScaDFX=  1.000000  1.000000  1.000000  1.000000
 Initial guess orbital symmetries:
      Occupied  (A) (B) (A) (B) (A) (B) (A) (B) (A) (B)
(A) (B)
                (A) (B) (A) (B) (A) (B) (A) (B) (A) (A)
(B) (A)
                (B) (B) (A) (A) (B) (B) (A) (A) (B) (B)
(A) (B)
      Virtual   (A) (B) (A) (B) (A) (A) (B) (A) (B) (A)
(A) (B)
                (B) (A) (A) (B) (A) (B) (B) (B) (A) (B)
(A) (A)
                (B) (B) (A) (A) (B) (A) (B) (B) (A) (B)
(A) (B)
                (A) (A) (B) (B) (A) (B) (A) (A) (B) (A)
(B) (A)
                (B) (A) (B) (A) (B) (A) (B) (B) (A) (A)
(B) (A)
                (B) (A) (B) (A) (B) (A) (B) (B) (A) (B)
(A) (A)
                (B) (B) (B) (A) (A) (B) (A) (B) (B) (A)
(B) (A)
                (B) (A) (B) (A) (B) (A) (B) (A) (A) (B)
(A) (B)
                (A) (A) (B) (B) (A) (B) (B) (A) (A) (B)
(A) (B)
                (A) (B) (A) (A) (B) (A) (B) (B) (A) (A)
(B) (A)
                (B) (A) (B) (B) (A) (A) (B) (B) (A) (B)
(A) (B)
                (A) (B) (A) (B) (A) (B)
 The electronic state of the initial guess is 1-A.
```

```
 Requested convergence on RMS density matrix=1.00D-08
within 128 cycles.
 Requested convergence on MAX density matrix=1.00D-06.
 Requested convergence on             energy=1.00D-06.
 No special actions if energy rises.
 Integral accuracy reduced to 1.0D-05 until final
iterations.
 Initial convergence to 1.0D-05 achieved.  Increase
integral accuracy.
 SCF Done:  E(RHF) =  -385.568706495     A.U. after   15
cycles
             Convg  =    0.1118D-08             -V/T =
2.0008
             S**2   =   0.0000
 ExpMin= 1.61D-01 ExpMax= 3.05D+03 ExpMxC= 4.57D+02 IAcc=1
IRadAn=         1 AccDes= 1.00D-06
 HarFok:  IExCor= 205 AccDes= 1.00D-06 IRadAn=         1
IDoV=1
 ScaDFX=  1.000000  1.000000  1.000000  1.000000
 Range of M.O.s used for correlation:    11   174
 NBasis=   174 NAE=    36 NBE=    36 NFC=    10 NFV=     0
 NROrb=    164 NOA=    26 NOB=    26 NVA=   138 NVB=   138
 Semi-Direct transformation.
 ModeAB=           4 MOrb=            26 LenV=
7801009
 LASXX=     25541776 LTotXX=    25541776 LenRXX=
51559950
 LTotAB=    26018174 MaxLAS=    26163904 LenRXY=
0
 NonZer=    77101726 LenScr=   123368960 LnRSAI=
26163904
 LnScr1=    44406272 LExtra=     2955347 Total=
248454433
 MaxDsk=   262144000 SrtSym=           T ITran=
4
 JobTyp=0 Pass  1:  I=   1 to  26.
 Spin components of T(2) and E(2):
     alpha-alpha T2 =       0.5681778885D-01 E2=     -
0.1570647527D+00
     alpha-beta  T2 =       0.3425774104D+00 E2=     -
0.9406427879D+00
     beta-beta   T2 =       0.5681778885D-01 E2=     -
0.1570647527D+00
 ANorm=    0.1206736503D+01
```

```
 E2=       -0.1254772293D+01 EUMP2=       -
0.38682347878844D+03
 GREENY: Electron Propagator Program
 Petite list used in FoFDir.
 MinBra= 0 MaxBra= 2 Meth= 1.
 IRaf=       0 NMat=   1 IRICut=       1 DoRegI=T DoRafI=F
ISym2E=-1 JSym2E=1.

 Orbital window will be selected automatically

    Alpha HOMO is orbital  26

 GREENY has selected a window containing alpha orbitals

             9 through  27

 from symmetry group number 1 of the 2 total symmetry
operations

 Summary of results for alpha spin-orbital   9  OVGF:
 Koopmans theorem:            -0.74575D+00 au  -20.293 eV
 Converged second order pole: -0.64219D+00 au  -17.475 eV
0.839 (PS)
 Converged third  order pole: -0.66809D+00 au  -18.180 eV
0.851 (PS)
 Outer Valence Approximation: -0.65873D+00 au  -17.925 eV
0.839 (PS)

 Summary of results for alpha spin-orbital  10  OVGF:
 Koopmans theorem:            -0.69766D+00 au  -18.984 eV
 Converged second order pole: -0.60117D+00 au  -16.359 eV
0.849 (PS)
 Converged third  order pole: -0.62593D+00 au  -17.032 eV
0.860 (PS)
 Outer Valence Approximation: -0.61692D+00 au  -16.787 eV
0.850 (PS)

 Summary of results for alpha spin-orbital  11  OVGF:
 Koopmans theorem:            -0.67932D+00 au  -18.485 eV
 Converged second order pole: -0.58115D+00 au  -15.814 eV
0.847 (PS)
 Converged third  order pole: -0.60932D+00 au  -16.580 eV
0.868 (PS)
 Outer Valence Approximation: -0.59753D+00 au  -16.260 eV
0.856 (PS)
```

```
 Summary of results for alpha spin-orbital  12  OVGF:
 Koopmans theorem:            -0.64142D+00 au  -17.454 eV
 Converged second order pole: -0.55180D+00 au  -15.015 eV
0.857 (PS)
 Converged third  order pole: -0.57510D+00 au  -15.649 eV
0.875 (PS)
 Outer Valence Approximation: -0.56510D+00 au  -15.377 eV
0.865 (PS)

 Summary of results for alpha spin-orbital  13  OVGF:
 Koopmans theorem:            -0.63920D+00 au  -17.393 eV
 Converged second order pole: -0.53922D+00 au  -14.673 eV
0.838 (PS)
 Converged third  order pole: -0.57355D+00 au  -15.607 eV
0.865 (PS)
 Outer Valence Approximation: -0.55935D+00 au  -15.221 eV
0.850 (PS)

 Summary of results for alpha spin-orbital  14  OVGF:
 Koopmans theorem:            -0.59937D+00 au  -16.310 eV
 Converged second order pole: -0.51467D+00 au  -14.005 eV
0.863 (PS)
 Converged third  order pole: -0.53642D+00 au  -14.597 eV
0.881 (PS)
 Outer Valence Approximation: -0.52686D+00 au  -14.336 eV
0.872 (PS)

 Summary of results for alpha spin-orbital  15  OVGF:
 Koopmans theorem:            -0.59861D+00 au  -16.289 eV
 Converged second order pole: -0.51598D+00 au  -14.041 eV
0.861 (PS)
 Converged third  order pole: -0.53877D+00 au  -14.661 eV
0.876 (PS)
 Outer Valence Approximation: -0.53025D+00 au  -14.429 eV
0.867 (PS)

 Summary of results for alpha spin-orbital  16  OVGF:
 Koopmans theorem:            -0.56135D+00 au  -15.275 eV
 Converged second order pole: -0.47809D+00 au  -13.010 eV
0.869 (PS)
 Converged third  order pole: -0.50023D+00 au  -13.612 eV
0.894 (PS)
 Outer Valence Approximation: -0.48934D+00 au  -13.316 eV
0.885 (PS)
```

```
 Summary of results for alpha spin-orbital  17  OVGF:
 Koopmans theorem:            -0.55736D+00 au  -15.166 eV
 Converged second order pole: -0.47932D+00 au  -13.043 eV
0.872 (PS)
 Converged third  order pole: -0.50110D+00 au  -13.636 eV
0.891 (PS)
 Outer Valence Approximation: -0.49222D+00 au  -13.394 eV
0.883 (PS)

 Summary of results for alpha spin-orbital  18  OVGF:
 Koopmans theorem:            -0.54375D+00 au  -14.796 eV
 Converged second order pole: -0.45680D+00 au  -12.430 eV
0.864 (PS)
 Converged third  order pole: -0.48296D+00 au  -13.142 eV
0.894 (PS)
 Outer Valence Approximation: -0.47038D+00 au  -12.800 eV
0.883 (PS)

 Summary of results for alpha spin-orbital  19  OVGF:
 Koopmans theorem:            -0.52268D+00 au  -14.223 eV
 Converged second order pole: -0.44766D+00 au  -12.182 eV
0.874 (PS)
 Converged third  order pole: -0.47007D+00 au  -12.791 eV
0.893 (PS)
 Outer Valence Approximation: -0.46105D+00 au  -12.546 eV
0.884 (PS)

 Summary of results for alpha spin-orbital  20  OVGF:
 Koopmans theorem:            -0.49136D+00 au  -13.371 eV
 Converged second order pole: -0.41929D+00 au  -11.409 eV
0.878 (PS)
 Converged third  order pole: -0.44128D+00 au  -12.008 eV
0.898 (PS)
 Outer Valence Approximation: -0.43200D+00 au  -11.755 eV
0.890 (PS)

 Summary of results for alpha spin-orbital  21  OVGF:
 Koopmans theorem:            -0.47984D+00 au  -13.057 eV
 Converged second order pole: -0.41343D+00 au  -11.250 eV
0.865 (PS)
 Converged third  order pole: -0.43493D+00 au  -11.835 eV
0.884 (PS)
 Outer Valence Approximation: -0.42490D+00 au  -11.562 eV
0.875 (PS)
```

```
 Summary of results for alpha spin-orbital  22  OVGF:
 Koopmans theorem:            -0.44460D+00 au  -12.098 eV
 Converged second order pole: -0.38405D+00 au  -10.451 eV
0.870 (PS)
 Converged third  order pole: -0.40379D+00 au  -10.988 eV
0.887 (PS)
 Outer Valence Approximation: -0.39468D+00 au  -10.740 eV
0.879 (PS)

 Summary of results for alpha spin-orbital  23  OVGF:
 Koopmans theorem:            -0.43134D+00 au  -11.737 eV
 Converged second order pole: -0.39013D+00 au  -10.616 eV
0.871 (PS)
 Converged third  order pole: -0.40216D+00 au  -10.943 eV
0.878 (PS)
 Outer Valence Approximation: -0.39541D+00 au  -10.760 eV
0.873 (PS)

 Summary of results for alpha spin-orbital  24  OVGF:
 Koopmans theorem:            -0.38742D+00 au  -10.542 eV
 Converged second order pole: -0.35675D+00 au   -9.708 eV
0.878 (PS)
 Converged third  order pole: -0.36612D+00 au   -9.963 eV
0.886 (PS)
 Outer Valence Approximation: -0.36013D+00 au   -9.800 eV
0.882 (PS)

 Summary of results for alpha spin-orbital  25  OVGF:
 Koopmans theorem:            -0.33385D+00 au   -9.084 eV
 Converged second order pole: -0.31393D+00 au   -8.542 eV
0.884 (PS)
 Converged third  order pole: -0.32086D+00 au   -8.731 eV
0.893 (PS)
 Outer Valence Approximation: -0.31939D+00 au   -8.691 eV
0.890 (PS)

 Summary of results for alpha spin-orbital  26  OVGF:
 Koopmans theorem:            -0.28168D+00 au   -7.665 eV
 Converged second order pole: -0.26705D+00 au   -7.267 eV
0.882 (PS)
 Converged third  order pole: -0.27335D+00 au   -7.438 eV
0.895 (PS)
 Outer Valence Approximation: -0.27198D+00 au   -7.401 eV
0.891 (PS)
```

```
 DD1Dir will call FoFDir   4 times, MxPair=       176
 NAB=   351 NAA=     0 NBB=     0 NumPrc=  1.

 Summary of results for alpha spin-orbital  27  OVGF:
 Koopmans theorem:             0.83066D-01 au    2.260 eV
 Converged second order pole:  0.22899D-01 au    0.623 eV
0.897 (PS)
 Converged third  order pole:  0.52954D-01 au    1.441 eV
0.903 (PS)
 Outer Valence Approximation:  0.47540D-01 au    1.294 eV
0.901 (PS)


**********************************************************
***********

           Population analysis using the SCF density.


**********************************************************
***********

 Orbital symmetries:
       Occupied  (A) (B) (A) (B) (A) (B) (A) (B) (A) (B)
(A) (B)
                 (A) (B) (A) (B) (A) (B) (A) (B) (A) (B)
(A) (A)
                 (B) (B) (A) (A) (B) (A) (B) (B) (A) (B)
(A) (B)
       Virtual   (A) (B) (A) (B) (A) (B) (A) (B) (A) (A)
(A) (B)
                 (B) (A) (B) (A) (B) (A) (B) (A) (B) (B)
(A) (A)
                 (B) (B) (A) (A) (B) (A) (A) (B) (B) (A)
(B) (B)
                 (A) (A) (A) (B) (B) (B) (A) (B) (A) (A)
(A) (B)
                 (B) (A) (B) (A) (B) (A) (B) (A) (A) (B)
(A) (B)
                 (B) (A) (B) (A) (B) (A) (B) (A) (B) (B)
(A) (A)
                 (B) (B) (A) (B) (A) (B) (A) (B) (B) (A)
(B) (B)
                 (A) (A) (B) (A) (B) (A) (B) (A) (A) (B)
(A) (B)
```

```
                 (A) (A) (B) (B) (A) (B) (B) (A) (A) (B)
(A) (B)
                 (A) (B) (A) (A) (B) (A) (B) (A) (B) (A)
(B) (A)
                 (B) (A) (B) (B) (A) (A) (B) (B) (A) (B)
(A) (B)
                 (A) (B) (A) (B) (A) (B)
 The electronic state is 1-A.
 Alpha  occ. eigenvalues --  -11.23437 -11.23437 -11.23361
-11.23355 -11.23334
 Alpha  occ. eigenvalues --  -11.23187 -11.23109 -11.23097
-11.22497 -11.22497
 Alpha  occ. eigenvalues --   -1.11695  -1.09378  -1.05737
-1.01260  -0.97273
 Alpha  occ. eigenvalues --   -0.84979  -0.82165  -0.78753
-0.74575  -0.69766
 Alpha  occ. eigenvalues --   -0.67932  -0.64142  -0.63920
-0.59937  -0.59861
 Alpha  occ. eigenvalues --   -0.56135  -0.55736  -0.54375
-0.52268  -0.49136
 Alpha  occ. eigenvalues --   -0.47984  -0.44460  -0.43134
-0.38742  -0.33385
 Alpha  occ. eigenvalues --   -0.28168
 Alpha virt. eigenvalues --    0.08307   0.14510   0.20168
0.24029   0.24032
 Alpha virt. eigenvalues --    0.27406   0.27622   0.27927
0.28981   0.29713
 Alpha virt. eigenvalues --    0.31237   0.31780   0.33619
0.34542   0.36538
 Alpha virt. eigenvalues --    0.36905   0.40253   0.41873
0.47147   0.49888
 Alpha virt. eigenvalues --    0.51838   0.53949   0.54580
0.58424   0.59777
 Alpha virt. eigenvalues --    0.65484   0.66923   0.69512
0.73121   0.76536
 Alpha virt. eigenvalues --    0.78250   0.78647   0.79065
0.80716   0.80721
 Alpha virt. eigenvalues --    0.82211   0.83191   0.84367
0.85356   0.85818
 Alpha virt. eigenvalues --    0.88527   0.90833   0.92682
0.93128   0.94229
 Alpha virt. eigenvalues --    0.96214   0.97087   0.97811
1.08220   1.11355
 Alpha virt. eigenvalues --    1.11813   1.12666   1.12906
1.13774   1.16137
```

```
 Alpha virt. eigenvalues --    1.16496   1.17530   1.17652
1.19095   1.19408
 Alpha virt. eigenvalues --    1.20043   1.22401   1.22513
1.24378   1.25300
 Alpha virt. eigenvalues --    1.26983   1.31117   1.31787
1.34135   1.35751
 Alpha virt. eigenvalues --    1.38900   1.42301   1.45451
1.50355   1.54388
 Alpha virt. eigenvalues --    1.55136   1.62131   1.62200
1.73199   1.74036
 Alpha virt. eigenvalues --    1.75260   1.78285   1.82619
1.86509   1.86729
 Alpha virt. eigenvalues --    1.89659   1.93961   2.02094
2.02335   2.04534
 Alpha virt. eigenvalues --    2.12244   2.17144   2.21914
2.22529   2.25467
 Alpha virt. eigenvalues --    2.29195   2.30577   2.31988
2.33778   2.35122
 Alpha virt. eigenvalues --    2.36673   2.39825   2.47662
2.48153   2.50296
 Alpha virt. eigenvalues --    2.52676   2.55093   2.61494
2.63552   2.69998
 Alpha virt. eigenvalues --    2.71228   2.74377   2.75706
2.80011   2.83327
 Alpha virt. eigenvalues --    2.91340   2.92316   2.93389
2.93895   3.03964
 Alpha virt. eigenvalues --    3.10194   3.13702   3.14891
3.30191   3.33227
 Alpha virt. eigenvalues --    3.46959   3.51630   3.53850
4.51323   4.52769
 Alpha virt. eigenvalues --    4.54677   4.56647   4.59746
4.64154   4.72394
 Alpha virt. eigenvalues --    4.81523   4.90681   4.98501
          Condensed to atoms (all electrons):
               1          2          3          4          5
6
     1  C    4.930504   0.649204   0.413326  -0.054015  -
0.005650   0.000208
     2  C    0.649204   4.914237  -0.053667   0.000036
0.000208  -0.000008
     3  C    0.413326  -0.053667   4.927373   0.648015  -
0.054015   0.000036
     4  C   -0.054015   0.000036   0.648015   4.927373
0.413326  -0.053667
```

```
     5  C   -0.005650   0.000208  -0.054015   0.413326
4.930504   0.649204
     6  C    0.000208  -0.000008   0.000036  -0.053667
0.649204   4.914237
     7  H   -0.037670  -0.001875   0.391524  -0.035746
0.002848  -0.000099
     8  H    0.002848  -0.000099  -0.035746   0.391524  -
0.037670  -0.001875
     9  H   -0.034627   0.391907   0.002873  -0.000096  -
0.000002   0.000000
    10  H    0.390937  -0.035000  -0.037980  -0.001932
0.002436   0.000314
    11  H   -0.000002   0.000000  -0.000096   0.002873  -
0.034627   0.391907
    12  H    0.002436   0.000314  -0.001932  -0.037980
0.390937  -0.035000
    13  C   -0.055033   0.411818  -0.005483   0.000200  -
0.000004   0.000000
    14  H   -0.001633  -0.036881   0.002188   0.000245  -
0.000003   0.000000
    15  C   -0.000160  -0.051979   0.000242  -0.000008
0.000000   0.000000
    16  H    0.000147  -0.002070   0.000008   0.000000
0.000000   0.000000
    17  H   -0.000080   0.002527  -0.000002   0.000000
0.000000   0.000000
    18  C   -0.000004   0.000000   0.000200  -0.005483  -
0.055033   0.411818
    19  H   -0.000003   0.000000   0.000245   0.002188  -
0.001633  -0.036881
    20  C    0.000000   0.000000  -0.000008   0.000242  -
0.000160  -0.051979
    21  H    0.000000   0.000000   0.000000  -0.000002  -
0.000080   0.002527
    22  H    0.000000   0.000000   0.000000   0.000008
0.000147  -0.002070
              7          8          9         10         11
12
     1  C   -0.037670   0.002848  -0.034627   0.390937  -
0.000002   0.002436
     2  C   -0.001875  -0.000099   0.391907  -0.035000
0.000000   0.000314
     3  C    0.391524  -0.035746   0.002873  -0.037980  -
0.000096  -0.001932
```

```
     4  C   -0.035746   0.391524  -0.000096  -0.001932
0.002873  -0.037980
     5  C    0.002848  -0.037670  -0.000002   0.002436  -
0.034627   0.390937
     6  C   -0.000099  -0.001875   0.000000   0.000314
0.391907  -0.035000
     7  H    0.485294  -0.003626  -0.000054   0.002704
0.000002  -0.000034
     8  H   -0.003626   0.485294   0.000002  -0.000034  -
0.000054   0.002704
     9  H   -0.000054   0.000002   0.488564  -0.003871
0.000000   0.000003
    10  H    0.002704  -0.000034  -0.003871   0.483948
0.000003  -0.000593
    11  H    0.000002  -0.000054   0.000000   0.000003
0.488564  -0.003871
    12  H   -0.000034   0.002704   0.000003  -0.000593  -
0.003871   0.483948
    13  C    0.001984  -0.000003  -0.040974   0.002980
0.000000  -0.000003
    14  H   -0.000456   0.000004   0.002740  -0.000038
0.000000  -0.000002
    15  C    0.000256   0.000000  -0.000265  -0.000113
0.000000   0.000000
    16  H   -0.000002   0.000000   0.002720  -0.000011
0.000000   0.000000
    17  H    0.000000   0.000000  -0.000042   0.000002
0.000000   0.000000
    18  C   -0.000003   0.001984   0.000000  -0.000003  -
0.040974   0.002980
    19  H    0.000004  -0.000456   0.000000  -0.000002
0.002740  -0.000038
    20  C    0.000000   0.000256   0.000000   0.000000  -
0.000265  -0.000113
    21  H    0.000000   0.000000   0.000000   0.000000  -
0.000042   0.000002
    22  H    0.000000  -0.000002   0.000000   0.000000
0.002720  -0.000011
             13         14         15         16         17
18
     1  C   -0.055033  -0.001633  -0.000160   0.000147  -
0.000080  -0.000004
     2  C    0.411818  -0.036881  -0.051979  -0.002070
0.002527   0.000000
```

```
     3  C   -0.005483   0.002188   0.000242   0.000008  -
0.000002   0.000200
     4  C    0.000200   0.000245  -0.000008   0.000000
0.000000  -0.005483
     5  C   -0.000004  -0.000003   0.000000   0.000000
0.000000  -0.055033
     6  C    0.000000   0.000000   0.000000   0.000000
0.000000   0.411818
     7  H    0.001984  -0.000456   0.000256  -0.000002
0.000000  -0.000003
     8  H   -0.000003   0.000004   0.000000   0.000000
0.000000   0.001984
     9  H   -0.040974   0.002740  -0.000265   0.002720  -
0.000042   0.000000
    10  H    0.002980  -0.000038  -0.000113  -0.000011
0.000002  -0.000003
    11  H    0.000000   0.000000   0.000000   0.000000
0.000000  -0.040974
    12  H   -0.000003  -0.000002   0.000000   0.000000
0.000000   0.002980
    13  C    4.887824   0.392911   0.638661  -0.045585  -
0.036067   0.000000
    14  H    0.392911   0.485777  -0.038169   0.003212  -
0.003169   0.000000
    15  C    0.638661  -0.038169   5.056198   0.397014
0.395299   0.000000
    16  H   -0.045585   0.003212   0.397014   0.492435  -
0.026719   0.000000
    17  H   -0.036067  -0.003169   0.395299  -0.026719
0.485992   0.000000
    18  C    0.000000   0.000000   0.000000   0.000000
0.000000   4.887824
    19  H    0.000000   0.000000   0.000000   0.000000
0.000000   0.392911
    20  C    0.000000   0.000000   0.000000   0.000000
0.000000   0.638661
    21  H    0.000000   0.000000   0.000000   0.000000
0.000000  -0.036067
    22  H    0.000000   0.000000   0.000000   0.000000
0.000000  -0.045585
              19         20         21         22
     1  C   -0.000003   0.000000   0.000000   0.000000
     2  C    0.000000   0.000000   0.000000   0.000000
     3  C    0.000245  -0.000008   0.000000   0.000000
     4  C    0.002188   0.000242  -0.000002   0.000008
```

5	C	-0.001633	-0.000160	-0.000080	0.000147
6	C	-0.036881	-0.051979	0.002527	-0.002070
7	H	0.000004	0.000000	0.000000	0.000000
8	H	-0.000456	0.000256	0.000000	-0.000002
9	H	0.000000	0.000000	0.000000	0.000000
10	H	-0.000002	0.000000	0.000000	0.000000
11	H	0.002740	-0.000265	-0.000042	0.002720
12	H	-0.000038	-0.000113	0.000002	-0.000011
13	C	0.000000	0.000000	0.000000	0.000000
14	H	0.000000	0.000000	0.000000	0.000000
15	C	0.000000	0.000000	0.000000	0.000000
16	H	0.000000	0.000000	0.000000	0.000000
17	H	0.000000	0.000000	0.000000	0.000000
18	C	0.392911	0.638661	-0.036067	-0.045585
19	H	0.485777	-0.038169	-0.003169	0.003212
20	C	-0.038169	5.056198	0.395299	0.397014
21	H	-0.003169	0.395299	0.485992	-0.026719
22	H	0.003212	0.397014	-0.026719	0.492435

Mulliken atomic charges:

		1
1	C	-0.200733
2	C	-0.188672
3	C	-0.197100
4	C	-0.197100
5	C	-0.200733
6	C	-0.188672
7	H	0.194951
8	H	0.194951
9	H	0.191123
10	H	0.196253
11	H	0.191123
12	H	0.196253
13	C	-0.153227
14	H	0.193273
15	C	-0.396975
16	H	0.178851
17	H	0.182258
18	C	-0.153227
19	H	0.193273
20	C	-0.396975
21	H	0.182258
22	H	0.178851

Sum of Mulliken charges= 0.00000

Atomic charges with hydrogens summed into heavy atoms:

		1

```
     1  C   -0.004480
     2  C    0.002451
     3  C   -0.002150
     4  C   -0.002150
     5  C   -0.004480
     6  C    0.002451
     7  H    0.000000
     8  H    0.000000
     9  H    0.000000
    10  H    0.000000
    11  H    0.000000
    12  H    0.000000
    13  C    0.040046
    14  H    0.000000
    15  C   -0.035867
    16  H    0.000000
    17  H    0.000000
    18  C    0.040046
    19  H    0.000000
    20  C   -0.035867
    21  H    0.000000
    22  H    0.000000
 Sum of Mulliken charges=   0.00000
 Electronic spatial extent (au):  <R**2>=  2965.9818
 Charge=     0.0000 electrons
 Dipole moment (field-independent basis, Debye):
    X=     0.0000    Y=     0.0000    Z=    -0.0733  Tot=
0.0733
 Quadrupole moment (field-independent basis, Debye-Ang):
   XX=   -65.9764   YY=   -54.2015   ZZ=   -56.4733
   XY=     0.2758   XZ=     0.0000   YZ=     0.0000
 Traceless Quadrupole moment (field-independent basis,
Debye-Ang):
   XX=    -7.0927   YY=     4.6822   ZZ=     2.4104
   XY=     0.2758   XZ=     0.0000   YZ=     0.0000
 Octapole moment (field-independent basis, Debye-Ang**2):
  XXX=     0.0000  YYY=     0.0000  ZZZ=     0.7308  XYY=
0.0000
  XXY=     0.0000  XXZ=    -3.0966  XZZ=     0.0000  YZZ=
0.0000
  YYZ=    -1.4245  XYZ=   -12.2564
 Hexadecapole moment (field-independent basis, Debye-
Ang**3):
 XXXX=  -158.8782 YYYY= -3410.8364 ZZZZ=  -234.8020 XXXY=
-229.3899
```

```
 XXXZ=     0.0000 YYYX=  -215.0683 YYYZ=     0.0000 ZZZX=
0.0000
 ZZZY=     0.0000 XXYY=  -708.2271 XXZZ=   -65.7509 YYZZ=
-622.8885
 XXYZ=     0.0000 YYXZ=     0.0000 ZZXY=   -61.7208
 N-N= 4.281033358716D+02 E-N=-1.753287885706D+03  KE=
3.852679012083D+02
 Symmetry A    KE= 1.928396429703D+02
 Symmetry B    KE= 1.924282582380D+02
 1|1|UNPC-UNK|SP|ROVGF-FC|6-31G(d)|C10H12|PCUSER|28-Feb-
2006|0||# HF/6-
 31G(D) GEOM=(MODREDUNDANT,CONNECTIVITY) SYMM=LOOSE
OVGF||150||0,1|C,0,
 -
0.1897035523,1.5121070599,0.6575580801|C,0,0.1897038565,2.7
848072503,
 0.7391178592|C,0,-0.0860126384,0.6601470471,-
0.5368119182|C,0,0.086012
 6384,-0.6601470471,-0.5368119182|C,0,0.1897035523,-
1.5121070599,0.6575
 580801|C,0,-0.1897038565,-2.7848072503,0.7391178592|H,0,-
0.1303256708,
 1.1578450449,-1.4899289179|H,0,0.1303256708,-
1.1578450449,-1.489928917
 9|H,0,0.0341379618,3.2999092628,1.6727228698|H,0,-
0.5828095178,1.04991
 90731,1.5461921023|H,0,-0.0341379618,-
3.2999092628,1.6727228698|H,0,0.
 5828095178,-
1.0499190731,1.5461921023|C,0,0.7274646395,3.60392527,-0.3
 587682323|H,0,1.239917549,3.0907822854,-
1.1544263005|C,0,0.5650210412,
 4.9143583383,-
0.4393469326|H,0,0.0524093553,5.4712853429,0.3263552743|
 H,0,0.9453020711,5.4787463893,-1.2714098843|C,0,-
0.7274646395,-3.60392
 527,-0.3587682323|H,0,-1.239917549,-3.0907822854,-
1.1544263005|C,0,-0.
 5650210412,-4.9143583383,-0.4393469326|H,0,-0.9453020711,-
5.4787463893
 ,-1.2714098843|H,0,-0.0524093553,-
5.4712853429,0.3263552743||Version=x
 86-Win32-G03RevB.05|State=1-A|HF=-385.5687065|MP2=-
386.8234788|RMSD=1.
 118e-009|PG=C02 [X(C10H12)]||@
```

```
 ANYONE WHO IS NOT SHOCKED BY QUANTUM THEORY HAS
 NOT UNDERSTOOD IT. -- NIELS BOHR(1885-1962)
 Job cpu time:  0 days  2 hours 52 minutes 10.0 seconds.
 File lengths (MBytes):  RWF=   1933 Int=      0 D2E=
0 Chk=     18 Scr=      1
 Normal termination of Gaussian 03 at Tue Feb 28 10:54:42
2006.
```

180 Degree Dihedral Angles:

```
Entering Link 1 = C:\G03W\l1.exe PID=      2200.

 Copyright (c) 1988,1990,1992,1993,1995,1998,2003,
Gaussian, Inc.
                  All Rights Reserved.

 This is the Gaussian(R) 03 program.  It is based on the
 the Gaussian(R) 98 system (copyright 1998, Gaussian,
Inc.),
 the Gaussian(R) 94 system (copyright 1995, Gaussian,
Inc.),
 the Gaussian 92(TM) system (copyright 1992, Gaussian,
Inc.),
 the Gaussian 90(TM) system (copyright 1990, Gaussian,
Inc.),
 the Gaussian 88(TM) system (copyright 1988, Gaussian,
Inc.),
 the Gaussian 86(TM) system (copyright 1986, Carnegie
Mellon
 University), and the Gaussian 82(TM) system (copyright
1983,
 Carnegie Mellon University). Gaussian is a federally
registered
 trademark of Gaussian, Inc.

 This software contains proprietary and confidential
information,
 including trade secrets, belonging to Gaussian, Inc.

 This software is provided under written license and may be
 used, copied, transmitted, or stored only in accord with
that
```

written license.

The following legend is applicable only to US Government contracts under DFARS:

RESTRICTED RIGHTS LEGEND

Use, duplication or disclosure by the US Government is subject to restrictions as set forth in subparagraph (c)(1)(ii) of the Rights in Technical Data and Computer Software clause at DFARS 252.227-7013.

Gaussian, Inc.
Carnegie Office Park, Building 6, Pittsburgh, PA 15106 USA

The following legend is applicable only to US Government contracts under FAR:

RESTRICTED RIGHTS LEGEND

Use, reproduction and disclosure by the US Government is subject to restrictions as set forth in subparagraph (c) of the Commercial Computer Software - Restricted Rights clause at FAR 52.227-19.

Gaussian, Inc.
Carnegie Office Park, Building 6, Pittsburgh, PA 15106 USA

Warning -- This program may not be used in any manner that competes with the business of Gaussian, Inc. or will provide assistance to any competitor of Gaussian, Inc. The licensee of this program is prohibited from giving any competitor of Gaussian, Inc. access to this program. By using this program,

Cite this work as:
Gaussian 03, Revision B.05,
M. J. Frisch, G. W. Trucks, H. B. Schlegel, G. E. Scuseria,
M. A. Robb, J. R. Cheeseman, J. A. Montgomery, Jr., T. Vreven,
K. N. Kudin, J. C. Burant, J. M. Millam, S. S. Iyengar, J. Tomasi,
V. Barone, B. Mennucci, M. Cossi, G. Scalmani, N. Rega,
G. A. Petersson, H. Nakatsuji, M. Hada, M. Ehara, K. Toyota,
R. Fukuda, J. Hasegawa, M. Ishida, T. Nakajima, Y. Honda, O. Kitao,
H. Nakai, M. Klene, X. Li, J. E. Knox, H. P. Hratchian, J. B. Cross,
C. Adamo, J. Jaramillo, R. Gomperts, R. E. Stratmann, O. Yazyev,
A. J. Austin, R. Cammi, C. Pomelli, J. W. Ochterski, P. Y. Ayala,
K. Morokuma, G. A. Voth, P. Salvador, J. J. Dannenberg,
V. G. Zakrzewski, S. Dapprich, A. D. Daniels, M. C. Strain,
O. Farkas, D. K. Malick, A. D. Rabuck, K. Raghavachari,
J. B. Foresman, J. V. Ortiz, Q. Cui, A. G. Baboul, S. Clifford,
J. Cioslowski, B. B. Stefanov, G. Liu, A. Liashenko, P. Piskorz,
I. Komaromi, R. L. Martin, D. J. Fox, T. Keith, M. A. Al-Laham,
C. Y. Peng, A. Nanayakkara, M. Challacombe, P. M. W. Gill,
B. Johnson, W. Chen, M. W. Wong, C. Gonzalez, and J. A. Pople,

```
 Gaussian, Inc., Pittsburgh PA, 2003.

 ******************************************
 Gaussian 03:  x86-Win32-G03RevB.05  8-Nov-2003
                27-Feb-2006
 ******************************************
 %chk=180.chk
 %mem=64MB
 %nproc=1
 Will use up to    1 processors via shared memory.
 Default route:  MaxDisk=2000MB
 ----------------------------------------------------------------
 # hf/6-31g(d) geom=(modredundant,connectivity) symm=loose
ovgf
 ----------------------------------------------------------------
 1/18=120,38=1,57=2/1;
 2/17=4,18=3,40=1/2;
 3/5=1,6=6,7=1,11=9,16=1,25=1,30=1/1,2,3;
 4//1;
 5/5=2,38=5/2;
 8/6=4,9=120000,10=2,27=262144000/1,4;
 9/11=20000,27=262144000/8;
 6/7=2,8=2,9=2,10=2/1;
 99/5=1,9=1/99;
 ---
 180
 ---
 Symbolic Z-matrix:
 Charge =  0 Multiplicity = 1
 C                     0.        1.53573   0.70004
 C                     0.        2.86706   0.69128
 C                     0.        0.6666   -0.47237
 C                     0.       -0.6666   -0.47237
 C                     0.       -1.53573   0.70004
 C                     0.       -2.86706   0.69128
 H                     0.        1.15367  -1.42795
 H                     0.       -1.15367  -1.42795
 H                     0.        3.37616   1.63857
 H                     0.        1.05341   1.65775
 H                     0.       -3.37616   1.63857
 H                     0.       -1.05341   1.65775
 C                     0.        3.74523  -0.4796
 H                     0.        3.28766  -1.44993
```

```
 C                     0.        5.06447  -0.39136
 H                     0.        5.56912   0.55716
 H                     0.        5.68843  -1.2636
 C                     0.       -3.74523  -0.4796
 H                     0.       -3.28766  -1.44993
 C                     0.       -5.06447  -0.39136
 H                     0.       -5.68843  -1.2636
 H                     0.       -5.56912   0.55716

 The following ModRedundant input section has been read:
 D    5    6   18   20 180.00 F
 D    3    4    5    6 180.00 F
 D    2    1    3    4 180.00 F
 D    1    2   13   15 180.00 F
 Iteration  1 RMS(Cart)=  0.00000000 RMS(Int)=  0.00000000
 Iteration  1 RMS(Cart)=  0.00000000 RMS(Int)=  0.00000000
                         Input orientation:
 ---------------------------------------------------------------
-----------
 Center     Atomic     Atomic              Coordinates
(Angstroms)
 Number     Number      Type              X           Y
Z
 ---------------------------------------------------------------
-----------
    1          6             0        0.000000    1.535727
0.700041
    2          6             0        0.000000    2.867060
0.691284
    3          6             0        0.000000    0.666598
-0.472368
    4          6             0        0.000000   -0.666598
-0.472368
    5          6             0        0.000000   -1.535727
0.700041
    6          6             0        0.000000   -2.867060
0.691284
    7          1             0        0.000000    1.153667
-1.427952
    8          1             0        0.000000   -1.153667
-1.427952
    9          1             0        0.000000    3.376157
1.638572
   10          1             0        0.000000    1.053410
1.657753
```

```
   11          1             0        0.000000   -3.376157
1.638572
   12          1             0        0.000000   -1.053410
1.657753
   13          6             0        0.000000    3.745227
-0.479598
   14          1             0        0.000000    3.287661
-1.449934
   15          6             0        0.000000    5.064465
-0.391358
   16          1             0        0.000000    5.569119
0.557159
   17          1             0        0.000000    5.688432
-1.263600
   18          6             0        0.000000   -3.745227
-0.479598
   19          1             0        0.000000   -3.287661
-1.449934
   20          6             0        0.000000   -5.064465
-0.391358
   21          1             0        0.000000   -5.688432
-1.263600
   22          1             0        0.000000   -5.569119
0.557159
 ---------------------------------------------------------
-----------
                    Distance matrix (angstroms):
                    1          2          3          4
5
     1  C    0.000000
     2  C    1.331362   0.000000
     3  C    1.459427   2.489200   0.000000
     4  C    2.494951   3.720326   1.333196   0.000000
     5  C    3.071454   4.402796   2.494951   1.459427
0.000000
     6  C    4.402796   5.734120   3.720326   2.489200
1.331362
     7  H    2.162019   2.725230   1.072556   2.055847
3.429460
     8  H    3.429460   4.545042   2.055847   1.072556
2.162019
     9  H    2.065919   1.075423   3.434789   4.560695
5.000744
    10  H    1.072307   2.055088   2.164957   2.737854
2.760587
```

11	H	5.000744	6.314674	4.560695	3.434789	2.065919
12	H	2.760587	4.037839	2.737854	2.164957	1.072307
13	C	2.504683	1.463606	3.078637	4.411831	5.411102
14	H	2.773385	2.182137	2.797429	4.073303	5.280858
15	C	3.693663	2.449633	4.398613	5.731636	6.689820
16	H	4.035922	2.705386	5.009455	6.320134	7.106283
17	H	4.593566	3.432450	5.083784	6.404097	7.486278
18	C	5.411102	6.715155	4.411831	3.078637	2.504683
19	H	5.280858	6.516549	4.073303	2.797429	2.773385
20	C	6.689820	8.005074	5.731636	4.398613	3.693663
21	H	7.486278	8.775991	6.404097	5.083784	4.593566
22	H	7.106283	8.437245	6.320134	5.009455	4.035922

		6	7	8	9	10
6	C	0.000000				
7	H	4.545042	0.000000			
8	H	2.725230	2.307334	0.000000		
9	H	6.314674	3.787219	5.470181	0.000000	
10	H	4.037839	3.087333	3.793780	2.322826	0.000000
11	H	1.075423	5.470181	3.787219	6.752314	4.429609
12	H	2.055088	3.793780	3.087333	4.429609	2.106820
13	C	6.715155	2.759630	4.989843	2.150083	3.437172
14	H	6.516549	2.134107	4.441382	3.089774	3.827479
15	C	8.005074	4.045846	6.303943	2.640265	4.504156
16	H	8.437245	4.841165	7.009744	2.445105	4.647896

```
    17  H    8.775991   4.537742   6.844073   3.710690
5.478844
    18  C    1.463606   4.989843   2.759630   7.429721
5.253112
    19  H    2.182137   4.441382   2.134107   7.344749
5.338784
    20  C    2.449633   6.303943   4.045846   8.681285
6.451918
    21  H    3.432450   6.844073   4.537742   9.517845
7.347567
    22  H    2.705386   7.009744   4.841165   9.010406
6.713360
                   11         12         13         14
15
    11  H    0.000000
    12  H    2.322826   0.000000
    13  C    7.429721   5.253112   0.000000
    14  H    7.344749   5.338784   1.072809   0.000000
    15  C    8.681285   6.451918   1.322186   2.068240
0.000000
    16  H    9.010406   6.713360   2.097963   3.038663
1.074412
    17  H    9.517845   7.347567   2.095401   2.407991
1.072446
    18  C    2.150083   3.437172   7.490454   7.099512
8.810134
    19  H    3.089774   3.827479   7.099512   6.575322
8.418942
    20  C    2.640265   4.504156   8.810134   8.418942
10.128930
    21  H    3.710690   5.478844   9.466181   8.978027
10.788216
    22  H    2.445105   4.647896   9.371868   9.081353
10.675804
                   16         17         18         19
20
    16  H    0.000000
    17  H    1.824664   0.000000
    18  C    9.371868   9.466181   0.000000
    19  H    9.081353   8.978027   1.072809   0.000000
    20  C   10.675804  10.788216   1.322186   2.068240
0.000000
    21  H   11.403842  11.376864   2.095401   2.407991
1.072446
```

```
    22  H   11.138238  11.403842   2.097963   3.038663
1.074412
                   21         22
    21  H    0.000000
    22  H    1.824664   0.000000
 Stoichiometry    C10H12
 Framework group  C2V[SGV(C10H12)]
 Deg. of freedom    21
 Full point group                 C2V     NOp   4
 Largest Abelian subgroup         C2V     NOp   4
 Largest concise Abelian subgroup C2      NOp   2
                         Standard orientation:
 ---------------------------------------------------------
-----------
 Center     Atomic     Atomic              Coordinates
(Angstroms)
 Number     Number      Type              X           Y
Z
 ---------------------------------------------------------
-----------
    1          6             0        0.000000    1.535727
0.700041
    2          6             0        0.000000    2.867060
0.691284
    3          6             0        0.000000    0.666598
-0.472368
    4          6             0        0.000000   -0.666598
-0.472368
    5          6             0        0.000000   -1.535727
0.700041
    6          6             0        0.000000   -2.867060
0.691284
    7          1             0        0.000000    1.153667
-1.427952
    8          1             0        0.000000   -1.153667
-1.427952
    9          1             0        0.000000    3.376157
1.638572
   10          1             0        0.000000    1.053410
1.657753
   11          1             0        0.000000   -3.376157
1.638572
   12          1             0        0.000000   -1.053410
1.657753
```

```
   13          6             0        0.000000    3.745227
-0.479598
   14          1             0        0.000000    3.287661
-1.449934
   15          6             0        0.000000    5.064465
-0.391358
   16          1             0        0.000000    5.569119
0.557159
   17          1             0        0.000000    5.688432
-1.263600
   18          6             0        0.000000   -3.745227
-0.479598
   19          1             0        0.000000   -3.287661
-1.449934
   20          6             0        0.000000   -5.064465
-0.391358
   21          1             0        0.000000   -5.688432
-1.263600
   22          1             0        0.000000   -5.569119
0.557159
 ---------------------------------------------------------
-----------
 Rotational constants (GHZ):      8.2955116      0.3624917
0.3473150
 Standard basis: 6-31G(d) (6D, 7F)
 There are    67 symmetry adapted basis functions of A1
symmetry.
 There are    20 symmetry adapted basis functions of A2
symmetry.
 There are    20 symmetry adapted basis functions of B1
symmetry.
 There are    67 symmetry adapted basis functions of B2
symmetry.
 Integral buffers will be    262144 words long.
 Raffenetti 1 integral format.
 Two-electron integral symmetry is turned on.
   174 basis functions,   328 primitive gaussians,   174
cartesian basis functions
    36 alpha electrons       36 beta electrons
       nuclear repulsion energy       426.3724773184
Hartrees.
 NAtoms=   22 NActive=   22 NUniq=   11 SFac= 5.66D+00
NAtFMM=   60 Big=F
 One-electron integrals computed using PRISM.
 NBasis=   174 RedAO= T  NBF=    67    20    20    67
```

```
 NBsUse=   174 1.00D-06 NBFU=    67    20    20    67
 Harris functional with IExCor=  205 diagonalized for
initial guess.
 ExpMin= 1.61D-01 ExpMax= 3.05D+03 ExpMxC= 4.57D+02 IAcc=1
IRadAn=         1 AccDes= 1.00D-06
 HarFok:  IExCor= 205 AccDes= 1.00D-06 IRadAn=         1
IDoV=1
 ScaDFX=  1.000000  1.000000  1.000000  1.000000
 Initial guess orbital symmetries:
       Occupied  (B2) (A1) (B2) (A1) (A1) (B2) (A1) (B2)
(A1) (B2)
                 (A1) (B2) (A1) (B2) (A1) (B2) (A1) (B2)
(A1) (A1)
                 (B2) (A1) (B2) (A1) (B2) (B2) (A1) (A1)
(B2) (B1)
                 (A1) (A2) (B2) (B1) (A2) (B1)
       Virtual   (A2) (B1) (A2) (B1) (A2) (A1) (A1) (B2)
(B2) (A1)
                 (A1) (B2) (B2) (A1) (A1) (A1) (B2) (B2)
(B2) (A1)
                 (B2) (B2) (A1) (A1) (A1) (B2) (B2) (A1)
(B1) (A2)
                 (B2) (B1) (B2) (A1) (A2) (A1) (B2) (A1)
(B1) (B2)
                 (A1) (A2) (B1) (B2) (B1) (A1) (A2) (A2)
(B2) (A1)
                 (A1) (B2) (A1) (B2) (A1) (B2) (A1) (B2)
(A1) (B2)
                 (A1) (A1) (B2) (B2) (B2) (A1) (B2) (A1)
(A1) (B2)
                 (B2) (B1) (A1) (B2) (A2) (B1) (B1) (A1)
(A2) (B2)
                 (B1) (A2) (B1) (A2) (A1) (B2) (B1) (A2)
(A1) (B2)
                 (B2) (A1) (A1) (B2) (A1) (B2) (A1) (B2)
(B1) (A1)
                 (B2) (A2) (A1) (B1) (A2) (B2) (A1) (B2)
(A1) (B2)
                 (B1) (A2) (A2) (A1) (B1) (A1) (B2) (B2)
(A2) (A1)
                 (B2) (A1) (B2) (B2) (A1) (A1) (B2) (B2)
(A1) (B2)
                 (A1) (B2) (A1) (B2) (A1) (B2) (A1) (B2)
 The electronic state of the initial guess is 1-A1.
```

```
 Requested convergence on RMS density matrix=1.00D-08
within 128 cycles.
 Requested convergence on MAX density matrix=1.00D-06.
 Requested convergence on                energy=1.00D-06.
 No special actions if energy rises.
 Integral accuracy reduced to 1.0D-05 until final
iterations.
 Initial convergence to 1.0D-05 achieved.  Increase
integral accuracy.
 SCF Done:  E(RHF) =  -385.575676450     A.U. after   14
cycles
             Convg  =    0.3523D-08             -V/T =
2.0005
             S**2   =   0.0000
 ExpMin= 1.61D-01 ExpMax= 3.05D+03 ExpMxC= 4.57D+02 IAcc=1
IRadAn=         1 AccDes= 1.00D-06
 HarFok:  IExCor= 205 AccDes= 1.00D-06 IRadAn=         1
IDoV=1
 ScaDFX=  1.000000  1.000000  1.000000  1.000000
 Range of M.O.s used for correlation:    11   174
 NBasis=   174 NAE=    36 NBE=    36 NFC=    10 NFV=     0
 NROrb=    164 NOA=    26 NOB=    26 NVA=   138 NVB=   138
 Semi-Direct transformation.
 ModeAB=           4 MOrb=            26 LenV=
7799870
 LASXX=     13774702 LTotXX=    13774702 LenRXX=
27854850
 LTotAB=    14080148 MaxLAS=    25447552 LenRXY=
0
 NonZer=    41629552 LenScr=    67624960 LnRSAI=
25447552
 LnScr1=    43309056 LExtra=     2955978 Total=
167192396
 MaxDsk=   262144000 SrtSym=           T ITran=
4
 JobTyp=0 Pass  1:  I=   1 to  26.
 Spin components of T(2) and E(2):
     alpha-alpha T2 =       0.5696733360D-01 E2=     -
0.1573098714D+00
     alpha-beta  T2 =       0.3416712483D+00 E2=     -
0.9390671214D+00
     beta-beta   T2 =       0.5696733360D-01 E2=     -
0.1573098714D+00
 ANorm=    0.1206484942D+01
```

```
 E2=       -0.1253686864D+01 EUMP2=       -
0.38682936331425D+03
 GREENY: Electron Propagator Program
 Petite list used in FoFDir.
 MinBra= 0 MaxBra= 2 Meth= 1.
 IRaf=       0 NMat=   1 IRICut=       1 DoRegI=T DoRafI=F
ISym2E=-1 JSym2E=1.

 Orbital window will be selected automatically

    Alpha HOMO is orbital  26

 GREENY has selected a window containing alpha orbitals

             9 through  27

 from symmetry group number 1 of the 4 total symmetry
operations

 Summary of results for alpha spin-orbital   9  OVGF:
 Koopmans theorem:            -0.74982D+00 au  -20.404 eV
 Converged second order pole: -0.64439D+00 au  -17.535 eV
0.838 (PS)
 Converged third  order pole: -0.67112D+00 au  -18.262 eV
0.850 (PS)
 Outer Valence Approximation: -0.66147D+00 au  -17.999 eV
0.837 (PS)

 Summary of results for alpha spin-orbital  10  OVGF:
 Koopmans theorem:            -0.69984D+00 au  -19.044 eV
 Converged second order pole: -0.60113D+00 au  -16.358 eV
0.845 (PS)
 Converged third  order pole: -0.62699D+00 au  -17.061 eV
0.860 (PS)
 Outer Valence Approximation: -0.61751D+00 au  -16.803 eV
0.848 (PS)

 Summary of results for alpha spin-orbital  11  OVGF:
 Koopmans theorem:            -0.69039D+00 au  -18.786 eV
 Converged second order pole: -0.58807D+00 au  -16.002 eV
0.841 (PS)
 Converged third  order pole: -0.61844D+00 au  -16.829 eV
0.864 (PS)
 Outer Valence Approximation: -0.60585D+00 au  -16.486 eV
0.851 (PS)
```

```
 Summary of results for alpha spin-orbital  12  OVGF:
 Koopmans theorem:            -0.64264D+00 au  -17.487 eV
 Converged second order pole: -0.55024D+00 au  -14.973 eV
0.853 (PS)
 Converged third  order pole: -0.57498D+00 au  -15.646 eV
0.873 (PS)
 Outer Valence Approximation: -0.56437D+00 au  -15.357 eV
0.863 (PS)

 Summary of results for alpha spin-orbital  13  OVGF:
 Koopmans theorem:            -0.64209D+00 au  -17.472 eV
 Converged second order pole: -0.53840D+00 au  -14.650 eV
0.832 (PS)
 Converged third  order pole: -0.57519D+00 au  -15.652 eV
0.865 (PS)
 Outer Valence Approximation: -0.55985D+00 au  -15.234 eV
0.848 (PS)

 Summary of results for alpha spin-orbital  14  OVGF:
 Koopmans theorem:            -0.59657D+00 au  -16.234 eV
 Converged second order pole: -0.51128D+00 au  -13.913 eV
0.857 (PS)
 Converged third  order pole: -0.53557D+00 au  -14.574 eV
0.874 (PS)
 Outer Valence Approximation: -0.52633D+00 au  -14.322 eV
0.863 (PS)

 Summary of results for alpha spin-orbital  15  OVGF:
 Koopmans theorem:            -0.59259D+00 au  -16.125 eV
 Converged second order pole: -0.50609D+00 au  -13.771 eV
0.860 (PS)
 Converged third  order pole: -0.52873D+00 au  -14.388 eV
0.880 (PS)
 Outer Valence Approximation: -0.51875D+00 au  -14.116 eV
0.871 (PS)

 Summary of results for alpha spin-orbital  16  OVGF:
 Koopmans theorem:            -0.56151D+00 au  -15.279 eV
 Converged second order pole: -0.48108D+00 au  -13.091 eV
0.868 (PS)
 Converged third  order pole: -0.50406D+00 au  -13.716 eV
0.887 (PS)
 Outer Valence Approximation: -0.49477D+00 au  -13.463 eV
0.878 (PS)
```

```
 Summary of results for alpha spin-orbital  17  OVGF:
 Koopmans theorem:            -0.55424D+00 au  -15.082 eV
 Converged second order pole: -0.46950D+00 au  -12.776 eV
0.868 (PS)
 Converged third  order pole: -0.49254D+00 au  -13.403 eV
0.894 (PS)
 Outer Valence Approximation: -0.48137D+00 au  -13.099 eV
0.884 (PS)

 Summary of results for alpha spin-orbital  18  OVGF:
 Koopmans theorem:            -0.53902D+00 au  -14.667 eV
 Converged second order pole: -0.45044D+00 au  -12.257 eV
0.862 (PS)
 Converged third  order pole: -0.47783D+00 au  -13.002 eV
0.894 (PS)
 Outer Valence Approximation: -0.46477D+00 au  -12.647 eV
0.883 (PS)

 Summary of results for alpha spin-orbital  19  OVGF:
 Koopmans theorem:            -0.52808D+00 au  -14.370 eV
 Converged second order pole: -0.45089D+00 au  -12.269 eV
0.870 (PS)
 Converged third  order pole: -0.47395D+00 au  -12.897 eV
0.888 (PS)
 Outer Valence Approximation: -0.46475D+00 au  -12.646 eV
0.879 (PS)

 Summary of results for alpha spin-orbital  20  OVGF:
 Koopmans theorem:            -0.49369D+00 au  -13.434 eV
 Converged second order pole: -0.42030D+00 au  -11.437 eV
0.876 (PS)
 Converged third  order pole: -0.44259D+00 au  -12.043 eV
0.895 (PS)
 Outer Valence Approximation: -0.43339D+00 au  -11.793 eV
0.886 (PS)

 Summary of results for alpha spin-orbital  21  OVGF:
 Koopmans theorem:            -0.47874D+00 au  -13.027 eV
 Converged second order pole: -0.42038D+00 au  -11.439 eV
0.849 (PS)
 Converged third  order pole: -0.43785D+00 au  -11.915 eV
0.855 (PS)
 Outer Valence Approximation: -0.42917D+00 au  -11.678 eV
0.848 (PS)
```

```
 Summary of results for alpha spin-orbital  22  OVGF:
 Koopmans theorem:            -0.46141D+00 au  -12.556 eV
 Converged second order pole: -0.38538D+00 au  -10.487 eV
0.872 (PS)
 Converged third  order pole: -0.41091D+00 au  -11.181 eV
0.900 (PS)
 Outer Valence Approximation: -0.39983D+00 au  -10.880 eV
0.890 (PS)

 Summary of results for alpha spin-orbital  23  OVGF:
 Koopmans theorem:            -0.44708D+00 au  -12.166 eV
 Converged second order pole: -0.40184D+00 au  -10.935 eV
0.861 (PS)
 Converged third  order pole: -0.41435D+00 au  -11.275 eV
0.864 (PS)
 Outer Valence Approximation: -0.40733D+00 au  -11.084 eV
0.859 (PS)

 Summary of results for alpha spin-orbital  24  OVGF:
 Koopmans theorem:            -0.39715D+00 au  -10.807 eV
 Converged second order pole: -0.36485D+00 au   -9.928 eV
0.871 (PS)
 Converged third  order pole: -0.37400D+00 au  -10.177 eV
0.876 (PS)
 Outer Valence Approximation: -0.36803D+00 au  -10.015 eV
0.872 (PS)

 Summary of results for alpha spin-orbital  25  OVGF:
 Koopmans theorem:            -0.33372D+00 au   -9.081 eV
 Converged second order pole: -0.31392D+00 au   -8.542 eV
0.880 (PS)
 Converged third  order pole: -0.32047D+00 au   -8.720 eV
0.888 (PS)
 Outer Valence Approximation: -0.31906D+00 au   -8.682 eV
0.884 (PS)

 Summary of results for alpha spin-orbital  26  OVGF:
 Koopmans theorem:            -0.27018D+00 au   -7.352 eV
 Converged second order pole: -0.25741D+00 au   -7.004 eV
0.880 (PS)
 Converged third  order pole: -0.26309D+00 au   -7.159 eV
0.893 (PS)
 Outer Valence Approximation: -0.26184D+00 au   -7.125 eV
0.889 (PS)
```

```
 DD1Dir will call FoFDir   4 times, MxPair=       176
 NAB=   351 NAA=     0 NBB=     0 NumPrc=  1.

 Summary of results for alpha spin-orbital  27  OVGF:
 Koopmans theorem:             0.82860D-01 au    2.255 eV
 Converged second order pole:  0.21427D-01 au    0.583 eV
0.890 (PS)
 Converged third  order pole:  0.52444D-01 au    1.427 eV
0.897 (PS)
 Outer Valence Approximation:  0.46790D-01 au    1.273 eV
0.895 (PS)


**************************************************************
***********

           Population analysis using the SCF density.


**************************************************************
***********

 Orbital symmetries:
       Occupied  (A1) (B2) (A1) (B2) (A1) (B2) (A1) (B2)
(B2) (A1)
                 (A1) (B2) (A1) (B2) (A1) (B2) (A1) (B2)
(A1) (B2)
                 (A1) (B2) (A1) (B2) (A1) (A1) (B2) (A1)
(B2) (A1)
                 (B1) (B2) (A2) (B1) (A2) (B1)
       Virtual   (A2) (B1) (A2) (A1) (B2) (A1) (B2) (B1)
(A1) (B2)
                 (A1) (B2) (A2) (A1) (A1) (B2) (A1) (B2)
(B2) (A1)
                 (B2) (A1) (B2) (B2) (A1) (A1) (A1) (B1)
(B2) (A2)
                 (A1) (B2) (B1) (B2) (A1) (B2) (A2) (B1)
(A1) (A1)
                 (A2) (B1) (B2) (B1) (B2) (A1) (A2) (A2)
(B2) (A1)
                 (B2) (A1) (A1) (B2) (A1) (B2) (A1) (B2)
(A1) (B2)
                 (A1) (B2) (B2) (A1) (A1) (B2) (B2) (A1)
(B2) (A1)
```

```
                 (B2) (A1) (B2) (B1) (A2) (A1) (B2) (B1)
(B1) (A2)
                 (A1) (B2) (B1) (A2) (B1) (A2) (B2) (B1)
(A2) (A1)
                 (B2) (A1) (B2) (A1) (A1) (A1) (B2) (B2)
(B1) (A2)
                 (A1) (B2) (B1) (A1) (A2) (B2) (A1) (B2)
(A1) (B2)
                 (B1) (A2) (A2) (A1) (B1) (A1) (B2) (B2)
(A2) (A1)
                 (B2) (A1) (B2) (B2) (A1) (A1) (B2) (B2)
(A1) (B2)
                 (A1) (B2) (A1) (B2) (A1) (B2) (A1) (B2)
 The electronic state is 1-A1.
 Alpha  occ. eigenvalues --  -11.23475 -11.23467 -11.23457
-11.23399 -11.23393
 Alpha  occ. eigenvalues --  -11.23304 -11.23211 -11.23202
-11.22478 -11.22478
 Alpha  occ. eigenvalues --   -1.12024  -1.09694  -1.06077
-1.01565  -0.97446
 Alpha  occ. eigenvalues --   -0.85287  -0.82612  -0.79255
-0.74982  -0.69984
 Alpha  occ. eigenvalues --   -0.69039  -0.64264  -0.64209
-0.59657  -0.59259
 Alpha  occ. eigenvalues --   -0.56151  -0.55424  -0.53902
-0.52808  -0.49369
 Alpha  occ. eigenvalues --   -0.47874  -0.46141  -0.44708
-0.39715  -0.33372
 Alpha  occ. eigenvalues --   -0.27018
 Alpha virt. eigenvalues --    0.08286   0.14129   0.20444
0.22963   0.26135
 Alpha virt. eigenvalues --    0.26548   0.26946   0.27229
0.27778   0.30481
 Alpha virt. eigenvalues --    0.30962   0.33693   0.33927
0.33964   0.38160
 Alpha virt. eigenvalues --    0.40886   0.41289   0.44493
0.48204   0.50035
 Alpha virt. eigenvalues --    0.53293   0.53399   0.56972
0.60762   0.62446
 Alpha virt. eigenvalues --    0.65381   0.69188   0.73578
0.74626   0.75794
 Alpha virt. eigenvalues --    0.77576   0.78811   0.79079
0.80107   0.80990
 Alpha virt. eigenvalues --    0.82702   0.82935   0.85504
0.85801   0.87125
```

```
 Alpha virt. eigenvalues --    0.89344   0.91118   0.91217
0.92372   0.93598
 Alpha virt. eigenvalues --    0.94704   0.96859   0.97838
1.11261   1.11508
 Alpha virt. eigenvalues --    1.12098   1.12831   1.13258
1.14307   1.15471
 Alpha virt. eigenvalues --    1.17514   1.18252   1.21558
1.21891   1.23239
 Alpha virt. eigenvalues --    1.23384   1.24570   1.25681
1.25701   1.28862
 Alpha virt. eigenvalues --    1.32721   1.34260   1.36255
1.39151   1.39812
 Alpha virt. eigenvalues --    1.44469   1.47069   1.51500
1.53692   1.59928
 Alpha virt. eigenvalues --    1.60678   1.62392   1.66796
1.68786   1.70113
 Alpha virt. eigenvalues --    1.78000   1.78849   1.80504
1.82245   1.84870
 Alpha virt. eigenvalues --    1.85254   1.96241   2.00636
2.02039   2.04473
 Alpha virt. eigenvalues --    2.14193   2.14193   2.20515
2.21206   2.26575
 Alpha virt. eigenvalues --    2.29048   2.30478   2.36459
2.37823   2.39346
 Alpha virt. eigenvalues --    2.39448   2.40856   2.42539
2.43245   2.43363
 Alpha virt. eigenvalues --    2.51669   2.54252   2.60141
2.65549   2.73254
 Alpha virt. eigenvalues --    2.75781   2.76322   2.78859
2.80449   2.86680
 Alpha virt. eigenvalues --    2.89580   2.89845   2.92929
2.94741   3.01377
 Alpha virt. eigenvalues --    3.14319   3.14816   3.22970
3.31251   3.34791
 Alpha virt. eigenvalues --    3.50300   3.56419   3.63866
4.50789   4.52657
 Alpha virt. eigenvalues --    4.54554   4.56557   4.59214
4.63193   4.71003
 Alpha virt. eigenvalues --    4.80797   4.92375   5.03073
          Condensed to atoms (all electrons):
               1          2          3          4          5
6
     1  C    4.906782   0.654676   0.418379  -0.048546  -
0.005730   0.000287
```

```
     2  C    0.654676   4.898892  -0.048014   0.001032
0.000287  -0.000003
     3  C    0.418379  -0.048014   4.906778   0.653207  -
0.048546   0.001032
     4  C   -0.048546   0.001032   0.653207   4.906778
0.418379  -0.048014
     5  C   -0.005730   0.000287  -0.048546   0.418379
4.906782   0.654676
     6  C    0.000287  -0.000003   0.001032  -0.048014
0.654676   4.898892
     7  H   -0.039353  -0.001180   0.389816  -0.033032
0.002654  -0.000104
     8  H    0.002654  -0.000104  -0.033032   0.389816  -
0.039353  -0.001180
     9  H   -0.032870   0.391659   0.002676  -0.000105
0.000000   0.000000
    10  H    0.388432  -0.032022  -0.039130  -0.001308
0.000556   0.000104
    11  H    0.000000   0.000000  -0.000105   0.002676  -
0.032870   0.391659
    12  H    0.000556   0.000104  -0.001308  -0.039130
0.388432  -0.032022
    13  C   -0.051554   0.417222  -0.005719   0.000289  -
0.000002   0.000000
    14  H   -0.001309  -0.037625   0.000498   0.000107  -
0.000001   0.000000
    15  C    0.001227  -0.048705   0.000270  -0.000004
0.000000   0.000000
    16  H    0.000144  -0.002356   0.000008   0.000000
0.000000   0.000000
    17  H   -0.000090   0.002394  -0.000002   0.000000
0.000000   0.000000
    18  C   -0.000002   0.000000   0.000289  -0.005719  -
0.051554   0.417222
    19  H   -0.000001   0.000000   0.000107   0.000498  -
0.001309  -0.037625
    20  C    0.000000   0.000000  -0.000004   0.000270
0.001227  -0.048705
    21  H    0.000000   0.000000   0.000000  -0.000002  -
0.000090   0.002394
    22  H    0.000000   0.000000   0.000000   0.000008
0.000144  -0.002356
              7          8          9         10         11
12
```

```
     1  C   -0.039353   0.002654  -0.032870   0.388432
0.000000   0.000556
     2  C   -0.001180  -0.000104   0.391659  -0.032022
0.000000   0.000104
     3  C    0.389816  -0.033032   0.002676  -0.039130  -
0.000105  -0.001308
     4  C   -0.033032   0.389816  -0.000105  -0.001308
0.002676  -0.039130
     5  C    0.002654  -0.039353   0.000000   0.000556  -
0.032870   0.388432
     6  C   -0.000104  -0.001180   0.000000   0.000104
0.391659  -0.032022
     7  H    0.487537  -0.003707  -0.000047   0.002738
0.000002  -0.000043
     8  H   -0.003707   0.487537   0.000002  -0.000043  -
0.000047   0.002738
     9  H   -0.000047   0.000002   0.488976  -0.003898
0.000000   0.000001
    10  H    0.002738  -0.000043  -0.003898   0.486405
0.000001   0.001240
    11  H    0.000002  -0.000047   0.000000   0.000001
0.488976  -0.003898
    12  H   -0.000043   0.002738   0.000001   0.001240  -
0.003898   0.486405
    13  C    0.000780  -0.000002  -0.042913   0.002875
0.000000  -0.000001
    14  H    0.001199   0.000000   0.002773  -0.000047
0.000000   0.000000
    15  C    0.000062   0.000000  -0.000018  -0.000117
0.000000   0.000000
    16  H    0.000001   0.000000   0.003348  -0.000013
0.000000   0.000000
    17  H   -0.000001   0.000000  -0.000013   0.000002
0.000000   0.000000
    18  C   -0.000002   0.000780   0.000000  -0.000001  -
0.042913   0.002875
    19  H    0.000000   0.001199   0.000000   0.000000
0.002773  -0.000047
    20  C    0.000000   0.000062   0.000000   0.000000  -
0.000018  -0.000117
    21  H    0.000000  -0.000001   0.000000   0.000000  -
0.000013   0.000002
    22  H    0.000000   0.000001   0.000000   0.000000
0.003348  -0.000013
```

```
             13         14         15         16         17
18
     1  C   -0.051554  -0.001309   0.001227   0.000144  -
0.000090  -0.000002
     2  C    0.417222  -0.037625  -0.048705  -0.002356
0.002394   0.000000
     3  C   -0.005719   0.000498   0.000270   0.000008  -
0.000002   0.000289
     4  C    0.000289   0.000107  -0.000004   0.000000
0.000000  -0.005719
     5  C   -0.000002  -0.000001   0.000000   0.000000
0.000000  -0.051554
     6  C    0.000000   0.000000   0.000000   0.000000
0.000000   0.417222
     7  H    0.000780   0.001199   0.000062   0.000001  -
0.000001  -0.000002
     8  H   -0.000002   0.000000   0.000000   0.000000
0.000000   0.000780
     9  H   -0.042913   0.002773  -0.000018   0.003348  -
0.000013   0.000000
    10  H    0.002875  -0.000047  -0.000117  -0.000013
0.000002  -0.000001
    11  H    0.000000   0.000000   0.000000   0.000000
0.000000  -0.042913
    12  H   -0.000001   0.000000   0.000000   0.000000
0.000000   0.002875
    13  C    4.865665   0.391793   0.639521  -0.045926  -
0.036442   0.000000
    14  H    0.391793   0.487913  -0.036762   0.003174  -
0.003020   0.000000
    15  C    0.639521  -0.036762   5.059944   0.397199
0.396283   0.000000
    16  H   -0.045926   0.003174   0.397199   0.491537  -
0.026721   0.000000
    17  H   -0.036442  -0.003020   0.396283  -0.026721
0.484225   0.000000
    18  C    0.000000   0.000000   0.000000   0.000000
0.000000   4.865665
    19  H    0.000000   0.000000   0.000000   0.000000
0.000000   0.391793
    20  C    0.000000   0.000000   0.000000   0.000000
0.000000   0.639521
    21  H    0.000000   0.000000   0.000000   0.000000
0.000000  -0.036442
```

```
    22  H    0.000000   0.000000   0.000000   0.000000
0.000000  -0.045926
              19         20         21         22
     1  C   -0.000001   0.000000   0.000000   0.000000
     2  C    0.000000   0.000000   0.000000   0.000000
     3  C    0.000107  -0.000004   0.000000   0.000000
     4  C    0.000498   0.000270  -0.000002   0.000008
     5  C   -0.001309   0.001227  -0.000090   0.000144
     6  C   -0.037625  -0.048705   0.002394  -0.002356
     7  H    0.000000   0.000000   0.000000   0.000000
     8  H    0.001199   0.000062  -0.000001   0.000001
     9  H    0.000000   0.000000   0.000000   0.000000
    10  H    0.000000   0.000000   0.000000   0.000000
    11  H    0.002773  -0.000018  -0.000013   0.003348
    12  H   -0.000047  -0.000117   0.000002  -0.000013
    13  C    0.000000   0.000000   0.000000   0.000000
    14  H    0.000000   0.000000   0.000000   0.000000
    15  C    0.000000   0.000000   0.000000   0.000000
    16  H    0.000000   0.000000   0.000000   0.000000
    17  H    0.000000   0.000000   0.000000   0.000000
    18  C    0.391793   0.639521  -0.036442  -0.045926
    19  H    0.487913  -0.036762  -0.003020   0.003174
    20  C   -0.036762   5.059944   0.396283   0.397199
    21  H   -0.003020   0.396283   0.484225  -0.026721
    22  H    0.003174   0.397199  -0.026721   0.491537
 Mulliken atomic charges:
              1
     1  C   -0.193682
     2  C   -0.196257
     3  C   -0.197199
     4  C   -0.197199
     5  C   -0.193682
     6  C   -0.196257
     7  H    0.192678
     8  H    0.192678
     9  H    0.190430
    10  H    0.194223
    11  H    0.190430
    12  H    0.194223
    13  C   -0.135587
    14  H    0.191305
    15  C   -0.408900
    16  H    0.179604
    17  H    0.183385
    18  C   -0.135587
```

```
    19  H    0.191305
    20  C   -0.408900
    21  H    0.183385
    22  H    0.179604
 Sum of Mulliken charges=   0.00000
 Atomic charges with hydrogens summed into heavy atoms:
              1
     1  C    0.000541
     2  C   -0.005828
     3  C   -0.004521
     4  C   -0.004521
     5  C    0.000541
     6  C   -0.005828
     7  H    0.000000
     8  H    0.000000
     9  H    0.000000
    10  H    0.000000
    11  H    0.000000
    12  H    0.000000
    13  C    0.055718
    14  H    0.000000
    15  C   -0.045911
    16  H    0.000000
    17  H    0.000000
    18  C    0.055718
    19  H    0.000000
    20  C   -0.045911
    21  H    0.000000
    22  H    0.000000
 Sum of Mulliken charges=   0.00000
 Electronic spatial extent (au):  <R**2>=  3082.0025
 Charge=     0.0000 electrons
 Dipole moment (field-independent basis, Debye):
    X=     0.0000    Y=     0.0000    Z=    -0.0573  Tot=
0.0573
 Quadrupole moment (field-independent basis, Debye-Ang):
   XX=   -68.3116   YY=   -53.7185   ZZ=   -54.5931
   XY=     0.0000   XZ=     0.0000   YZ=     0.0000
 Traceless Quadrupole moment (field-independent basis,
Debye-Ang):
   XX=    -9.4372   YY=     5.1558   ZZ=     4.2813
   XY=     0.0000   XZ=     0.0000   YZ=     0.0000
 Octapole moment (field-independent basis, Debye-Ang**2):
  XXX=     0.0000  YYY=     0.0000  ZZZ=    -0.0717  XYY=
0.0000
```

```
  XXY=     0.0000  XXZ=     0.0358  XZZ=     0.0000  YZZ=
0.0000
  YYZ=     0.6154  XYZ=     0.0000
 Hexadecapole moment (field-independent basis, Debye-
Ang**3):
 XXXX=   -73.4248 YYYY= -3601.1922 ZZZZ=  -234.4414 XXXY=
0.0000
 XXXZ=     0.0000 YYYX=     0.0000 YYYZ=     0.0000 ZZZX=
0.0000
 ZZZY=     0.0000 XXYY=  -766.4134 XXZZ=   -59.5966 YYZZ=
-635.0529
 XXYZ=     0.0000 YYXZ=     0.0000 ZZXY=     0.0000
 N-N= 4.263724773184D+02 E-N=-1.749794918536D+03  KE=
3.853726606116D+02
 Symmetry A1   KE= 1.889058739230D+02
 Symmetry A2   KE= 3.947562961623D+00
 Symmetry B1   KE= 5.979873458932D+00
 Symmetry B2   KE= 1.865393502680D+02
 1|1|UNPC-UNK|SP|ROVGF-FC|6-31G(d)|C10H12|PCUSER|27-Feb-
2006|0||# HF/6-
 31G(D) GEOM=(MODREDUNDANT,CONNECTIVITY) SYMM=LOOSE
OVGF||180||0,1|C,0,

0.,1.535727,0.700041|C,0,0.,2.86706,0.691284|C,0,0.,0.66659
8,-0.472368
 |C,0,0.,-0.666598,-0.472368|C,0,0.,-
1.535727,0.700041|C,0,0.,-2.86706,
 0.691284|H,0,0.,1.153667,-1.427952|H,0,0.,-1.153667,-
1.427952|H,0,0.,3
 .376157,1.638572|H,0,0.,1.05341,1.657753|H,0,0.,-
3.376157,1.638572|H,0
 ,0.,-1.05341,1.657753|C,0,0.,3.745227,-
0.479598|H,0,0.,3.287661,-1.449
 934|C,0,0.,5.064465,-
0.391358|H,0,0.,5.569119,0.557159|H,0,0.,5.688432
 ,-1.2636|C,0,0.,-3.745227,-0.479598|H,0,0.,-3.287661,-
1.449934|C,0,0.,
 -5.064465,-0.391358|H,0,0.,-5.688432,-1.2636|H,0,0.,-
5.569119,0.557159
 ||Version=x86-Win32-G03RevB.05|State=1-A1|HF=-
385.5756764|MP2=-386.829
 3633|RMSD=3.523e-009|PG=C02V [SGV(C10H12)]||@


 THE CAUTIOUS SELDOM ERR...CONFUCIUS
```

```
 Job cpu time:  0 days  0 hours 59 minutes  6.0 seconds.
 File lengths (MBytes):  RWF=   1280 Int=      0 D2E=
0 Chk=     14 Scr=      1
 Normal termination of Gaussian 03 at Mon Feb 27 18:20:41
2006.
```

Appendix C

Calculations for Compounds in Chapter 5

Dynamic Calculations:

All calculations were done using mm3 parameters, built in PC Model, minimized in Tinker Minimize. Dynamic calculations were done using Tinker Dynamics, viewed in VMD 1.8.6, and analyzed in Microsoft excel. Dynamic calculations were performed at a temperature of 298 K, except for **Compound 52** which was done at 445 K, with some or all of the following keywords: Archive, Rattle, SAVE-FORCE, SAVE-VELOCITY, # Partial Structure Inactive 2 4 6. Cartesian Coordinates for the optimized structures are below:

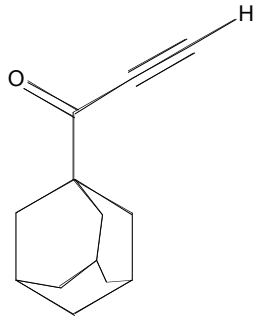

1-Adamantan-1-yl-propynone

```
HEADER    Untitled
COMPND
SOURCE
HETATM    1  C     1     1      -2.135  -1.276   1.161
HETATM    2  C     1     1      -1.015  -2.324   1.288
HETATM    3  C     1     1       0.039  -2.095   0.190
HETATM    4  C     1     1      -0.627  -2.215  -1.193
HETATM    5  C     1     1      -1.746  -1.167  -1.324
HETATM    6  C     1     1      -2.796  -1.402  -0.223
HETATM    7  C     1     1      -1.529   0.130   1.304
HETATM    8  C     1     1       0.629  -0.684   0.344
HETATM    9  C     1     1      -1.145   0.238  -1.154
HETATM   10  C     1     1      -0.466   0.393   0.220
HETATM   11  C     3     1       0.086   1.821   0.369
HETATM   12  O     7     1      -0.621   2.802   0.299
HETATM   13  C     4     1       1.372   1.984   0.581
```

```
HETATM   14  C     4     1       2.556   2.141   0.776
HETATM   15  H     5     1      -2.897  -1.441   1.959
HETATM   16  H     5     1      -0.541  -2.258   2.294
HETATM   17  H     5     1      -1.440  -3.350   1.203
HETATM   18  H     5     1       0.851  -2.856   0.283
HETATM   19  H     5     1       0.130  -2.070  -1.997
HETATM   20  H     5     1      -1.044  -3.239  -1.330
HETATM   21  H     5     1      -2.227  -1.253  -2.328
HETATM   22  H     5     1      -3.253  -2.411  -0.339
HETATM   23  H     5     1      -3.625  -0.664  -0.320
HETATM   24  H     5     1      -1.073   0.242   2.314
HETATM   25  H     5     1      -2.340   0.891   1.240
HETATM   26  H     5     1       1.137  -0.605   1.333
HETATM   27  H     5     1       1.413  -0.527  -0.432
HETATM   28  H     5     1      -1.947   1.001  -1.276
HETATM   29  H     5     1      -0.405   0.430  -1.965
HETATM   30  H     5     1       3.633   2.283   0.954
CONECT    1    2    6    7   15
CONECT    2    1    3   16   17
CONECT    3    2    4    8   18
CONECT    4    3    5   19   20
CONECT    5    4    6    9   21
CONECT    6    1    5   22   23
CONECT    7    1   10   24   25
CONECT    8    3   10   26   27
CONECT    9    5   10   28   29
CONECT   10    7    8    9   11
CONECT   11   10   12   13
CONECT   12   11
CONECT   13   11   14
CONECT   14   13   30
CONECT   15    1
CONECT   16    2
CONECT   17    2
CONECT   18    3
CONECT   19    4
CONECT   20    4
CONECT   21    5
CONECT   22    6
CONECT   23    6
CONECT   24    7
CONECT   25    7
CONECT   26    8
CONECT   27    8
CONECT   28    9
CONECT   29    9
CONECT   30   14
END
```

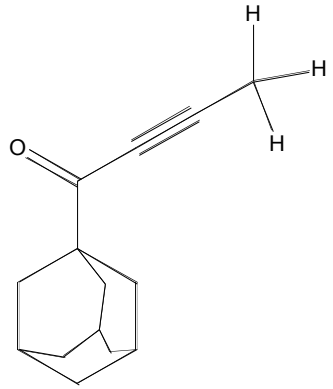

1-Adamantan-1-yl-but-2-yn-1-one

```
HEADER    Untitled
COMPND
SOURCE
HETATM    1  C      1      1       -2.561  -1.159   1.162
HETATM    2  C      1      1       -1.441  -2.207   1.289
HETATM    3  C      1      1       -0.387  -1.978   0.191
HETATM    4  C      1      1       -1.053  -2.098  -1.192
HETATM    5  C      1      1       -2.172  -1.050  -1.323
HETATM    6  C      1      1       -3.222  -1.285  -0.222
HETATM    7  C      1      1       -1.956   0.247   1.305
HETATM    8  C      1      1        0.202  -0.566   0.345
HETATM    9  C      1      1       -1.572   0.355  -1.154
HETATM   10  C      1      1       -0.893   0.511   0.221
HETATM   11  C      3      1       -0.343   1.940   0.370
HETATM   12  O      7      1       -1.051   2.919   0.300
HETATM   13  C      4      1        0.943   2.099   0.582
HETATM   14  C      4      1        2.128   2.247   0.777
HETATM   15  C      1      1        3.563   2.428   1.013
HETATM   16  H      5      1       -3.324  -1.325   1.960
HETATM   17  H      5      1       -0.967  -2.141   2.295
HETATM   18  H      5      1       -1.866  -3.233   1.204
HETATM   19  H      5      1        0.425  -2.738   0.284
HETATM   20  H      5      1       -0.296  -1.953  -1.996
HETATM   21  H      5      1       -1.470  -3.122  -1.328
HETATM   22  H      5      1       -2.653  -1.136  -2.327
HETATM   23  H      5      1       -3.679  -2.294  -0.338
HETATM   24  H      5      1       -4.051  -0.547  -0.319
HETATM   25  H      5      1       -1.500   0.359   2.315
HETATM   26  H      5      1       -2.768   1.007   1.241
HETATM   27  H      5      1        0.710  -0.487   1.334
HETATM   28  H      5      1        0.986  -0.409  -0.431
HETATM   29  H      5      1       -2.375   1.118  -1.275
HETATM   30  H      5      1       -0.831   0.547  -1.964
HETATM   31  H      5      1        3.965   3.205   0.328
HETATM   32  H      5      1        4.101   1.472   0.831
HETATM   33  H      5      1        3.737   2.747   2.064
CONECT    1    2    6    7   16
```

```
CONECT    2    1    3   17   18
CONECT    3    2    4    8   19
CONECT    4    3    5   20   21
CONECT    5    4    6    9   22
CONECT    6    1    5   23   24
CONECT    7    1   10   25   26
CONECT    8    3   10   27   28
CONECT    9    5   10   29   30
CONECT   10    7    8    9   11
CONECT   11   10   12   13
CONECT   12   11
CONECT   13   11   14
CONECT   14   13   15
CONECT   15   14   31   32   33
CONECT   16    1
CONECT   17    2
CONECT   18    2
CONECT   19    3
CONECT   20    4
CONECT   21    4
CONECT   22    5
CONECT   23    6
CONECT   24    6
CONECT   25    7
CONECT   26    7
CONECT   27    8
CONECT   28    8
CONECT   29    9
CONECT   30    9
CONECT   31   15
CONECT   32   15
CONECT   33   15
END
```

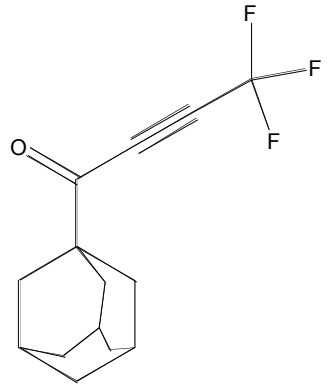

1-Adamantan-1-yl-4,4,4-trifluoro-but-2-yn-1-one

```
HEADER    Untitled
COMPND
SOURCE
HETATM    1  C     1     1      -2.689  -1.244   0.982
HETATM    2  C     1     1      -1.560  -2.284   1.096
HETATM    3  C     1     1      -0.507  -2.030   0.002
HETATM    4  C     1     1      -1.171  -2.139  -1.383
HETATM    5  C     1     1      -2.299  -1.099  -1.502
HETATM    6  C     1     1      -3.347  -1.357  -0.405
HETATM    7  C     1     1      -2.097   0.165   1.144
HETATM    8  C     1     1       0.070  -0.616   0.175
HETATM    9  C     1     1      -1.711   0.309  -1.313
HETATM   10  C     1     1      -1.036   0.453   0.064
HETATM   11  C     3     1      -0.500   1.885   0.232
HETATM   12  O     7     1      -1.216   2.858   0.180
HETATM   13  C     4     1       0.786   2.057   0.441
HETATM   14  C     4     1       1.969   2.223   0.633
HETATM   15  C     1     1       3.405   2.424   0.867
HETATM   16  F    11     1       3.966   3.160  -0.085
HETATM   17  F    11     1       4.080   1.245   0.903
HETATM   18  F    11     1       3.651   3.067   2.073
HETATM   19  H     5     1      -3.451  -1.427   1.777
HETATM   20  H     5     1      -1.087  -2.227   2.103
HETATM   21  H     5     1      -1.975  -3.313   0.996
HETATM   22  H     5     1       0.312  -2.784   0.086
HETATM   23  H     5     1      -0.414  -1.977  -2.184
HETATM   24  H     5     1      -1.579  -3.165  -1.532
HETATM   25  H     5     1      -2.778  -1.176  -2.507
HETATM   26  H     5     1      -3.796  -2.368  -0.535
HETATM   27  H     5     1      -4.182  -0.625  -0.493
HETATM   28  H     5     1      -1.643   0.267   2.156
HETATM   29  H     5     1      -2.915   0.919   1.089
HETATM   30  H     5     1       0.576  -0.544   1.165
HETATM   31  H     5     1       0.852  -0.441  -0.598
HETATM   32  H     5     1      -2.520   1.066  -1.427
HETATM   33  H     5     1      -0.971   0.518  -2.120
CONECT    1    2    6    7   19
```

```
CONECT    2    1    3   20   21
CONECT    3    2    4    8   22
CONECT    4    3    5   23   24
CONECT    5    4    6    9   25
CONECT    6    1    5   26   27
CONECT    7    1   10   28   29
CONECT    8    3   10   30   31
CONECT    9    5   10   32   33
CONECT   10    7    8    9   11
CONECT   11   10   12   13
CONECT   12   11
CONECT   13   11   14
CONECT   14   13   15
CONECT   15   14   16   17   18
CONECT   16   15
CONECT   17   15
CONECT   18   15
CONECT   19    1
CONECT   20    2
CONECT   21    2
CONECT   22    3
CONECT   23    4
CONECT   24    4
CONECT   25    5
CONECT   26    6
CONECT   27    6
CONECT   28    7
CONECT   29    7
CONECT   30    8
CONECT   31    8
CONECT   32    9
CONECT   33    9
END
```

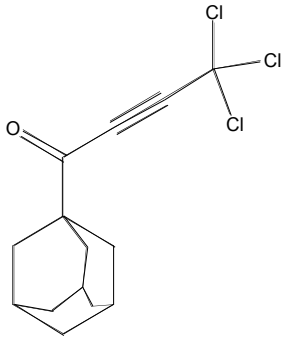

1-Adamantan-1-yl-4,4,4-trichloro-but-2-yn-1-one

```
HEADER    Untitled
COMPND
SOURCE
HETATM    1  C     1     1      -2.645  -1.192   1.053
HETATM    2  C     1     1      -1.516  -2.229   1.186
HETATM    3  C     1     1      -0.463  -1.996   0.087
HETATM    4  C     1     1      -1.126  -2.129  -1.296
HETATM    5  C     1     1      -2.255  -1.092  -1.433
HETATM    6  C     1     1      -3.304  -1.331  -0.332
HETATM    7  C     1     1      -2.054   0.220   1.188
HETATM    8  C     1     1       0.113  -0.578   0.235
HETATM    9  C     1     1      -1.668   0.319  -1.271
HETATM   10  C     1     1      -0.993   0.488   0.104
HETATM   11  C     3     1      -0.454   1.921   0.246
HETATM   12  O     7     1      -1.167   2.897   0.176
HETATM   13  C     4     1       0.832   2.090   0.452
HETATM   14  C     4     1       2.018   2.238   0.642
HETATM   15  C     1     1       3.460   2.403   0.873
HETATM   16  Cl   12     1       4.183   3.336  -0.419
HETATM   17  Cl   12     1       4.243   0.817   0.933
HETATM   18  Cl   12     1       3.750   3.244   2.426
HETATM   19  H     5     1      -3.408  -1.360   1.851
HETATM   20  H     5     1      -1.043  -2.153   2.192
HETATM   21  H     5     1      -1.931  -3.260   1.106
HETATM   22  H     5     1       0.356  -2.748   0.186
HETATM   23  H     5     1      -0.369  -1.980  -2.100
HETATM   24  H     5     1      -1.533  -3.158  -1.428
HETATM   25  H     5     1      -2.734  -1.188  -2.437
HETATM   26  H     5     1      -3.752  -2.345  -0.443
HETATM   27  H     5     1      -4.139  -0.601  -0.434
HETATM   28  H     5     1      -1.600   0.342   2.199
HETATM   29  H     5     1      -2.873   0.973   1.120
HETATM   30  H     5     1       0.619  -0.489   1.223
HETATM   31  H     5     1       0.896  -0.418  -0.542
HETATM   32  H     5     1      -2.477   1.074  -1.397
HETATM   33  H     5     1      -0.928   0.514  -2.081
CONECT    1    2    6    7   19
CONECT    2    1    3   20   21
CONECT    3    2    4    8   22
```

```
CONECT    4    3    5   23   24
CONECT    5    4    6    9   25
CONECT    6    1    5   26   27
CONECT    7    1   10   28   29
CONECT    8    3   10   30   31
CONECT    9    5   10   32   33
CONECT   10    7    8    9   11
CONECT   11   10   12   13
CONECT   12   11
CONECT   13   11   14
CONECT   14   13   15
CONECT   15   14   16   17   18
CONECT   16   15
CONECT   17   15
CONECT   18   15
CONECT   19    1
CONECT   20    2
CONECT   21    2
CONECT   22    3
CONECT   23    4
CONECT   24    4
CONECT   25    5
CONECT   26    6
CONECT   27    6
CONECT   28    7
CONECT   29    7
CONECT   30    8
CONECT   31    8
CONECT   32    9
CONECT   33    9
END
```

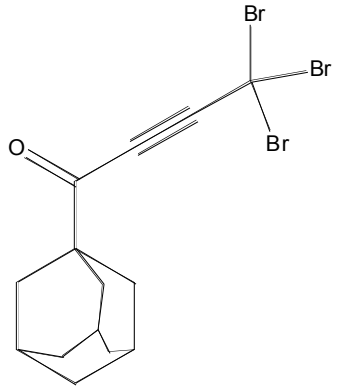

1-Adamantan-1-yl-4,4,4-tribromo-but-2-yn-1-one

```
HEADER    Untitled
COMPND
SOURCE
HETATM    1  C     1     1      -2.696  -1.230   0.985
HETATM    2  C     1     1      -1.563  -2.264   1.120
HETATM    3  C     1     1      -0.511  -2.029   0.021
HETATM    4  C     1     1      -1.173  -2.165  -1.362
HETATM    5  C     1     1      -2.305  -1.131  -1.500
HETATM    6  C     1     1      -3.354  -1.372  -0.399
HETATM    7  C     1     1      -2.108   0.184   1.120
HETATM    8  C     1     1       0.061  -0.610   0.168
HETATM    9  C     1     1      -1.722   0.282  -1.339
HETATM   10  C     1     1      -1.047   0.453   0.036
HETATM   11  C     3     1      -0.513   1.889   0.177
HETATM   12  O     7     1      -1.227   2.862   0.104
HETATM   13  C     4     1       0.773   2.059   0.386
HETATM   14  C     4     1       1.959   2.208   0.578
HETATM   15  C     1     1       3.401   2.373   0.811
HETATM   16  Br   13     1       4.175   3.414  -0.637
HETATM   17  Br   13     1       4.236   0.617   0.872
HETATM   18  Br   13     1       3.682   3.288   2.503
HETATM   19  H     5     1      -3.457  -1.400   1.784
HETATM   20  H     5     1      -1.091  -2.186   2.126
HETATM   21  H     5     1      -1.975  -3.296   1.041
HETATM   22  H     5     1       0.310  -2.778   0.120
HETATM   23  H     5     1      -0.417  -2.015  -2.166
HETATM   24  H     5     1      -1.577  -3.195  -1.493
HETATM   25  H     5     1      -2.784  -1.229  -2.504
HETATM   26  H     5     1      -3.799  -2.387  -0.509
HETATM   27  H     5     1      -4.191  -0.644  -0.501
HETATM   28  H     5     1      -1.654   0.307   2.131
HETATM   29  H     5     1      -2.928   0.934   1.051
HETATM   30  H     5     1       0.567  -0.518   1.156
HETATM   31  H     5     1       0.844  -0.448  -0.609
HETATM   32  H     5     1      -2.533   1.034  -1.466
HETATM   33  H     5     1      -0.983   0.478  -2.149
CONECT    1    2    6    7   19
```

```
CONECT    2    1    3   20   21
CONECT    3    2    4    8   22
CONECT    4    3    5   23   24
CONECT    5    4    6    9   25
CONECT    6    1    5   26   27
CONECT    7    1   10   28   29
CONECT    8    3   10   30   31
CONECT    9    5   10   32   33
CONECT   10    7    8    9   11
CONECT   11   10   12   13
CONECT   12   11
CONECT   13   11   14
CONECT   14   13   15
CONECT   15   14   16   17   18
CONECT   16   15
CONECT   17   15
CONECT   18   15
CONECT   19    1
CONECT   20    2
CONECT   21    2
CONECT   22    3
CONECT   23    4
CONECT   24    4
CONECT   25    5
CONECT   26    6
CONECT   27    6
CONECT   28    7
CONECT   29    7
CONECT   30    8
CONECT   31    8
CONECT   32    9
CONECT   33    9
END
```

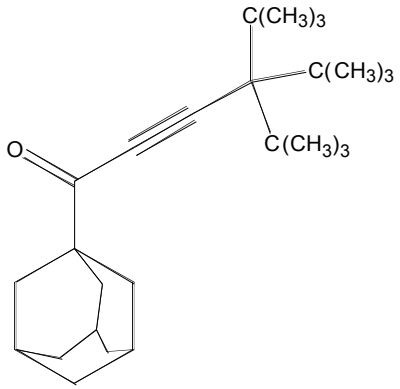

1-Adamantan-1-yl-4,4-di-tert-butyl-5,5-dimethyl-hex-2-yn-1-one

```
HEADER    Untitled
COMPND
SOURCE
HETATM    1  C     1     1      -3.031  -1.792   0.690
HETATM    2  C     1     1      -1.849  -2.777   0.736
HETATM    3  C     1     1      -0.835  -2.426  -0.367
HETATM    4  C     1     1      -1.523  -2.509  -1.741
HETATM    5  C     1     1      -2.704  -1.523  -1.792
HETATM    6  C     1     1      -3.714  -1.880  -0.687
HETATM    7  C     1     1      -2.506  -0.362   0.900
HETATM    8  C     1     1      -0.325  -0.992  -0.145
HETATM    9  C     1     1      -2.182  -0.097  -1.556
HETATM   10  C     1     1      -1.484   0.023  -0.188
HETATM   11  C     3     1      -1.014   1.472   0.031
HETATM   12  O     7     1      -1.777   2.411   0.032
HETATM   13  C     4     1       0.266   1.689   0.223
HETATM   14  C     4     1       1.449   1.880   0.399
HETATM   15  C     1     1       2.894   2.097   0.613
HETATM   16  C     1     1       3.425   3.020  -0.497
HETATM   17  C     1     1       3.608   0.736   0.561
HETATM   18  C     1     1       3.097   2.751   1.991
HETATM   19  H     5     1      -3.764  -2.046   1.491
HETATM   20  H     5     1      -1.357  -2.739   1.735
HETATM   21  H     5     1      -2.215  -3.820   0.601
HETATM   22  H     5     1       0.022  -3.140  -0.331
HETATM   23  H     5     1      -0.794  -2.275  -2.550
HETATM   24  H     5     1      -1.882  -3.547  -1.927
HETATM   25  H     5     1      -3.201  -1.583  -2.790
HETATM   26  H     5     1      -4.114  -2.906  -0.851
HETATM   27  H     5     1      -4.586  -1.188  -0.727
HETATM   28  H     5     1      -2.035  -0.280   1.906
HETATM   29  H     5     1      -3.361   0.351   0.894
HETATM   30  H     5     1       0.199  -0.938   0.837
HETATM   31  H     5     1       0.431  -0.747  -0.926
HETATM   32  H     5     1      -3.030   0.623  -1.620
HETATM   33  H     5     1      -1.472   0.182  -2.367
HETATM   34  H     5     1       3.276   2.576  -1.507
HETATM   35  H     5     1       2.911   4.007  -0.492
```

```
HETATM   36  H     5     1       4.514   3.215  -0.381
HETATM   37  H     5     1       3.463   0.233  -0.422
HETATM   38  H     5     1       4.705   0.843   0.717
HETATM   39  H     5     1       3.230   0.042   1.344
HETATM   40  H     5     1       2.575   3.731   2.062
HETATM   41  H     5     1       2.707   2.109   2.812
HETATM   42  H     5     1       4.174   2.936   2.201
CONECT    1    2    6    7   19
CONECT    2    1    3   20   21
CONECT    3    2    4    8   22
CONECT    4    3    5   23   24
CONECT    5    4    6    9   25
CONECT    6    1    5   26   27
CONECT    7    1   10   28   29
CONECT    8    3   10   30   31
CONECT    9    5   10   32   33
CONECT   10    7    8    9   11
CONECT   11   10   12   13
CONECT   12   11
CONECT   13   11   14
CONECT   14   13   15
CONECT   15   14   16   17   18
CONECT   16   15   34   35   36
CONECT   17   15   37   38   39
CONECT   18   15   40   41   42
CONECT   19    1
CONECT   20    2
CONECT   21    2
CONECT   22    3
CONECT   23    4
CONECT   24    4
CONECT   25    5
CONECT   26    6
CONECT   27    6
CONECT   28    7
CONECT   29    7
CONECT   30    8
CONECT   31    8
CONECT   32    9
CONECT   33    9
CONECT   34   16
CONECT   35   16
CONECT   36   16
CONECT   37   17
CONECT   38   17
CONECT   39   17
CONECT   40   18
CONECT   41   18
CONECT   42   18
END
```

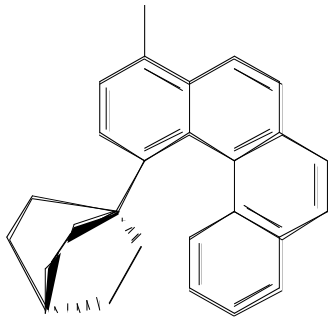

Compound 52b

```
HEADER    Untitled
COMPND
SOURCE
HETATM    1  C     2     1      -3.451   1.378  -1.437
HETATM    2  C     2     1      -2.179   1.776  -1.247
HETATM    3  C     1     1      -3.607  -0.139  -1.399
HETATM    4  C     2     1      -2.662  -0.682  -2.461
HETATM    5  C     2     1      -1.393  -0.272  -2.292
HETATM    6  C     1     1      -1.155   0.633  -1.070
HETATM    7  C     2     1      -1.761  -0.115   0.127
HETATM    8  C    50     1       0.889  -1.406   0.522
HETATM    9  C    50     1       0.655  -2.402   1.492
HETATM   10  C    50     1       0.864  -2.111   2.842
HETATM   11  C    50     1       1.420  -0.889   3.211
HETATM   12  C    50     1       1.646   0.101   2.250
HETATM   13  C    50     1       1.204  -0.088   0.928
HETATM   14  C    50     1       2.349   1.261   2.578
HETATM   15  C    50     1       1.185   1.028   0.056
HETATM   16  C    50     1       2.095   2.081   0.309
HETATM   17  C    50     1       2.659   2.188   1.587
HETATM   18  C    50     1       2.390   3.021  -0.698
HETATM   19  C    50     1       0.267   1.184  -1.014
HETATM   20  C    50     1       0.601   2.089  -2.035
HETATM   21  C    50     1       1.677   2.961  -1.899
HETATM   22  C     1     1       3.463   4.075  -0.539
HETATM   23  C    50     1       0.925  -1.793  -0.827
HETATM   24  C    50     1       0.583  -3.090  -1.216
HETATM   25  C    50     1       0.225  -4.033  -0.255
HETATM   26  C    50     1       0.277  -3.692   1.096
HETATM   27  C     2     1      -3.025  -0.544  -0.049
HETATM   28  H     5     1      -4.312   2.059  -1.534
HETATM   29  H     5     1      -1.900   2.838  -1.151
HETATM   30  H     5     1      -4.657  -0.474  -1.539
HETATM   31  H     5     1      -3.013  -1.310  -3.295
HETATM   32  H     5     1      -0.591  -0.536  -2.998
HETATM   33  H     5     1      -1.267  -0.184   1.106
HETATM   34  H     5     1       0.703  -2.884   3.614
HETATM   35  H     5     1       1.710  -0.726   4.263
HETATM   36  H     5     1       2.742   1.407   3.599
```

```
HETATM   37  H     5     1       3.311   3.036   1.855
HETATM   38  H     5     1      -0.036   2.182  -2.932
HETATM   39  H     5     1       1.898   3.673  -2.713
HETATM   40  H     5     1       3.671   4.615  -1.489
HETATM   41  H     5     1       4.430   3.631  -0.215
HETATM   42  H     5     1       3.168   4.846   0.208
HETATM   43  H     5     1       1.289  -1.092  -1.594
HETATM   44  H     5     1       0.629  -3.385  -2.278
HETATM   45  H     5     1      -0.033  -5.063  -0.556
HETATM   46  H     5     1       0.071  -4.471   1.851
HETATM   47  H     5     1      -3.635  -1.020   0.735
CONECT    1    2    3   28
CONECT    2    1    6   29
CONECT    3    1    4   27   30
CONECT    4    3    5   31
CONECT    5    4    6   32
CONECT    6    2    5    7   19
CONECT    7    6   27   33
CONECT    8    9   13   23
CONECT    9    8   10   26
CONECT   10    9   11   34
CONECT   11   10   12   35
CONECT   12   11   13   14
CONECT   13    8   12   15
CONECT   14   12   17   36
CONECT   15   13   16   19
CONECT   16   15   17   18
CONECT   17   14   16   37
CONECT   18   16   21   22
CONECT   19    6   15   20
CONECT   20   19   21   38
CONECT   21   18   20   39
CONECT   22   18   40   41   42
CONECT   23    8   24   43
CONECT   24   23   25   44
CONECT   25   24   26   45
CONECT   26    9   25   46
CONECT   27    3    7   47
CONECT   28    1
CONECT   29    2
CONECT   30    3
CONECT   31    4
CONECT   32    5
CONECT   33    7
CONECT   34   10
CONECT   35   11
CONECT   36   14
CONECT   37   17
CONECT   38   20
CONECT   39   21
CONECT   40   22
CONECT   41   22
CONECT   42   22
CONECT   43   23
```

```
CONECT   44   24
CONECT   45   25
CONECT   46   26
CONECT   47   27
END
```

Energy Barrier Calculations:

All energy barrier calculations were done using Spartan 06, Molecular Mechanics MMFF, starting with optimized structures. In the case of Compound 52a and 52b semi-emperical AM1 was used.

Cartesian coordinates for the optimized structures are below:

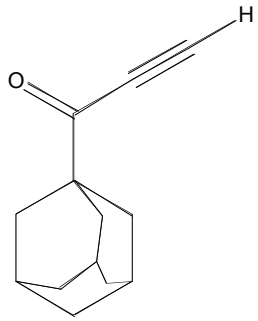

1-Adamantan-1-yl-propynone

```
HEADER
REMARK Spartan `04 exported M001
HETATM    1  H   UNK  0001       2.724  -1.335  -0.003
HETATM    2  C   UNK  0001       1.837  -0.708  -0.002
HETATM    3  C   UNK  0001       0.573   1.056   1.256
HETATM    4  C   UNK  0001       0.572   1.059  -1.254
HETATM    5  C   UNK  0001       0.564   1.943   0.002
HETATM    6  C   UNK  0001       1.832   0.180  -1.255
HETATM    7  C   UNK  0001       1.833   0.177   1.254
HETATM    8  H   UNK  0001       1.433   2.597   0.002
HETATM    9  H   UNK  0001       2.722   0.805  -1.276
HETATM   10  H   UNK  0001       2.723   0.802   1.276
HETATM   11  H   UNK  0001       0.562   1.680   2.146
HETATM   12  H   UNK  0001       0.560   1.685  -2.142
HETATM   13  H   UNK  0001      -0.314   2.585   0.003
HETATM   14  H   UNK  0001       1.858  -0.436  -2.150
HETATM   15  H   UNK  0001       1.860  -0.441   2.148
HETATM   16  C   UNK  0001       0.590  -1.605  -0.002
HETATM   17  H   UNK  0001       0.592  -2.255   0.867
HETATM   18  H   UNK  0001       0.591  -2.253  -0.872
HETATM   19  C   UNK  0001      -0.680  -0.737  -0.000
HETATM   20  C   UNK  0001      -0.679   0.166  -1.257
HETATM   21  H   UNK  0001      -0.693  -0.452  -2.152
```

```
HETATM   22  H   UNK  0001      -1.573   0.780  -1.280
HETATM   23  C   UNK  0001      -0.677   0.163   1.259
HETATM   24  H   UNK  0001      -0.691  -0.457   2.152
HETATM   25  H   UNK  0001      -1.572   0.777   1.284
HETATM   26  C   UNK  0001      -1.915  -1.627  -0.001
HETATM   27  O   UNK  0001      -1.870  -2.818  -0.002
HETATM   28  C   UNK  0001      -3.227  -0.955   0.000
HETATM   29  C   UNK  0001      -4.287  -0.421   0.002
HETATM   30  H   UNK  0001      -5.238   0.042   0.003
CONECT    1    2
CONECT    2    1    6    7   16
CONECT    3   11    5    7   23
CONECT    4   12    6    5   20
CONECT    5    3    4    8   13
CONECT    6    2    4    9   14
CONECT    7    2    3   10   15
CONECT    8    5
CONECT    9    6
CONECT   10    7
CONECT   11    3
CONECT   12    4
CONECT   13    5
CONECT   14    6
CONECT   15    7
CONECT   16   17   18    2   19
CONECT   17   16
CONECT   18   16
CONECT   19   16   23   20   26
CONECT   20   21   22    4   19
CONECT   21   20
CONECT   22   20
CONECT   23   24   25    3   19
CONECT   24   23
CONECT   25   23
CONECT   26   19   27   28
CONECT   27   26
CONECT   28   26   29
CONECT   29   28   30
CONECT   30   29
END
```

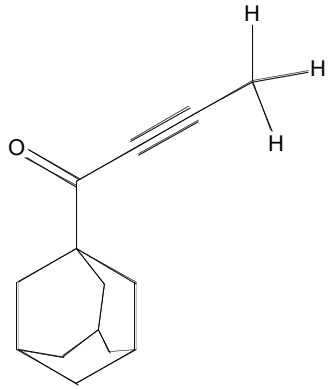

1-Adamantan-1-yl-but-2-yn-1-one

```
HEADER
REMARK Spartan `04 exported M001
HETATM    1  H   UNK  0001       3.214  -1.640  -0.000
HETATM    2  C   UNK  0001       2.435  -0.882  -0.000
HETATM    3  C   UNK  0001       1.462   1.059   1.255
HETATM    4  C   UNK  0001       1.463   1.060  -1.255
HETATM    5  C   UNK  0001       1.593   1.936   0.000
HETATM    6  C   UNK  0001       2.570  -0.005  -1.254
HETATM    7  C   UNK  0001       2.570  -0.005   1.254
HETATM    8  H   UNK  0001       2.553   2.446   0.000
HETATM    9  H   UNK  0001       3.546   0.473  -1.275
HETATM   10  H   UNK  0001       3.546   0.473   1.276
HETATM   11  H   UNK  0001       1.549   1.678   2.144
HETATM   12  H   UNK  0001       1.549   1.679  -2.144
HETATM   13  H   UNK  0001       0.826   2.707   0.000
HETATM   14  H   UNK  0001       2.499  -0.619  -2.149
HETATM   15  H   UNK  0001       2.499  -0.619   2.149
HETATM   16  C   UNK  0001       1.063  -1.572  -0.000
HETATM   17  H   UNK  0001       0.963  -2.214   0.869
HETATM   18  H   UNK  0001       0.963  -2.214  -0.870
HETATM   19  C   UNK  0001      -0.057  -0.517  -0.000
HETATM   20  C   UNK  0001       0.088   0.373  -1.257
HETATM   21  H   UNK  0001      -0.023  -0.236  -2.152
HETATM   22  H   UNK  0001      -0.700   1.120  -1.281
HETATM   23  C   UNK  0001       0.088   0.373   1.258
HETATM   24  H   UNK  0001      -0.023  -0.237   2.152
HETATM   25  H   UNK  0001      -0.700   1.119   1.282
HETATM   26  C   UNK  0001      -1.418  -1.203  -0.000
HETATM   27  O   UNK  0001      -1.551  -2.388   0.001
HETATM   28  C   UNK  0001      -2.605  -0.336  -0.001
HETATM   29  C   UNK  0001      -3.572   0.355  -0.002
HETATM   30  C   UNK  0001      -4.777   1.193  -0.000
HETATM   31  H   UNK  0001      -5.147   1.311   1.012
HETATM   32  H   UNK  0001      -5.558   0.735  -0.596
HETATM   33  H   UNK  0001      -4.565   2.176  -0.404
CONECT    1    2
CONECT    2    1    6    7   16
CONECT    3   11    5    7   23
```

```
CONECT    4   12    6    5   20
CONECT    5    3    4    8   13
CONECT    6    2    4    9   14
CONECT    7    2    3   10   15
CONECT    8    5
CONECT    9    6
CONECT   10    7
CONECT   11    3
CONECT   12    4
CONECT   13    5
CONECT   14    6
CONECT   15    7
CONECT   16   17   18    2   19
CONECT   17   16
CONECT   18   16
CONECT   19   16   23   20   26
CONECT   20   21   22    4   19
CONECT   21   20
CONECT   22   20
CONECT   23   24   25    3   19
CONECT   24   23
CONECT   25   23
CONECT   26   19   27   28
CONECT   27   26
CONECT   28   26   29
CONECT   29   28   30
CONECT   30   31   32   33   29
CONECT   31   30
CONECT   32   30
CONECT   33   30
END
```

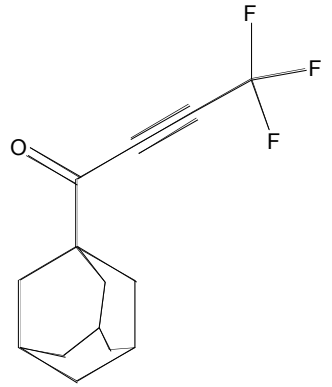

1-Adamantan-1-yl-4,4,4-trifluoro-but-2-yn-1-one

```
HEADER
REMARK Spartan `04 exported M001
HETATM    1  H   UNK  0001       4.379  -1.239  -0.004
HETATM    2  C   UNK  0001       3.492  -0.613  -0.002
HETATM    3  C   UNK  0001       2.226   1.149   1.256
HETATM    4  C   UNK  0001       2.224   1.152  -1.254
HETATM    5  C   UNK  0001       2.215   2.037   0.002
HETATM    6  C   UNK  0001       3.484   0.275  -1.255
HETATM    7  C   UNK  0001       3.487   0.272   1.253
HETATM    8  H   UNK  0001       3.083   2.692   0.002
HETATM    9  H   UNK  0001       4.373   0.902  -1.277
HETATM   10  H   UNK  0001       4.375   0.898   1.275
HETATM   11  H   UNK  0001       2.214   1.773   2.146
HETATM   12  H   UNK  0001       2.210   1.778  -2.142
HETATM   13  H   UNK  0001       1.336   2.678   0.004
HETATM   14  H   UNK  0001       3.511  -0.341  -2.151
HETATM   15  H   UNK  0001       3.515  -0.346   2.148
HETATM   16  C   UNK  0001       2.247  -1.512  -0.002
HETATM   17  H   UNK  0001       2.249  -2.162   0.867
HETATM   18  H   UNK  0001       2.248  -2.160  -0.873
HETATM   19  C   UNK  0001       0.976  -0.644  -0.000
HETATM   20  C   UNK  0001       0.974   0.258  -1.258
HETATM   21  H   UNK  0001       0.960  -0.360  -2.153
HETATM   22  H   UNK  0001       0.080   0.874  -1.281
HETATM   23  C   UNK  0001       0.976   0.255   1.260
HETATM   24  H   UNK  0001       0.964  -0.365   2.153
HETATM   25  H   UNK  0001       0.082   0.871   1.286
HETATM   26  C   UNK  0001      -0.255  -1.536   0.000
HETATM   27  O   UNK  0001      -0.226  -2.724   0.001
HETATM   28  C   UNK  0001      -1.574  -0.860  -0.001
HETATM   29  C   UNK  0001      -2.633  -0.331  -0.002
HETATM   30  C   UNK  0001      -3.950   0.327  -0.001
HETATM   31  F   UNK  0001      -3.874   1.535  -0.521
HETATM   32  F   UNK  0001      -4.825  -0.359  -0.705
HETATM   33  F   UNK  0001      -4.412   0.442   1.226
CONECT    1    2
CONECT    2    1    6    7   16
```

```
CONECT    3   11    5    7   23
CONECT    4   12    6    5   20
CONECT    5    3    4    8   13
CONECT    6    2    4    9   14
CONECT    7    2    3   10   15
CONECT    8    5
CONECT    9    6
CONECT   10    7
CONECT   11    3
CONECT   12    4
CONECT   13    5
CONECT   14    6
CONECT   15    7
CONECT   16   17   18    2   19
CONECT   17   16
CONECT   18   16
CONECT   19   16   23   20   26
CONECT   20   21   22    4   19
CONECT   21   20
CONECT   22   20
CONECT   23   24   25    3   19
CONECT   24   23
CONECT   25   23
CONECT   26   19   27   28
CONECT   27   26
CONECT   28   26   29
CONECT   29   28   30
CONECT   30   29   31   32   33
CONECT   31   30
CONECT   32   30
CONECT   33   30
END
```

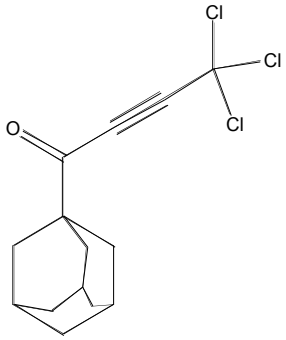

1-Adamantan-1-yl-4,4,4-trichloro-but-2-yn-1-one

```
HEADER
REMARK Spartan `04 exported M001
HETATM    1  H   UNK  0001      -3.041   0.001   1.874
HETATM    2  C   UNK  0001      -2.261   0.001   1.118
HETATM    3  C   UNK  0001      -1.282  -1.254  -0.821
HETATM    4  C   UNK  0001      -1.279   1.257  -0.818
HETATM    5  C   UNK  0001      -1.407   0.002  -1.696
HETATM    6  C   UNK  0001      -2.390   1.256   0.243
HETATM    7  C   UNK  0001      -2.393  -1.253   0.240
HETATM    8  H   UNK  0001      -2.366   0.004  -2.210
HETATM    9  H   UNK  0001      -3.364   1.279  -0.239
HETATM   10  H   UNK  0001      -3.368  -1.272  -0.242
HETATM   11  H   UNK  0001      -1.367  -2.142  -1.441
HETATM   12  H   UNK  0001      -1.362   2.146  -1.436
HETATM   13  H   UNK  0001      -0.638   0.002  -2.465
HETATM   14  H   UNK  0001      -2.321   2.150   0.858
HETATM   15  H   UNK  0001      -2.326  -2.148   0.853
HETATM   16  C   UNK  0001      -0.892  -0.002   1.815
HETATM   17  H   UNK  0001      -0.795  -0.872   2.455
HETATM   18  H   UNK  0001      -0.793   0.867   2.457
HETATM   19  C   UNK  0001       0.230  -0.002   0.762
HETATM   20  C   UNK  0001       0.093   1.258  -0.127
HETATM   21  H   UNK  0001       0.203   2.151   0.483
HETATM   22  H   UNK  0001       0.882   1.282  -0.873
HETATM   23  C   UNK  0001       0.090  -1.260  -0.130
HETATM   24  H   UNK  0001       0.198  -2.155   0.479
HETATM   25  H   UNK  0001       0.879  -1.285  -0.876
HETATM   26  C   UNK  0001       1.584  -0.004   1.453
HETATM   27  O   UNK  0001       1.737  -0.008   2.632
HETATM   28  C   UNK  0001       2.781  -0.002   0.583
HETATM   29  C   UNK  0001       3.747   0.000  -0.105
HETATM   30  C   UNK  0001       4.939   0.002  -0.945
HETATM   31 Cl   UNK  0001       4.552   0.692  -2.539
HETATM   32 Cl   UNK  0001       5.514  -1.666  -1.156
HETATM   33 Cl   UNK  0001       6.216   0.974  -0.186
CONECT    1    2
CONECT    2    1    6    7   16
CONECT    3   11    5    7   23
CONECT    4   12    6    5   20
```

```
CONECT    5    3    4    8   13
CONECT    6    2    4    9   14
CONECT    7    2    3   10   15
CONECT    8    5
CONECT    9    6
CONECT   10    7
CONECT   11    3
CONECT   12    4
CONECT   13    5
CONECT   14    6
CONECT   15    7
CONECT   16   17   18    2   19
CONECT   17   16
CONECT   18   16
CONECT   19   16   23   20   26
CONECT   20   21   22    4   19
CONECT   21   20
CONECT   22   20
CONECT   23   24   25    3   19
CONECT   24   23
CONECT   25   23
CONECT   26   19   27   28
CONECT   27   26
CONECT   28   26   29
CONECT   29   28   30
CONECT   30   29   31   32   33
CONECT   31   30
CONECT   32   30
CONECT   33   30
END
```

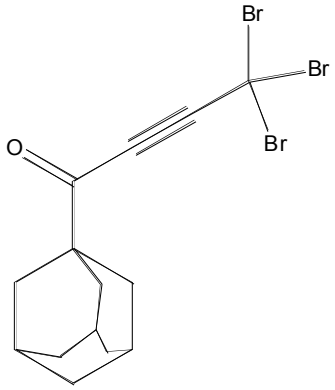

1-Adamantan-1-yl-4,4,4-tribromo-but-2-yn-1-one

```
HEADER
REMARK Spartan `04 exported M001
HETATM    1  H   UNK  0001       3.297  -1.390   0.025
HETATM    2  C   UNK  0001       2.410  -0.762   0.009
HETATM    3  C   UNK  0001       1.153   1.045   1.212
HETATM    4  C   UNK  0001       1.136   0.958  -1.297
HETATM    5  C   UNK  0001       1.135   1.887  -0.073
HETATM    6  C   UNK  0001       2.396   0.080  -1.275
HETATM    7  C   UNK  0001       2.413   0.167   1.232
HETATM    8  H   UNK  0001       2.003   2.541  -0.102
HETATM    9  H   UNK  0001       3.285   0.704  -1.324
HETATM   10  H   UNK  0001       3.303   0.792   1.226
HETATM   11  H   UNK  0001       1.147   1.700   2.078
HETATM   12  H   UNK  0001       1.117   1.551  -2.207
HETATM   13  H   UNK  0001       0.257   2.528  -0.089
HETATM   14  H   UNK  0001       2.416  -0.568  -2.148
HETATM   15  H   UNK  0001       2.447  -0.419   2.148
HETATM   16  C   UNK  0001       1.164  -1.660   0.049
HETATM   17  H   UNK  0001       1.171  -2.278   0.941
HETATM   18  H   UNK  0001       1.159  -2.338  -0.798
HETATM   19  C   UNK  0001      -0.107  -0.791   0.028
HETATM   20  C   UNK  0001      -0.115   0.065  -1.261
HETATM   21  H   UNK  0001      -0.135  -0.584  -2.133
HETATM   22  H   UNK  0001      -1.009   0.681  -1.301
HETATM   23  C   UNK  0001      -0.097   0.152   1.255
HETATM   24  H   UNK  0001      -0.105  -0.435   2.170
HETATM   25  H   UNK  0001      -0.990   0.770   1.265
HETATM   26  C   UNK  0001      -1.339  -1.680   0.068
HETATM   27  O   UNK  0001      -1.308  -2.869   0.108
HETATM   28  C   UNK  0001      -2.654  -1.004   0.053
HETATM   29  C   UNK  0001      -3.714  -0.470   0.043
HETATM   30  C   UNK  0001      -5.011   0.178   0.029
HETATM   31 Br   UNK  0001      -5.987  -0.299   1.646
HETATM   32 Br   UNK  0001      -4.778   2.115  -0.039
HETATM   33 Br   UNK  0001      -6.009  -0.409  -1.537
CONECT    1    2
CONECT    2    1    6    7   16
```

```
CONECT    3   11    5    7   23
CONECT    4   12    6    5   20
CONECT    5    3    4    8   13
CONECT    6    2    4    9   14
CONECT    7    2    3   10   15
CONECT    8    5
CONECT    9    6
CONECT   10    7
CONECT   11    3
CONECT   12    4
CONECT   13    5
CONECT   14    6
CONECT   15    7
CONECT   16   17   18    2   19
CONECT   17   16
CONECT   18   16
CONECT   19   16   23   20   26
CONECT   20   21   22    4   19
CONECT   21   20
CONECT   22   20
CONECT   23   24   25    3   19
CONECT   24   23
CONECT   25   23
CONECT   26   19   27   28
CONECT   27   26
CONECT   28   26   29
CONECT   29   28   30
CONECT   30   29   31   32   33
CONECT   31   30
CONECT   32   30
CONECT   33   30
END
```

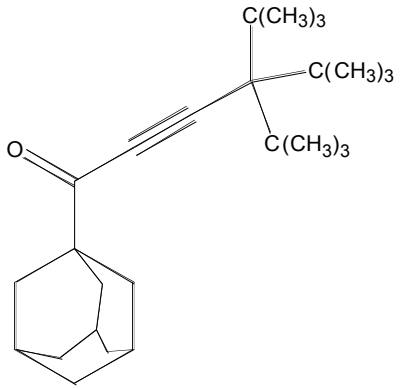

1-Adamantan-1-yl-4,4-di-tert-butyl-5,5-dimethyl-hex-2-yn-1-one

```
HEADER
REMARK Spartan `04 exported M001
HETATM    1  H   UNK  0001      -4.205  -0.061   2.168
HETATM    2  C   UNK  0001      -3.429  -0.026   1.409
HETATM    3  C   UNK  0001      -2.484  -1.168  -0.614
HETATM    4  C   UNK  0001      -2.436   1.336  -0.448
HETATM    5  C   UNK  0001      -2.592   0.145  -1.405
HETATM    6  C   UNK  0001      -3.540   1.286   0.617
HETATM    7  C   UNK  0001      -3.589  -1.216   0.451
HETATM    8  H   UNK  0001      -3.554   0.197  -1.911
HETATM    9  H   UNK  0001      -4.518   1.358   0.145
HETATM   10  H   UNK  0001      -4.567  -1.187  -0.024
HETATM   11  H   UNK  0001      -2.590  -2.012  -1.291
HETATM   12  H   UNK  0001      -2.507   2.266  -1.007
HETATM   13  H   UNK  0001      -1.827   0.181  -2.177
HETATM   14  H   UNK  0001      -3.451   2.137   1.289
HETATM   15  H   UNK  0001      -3.535  -2.151   1.005
HETATM   16  C   UNK  0001      -2.055  -0.098   2.093
HETATM   17  H   UNK  0001      -1.971  -1.010   2.676
HETATM   18  H   UNK  0001      -1.937   0.725   2.791
HETATM   19  C   UNK  0001      -0.937  -0.049   1.037
HETATM   20  C   UNK  0001      -1.060   1.267   0.233
HETATM   21  H   UNK  0001      -0.930   2.117   0.899
HETATM   22  H   UNK  0001      -0.273   1.325  -0.513
HETATM   23  C   UNK  0001      -1.108  -1.242   0.066
HETATM   24  H   UNK  0001      -1.014  -2.177   0.614
HETATM   25  H   UNK  0001      -0.323  -1.232  -0.683
HETATM   26  C   UNK  0001       0.425  -0.121   1.717
HETATM   27  O   UNK  0001       0.558  -0.202   2.900
HETATM   28  C   UNK  0001       1.610  -0.086   0.849
HETATM   29  C   UNK  0001       2.576  -0.059   0.155
HETATM   30  C   UNK  0001       3.794  -0.029  -0.689
HETATM   31  C   UNK  0001       3.408   0.343  -2.130
HETATM   32  H   UNK  0001       4.293   0.368  -2.758
HETATM   33  H   UNK  0001       2.938   1.320  -2.168
HETATM   34  H   UNK  0001       2.716  -0.381  -2.548
HETATM   35  C   UNK  0001       4.446  -1.422  -0.662
```

```
HETATM   36  H   UNK  0001       5.345  -1.421  -1.272
HETATM   37  H   UNK  0001       3.772  -2.177  -1.052
HETATM   38  H   UNK  0001       4.720  -1.704   0.349
HETATM   39  C   UNK  0001       4.768   1.017  -0.118
HETATM   40  H   UNK  0001       5.670   1.051  -0.721
HETATM   41  H   UNK  0001       5.047   0.773   0.901
HETATM   42  H   UNK  0001       4.322   2.006  -0.118
CONECT    1    2
CONECT    2    1    6    7   16
CONECT    3   11    5    7   23
CONECT    4   12    6    5   20
CONECT    5    3    4    8   13
CONECT    6    2    4    9   14
CONECT    7    2    3   10   15
CONECT    8    5
CONECT    9    6
CONECT   10    7
CONECT   11    3
CONECT   12    4
CONECT   13    5
CONECT   14    6
CONECT   15    7
CONECT   16   17   18    2   19
CONECT   17   16
CONECT   18   16
CONECT   19   16   23   20   26
CONECT   20   21   22    4   19
CONECT   21   20
CONECT   22   20
CONECT   23   24   25    3   19
CONECT   24   23
CONECT   25   23
CONECT   26   19   27   28
CONECT   27   26
CONECT   28   26   29
CONECT   29   28   30
CONECT   30   29   31   35   39
CONECT   31   32   33   34   30
CONECT   32   31
CONECT   33   31
CONECT   34   31
CONECT   35   36   37   38   30
CONECT   36   35
CONECT   37   35
CONECT   38   35
CONECT   39   40   41   42   30
CONECT   40   39
CONECT   41   39
CONECT   42   39
END
```

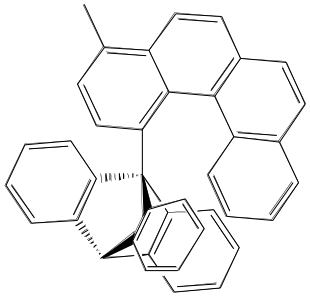

Compound 52a

```
HEADER
REMARK Spartan `06 exported M001
HETATM    1  H   UNK  0001      -2.269  -2.372  -3.610
HETATM    2  C   UNK  0001      -1.796  -1.516  -3.135
HETATM    3  C   UNK  0001      -1.794  -0.268  -3.737
HETATM    4  C   UNK  0001      -0.676  -0.571  -1.162
HETATM    5  C   UNK  0001      -1.139   0.823  -3.105
HETATM    6  C   UNK  0001      -1.279  -1.651  -1.862
HETATM    7  C   UNK  0001      -0.378   0.659  -1.902
HETATM    8  C   UNK  0001      -1.270   2.100  -3.668
HETATM    9  H   UNK  0001      -1.394  -2.623  -1.380
HETATM   10  C   UNK  0001      -0.664   3.214  -3.113
HETATM   11  H   UNK  0001      -1.902   2.273  -4.536
HETATM   12  H   UNK  0001      -0.870   4.189  -3.548
HETATM   13  C   UNK  0001       0.256   3.065  -2.091
HETATM   14  C   UNK  0001       0.881   4.225  -1.616
HETATM   15  C   UNK  0001       0.556   1.778  -1.574
HETATM   16  C   UNK  0001       1.894   4.154  -0.674
HETATM   17  H   UNK  0001       0.586   5.206  -1.983
HETATM   18  H   UNK  0001       2.348   5.074  -0.314
HETATM   19  C   UNK  0001       2.387   2.914  -0.290
HETATM   20  C   UNK  0001       1.776   1.733  -0.790
HETATM   21  C   UNK  0001       2.482   0.546  -0.549
HETATM   22  C   UNK  0001       3.512   2.852   0.550
HETATM   23  H   UNK  0001       3.946   3.761   0.961
HETATM   24  C   UNK  0001       3.613   0.479   0.270
HETATM   25  H   UNK  0001       4.097  -0.478   0.444
HETATM   26  C   UNK  0001       4.111   1.634   0.848
HETATM   27  H   UNK  0001       4.984   1.593   1.493
HETATM   28  C   UNK  0001      -2.507  -0.139  -5.063
HETATM   29  H   UNK  0001      -1.838   0.281  -5.820
HETATM   30  H   UNK  0001      -3.396   0.493  -4.957
HETATM   31  H   UNK  0001      -2.841  -1.113  -5.439
HETATM   32  C   UNK  0001      -0.470  -0.860   0.377
HETATM   33  C   UNK  0001       0.713  -1.926   0.597
HETATM   34  C   UNK  0001       2.687  -3.799   1.331
HETATM   35  C   UNK  0001       0.968  -2.246   1.958
HETATM   36  C   UNK  0001       1.431  -2.620  -0.384
HETATM   37  C   UNK  0001       2.420  -3.538  -0.015
HETATM   38  C   UNK  0001       1.952  -3.162   2.326
```

```
HETATM   39  H   UNK  0001       1.257  -2.455  -1.443
HETATM   40  H   UNK  0001       2.985  -4.057  -0.786
HETATM   41  H   UNK  0001       2.133  -3.395   3.371
HETATM   42  H   UNK  0001       3.456  -4.519   1.600
HETATM   43  C   UNK  0001      -0.275   0.343   1.386
HETATM   44  C   UNK  0001       0.023   2.190   3.501
HETATM   45  C   UNK  0001       0.096  -0.069   2.708
HETATM   46  C   UNK  0001      -0.686   1.665   1.232
HETATM   47  C   UNK  0001      -0.494   2.590   2.265
HETATM   48  C   UNK  0001       0.285   0.846   3.743
HETATM   49  H   UNK  0001      -1.180   2.004   0.329
HETATM   50  H   UNK  0001      -0.771   3.630   2.108
HETATM   51  H   UNK  0001       0.576   0.517   4.735
HETATM   52  H   UNK  0001       0.155   2.922   4.293
HETATM   53  C   UNK  0001      -1.719  -1.563   1.117
HETATM   54  C   UNK  0001      -3.654  -2.744   2.769
HETATM   55  C   UNK  0001      -3.033  -1.671   0.668
HETATM   56  C   UNK  0001      -1.408  -1.977   2.462
HETATM   57  C   UNK  0001      -2.365  -2.579   3.272
HETATM   58  C   UNK  0001      -3.988  -2.281   1.488
HETATM   59  H   UNK  0001      -3.344  -1.277  -0.294
HETATM   60  H   UNK  0001      -2.127  -2.890   4.284
HETATM   61  H   UNK  0001      -5.011  -2.382   1.134
HETATM   62  H   UNK  0001      -4.420  -3.206   3.388
HETATM   63  C   UNK  0001       0.012  -1.584   2.927
HETATM   64  H   UNK  0001       0.199  -1.868   3.968
HETATM   65  H   UNK  0001       2.176  -0.354  -1.063
CONECT    1    2
CONECT    2    1    3    6
CONECT    3    2    5   28
CONECT    4    6    7   32
CONECT    5    3    7    8
CONECT    6    2    4    9
CONECT    7    5    4   15
CONECT    8    5   10   11
CONECT    9    6
CONECT   10    8   13   12
CONECT   11    8
CONECT   12   10
CONECT   13   15   14   10
CONECT   14   16   13   17
CONECT   15    7   13   20
CONECT   16   14   19   18
CONECT   17   14
CONECT   18   16
CONECT   19   16   20   22
CONECT   20   19   15   21
CONECT   21   20   24   65
CONECT   22   23   19   26
CONECT   23   22
CONECT   24   25   21   26
CONECT   25   24
CONECT   26   27   24   22
CONECT   27   26
```

```
CONECT   28   29   30   31    3
CONECT   29   28
CONECT   30   28
CONECT   31   28
CONECT   32    4   33   43   53
CONECT   33   36   35   32
CONECT   34   37   38   42
CONECT   35   38   33   63
CONECT   36   33   37   39
CONECT   37   36   34   40
CONECT   38   34   35   41
CONECT   39   36
CONECT   40   37
CONECT   41   38
CONECT   42   34
CONECT   43   46   45   32
CONECT   44   47   48   52
CONECT   45   48   43   63
CONECT   46   43   47   49
CONECT   47   46   44   50
CONECT   48   44   45   51
CONECT   49   46
CONECT   50   47
CONECT   51   48
CONECT   52   44
CONECT   53   56   55   32
CONECT   54   57   58   62
CONECT   55   58   53   59
CONECT   56   53   57   63
CONECT   57   56   54   60
CONECT   58   54   55   61
CONECT   59   55
CONECT   60   57
CONECT   61   58
CONECT   62   54
CONECT   63   64   45   56   35
CONECT   64   63
CONECT   65   21
END
```

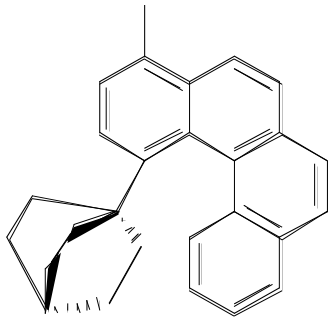

Compound 52b

```
HEADER
REMARK Spartan `06 exported M001
HETATM    1  C   UNK  0001      -0.185   0.225   1.749
HETATM    2  C   UNK  0001      -0.458   2.605   2.014
HETATM    3  C   UNK  0001      -2.062   1.092   3.000
HETATM    4  C   UNK  0001      -0.981   2.098   3.346
HETATM    5  C   UNK  0001      -1.648   0.112   2.178
HETATM    6  C   UNK  0001      -0.028   1.632   1.189
HETATM    7  H   UNK  0001      -0.446   3.677   1.813
HETATM    8  H   UNK  0001      -1.325   2.906   4.027
HETATM    9  H   UNK  0001       0.430   1.785   0.210
HETATM   10  H   UNK  0001      -3.061   1.208   3.422
HETATM   11  H   UNK  0001      -2.243  -0.732   1.824
HETATM   12  C   UNK  0001       0.583   0.297   3.083
HETATM   13  H   UNK  0001       1.399  -0.406   3.264
HETATM   14  C   UNK  0001       0.160   1.268   3.910
HETATM   15  H   UNK  0001       0.556   1.499   4.900
HETATM   16  C   UNK  0001       1.129  -3.221   1.130
HETATM   17  C   UNK  0001       1.856  -3.083  -0.040
HETATM   18  C   UNK  0001       0.291  -0.936   0.930
HETATM   19  C   UNK  0001       1.729  -1.884  -0.791
HETATM   20  C   UNK  0001       0.406  -2.133   1.634
HETATM   21  C   UNK  0001       0.779  -0.892  -0.410
HETATM   22  C   UNK  0001       2.592  -1.629  -1.906
HETATM   23  H   UNK  0001      -0.049  -2.215   2.635
HETATM   24  C   UNK  0001       2.474  -0.486  -2.634
HETATM   25  H   UNK  0001       3.381  -2.361  -2.135
HETATM   26  H   UNK  0001       3.192  -0.234  -3.428
HETATM   27  C   UNK  0001       1.353   0.377  -2.428
HETATM   28  C   UNK  0001       1.147   1.494  -3.296
HETATM   29  C   UNK  0001       0.419   0.079  -1.421
HETATM   30  C   UNK  0001      -0.019   2.196  -3.258
HETATM   31  H   UNK  0001       1.955   1.766  -3.992
HETATM   32  H   UNK  0001      -0.177   3.078  -3.897
HETATM   33  C   UNK  0001      -1.092   1.760  -2.419
HETATM   34  C   UNK  0001      -0.890   0.675  -1.530
HETATM   35  H   UNK  0001       1.159  -4.162   1.700
HETATM   36  C   UNK  0001      -2.019   0.139  -0.863
HETATM   37  H   UNK  0001      -1.886  -0.761  -0.243
HETATM   38  C   UNK  0001      -2.373   2.356  -2.522
```

```
HETATM   39  H   UNK  0001      -2.500   3.225  -3.185
HETATM   40  C   UNK  0001      -3.442   1.844  -1.821
HETATM   41  H   UNK  0001      -4.438   2.303  -1.904
HETATM   42  C   UNK  0001      -3.266   0.708  -1.005
HETATM   43  H   UNK  0001      -4.135   0.278  -0.485
HETATM   44  C   UNK  0001       2.752  -4.171  -0.495
HETATM   45  H   UNK  0001       3.821  -3.845  -0.434
HETATM   46  H   UNK  0001       2.529  -4.448  -1.556
HETATM   47  H   UNK  0001       2.629  -5.084   0.138
CONECT    1    5    6   12   18
CONECT    2    7    4    6
CONECT    3   10    5    4
CONECT    4    2    3    8   14
CONECT    5    1    3   11
CONECT    6    1    2    9
CONECT    7    2
CONECT    8    4
CONECT    9    6
CONECT   10    3
CONECT   11    5
CONECT   12   13    1   14
CONECT   13   12
CONECT   14   15   12    4
CONECT   15   14
CONECT   16   17   20   35
CONECT   17   16   19   44
CONECT   18   20   21    1
CONECT   19   17   21   22
CONECT   20   16   18   23
CONECT   21   19   18   29
CONECT   22   19   24   25
CONECT   23   20
CONECT   24   22   27   26
CONECT   25   22
CONECT   26   24
CONECT   27   29   28   24
CONECT   28   30   27   31
CONECT   29   21   27   34
CONECT   30   28   33   32
CONECT   31   28
CONECT   32   30
CONECT   33   30   34   38
CONECT   34   33   29   36
CONECT   35   16
CONECT   36   37   34   42
CONECT   37   36
CONECT   38   39   33   40
CONECT   39   38
CONECT   40   41   38   42
CONECT   41   40
CONECT   42   43   40   36
CONECT   43   42
CONECT   44   45   46   47   17
CONECT   45   44
```

```
CONECT   46   44
CONECT   47   44
END
```